NUMERICAL ANALYSIS OF AIR COOLED CONDENSER AND SELECTION OF OPTIMAL DESIGN PARAMETERS

By
ANKUR KUMAR
ENGG01201104019

Bhabha Atomic Research Center, Mumbai

A thesis submitted to the

Board of Studies in Engineering Sciences

In partial fulfillment of requirements for the Degree of

DOCTOR OF PHILOSOPHY ***of***

HOMI BHABHA NATIONAL INSTITUTE

April, 2017

Homi Bhabha National Institute

Recommendations of the Viva Voce Committee

As members of the Viva Voce Committee, we certify that we have read the dissertation prepared by Ankur Kumar entitled "Simulation and Design of Air Cooled Condenser" and recommend that it may be accepted as fulfilling the thesis requirement for the award of Degree of Doctor of Philosophy.

Chairman – Dr. P. K. Vijayan   Date: 1/2/17

Guide / Convener – Dr. A. K. Nayak   Date: 1/2/17

Co-guide - Prof. J.B. Joshi   Date: 1/2/17

Examiner – Prof. A.K. Suresh   Date: 1/2/17

Member 1- Dr. K. Velusamy   Date: 1/2/2017

Member 2- Prof. Atul Sharma   Date: 1/2/17

Final approval and acceptance of this thesis is contingent upon the candidate's submission of the final copies of the thesis to HBNI.

I/We hereby certify that I/we have read this thesis prepared under my/our direction and recommend that it may be accepted as fulfilling the thesis requirement.

Date: 1/2/2017

Place: MUMBAI

Co-guide   **Guide**

STATEMENT BY AUTHOR

This dissertation has been submitted in partial fulfillment of requirements for an advanced degree at Homi Bhabha National Institute (HBNI) and is deposited in the Library to be made available to borrowers under rules of the HBNI.

Brief quotations from this dissertation are allowable without special permission, provided that accurate acknowledgement of source is made. Requests for permission for extended quotation from or reproduction of this manuscript in whole or in part may be granted by the Competent Authority of HBNI when in his or her judgment the proposed use of the material is in the interests of scholarship. In all other instances, however, permission must be obtained from the author.

Ankur Kumar

DECLARATION

I, hereby declare that the investigation presented in the thesis has been carried out by me. The work is original and has not been submitted earlier as a whole or in part for a degree / diploma at this or any other Institution / University.

Ankur Kumar

List of Publications arising from the thesis

Journal

1. "3D CFD simulation of air cooled condenser-I: Natural convection over a circular cylinder", A. Kumar, J.B. Joshi, A.K. Nayak, P.K. Vijayan, **Int. J. Heat Mass Transfer, 2014**, 78., 1265-1283.
2. "A review on the thermal-hydraulic characteristics of air cooled heat exchangers in forced convection", A. Kumar, J.B. Joshi, A.K. Nayak, P.K. Vijayan, **Sadhana, 40 (3)**., 673-655.
3. "3D CFD simulation of air cooled condenser-II: Natural draft around a single finned tube kept in a small chimney", A. Kumar, J.B. Joshi, A.K. Nayak, P.K. Vijayan, **Int. J. Heat Mass Transfer, 2016**, 92., 507-522.
4. "3D CFD simulation of air cooled condenser-III: thermal-hydraulic characteristics and design optimization under forced convection conditions", A. Kumar, J.B. Joshi, A.K. Nayak, P.K. Vijayan, **Int. J. Heat Mass Transfer, 2016**, 93., 1227-1247.
5. "A comparison of thermal-hydraulic performance of various fin patterns using 3D CFD simulations", A. Kumar, J.B. Joshi, A.K. Nayak, **Int. J. Heat Mass Transfer, 2017,** 109., 336-356.

Conferences

1. "3D numerical simulations to investigate the thermal-hydraulic performance of the A-type air cooled condenser (ACC)", A. Kumar, J.B. Joshi, A.K. Nayak, P.K. Vijayan, Fluid Mechanics Fluid Power Conference 2014.
2. "Thermal-hydraulic performance of the Air Cooled Condensers", A. Kumar, J.B. Joshi, A.K. Nayak, P.K. Vijayan, Int. Workshop on New Horizons in Nuc. Reac. Th. Hydraulics and Safety 2013.
3. "3D CFD simulation of natural convection over a circular cylinder in a cuboidal box. Int. Workshop on New Horizons in Nuc. Reac. Th. Hydraulics and Safety 2013", A. Kumar, J.B. Joshi, A.K. Nayak, P.K. Vijayan 2013.

ACKNOWLEDGEMENTS

First of all I would like to express my gratitude to my guide Dr. A.K. Nayak for his encouragement and support during my thesis work. He has always given critical and constructive comments, which helped in improving the quality of the thesis. He has always asked me to focus on the applicability of my work for real use.

My deepest gratitude goes to my Co-Guide Prof. J.B. Joshi for his motivation and encouragement to do innovation and make my work useful for the society. Beside a good scientist, he is one of the best teacher I have had in my life. He always supports new ideas and try to transform them to applicable work. I am highly thankful to him for the confidence he showed in me and giving me complete freedom to carry out my research work. Which has made me strong and confident to take up any task and executing it successfully. Apart from the research, he has taught me to stay positive in any circumstances and work positively towards the welfare of the society.

Beside my advisors, I am thankful to my doctoral committee members, Dr. P.K. Vijayan, Prof. J.C. Mandal and Dr. K. Velusamy for providing useful and critical comments, which helped in making a good roadmap for the Ph.D. Apart from being a committee member, Dr. K. Velusamy has given me good ideas and encouragement during our interactions. He provided a good support during my IGCAR visit and I am very thankful to him.

My special thanks to Mayur Gandhi, who taught me Openfoam and have always been a phone call away whenever I had any problem with my Ph.D. work.

When it comes to friends, I wish to thanks Joyeeta Sinha for her continuous support since my masters. She has always been my biggest strength, who has always shown confidence in me and supported me with all my ideas. Also, she has a habit of making good notes in the class, which allowed me to skip all the writing work during our masters classes :P, so a special thanks to her for that also.

Parul Goel has also given a good support during my Ph.D. She loves cooking and provided me with a good food support haha :P. Apart from this, I had a good time with

her during many trips we had and also while exploring many new restaurants. She has been supportive in all matters of my life, may be emotional or related to my work. Shuchi Vaishnav is also one my close friends, she can make anyone smile with her funny sense of humor. She is one of those people, whom I can trust with my secrets and emotional matters. I would like to thank Bharti Kansal for her support and encouragement. She has been a good friend and due to her I visited many new places.

My special thanks to Priya (Priyasmita) for her encouragement and motivation for last 7-8 years. She is one of my best friends, she gave me ideas and motivated me to do hard work, also she scolded me sometimes for not being sincere during my masters. I am grateful to have her as my friend.

Moving on to a big friends list, I am happy to share me gratitude to Nitin, Eshita and Vishal. Nitin is a calm person and a good roommate. He can be found in two states inside the room, sleeping or studying. He is very hardworking and sincere towards his work, specially TURBULENCE :P. Eshita has been a good teacher of softwares for me and for all the people in group. She learned many new things and passed it to me also, I am thankful to her for that. Vishal was the first teacher I had here in HBNI, although it lasted only for two chapters, but in those two chapters we learned how to skip homework and numericals. :P He has been a good friend to me with similar sense of humor and IQ in jokes. Annii aka Anita has also been a good friend, she has a similar obsession for cats as do I have. She is quite strong and can give me a good competition in boxing :P. Sunil is the fastest bowler I have ever met, he is so fast that normally he runs faster than his ball. He is very hard working and spend most of his time working at office and after that working at home on skype. Nitendra is known for his contacts around the world, he spends most of his time and money in travelling. He is a good finisher when it comes to food because of his infinite capacity. Archana is similar to Sunil when it comes to hard work and tension related to work, she can eat the whole cake by herself. Ruchi is a rebellious one, unlike our cases, her guide is scared of her. She has a temptation towards nonveg food in other’s plates specially Eshita’s plate.

I would like to thank Ram for encouraging me towards body building and fitness though he himself do yoga only while sleeping. He is one of the most soft spoken and well-mannered guy I have ever met.

I would like to thank Yogesh, Swapnil, Varsha and Zoheb for their support with trips and timepass talks in ICT. Being part of the same CFD group we hardly talked about it, which has been the best part.

Preeti and Shweta are two friends who have been with me since my graduation. I share a very special emotional bond with them. Shweta is a little sweet girl with a lot of ambitions. She is one of the most intelligent friends I have ever knows. She is very hardworking and a good teacher. I always had a very special place for her in my life. On the contrary, Preeti is a tall sweet girl :P. She is a good teacher too and takes her profession very seriously. She has been a good emotional support in all these years.

Also I would like to thank my friend Mohit Goyal, He is one friend with whom I meet one or two times a year, but it feels the same as if we are meeting daily.

Lastly, I would like to thank my family, specially my mother. She has taught me to do hardwork and stay positive in any circumstances. Also, a cute addition to my family is Kittu, though she is a kitten, but she is the one who always keeps my energy high and positive. I can never get negative when she is around.

CONTENTS

LIST OF FIGURES

LIST OF TABLES

Homi Bhabha National Institute

SYNOPSIS

1. **Name of the Student:** Ankur Kumar
2. **Name of the Constituent Institution:** Homi Bhabha National Institute
3. **Enrollment No.:** ENGG01201104019
4. **Title of the Thesis:** Computational analysis of air cooled condenser and selection of optimal design parameters
5. **Board of Studies:** Engineering Science

Conventional power plants use river water or sea water as the ultimate heat sink. The steam coming from the turbine is condensed using the water coming from the cooling towers and then the water is recirculated back to the cooling towers (for the case: river as ultimate heat sink). However, for this type of cooling, approximately 2.44 litres of water is needed per kWh of energy produced. Therefore, in the regions, where water is scarce, the use of air cooled condenser is very useful. Also, in the case of station blackout in a nuclear reactor, passive air cooled condenser can be used to remove the decay heat. The performance of the air-cooled heat exchangers depends upon many geometrical parameters, like tube type, fin type, fin spacing, number of tube rows, tube pitch, etc. One of the major problems with the air cooling technology is the low heat transfer coefficient provided by air, which results in a large heat transfer area of the condenser, and therefore, a high associated capital cost as compared to the water cooled condensers. The total cost associated with the A-type air-cooled condensers (Fig. 1) includes the capital cost, operating cost, and the cost of the space used, and hence, the design must be optimized to obtain an efficient and economic air cooled condenser.

Based on the literature survey, it is now known that there exists many unresolved issues for the design of air cooled condenser. Briefly, they are:

1. Design of passive air cooled condenser require 3D natural convection simulation due to complex geometry of air cooled condenser having a large number of fins on the tubes, spacing between fins and tubes, and large chimneys. Currently natural convection with air as cooling medium has been mostly limited to closed cavities and have been studied using 2D numerical simulations only. In few experimental studies, it was observed that the flow becomes 3D, complex and unstable. Therefore, it is important to perform 3D numerical simulations and hence establishing the 3D CFD model (laminar and turbulent) for closed cavities as well as for air cooled heat exchangers.

2. As stated above, the passive Air Cooled Heat Exchangers have large chimneys to induce buoyancy to remove heat. There are almost no studies for air flow around heat exchangers in chimney in the past.

3. Despite the advancement in the computational methodology, the design of the Air Cooled Condensers have been based mainly on empirical approach [Kumar et al. (2015)]. Therefore, it is important to understand the flow patterns and its relationship with the thermal-hydraulic performance of the Air Cooled Condenser.

4. Various types of fins have been used in the industry in the design of conventional Air Cooled Heat Exchangers. Optimization of the fin design for efficient heat removal has rarely been done in the past. Only few designs of them have been investigated by using 3D numerical simulations.

Therefore, the main objective of this thesis is to develop procedures for the design the Air Cooled Steam Condenser (Fig. 1) for application in classical fossil fuel thermal power plants as well as in nuclear reactors for efficient decay heat removal in case of station black out, which includes:

1. To establish the CFD model for simulation of natural convection in cavities and Air Cooled Heat Exchangers under laminar and turbulent flow conditions.
2. To understand the multi-dimensional convection around finned-tubes of Air Cooled Heat Exchangers under natural convection conditions in a chimney.
3. To analyze systematically the various types of fins and a comparison of their thermal-hydraulic performance.
4. Optimization of the geometry of the heat exchangers (effect of various geometrical parameters like, fin spacing, fin height, tube pitch, chimney height, tube surface temperature, and tube geometry) on the thermal-hydraulic performance of a forced draft air cooled condenser using 3D numerical simulations.

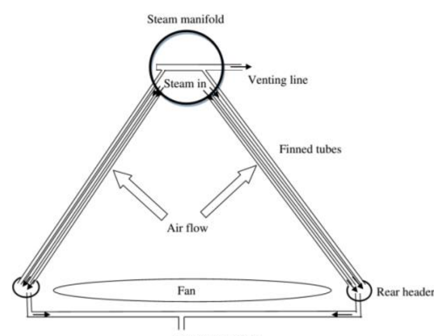

Figure 1: A schematic of forced draft air cooled condenser.

The first objective was achieved by comparing the numerical results with the previous experimental results under forced convection and natural convection conditions. For natural convection around bare tubes, the results were compared with the correlation of Churchill and Chu (1975) and Morgan(1975). SST k-omega and laminar model were used for the simulations. The geometry consisted of a bare circular cylinder (D = 76 mm) kept in a cavity of dimensions 1200 ×

600 × 1000 mm (Fig. 2A). Both the SST k-omega and laminar models perform equally well, however, due to low Rayleigh number ($Ra < 10^6$), laminar model was used and the results are shown in Fig. 3A. A good agreement between the numerical and correlations can be observed in Fig. 3. Further, the CFD predictions were compared with the results of Cesini et al. (1999) and Newport et al. (2001) [kumar et al. (2014)]. Under forced convection conditions, the CFD predictions were compared with the experimental results of Pongsoi et al. (2013) for a two row air cooled heat exchanger (D = 16.85 mm, h_f = 8.97 mm, S = 3.2 mm) (Fig. 2B). The Reynolds number ranged from 3000 to 6000, therefore, standard k- ε model was used for the numerical simulations. The results for heat transfer coefficient are shown in Fig. 3B. The CFD results deviated from the experimental results by 5-15%, which can be considered as reasonable agreement. Therefore, standard k- ε turbulent model has been used to carry out the numerical simulation in the present work.

Table 1: Comparison of various turbulence models with the experimental results of Pongsoi et al. (2013)

U_{fr} (m/s)	**Experimental [h (W/m^{2}K)]**	**RNG k- ε model [h (W/m^{2}K)]**	**SST k-omega [h (W/m^{2}K)]**	**Standard k- ε model [h (W/m^{2}K)]**	**Laminar [h (W/m^{2}K)]**	**Launder Sharma k- ε model [h (W/m^{2}K)]**
2.45	46.44	51.54	52.45	54.32	63.50	54.52
4.76	68.22	78.76	77.53	79.75	86.76	79.54
6.32	80.07	88.45	89.96	91.80	95.60	89.21

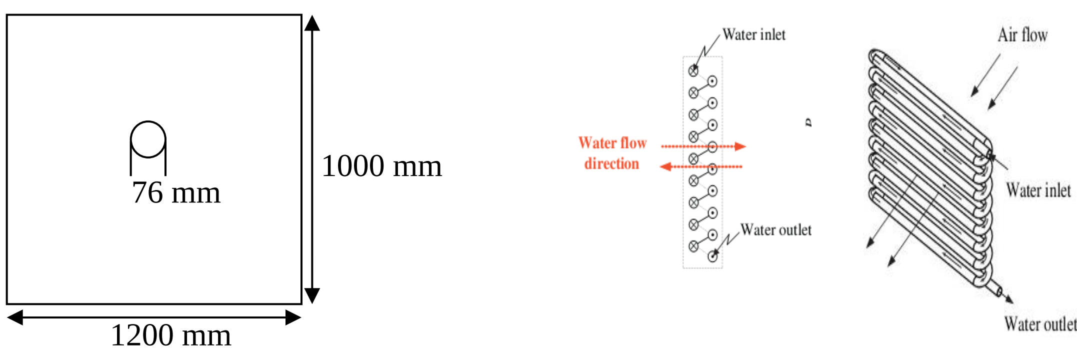

(A) (B)

Fig. 2: Geometries for the validation of the code

Also, a comparison of various turbulence models [standard k- ε (used presently), SST k-omega, Re-normalization group (RNG) k- ε, laminar and Launder Sharma k- ε] was carried out under forced convection conditions. Based on the results, Re-normalization group (RNG) k- ε, SST k-omega and standard k- ε were found to be better [Kumar et al. (2016b)]. Therefore, in some studies RNG k- ε model has been used. The results are shown in Table 1.

The current understanding of natural convection flow has been limited to 2D numerical simulations in closed cavities, which has been found to be inadequate as observed by many experiments performed by previous researchers. Therefore, to start with, it was important to

1975)

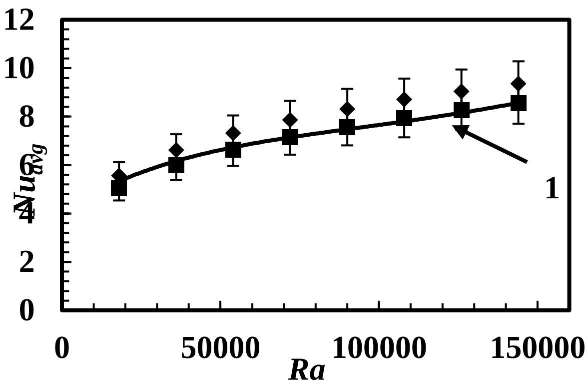

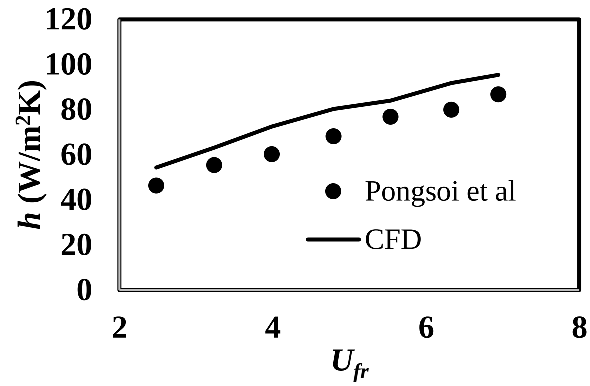

Fig. 3: Validation of the code (A) natural convection, (B) forced draft Air Cooled Heat Exchanger

understand the multidimensional natural convection of air around bare tubes and also to establish the validity of OpenFoam code for natural convection, which fulfils our first objective. Also, this provided us the confidence of performing 3D numerical simulations for commercial Air Cooled Condenser. In the first case, a small cavity was chosen with dimensions of 57 × 30 × 420 mm with a cylinder of 14 mm diameter, in the second case the cavity dimensions were 470 × 470 × 300 mm with cylinder of 20 mm diameter kept at the center, and in the third case the cavity dimensions were 1000 × 1200 × 600 mm with a cylinder of 76 mm diameter kept close to the top wall. A constant temperature boundary condition was applied at the cylinder for all the cases with a combination of adiabatic and isothermal enclosure walls. The corresponding range of *Ra* varied from 1.3×10^3 - 1×10^6 for various cases and hence laminar model was used. From all the simulations performed, it was observed that the flow becomes 3D, oscillating, and complex whenever there is an interaction between the cylinder and the enclosure walls. For example in the first case the distance between the inner cylinder and cavity walls was small due to smaller size of cavity and this resulted in 3D complex flow due to cavity wall interaction (see Fig. 4), in the second case, the distance between the wall and cylinder was larger and resulted in 2D stable flow, and in the third case, the flow became unstable as the clearance of cylinder from top was

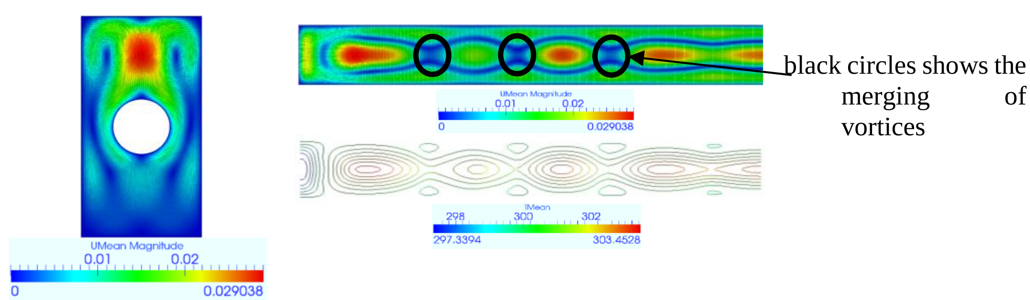

Fig. 4: Flow patterns showing 3D unstable flow in a cavity at Ra = 1300

decreased. The transient behavior of the natural convection flow and its startup from the rest was also studied. It was emphasized that 3D numerical simulations must be performed to capture the 3D flow phenomenon in natural convection especially in the presence of cylinder-cavity interaction. This work has been published in Kumar et al. (2014).

After studying the natural convection in closed cavities, an attempt was made to understand the natural convection flow around finned tube heat exchanger kept under a chimney, which addresses the second unresolved issue and objective. 3D numerical simulations were performed and the effect of tube shape and size, fin spacing, fin height, chimney height, and tube surface temperature were studies on the heat transfer and driving force. At the inlet, a zero fixed velocity was given as the boundary condition, and at the finned-tube, a constant temperature boundary condition (310 K-365 K) was provided. The flow was generated in the chimney by buoyancy force alone (Fig. 5A). The flow development with time (Fig. 5B) showed that the heat transfer coefficient decreases for $t < 7$ s, and then increases again and attains steady state at about 60 s. It was observed that the heat transfer coefficient is maximum for optimized fin spacing (Fig. 6). The phenomena of merging of thermal boundary layers at low fin spacing and bypass flow at higher fin spacing was explained in detail. The rate of increase in the heat transfer coefficient decreases as the fin diameter increases. The heat transfer coefficient increases with an increase in the chimney height (due to increase in the driving force) and tube surface temperature. It was also shown that attaching fins lead to an increase in the overall heat transfer for tubes, however, the heat transfer coefficient deteriorates for finned tubes as compared to the bare tubes. These findings are published in Kumar et al. (2016a).

To reduce the empiricism in the design of air cooled condensers, we have made an attempt to understand the relationship between the flow pattern and the rate of heat transfer. This understanding is expected to evolve a rational and reliable procedure for the optimum design of an air cooled condenser under forced convection conditions using 3D numerical simulations. A typical A type air cooled condenser (shown in Fig. 1) has been considered for the analysis. Standard k- ε model was used for the simulations.

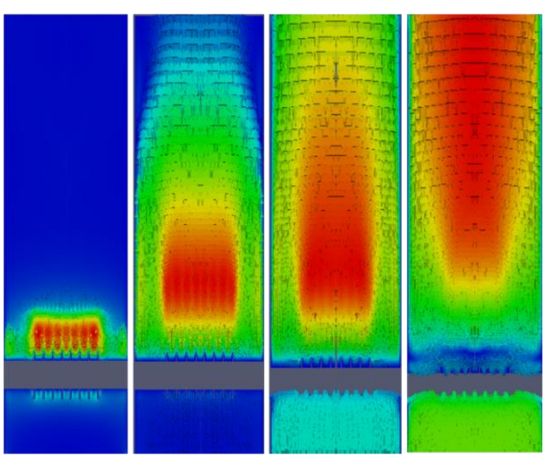

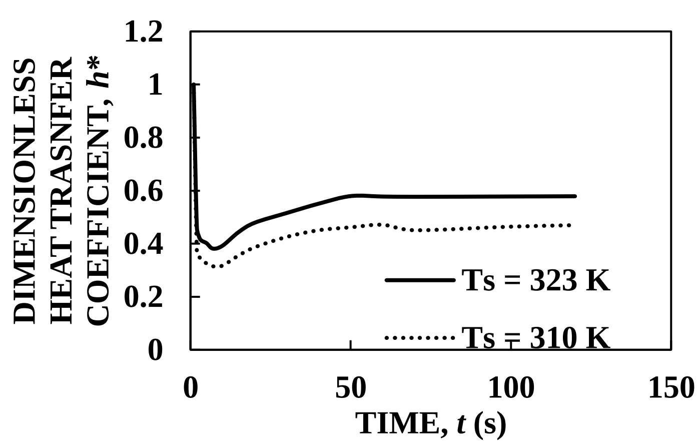

(B)

1 s 5 s 10 s 80 s

(A)

Fig. 5: Flow development with time in the chimney

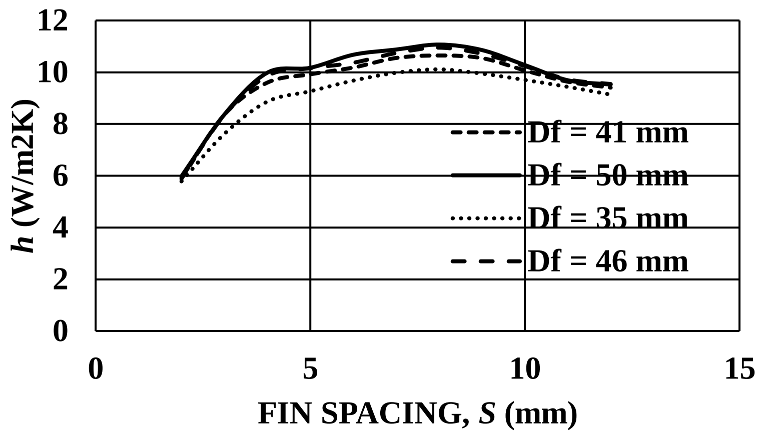

Fig. 6: Effect of fin spacing on the heat transfer coefficient

The effect of tube shape (elliptical and round), tube diameter [7-24 mm (circular), 30 ×10-30 × 20 mm (elliptical)], fin spacing (2-10 mm),number of rows (2-10), fin height (5-10 mm), air frontal velocity (4.76 – 6.32 m/s), transverse tube pitch (36.8 – 44 mm) on the thermal-hydraulic performance has been studied. The tube temperature was set at 323 K (steam temperature in TPPs). It was observed that, with an increase in the fin spacing, the heat transfer coefficient increases (by 35-40%) at a constant inlet velocity and the pressure drop decreases (by 60-80%). The frontal area requirement increased by 100-150% with an increase in the fin spacing for the same heat removal capacity. As the number of rows was increased, the heat transfer coefficient increased initially for $N_r < 4$ by 7-8%, and for $N_r > 4$, the heat transfer coefficient decreased by 23%. This was due to the increase in the wake region behind the tubes at larger number of tube rows (Fig. 7). An increase in the tube pitch increased the heat transfer coefficient per unit pressure drop by 40%. The fin efficiency was found to decrease with an increase in the Reynolds number, fin spacing and number of tube rows. Further, the optimization of the design was performed by Taguchi method. It has been observed that the number of tube rows must be kept between 2-4, fin spacing 3-5 mm, tube pitch around 40 mm, and fin height 5 mm for better performance of the condenser. This work has been published in Kumar et al. (2016b). To compare with the empirical results, the Nusselt number obtained from CFD and other empirical correlations is shown in Fig. 8.

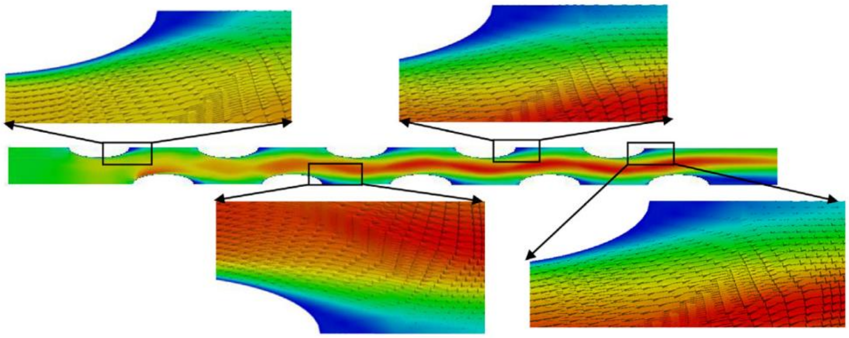

Fig. 7: Velocity vectors showing wake region behind the tubes.

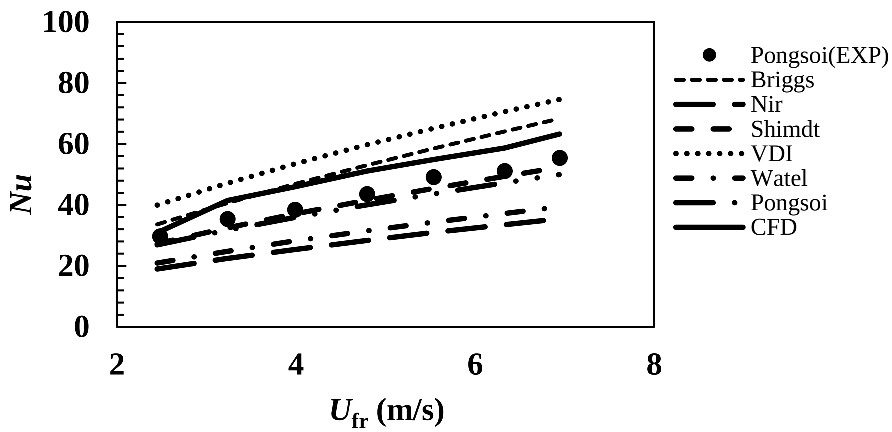

Fig. 8: Comparison of numerical results with empirical models and experiment by Pongsoi et al. (2013).

In an extension to the optimization of the air cooled condenser, numerical studies were carried out to compare the thermal-hydraulic performance of various fins (plain annular fin, crimped spiral fin, serrated fin, plain plate fin, and wavy fin) (Fig. 9). The geometrical parameters are, tube outer diameter (OD) = 7 mm, fin spacing (S) = 3-7 mm, fin height (h_f) = 5 mm, number of tube rows (N_r) = 2, transverse tube pitch (P_t) = 23 mm and longitudinal tube pitch (P_l) = 18 mm. The air frontal velocity has been varied from 4.76 m /s to 6.32 m/s. It is observed that, with an increase in the fin spacing, the heat transfer coefficient increases (by 35-40%) at a constant inlet velocity and the pressure drop decreases(by 60-80%) for all the fin types. It has been observed that the serrated fins provides the highest heat transfer per unit pumping power. This is due the 3D vortices and turbulence generation by the segments of the fin. A detailed analysis has been carried out to see the development of thermal boundary layer, generation of vortices and turbulence for all the fins. 3D flow patterns around serrated fins and crimped fins are shown in Fig. 10.

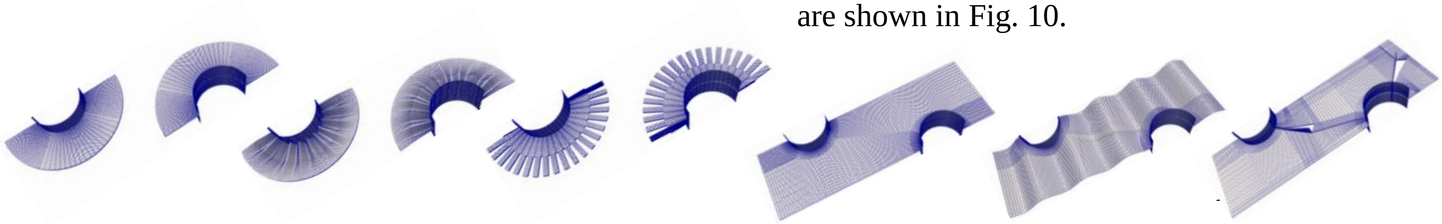

A B C xx D E F

Fig. 9: Fins considered (A) plain annular, (B) crimped fins (C) serrated fins (D) plate fins (E) wavy fins

It can be observed that the flow penetrates into the segments of serrated fin, and similarly crimped fin disturbs the flow and inner circulations can also be observed. In both the cases the mixing and heat transfer improve as compared to the plain fins (Fig. 11).

de view side view side view

B B

Fig. 10: 3D flow patterns (A) serrated fins, (B) crimped fins

The main conclusions of the thesis were:

1. The natural convection of air around bare tubes can become 3D, unstable and complex in the presence of wall-cylinder interaction (Fig. 4), which affects the heat transfer. Therefore, 3D numerical simulations are important to perform in such cases.

2. A comparison of various turbulence models [standard k- ε (used presently), SST k-omega, Re-normalization group (RNG) k- ε, laminar and Launder Sharma k- ε] revealed that standard k- ε (used presently), SST k-omega, Re-normalization group (RNG) k- ε performed better than other models. However, SST k-omega and Re-normalization group (RNG) k- ε requires a finer meshing as compared to standard k- ε model.

3. It was observed that natural convection around finned-tubes in chimney is multidimensional in nature. The flow initiation and its development with time (Fig. 5) are important in order to understand the flow physics and related heat transfer. The heat transfer coefficient is highest of an optimum fin spacing, and increases with an increase in the chimney height, fin diameter and tube surface temperature.

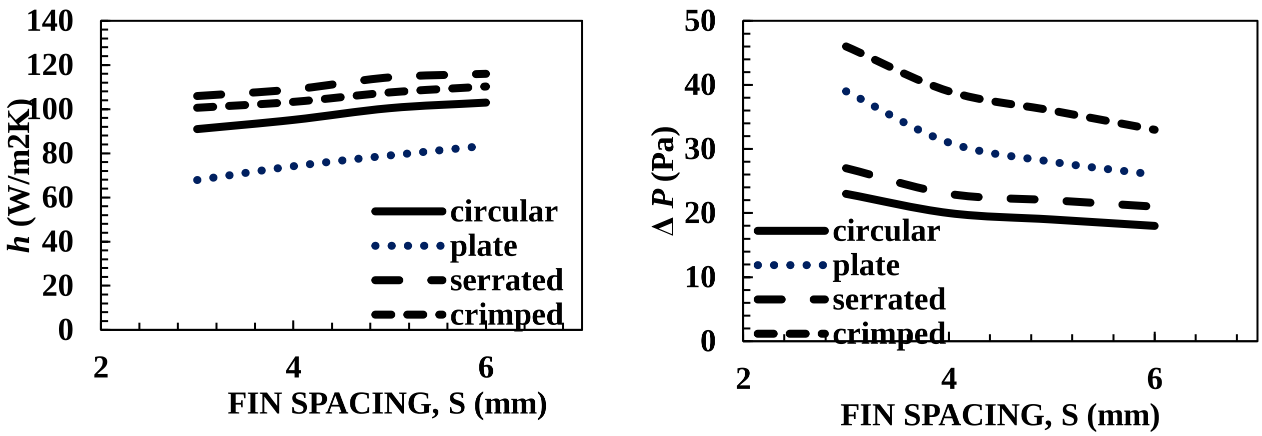

Fig. 11: Thermal-hydraulic performance of various fins (A) heat transfer coefficient, (B) pressure drop

4. An optimization of the design has been performed using Taguchi method. It has been recommended that the tube rows need to be kept between 2-4, dimensionless fin spacing 0.6-1, dimensionless tube pitch around 4, and dimensionless fin height 1 for better performance of the condenser. (Parameters are made dimensionless w.r.t. tube semi-minor axis)

5. Some of the fins (serrated, crimped spiral and wavy) promotes turbulence, generates 3D vortices in the flow (Fig. 9), which results in larger heat transfer coefficient as compared to plain fins. However, the associated pumping power also increases.

The Recommendation for future work can be given as:

1. The finned-tube design parameters are important for the performance of the Air Cooled Condenser and therefore must be optimized. In the present work, the optimization has been performed for the plain annular finned-tube. However, it can be performed for other fins also in the future.

2. The natural convection studies can be extended to big chimney and larger size of the condenser. However, it takes large computational time and a lot of efforts in the modeling part. Therefore, it is recommended to find a efficient way of performing numerical simulations for larger heat removal capacity. The use of periodic boundary condition is one of the possible ways.

Chapter 1
Introduction

1.1. Importance

In power plants (nuclear or thermal) water is converted into steam by using heat from nuclear fission or from burning of coal and then the steam is used to drive the electric generator using turbines. After passing through the turbines, steam is condensed using condensers. Conventionally, water is used on the tube side of the condensers to condense the steam. A typical condenser is shown in Fig. 1.1.

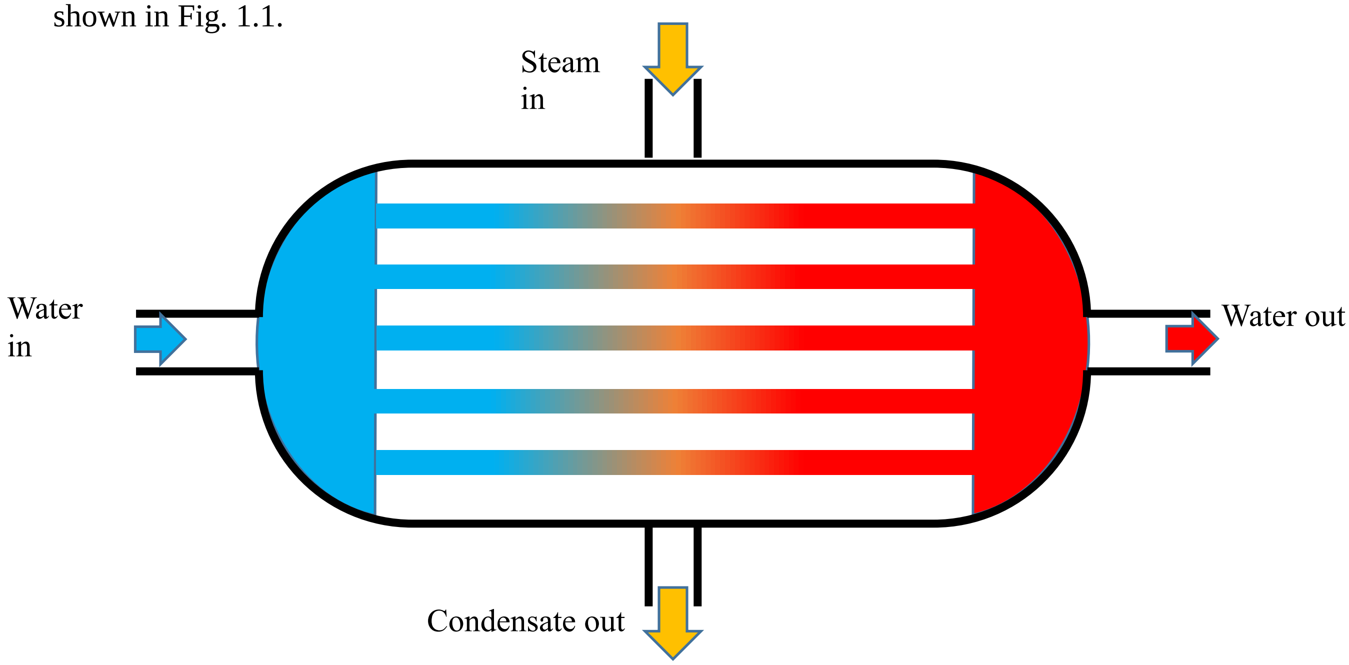

Fig. 1.1. Schematic representation of water cooled condenser.

Typical power plants have an efficiency of 30-40% and if we consider a 500 MWe power plant, then around 30000 m^3 of water is evaporated per day in the cooling towers. Also, the water reservoirs are very rare at some places, e.g. some part of western India, north China, therefore, the power plants having water as the ultimate heat sink cannot be located at these locations. The air cooled condenser can become a better alternative to solve this water scarcity problem. The current design of air cooled condensers are A Frame type condensers (Fig. 1.2). This technology was started by GEA in Essen, Germany in 1939. Nowadays there are lots of power plants around the world employed with this kind of condensers. It is a forced convection type condensers, air blows using a large fan on the base of the condenser, and steam is condensed inside the inclined finned tubes above it. The biggest plant operating with this kind of condenser is Kendal Power station in South Africa containing six units of 686 MW.

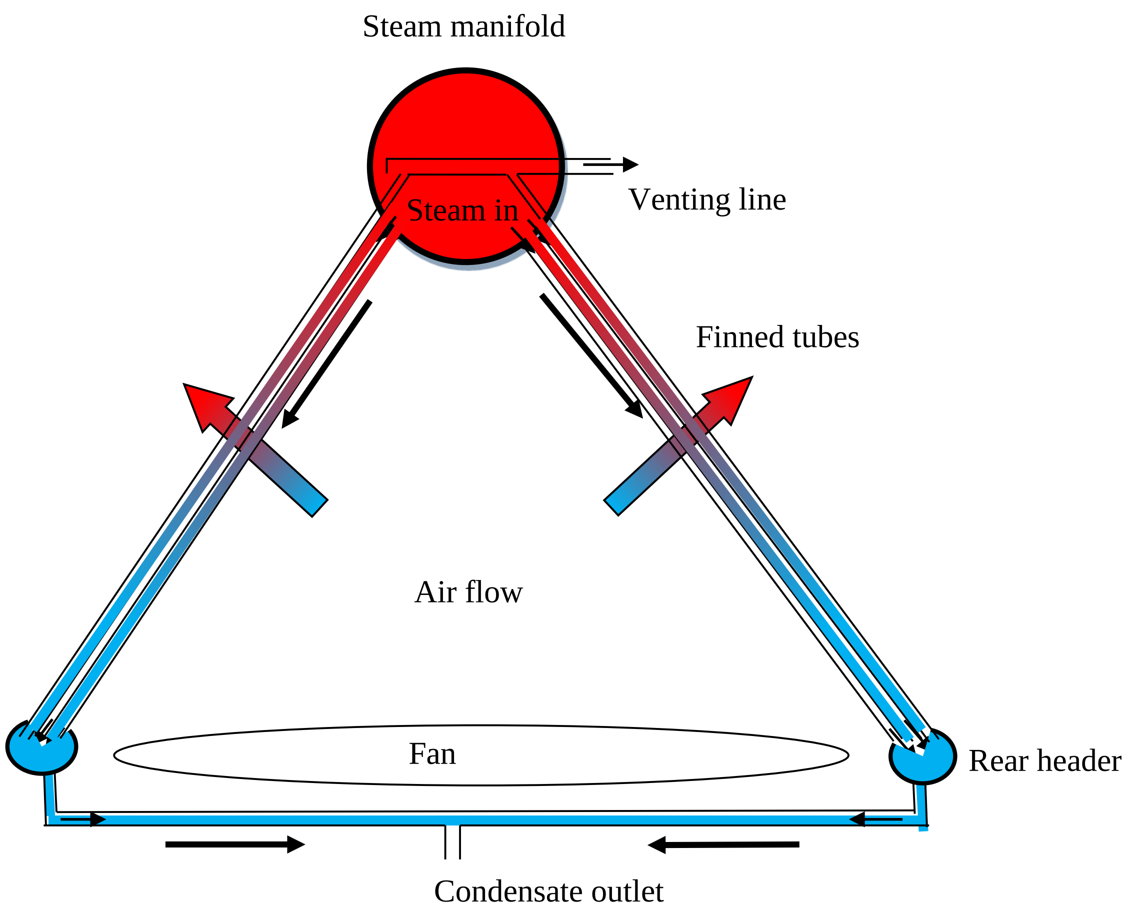

Fig. 1.2. Schematic representation of A type air cooled condenser

Air cooled heat exchanger or condenser is a finned tube type heat exchanger. Due to low thermal conductivity of air, fins are used to enhance the heat transfer area on the air side and therefore increasing the heat transfer rate. The large heat transfer area requirement makes the capital cost of air cooled condensers larger than the water cooled condensers. Also, forced draft air cooled condensers have limitation during station black out, in which case no power is available for the blowers. To avoid such circumstances, these air cooled condenser units can be placed with chimneys to obtain a natural draft of air for condensing the steam. Currently, no passive air cooled condenser is in operation.

In the present work, the optimization of the design of air cooled condenser under forced convection conditions has been performed. Also, natural convection around passive air cooled condenser has been studied.

1.2. Motivation

The motivation behind present work is to make the design of air cooled condenser economical and efficient so that it can be put in power plants to cut the water consumption as much as possible. Also, in the areas where water is scarce, it is very difficult to operate power plants, therefore, air cooled condensers are good alternatives for water requirement. Further, in the present work, passive air cooled condensers have also been investigated, which is important in station blackout conditions. Various researchers have performed studies on the thermal-hydraulic characteristics of air cooled heat exchangers, however by going through an extensive literature survey (chapter 2), the unresolved issues can be stated as:

1. Design of passive air cooled condenser require 3D natural convection simulation due to complex geometry of air cooled condenser having a large number of fins on the tubes, spacing between fins and tubes, and large chimneys. Currently natural convection with air as cooling medium has been mostly limited to closed cavities and have been studied using 2D numerical simulations only. In few experimental studies, it was observed that the flow becomes 3D, complex and unstable.

Therefore, it is important to perform 3D numerical simulations and hence establishing the 3D CFD model (laminar and turbulent) for closed cavities as well as for air cooled heat exchangers.

2. As said before, the passive Air Cooled Heat Exchangers have large chimneys to induce buoyancy to remove heat. There are almost no studies for air flow around heat exchangers in chimney in the past.

3. Despite the advancement in the computational methodology, the design of the Air Cooled Condensers have been based mainly on empirical approach (Chapter 2). Therefore, it is important to understand the flow patterns and its relationship with the thermal-hydraulic performance of the Air-Cooled Condenser.

4. Various types of fins have been used in the industry in the design of conventional Air Cooled Heat Exchangers. Optimization of the fin design for efficient heat removal have never been done in the past. Only few designs of them have been investigated by using 3D numerical simulations.

1.3. Objectives

The main objective of this thesis is to design the Air Cooled Steam Condenser (Fig. 1.2) for application to future Nuclear Reactors for efficient decay heat removal in case of station black out, which includes:

1. To establish the CFD turbulent model for simulation of natural convection in cavities and Air Cooled Heat Exchangers under laminar and turbulent flow conditions.

2. To understand the multi-dimensional convection around finned-tubes of Air Cooled Heat Exchangers under natural convection conditions in a chimney.

3. To investigate various type of fins and a comparison of their thermal-hydraulic performance.

4. Optimization of the geometry of the heat exchangers (effect of various geometrical parameters like, fin spacing, fin height, tube pitch, chimney height, tube surface temperature, and tube geometry) on the thermal-hydraulic performance of a forced draft air cooled condenser using 3D numerical simulations.

The above objectives are based on the unresolved issues found in the literature.

1.4. Outline of the thesis

Present work has been divided into 8 chapters, which includes:

Chapter 1 is the introduction including importance, motivation and objectives of the present work.

Chapter 2 is the detailed literature survey, which is further divided in three parts. First part describes the literature in the area of natural convection around bare cylinders in cavities. Second part describes the literature related to the natural convection around finned-tubes. The third part is about the previous published work in the area of forced convection air cooled heat exchangers.

Chapter 3 is an introduction to the computational fluid dynamics. It explains the numerical methodology used in the present work including all the turbulence models used, governing equations, discretization schemes and solution algorithm used.

Chapter 4 describes the 3D CFD simulation of natural convection around bare circular cylinder in various sizes of cavities.

Chapter 5 includes the 3 CFD simulations performed to study the natural convection of air around finned-tubes kept in a chimney.

Chapter 6 represents 3D numerical simulations on the comparison of thermal-hydraulic performance of five types of fins (plain circular, crimped, serrated, plate fin and wavy fin).

Chapter 7 represents optimization of an air cooled condenser using 3D CFD simulations and Taguchi method.

Chapter 8 is the conclusion of the thesis and recommendation for future work.

Chapter 2
Literature survey

2.1. Introduction

The air cooling technology is used in a variety of applications, for example automobile industry, power plants, computer systems, air conditioners etc. In the power plants, the air cooling is used in the air cooled condensers, and dry and wet cooling towers. The A-type air-cooled condensers (Fig. 2.1) are used to condense the exhaust steam from the turbine, whereas the dry and wet cooling towers are used to remove the heat from the secondary water loop by forced or natural draft of air. For wet cooling towers, approximately 2.11 litres of water are needed per kWh of energy produced. Due to heavy demand of water in cooling towers, substantial amount of research work has been published in the past 50 years. The performance of the air-cooled heat exchangers depends upon many geometrical parameters, like fin type, fin spacing, number of tube rows, tube pitch, etc. The ambient parameters like wind, humidity, etc. are also important in determining the efficiency of the air-cooled heat exchangers. One of the major problems with the air cooling technology is the low heat transfer coefficient provided by air, which results in a large heat transfer area of the heat exchanger and therefore, a high associated capital cost as compared to the water cooled heat exchanger. The total cost associated with the A-type air-cooled condensers includes the capital cost, operating cost, and the cost of the space used, and these three parameters must be optimized to obtain an economical air cooled condenser. Continuous efforts have been going on to improve the performance and the efficiency of the air-cooled heat exchangers, still, there is a lot of scope to make the air cooling technology more economical and efficient.

In the case of a station black out (e.g., Fukushima nuclear accident), the use of forced draft air cooled condenser can cause various safety concerns (e.g., core melt). Therefore, the use of a natural air-cooled condenser should also be considered in the power plants and we should design and optimize the air cooled condenser with large chimneys to induce natural draft of air.

The literature survey has been divided mainly into three categories:

(1) Natural convection in cavities.

(2) Natural draft around finned-tube heat exchangers.

(3) Forced convection air cooled heat exchangers and condensers.

The abovementioned three categories of literature will be explained in detail in next sections.

2.2. Natural convection in cavities

Churchill and Chou (1975) have analyzed the experimental data on natural convection over a horizontal cylinder of various researchers and proposed the following correlations,

$$Nu = \left[0.60 + \frac{0.387.Ra^{\left(\frac{1}{6}\right)}}{\left[1+\left(\frac{0.559}{Pr}\right)^{\frac{9}{16}}\right]^{8/27}}\right]^2 \qquad 10^{-6} < Ra < 10^{9} \qquad \ldots (2.1)$$

In a similar manner Morgan (1975) proposed the following correlations,

$$Nu = 0.48.Ra^{0.25} \qquad 10^{4} < Ra < 10^{7}. \qquad \ldots (2.2)$$

Ghaddar (1992) performed numerical simulations to study the natural convection over a circular cylinder (63 mm *OD*) in a rectangular cavity with varying Rayleigh number. It was found that the plume developing from the hot cylinder reaches a maximum velocity at some height from the cylinder and then attains second local maxima near the top wall. Koizumi and Hosokawa (1996) performed experiments to determine the effect of adiabatic and conducting ceiling on the natural convection heat transfer from a horizontal cylinder for a Rayleigh number range from 4.8

$\times 10^4$ to 1.0×10^7. A 3D unsteady flow was observed for H^*/D =0.2 and as the H^*/D ratio was increased to 0.4, the flow became stable and 2D. Cesini et al., (1999) performed 2D numerical simulations and experiments to study the natural convection over a circular cylinder in a cavity for a range of Rayleigh number from 1.3×10^3 to 7.5×10^4. A non-stationary oscillating solution was encountered for $Ra = 10^5$. Shu et al., (2002) studied the natural convection inside an annulus with circular inner cylinder and square outer cylinder using the differential quadrature method for a fixed Rayleigh number of 10^5. Newport et al., (2001) studied the thermal interaction between an isothermal cylinder and isothermal cubical enclosure for a range of Rayleigh number from 6800 to 21800. Harrez et al., (2002) performed experiments using holographic interferometry to study the temperature field and the Nusselt number for the natural convection over circular heated cylinders (10 and 30 mm *OD*). Atmane et al., (2003) experimentally investigated the effect of vertical confinement on the heat transfer from a horizontal cylinder in a water tank of dimensions 700 mm × 600 mm × 300 mm. The transition to the unstable flow was found to be dependent on the distance between the free surface and the cylinder. Misumi et al., (2003) performed experiments to understand the transition to turbulent flow and local heat transfer characteristics of natural convection. It was shown that the transition to turbulent flow occurred following the flow separation at the trailing edge of the cylinder at a Rayleigh number of 3.5×10^9. Ding et al. (2005) applied the multiquadric-based differential quadrature (MQ-DQ) method to study the natural convection of annuli with inner circular cylinder and square outer cylinder with aspect ratio varying from 1.67 to 5 for a range of Rayleigh number from 10^4 to 10^6. Kim et al., (2008) carried out 2D numerical simulations to study the effect of the location of the cylinder on the flow field and heat transfer in square cavity (AR = 2.5) within a range of Rayleigh number from 10^3 to 10^6. The formation of secondary and tertiary cells was observed at higher Rayleigh number, which had a significant effect on the heat transfer. Ganguly et al., (2009) performed numerical simulations to study the heat transfer from natural convection in a 2D differentially heated vertical enclosure ($4 \leq H/L \leq 200$) for a range of $5.99 \times 10^2 \leq Ra \leq 3.15 \times 10^5$. Yu et al., (2011) performed 2D numerical simulations to study the unsteady natural convection over an isothermal circular cylinder inside an isothermal triangular enclosure for an aspect ratio (R_{out}/R_{cyl}) range of 3-5 and the Rayleigh number was varied from 10^3 to 10^7. The effect of the orientation of the enclosure was also studied. Lee et al., (2010) carried out 2D numerical simulations for a hot circular cylinder and a cold outer square and the position of the cylinder was changed horizontally and diagonally and the range of Rayleigh number was varied from 10^3 to 10^6. It was found that, at high Rayleigh number, the Nusselt number of the outer enclosure becomes independent of the cylinder movement, showing that the convection heat transfer dominates at high Rayleigh number. Hussain and Hussein (2010) performed 2D numerical simulations to study the effect of the vertical location of circular cylinder enclosed in a square enclosure for an aspect ratio of 5 and a Rayleigh number range from 10^3 to 10^6. The vertical upward and downward displacement of the cylinder resulted in more heat transfer and the secondary cells at the corners were observed. Ashjaee et al., (2012) performed experiments and numerical simulations to study the local and average Nusselt number of a heated cylinder kept over an adiabatic surface. As the cylinder was moved vertically upward, the heat transfer increased. Ganguly et al., (2012) performed experiments and numerical simulations to study the transient temperature variation in an insulated cooking device. A method was proposed for the optimization of the gap-width for the double-walled cylindrical vessel ($28 \leq H/L \leq 174$) for a range of $9.07 \times 10^2 \leq Ra \leq 2.61 \times 10^5$. Butler et al., (2013) performed experiments to study the heat transfer from a heated cylinder inside a cubical enclosure with a temperature difference between enclosure walls. The interaction between the cubical enclosure and the cylinder was studied. Ghasemi et al., (2012) performed 2D numerical simulations to investigate the natural convection of air inside an elliptical annulus for a range of Rayleigh number from 10^3 to 10^6. Zhang et al. (2013) performed numerical simulations to study the radiation and natural convection heat transfer by a circular cylinder inside a square enclosure for an aspect ratio of 5 and the Rayleigh number was varied from 10^3 to 10^6. The Nusselt number and the heat transfer decreased with an increase in the optical thickness. Patil et al., (2014) performed numerical simulations to study the effect of different parameters like average temperature of the pipe, non-uniformity in the temperature along the pipe surface, hour angle, denoting position of the sun in the sky and radius ratio on the heat loss from a non-evacuated solar collector. The heat loss was reduced by 10-25% by optimization of the different parameters.

Table 2.1. Summary of previous work on natural convection in a cavity (Experimental)

Sr. No.	Author and Year	Geometry		Source	Rayleigh number	Method of measurements	Results
		Diameter of the cylinder, *D* (mm)	Enclosure dimensions, $L \times W \times H$ (mm^3)				
1.	Koizumi and Hosokawa (1996)	25.4-152.4	1000 × 600 × 1200	Electrical	4.8×10^4 – 1.0×10^7	Heat flow Sensor	2D and 3D flow patterns were observed for different values of the *H/D* ratio.
2.	Cesini et al., (1999)	14	420 × 57 × 30 to 420 × 57 × 50	Hot fluid	1.3×10^3 – 3.4×10^3	Thermocouples	The fluid motion was found be a strong function of the cavity aspect ratio and Rayleigh number. The Nusselt number increased with the increase in Rayleigh number and decrease in the aspect ratio.
3.	Newport et al., (2001)	20	470 × 470 × 470	Electrical (310.2-350.2 K)	6.8×10^3 – 2.2×10^4	Mach-Zehnder interferometer and thermocouples	The experimental results showed some discrepancy with the numerical results at low Rayleigh number because of the slight misalignment between the circular cylinder and enclosure center. At high Rayleigh number, the 3D nature of the flow lead to some discrepancy between numerical results and experimental results in the vicinity of the ceiling.
4.	Harraez and Belda (2002)	10-30		Electrical (333-533K)	2.2×10^3 – 1.6×10^5	Thermocouples	The heat transfer coefficient and the Nusselt number was calculated with the help of temperature isotherms measurements.

5.	Misumi et al. (2003)	200-1200	2700 × 2000 × 2300	Electrical	$1.0 \times 10^8 \times 5.5 \times 10^{11}$	Thermocouples and smoke visualization	The laminar boundary layer, flow separation, transitional flow, and fully developed flow were shown with the varying range of Rayleigh number.
6.	Ashjaee et al. (2012)	8-22	3000 × 500 ×1500		$5 \times 10^2 – 1.5 \times 10^4$	Mach-Zehnder interferometer	The Nusselt number increased with the increase in the spacing between cylinder and adiabatic surface.
7.	Butler et al. (2014)	30	310 × 310 × 310	Electrical (3-13 W)	$2 \times 10^4 – 8 \times 10^4$	PIV	The interaction between flow generated due to the cylinder and the cavity leads to an increase in the Nusselt number.

Table 2.2. Summary of previous work on natural convection in a cavity (Numerical)

Sr. No.	Author and year	Computational domain			Range of		Grid size, Discretization	Model, Solution procedure	Results
		Diameter of the cylinder, *D* (mm)	Enclosure dimensions, *H* × *W* (mm^2)	Aspect Ratio, (*W*/*D*)	Temperature (K) or Flux (W)	Rayleigh number, *Ra*			
1.	Ghaddar (1992)	63	2520 × 945		48 W (per m^2)		2352, Adams Bashforth Scheme	Laminar, Adams Bashforth method	The heat transfer increased with the increase in the Rayleigh number. The maximum heat transfer of enclosure occurred at the middle of the top wall.

2.	Cesini et al. (1999)			2.1-3.6		1.3×10^3– 7.5×10^4		Laminar	Same as given in Table 4.1.
3.	Shu et al. (2002)			2.6		3×10^5	31 × 21, DQ scheme	Laminar	It was shown that DQ method with transformed coordinates can be applied successfully to study the natural convection problem inside an annulus.
4.	Newport et al. (2001)	20	470 × 470		310.2-350.2 K	6.8×10^3 – 2.2×10^4	11,172, First and second order Upwind	Laminar	Same as given in Table 4.1.
5.	Ding et al. (2005)			1.67 – 5		10^4 - 10^6	18480, 30076, First order upwind	Laminar	The numerical results showed a higher Nusselt number as compared to the experimental Nusselt number.
6.	Kim et al. (2008)			2.5		10^3- 10^6	201 × 201, Central difference scheme	Laminar	The formation of secondary and tertiary cells was observed at higher Rayleigh number, which had a significant effect on the heat transfer
7.	Yu et al. (2011)			3-5	320 K	10^3- 10^7	10000, Second order upwind	Laminar, SIMPLE	As the Grashof number was increased, the flow development time increased and flow became more oscillating and less stable.
8.	Lee et al. (2010)			5		10^3- 10^6	201 × 201, Central difference Scheme	Laminar	At high Rayleigh number, the Nusselt number of the enclosure became independent of the cylinder movement, showing that convection heat transfer dominates at high Rayleigh number.

9.	Hussain and Hussein (2010)	5		10^3- 10^6	200 × 200, Power Scheme	Laminar, SIMPLE	The displacement of the cylinder vertically resulted in more heat transfer, and the secondary cells were observed at the corners.
10.	Ashajaee et al. (2012)	20		10^2- 10^6	600 × 900, Hybrid Scheme	Laminar	Same as given in Table 4.1.
11.	Ghasemi et al. (2012)	0.4-0.8 (elliptical geometry)		10^3- 10^6	61 × 181	Laminar	The Nusselt number was larger at higher Rayleigh number and smaller diameter of the inner cylinder.
12.	Zhang et al. (2013)	5	330-700 K	10^3- 10^6	49 × 49, QUICK	Laminar	It was found that the Nusselt number and heat transfer decreases with the increase in the optical thickness. The radiation heat transfer was found to be very important especially at higher Rayleigh numbers.

2.3. Natural convection around finned-tube heat exchangers.

Kayansayan (1993) studied the natural convection of air over an annular finned tube and observed the effects of the fin spacing, fin diameter to tube diameter ratio and Rayleigh number on the heat transfer. A critical Rayleigh number was found, above which the effect of fin spacing and fin to tube diameter ratio diminishes. Hahne and Zhu (1994) performed experiments on a circular finned tube (OD=16 mm). It was found that the smaller diameter fin (D_f =70 mm) gives better heat transfer coefficient and more uniform heat transfer as compared to larger diameter fin (D_f=110 mm). Aziz and Kraus (1996) presented a review on the optimized design of the radiating and convecting-radiating fins. Lack of experimental data on the natural convection around the annular fins motivated Yildiz and Yuncu (2004) to perform the experimental investigation on the annular finned tube. The convective heat transfer rate was found to be maximum for optimized fin spacing. Farhadi et al., (2005) studied the effects of steam pressure, mechanical fouling and existing two phase regimes on the temperature distribution of the A type air cooled condenser in natural convection. The temperature distribution in the air cooled condenser was studied and the air side heat transfer correlations were proposed for the superheating and subcooled regions. Chen and Chou (2006) applied the finite difference method in conjunction with the least square scheme on the plate fin and validated the predictions with the experiments performed. It was found that the heat transfer coefficient increases with an increase in the fin spacing and reaches an asymptotic value as fin spacing approaches infinity. In a similar manner, Chen and Hsu (2007) carried out experiments on the annular fin. The results obtained were similar to the results obtained for plate fin. Dogan et al., (2012) performed numerical simulations to study the natural convection over a horizontal annular-finned tube. An optimum fin spacing of 8.7 mm was observed for the fin diameter ranging from 35 mm to 160 mm. Yaghoubi and Mahdavi (2013) performed experiments and numerical simulation to study the natural convection around a circular finned-tube. The effect of the geometrical parameters on the convective to radiative heat transfer ratio was investigated. It was observed that, the temperature distribution over the fin surface was almost uniform. Kannan et al., (2015) studied the thermal-hydraulic effects of the geometrical parameters for a sodium to air heat exchanger. An improvement of 22% in heat transfer was observed with a variation in the transverse and longitudinal tube pitch. A design of a passive residual heat removal system (10 MW) was put forward by Zhao et al., (2015) for a molten salt reactor. It was concluded that the design could fulfil the requirements for a residual heat removal system. Katsuki et al., (2015) performed experiments to study the heat transfer characteristics of an array of finned-tubes under natural convection conditions. The heat transfer coefficient was 1.4 times higher for the case with chimney as compared to the case of free convection in open space. Pathak et al., (2015) carried out numerical and experimental investigation on a sodium to air heat exchanger. Correlations were proposed for the Nusselt number and the fin effectiveness.

From the forgoing discussion it may be seen that all the experimental studies on the natural convection of air around finned tube have been performed in a closed system. The numerical studies have also been performed in the similar manner and only one or two fins are considered in the numerical domain and the flow is assumed to be uniform along the length of the tube. However, no 3D numerical simulations have been reported in the published literature on a system where finned-tube heat exchanger is placed under a chimney to generate a natural draft.

2.4. Forced convection air cooled heat exchangers and condensers

A large number of researchers have studied the effect of the geometric parameters on the heat transfer and pressure drop characteristics of the air-cooled heat exchangers. The experimental as well as the numerical simulations have been performed to investigate the effects of various parameters. Ota et al. (1984), and Badr (1994) have reviewed the studies performed on the heat transfer and flow field around the bare elliptical tubes. Theoretical studies on the natural and the forced convection over elliptical tubes have been performed by Chao and fagbenle (1974), and Merkin (1977). In early 90s, Kayansayan (1993) experimentally studied the effects of fin spacing, number of rows, and number of tubes per row on the heat transfer and the pressure drop characteristics of the plate- finned-tube heat exchangers. Other researchers, Wang and coworkers (1996, 1997, 2000), Jang and Yang (1998), Ay and group (2002, 2003, 2009), Nuntaphan et al. (2005a, 2005b), He and group (2005, 2007, 2009, 2011, 2012) etc., have performed studies on the effect of geometric parameters on the heat transfer and the pressure drop characteristics of the air-cooled heat exchanger. Many correlations have been proposed for the air-side heat transfer coefficient for various types of fins. It is well known that the temperature distribution on the fin surface is not uniform, and the heat transfer coefficient varies over the fin surface. Chen and group (2005, 2007, 2008, 2012) conducted various studies to determine the heat transfer coefficient variation on the fin surface. Previous work on the air-cooled heat exchangers shows that the thermal-hydraulic behavior of various types of fins vary from each other, therefore, depending on the application, the design of the finned tube has to be optimized to obtain a maximum heat transfer rate per unit power consumption. The thermal and the mechanical properties of the materials play an important role in determining the thermal-hydraulic performance of heat exchangers. Aluminum, copper, steel, and nickel alloys are mostly used as fin and tube materials. Out of these, copper has the highest thermal conductivity, and hence provides a better fin efficiency than the other materials. Aluminum has the second best thermal conductivity, and hence, provides the second best fin efficiency (slightly lower than Cu). However, copper finned-tubes are almost twice as costly as aluminum finned-tubes, therefore, this factor must be taken into account along with the fin efficiency while designing an economical and efficient air-cooled heat exchanger.

The system details for the experiments and the numerical simulations of the previous studies are given in Table 2.3 and Table 2.4, respectively. The correlations proposed by various authors for the heat transfer and the pressure loss are provided in Table 2.5 and Table 2.6, respectively.

2.4.1. Important parameters

In this section, role of three important parameters (Reynolds number, area goodness factor and the volume goodness factor) has been discussed. The first parameter is the Reynolds number, which is a dimensionless number and is defined as the ratio of the inertial forces to the viscous forces. The Reynolds number is used to predict the different flow regimes, such as creepy, laminar and turbulent in fluid flows. The Reynolds number is defined as:

$$Re = \frac{\rho U_{max} l}{\mu} \qquad \ldots \quad (2.3)$$

where l is the characteristic length. In literature, the definition of the characteristic length has been different for different authors. One category of the authors considers the outer tube diameter or the tube collar diameter as the characteristic length, the second category of the authors considers the fin spacing as the characteristics length, and in the third category, the hydraulic diameter of the heat exchanger is considered as the characteristic length. However, in most of the cases, the outer tube diameter is considered as the characteristic length, therefore, in the present review, we have used the outer tube diameter (or tube collar diameter) as the length dimension in the Reynolds number and wherever it was possible, we have converted the Reynolds number based on other characteristics length to the Reynolds number based on the outer tube diameter and the results are given in Table 2.3 and Table 2.4. However, in some studies we have retained the Reynolds number as it was used by the authors, and in Tables 2.3 and 2.4 they have been provided with a separate subscript.

The performance evaluation criteria (PEC) for any heat exchanger comprises mainly of two parameters, area goodness factor and the volume goodness factor [Sahiti et al. (2006)]. When the frontal area of the heat exchanger is the parameter of interest, then the area goodness factor is compared for the heat exchangers. The area goodness factor is used to optimize the heat exchanger frontal area. A maximum value of the area goodness factor indicates a minimum frontal area of the heat exchanger. It can be observed by using the equations.

The definition of *j* can be given as: $\frac{Nu}{RePr^{\frac{1}{3}}}$ … (2.4)

The definition of *f* can be given as: $\frac{2\Delta PA_c\,\sigma^2}{A\rho U_{fr}^2}$ … (2.5)

The *j/f* factor results into an expression given as: $\frac{1}{A_{fr}^2}\left(\frac{Pr^{2/3}NTU\dot{m}^2}{G\Delta PG}\right)$

… (2.6)

The quantities in the bracket are dependent on the operating conditions. Therefore, for a fixed operating condition, a higher *j/f* indicates a lower frontal area (A_{fr}). This factor is important in determining the frontal size of the heat exchangers. However, when the volume of the heat exchanger is the parameter to be considered, then the optimization of area goodness factor is not sufficient and in that case, the volume goodness factor is taken into consideration. Colburn (1942) proposed this method, which was adopted by London and Ferguson (1949). In this method, the heat transfer coefficient (h) is plotted with the normalized power requirement (P_n).

Table 2.3. Summary of published work on air cooled heat exchanger (experimental).

Sr. No.	Author/s and year	Design of the tube assembly			Design of the fins			Geometry of the shell (m^3 or m^2) / thermal source (℃ or W)	Inlet Velocity (Reynolds number)	Remarks
		Diameter of the tubes, D (mm)	Number of rows, N_r	Tube Pitch (S_t (mm)/ S_l (mm))	Type of fins	Length or Diameter (mm) / Thickness, t_f (mm)	Pitch, S_f (mm)			
1.	Saboya and Sparrow (1976)	8.53	2	21.3/	Plate	37 mm (along the flow) /	16.5		(211-1089, Re_h)	The mass transfer coefficient was affected by the boundary layer development for the first row, while the vortex generation gave more contribution to the mass transfer coefficient for the second row.
2.	Fiebig et al. (1993)	32	3	64/47.25	Plate with DWP	216 mm (along the flow) / 0.84	7.84	160 × 320 / Electrical heating	1.45-6.3 (2700-12340)	The increment in the heat transfer and pressure drop for the inline arrangement with the DWP was 55-60 % and 20-45 %, respectively.
3.	Kayansayan (1993)	9.52, 12.5, 16.3	4	25.4-40 / 22-34.67	Plate	88 – 139 / 0.2 mm	0.0022 to 0.0042	50 × 50 / Hot water (80)	0-15 (100-30000)	The Colburn factor (j) decreases with an increase in the finning factor and the Reynolds number.
4.	Mirth and Ramadhyani (1993)	13.2-16.4	4-8		Wavy	/ 0.15	1.62-3.20	/ Cold Water (3-6.3)	1-2.9 (1350-4570)	The Nusselt number correlation for the dry surface predicted the heat transfer for wet surface within ±5%.

5.	Hu and Jacobi (1993)	38.1	1	76.2/	Annular	76.2 / 1.02	7.1	40 × 40 × 135	13711-49858	The heat and mass transfer analogy was applied to obtain the fin efficiency as a function of the fin parameter (fin diameter, thermal conductivity and heat transfer coefficient).
6.	Mirth and Ramadhyani (1994)	13.2-16.4	4-8		Wavy	/0.15	1.47-3.05	/ Cold Water (3-6.3)	1-2.9 (1350-4570)	The length of the coil and the fin spacing affected the Nusselt number for all the coils. However, the friction factor for one set of coil was a function of the fin spacing only, and for the other set, it was a function of both the fin spacing and length of the coil.
7.	Fiebig et al. (1994)	32 (round tubes) 69.6 × 12 (elliptical)	3	64/47.25	Plate with DWP	216 mm (along the flow) / 0.84	7.84	160 × 320 / Electrical heating	1.45-6.3 (2700-12340)	The DWP affected the flat tubes to a larger extent as compared to the round tubes. The increment in the heat transfer for the flat tubes was 80-120% and for round tubes it was 10%.
8.	Tigglebeck et al. (1994)				Plate with VGs			/ Hot air, 50	(2000-9000, Re_h)	The performance of the DWP and the RWP was studied at various attack angles. It was found that, the maxima in the Nusselt number occurs between 50° and 70° for DWP and between 45° and 65° for RWP.
9.	Wang et al. (1996)	9.52	2-6	25.4/22	Plate	/ 0.13-2	1.74-3.20	/ Hot water (60)	280-6980	The Colburn factor was found to be independent of the number of tube rows and slightly dependent on the fin thickness and fin spacing.
10	Wang et al. (1997)	9.53	1-4	25.4, 29.4/19.05, 29.4	Wavy	/ 0.12, 0.2	1.69 to 3.53	/ Hot water (60)	0.3-5.5 (372-7456)	The heat transfer increased with an increase in the number of rows for *Re* < 900, and for *Re* > 900, the heat transfer decreased with an increase in the number of rows for the staggered arrangement and did not show any

										variation for the inline arrangement. The friction factor was almost independent of the number of rows.
11	Jang and Yang (1998)	36 × 12.7 (elliptical), 27.2	4	34, 42/50, 37	Annular and elliptical	50 × 26.7 (elliptical), 41 / 0.5	3.175	/ Hot and cold water (70 and 7)	1-7 (20000-80000, Re_p)	The heat transfer per unit pressure drop was 50% higher for the elliptical finned tubes as compared to the circular finned tubes.
12	Madi et al. (1998)	9.956	1-4	19-25.4/16-22	Plain and wavy	/ 0.12-0.2	1.615-4.129	/ Hot water, 84	1-20 (220-6700, Re_h)	The wavy fin was found to have a larger Colburn factor and friction factor as compared to the plain fins.
13	Yun and Lee (1999)	22.5/7.5	2	63, 21/38.1,12.7	Plate with slits and louver	/ 0.3, 0.1	3.6/1.2	/ Hot water at 45	0.2-1.5 (300-2230, Re_h)	Different slit patterns had a negligible effect on the heat transfer coefficient but the effect on the pressure drop was quite significant. The strips in the rear part of the plain fin were recommended.
14	Kang and Kim (1999)	22.5(large model), 7.5 (prototype model)	2	63, 21/38.1, 12.7	Plate with slits and louver	/0.3, 0.1	3.63, 1.21	0.315 × 0.0292 / Hot water	(500-2000)	The strip fin with strips in the half rear part of the fin was found to be the best.
15	Watel et al. (1999)	58	1		Annular	100 / 1	3-41	0.4 × 0.3 / Radiant panel with infrared waves	0.9-14 (2550-42000)	The Nusselt number increased with an increase in the fin spacing and Reynolds number, and the reason was believed to be the decrease in the interaction between the boundary layers on two fins.
16	Watel et al. (2000a)	58	1		Annular	100/ 1	3-41	0.4 × 0.3 / Radiant panel with infrared waves		The Nusselt number increased with an increase in the fin spacing.

17	Wang and Chi (2000)	7.3 - 9.52	1-4	21, 25.4 / 12.7, 19.05	Plate	/ 0.115	1.19-2.31	/ Hot water	0.3-6.5 (300-9000)	The effect of the number of tube rows, fin pitch and the tube diameter was significant on the heat transfer and the pressure drop.
18	Romero-Mendez et al. (2000)		1		Plain			0.381 × 0.508 × 1.626 /	0.09-0.15 (260-1450)	The Nusselt number per unit pressure drop per unit fin spacing was maximum for an optimum fin spacing. The fin pitch, angle of slit pattern, slit length and the slit height were the important factors affecting the performance of the heat exchanger.
19	Du and Wang (2000)	7.3-14.8	1-6	17.32-38 / 15-33	Slit	/ 0.11-0.18	1.20-2.50		(200-8000)	The effect of fin pitch on the heat transfer performance varied for two types of fins, and the difference was found to be because of the difference in the manufacturing design of the fins.
20	Yun and Lee (2000)	22.5/7.5	2	63,21 / 38.1,12.7	Plate with slits	/ 0.3, 0.1	3.6/1.2	/ Electric heating	0.2-1.5 (300-2230, Re_h)	It was found that the effect of four factors fin pitch (39%), angle of slit pattern (28%), slit length (20%), and slit height (9%) was significant on the performance of the heat exchanger.
21	Yan and Sheen (2000)	9.53	1-4	25.4 / 19.05	Plate, wavy and louver		1.4-2	0.6 × 0.4 / Hot water (60)	0.47-3.19 (650-3500)	The heat transfer per unit pumping power, the volume goodness factor, and surface area reduction for a fixed power was maximum for the louver fin.
22	Watel et al. (2000b)	58	1		Annular	100 / 1	3-41	0.4 × 0.3 / Hot water (65)	0.9-6 (2550-18200)	The Nusselt number was found to be largely dependent on the air flow Re number as compared to the rotational Re number.

23	Wang et al. (2000b)	8.62	2, 4	25.4/19.05	Plain and Wavy	/ 0.12	1.70-3.14	0.85 × 0.55 / Cold water (7)	0.3-3.5 (150-1800)	The effect of the waffle height on the heat transfer was negligible, but the effect on the pressure drop was significant. The heat transfer was found to be a strong function of the fin pitch for the larger waffle height.
24	Saboya and Saboya (2001)	12.06 × 6.03-17.06 × 8.53 (elliptical)	1-2	21.35/18.5	Plate		1.70		150-1300	The elliptical tubes did not provide adverse change in the average Sherwood number, however, elliptical tubes provided a higher fin efficiency.
25	Tori et al. (2002)	30	3	75/75	Plate with DWP		5.6	0.15 × 0.1 x 0.3 / Electrical heating	0.5-3.5 (937-6428, Re_{fr})	The common flow up configuration of the DWP enhanced the heat transfer and reduced the pressure drop as compared to the common flow down configuration.
26	Kwak et al. (2002)	30	1-3	75/75	Plate with DWP		5.6	0.15 × 0.1 × 0.3 / Electrical heating	0.5-3.5 (937-6428, Re_{fr})	An increment of 10-25 % in the heat transfer and 20-30% in the pressure drop was observed with DWP included for the inline arrangement.
27	Elsharbini and Jacobi (2002)	9.5	8		Plate with DWP		5	0.058 × 0.61 / Electrical heating	(700-2300, Re_h)	An overall enhancement of 29-33 % in the heat transfer was observed for the larger DWP. The smaller delta winglet enhanced the heat transfer by 17-20 %.
28	Ay et al. (2002)	25.4	3	60.7/52.6, 60.7	Plate	196 × 240 / 0.5	10.5-20.5	/ Electrical heating	0.5-7.5 (730-11000)	The heat transfer coefficient was found to be 14-32% larger for the staggered arrangement as compared to the inline arrangement.
29	Hashizume et al. (2002)	31.8	5		Serrated	68.5 / 1	5.1	/ Electrical heating	(5000-50000)	The correlation for the fin efficiency was proposed.

30	Kwak et al. (2003)	30	2-5	75/75	Plate with DWP		5.6	0.15 × 0.1 × 0.3 / Electrical heating	0.5-3.5 (937-6428, Re_{fr})	The three rows of finned tube with DWP performed better than the 2, 4, and 5 rows. The increment in the heat transfer was 30-10 % with a reduction of 55-34 % in the pressure drop.
31	Wongwises and Chokeman (2004)	9.53	2-6	25.4/19.05	Wavy	/ 0.115-0.250	1.41-2.54	0.43 × 0.48 / Hot water (55-65)	1-6 (900-5400)	The Colburn factor and the friction factor both increased with an increase in the fin thickness for 2 row coil. For 4 and 6 row coil, the Colburn factor decreased with an increase in the fin thickness at low *Re*, and at higher *Re*, the effect was same as was for 2 row coil.
32	Matos et al. (2004a)	15.875-28.58 (circular) Elliptical tubes with *e* = 0.4-1	4		Plate	150 × 130 / 0.3		0.161 × 0.152 / Electrical heating	0.1-1 (100-1000)	The tube spacing and tube eccentricity were optimized for the best performance of the heat exchanger.
33	Matos et al. (2004b)	15.875-28.58 (circular) lliptical tubes with *e* = 0.4-1	4		Plate	150 × 130 / 0.3		0.161 × 0.152 / Electrical heating	0.1-1 (100-1000)	The optimum value of the parameters [dimensionless tube spacing (0.5), eccentricity (0.5) and dimensionless fin spacing (0.006)] were obtained..
34	Nantaphan et al. (2005a)	17.3-27.2	4	50-84 / 24.2-50	Crimped spiral	37.3, 57.2 / 0.4	2.85-6.10	/ Hot water (65)	0.6-1.7 (600-2700)	The effect of the tube diameter, fin height, and the fin spacing was studied for the staggered and the inline arrangement of the crimped-spiral-finned tubes.
35	Nantaphan et al. (2005b)	17.3-27.2	4	50-84/24.2-50	Crimped spiral	37.3, 57.2 / 0.4	3.25-6.50	/ Cold water (65)	0.6-1.7 (600-2700)	The effect of the tube diameter, fin height, and the fin spacing was studied for the staggered and the inline arrangement of the

									crimped-spiral-finned tubes in the wet conditions.
36	Kawaguchi et al. (2004)	17.3	3-6	40-45/30-40	Spiral annular and serrated	35.3 / 0.9	3.3-5	/ Hot water (60)	(2000-27000, Re_h)	The thermal-hydraulic performance of the serrated fin and the spiral-annular fin was compared.
37	Kwak et al. (2005)	30	3	75/75	Plate with DWP		5.6	0.15 × 0.1 × 0.3 / Electrical heating	0.5-3.5 (937-6428, Re_{fr})	The inline arrangement performed better than the staggered arrangement for the two rows of DWP in the common flow up configuration.
38	Wongwises and Chokeman (2005)	9.53	2-6	25.4/19.05	Wavy	/ 0.115-0.250	1.41-2.54	0.43 × 0.48 / Hot water (55-65)	1-6 (900-5600)	The effect of fin pitch, number of tube rows and the Reynolds number on the performance of wavy finned-tube heat exchanger was studied.
39	Chokeman and Wongwises (2005)	9.53	2	25.4/22	Wavy	/ 0.115	1.81	0.43 × 0.48 / Hot water (55-65)	1.4-6 (1400-5600)	The fin pattern and edge corrugation affected the performance of the heat exchangers significantly.
40	Pirompugd et al. (2005)	8.51-10.34	2-6	25.4/19.05-22	Plate	/ 0.115-0.130	1.195-3.16	0.85 × 0.55 / Cold water (7)	0.3-4.5 (300-5500)	The effect of the inlet conditions and geometric parameters on the heat and mass transfer was observed for 1 and 2 row coils in wet conditions.
41	Naphon and Wongwises (2005)	9.6 (spiral coiled tubes)	6		Crimped spiral	28.2 / 0.35	3.1	300 mm diameter (cylindrical tunnel) / Water , wet conditions		The effect of the inlet air temperature, air mass flow rate, water inlet temperature, and the water flow rate was described on the heat transfer performance.

								(12.5), dry conditions (30)		
42	Chen et al. (2005)	40	1		Plate	100 × 100 / 0.2	-	/ Hot and cold water (75 and 7)	0.3-6.5 (2500 to 13000, Re_{fr})	The average heat transfer increased and the fin efficiency decreased with an increase in the base to ambient temperature difference and inlet air velocity.
43	Pesteei et al. (2006)	50.8	1		Plate with DWP	300 × 204 / 3	15	300 × 300 × 600 / Electrical heating	(9525)	The best location for the DWP was at Δx = 0.5D and Δy = 0.5D, where Δx and Δy were the streamwise and cross-stream distances.
44	Pirompugd et al. (2006)	8.62-10.38	1-6	25.4/19.63-26.27	Wavy	/ 0.12	1.57-3.63	0.85 × 0.55 / Hot water (7)	0.3-3.8 (400-5000)	The ratio of the heat transfer to the mass transfer coefficient varied from 0.6 to 1.1, and was insensitive to the fin spacing.
45	Wongwises and Naphon (2006a)	9.6 (spiral coiled tubes)	6		Crimped spiral	28.2 / 0.35	3.1	300 mm diameter (cylindrical tunnel) / Cold Water (7.5-20)		The enthalpy effectiveness and humidity effectiveness were defined and their behaviour was also described. The liquid film had significant effect on the heat transfer performance of the heat exchanger.
46	Wongwises and Naphon (2006b)	9.6 (spiral coiled tubes)	6		Crimped spiral	28.2 / 0.35	3.1	300 mm diameter (cylindrical tunnel) / Cold Water (30-35)		
47	Kuvannarat et al. (2006)	9.53	2-6	25.4/19.05	Wavy	/ 0.115-0.250	1.41-2.54	480 × 460 / Cold Water (7)	0.5-6 (450-5400)	The effect of the fin thickness on the heat transfer was pronounced only at lower fin spacing.

48	Chen et al. (2006)	27.3	1		Plate	100 x 100 / 0.1	5.1-50	0.2 × 0.2 / Electrical heating	1-5 (1550-7760, Re_{fr})	The fin efficiency decreased and the heat transfer coefficient increased with an increase in the air velocity and base to ambient temperature difference.
49	Jaordar and Jacobi (2007)							0.101 × 0.610 / Electrical heating	0.7-1.8 (220-960, Re_h)	The *j*/*f* factor was higher (35.7 % to 50.8%) for the one row of the DWP as compared to the three rows of the DWP. However, the volume goodness factor was better for the three rows of the DWP as compared to the one row of the DWP.
50	Chen et al. (2007)	27.3	1		Annular	99 / 0.1	5.1-50	0.2 × 0.2 / Electrical heating	1-5 (1550-7760, Re_{fr})	
51	Pirompugd et al. (2007)	8.51-10.23	1-6	25.4/12.7-22.0	Plate	/ 0.115-0.130	1.315-3.33	0.85 × 0.55 / Hot water (7)	0.3-3.8 (525-7650)	A new mathematical model [FCFM (Finite circular fin method)] was developed to determine the performance of the plain finned-tube heat exchangers under wet surfaces condition.
52	Saechan et al. (2008)	9.53	2-5		Plate	/ 0.3	6.6		(940-20000)	The second law of thermodynamics was used to optimize the performance of the plain-finned-tube heat exchanger.
53	Pirompugd et al. (2008)	8.62-10.38	1-6	25.4/19.05	Wavy	/ 0.12	1.45-3.51	0.85 × 0.55 / Hot water (7)	0.3-3.8 (525-7650)	The effect of the fin spacing and the Reynolds number on the thermal-hydraulic performance of the wavy finned-tube heat exchanger was studied.
54	Paeng et al. (2008)	10.2	3	25/22	Plate	/ 0.33	3.2	0.36 × 0.27 × 1.5 / R-22	1.13-1.61 (1082-1649)	The correlation for the Nusselt number was derived, and the error between the numerical and the experimental results was 6 %.

55	Huang et al. (2009)	25.4	3	52.6, 60.7/60.7	Plate	196 x 240 / 1	10-15	0.3 × 0.3 / Electrical heating	0.5-1.5	The heat transfer coefficient for the staggered arrangement was higher than the heat transfer coefficient for the inline arrangement.
56	Ibrahim and Gomaa (2009)	12.7 (circular), 5.2 x 7.8-3.2 x 12.7 (elliptic tubes)	5	30/26				/ Hot water, 80	3.8-20 (5300-28000, Re_h)	Four criterions for the thermal performance were identified, (1) comparison of heat transfer and pressure drop (2) heat transfer per unit pressure drop (3) area goodness factor and (4) efficiency index.
57	Tang et al. (2009a)	18	6-12	42/34	Plain, slit, vortex	/ 0.3	3.1	/ Superheated steam (65)	2.5-5 (3870-9677)	The *j*/*f* ratio for the slit fin increased at a higher rate as compared to the plain fin and fin with DWP.
58	Tang et al. (2009b)	18	6-12	42/34	Crimped Spiral , Plain, slit, Plate with DWP, mixed (DWP + slit)	/ 0.3	3.1	/ Superheated steam (65)	2.5-5 (3870-9677)	After optimization, it was found that the fin with DWP could perform better than the slit fin.
59	Choi et al. (2010)	8	1-4	26/28-34	Discrete plate	62 × 27 /	7.5-15	1.4 × 0.4 × (0.44-0.6) / Ethylene glycol-water mixture, 33	1-1.65 (500-800)	The Colburn factor for the discrete plate finned-tube was found to be 6-11 % more than the continuous plate finned-tube heat exchanger for a fin pitch of 7.5-15 mm.
60	Naess (2010)	19.07-31.77	4	46.1-79.8/23.1-50.9	Serrated	/ 0.91	3.62-5.08	/ Water-glycol	(2282-47290)	It was found that the Nusselt number shows a maxima when the flow areas in the transverse and diagonal directions become equal.

61	Martinez et al. (2010)	50.8	8	114.3/99.06	Serrated	101.6 / 1.24	4.23	1.4 × 0.8-1.4 × 0.8 / Water (105-108)	(6200-11200)	Various correlation for the heat transfer and pressure drop performance of the serrated fins were compared.
62	Liu et al. (2010)	16.44	2-8	38.1/33	Plate	/ 0.12	2.06-3.17	0.85 × 0.55 / Cold Water (7)	1-4 (1970-7885)	The heat transfer was maximum for an optimized fin spacing of 2.54 mm.
63	Pongsoi et al. (2011)	16.35	2	39/35	Crimped spiral	34.8 / 0.4	3.2-6.2	0.43 × 0.48 / Hot water (60)	2-6 (4000-13000)	It was found that, the effect of fin pitch on the Colburn factor was very small for 2 row coil due to better mixing at high Re number.
64	Ma et al. (2012)	38.1	12	88-120/92-117	Serrated	70.1 / 1	3.9-4.1		4000-30000	A critical *Re* was found, above which the effect of the fin height-spacing ratio on the heat transfer was negligible.
65	Chen and Lai (2012)	27	2	214.28/214.28	Plate	126 x 126 / 1	5-50	0.22 × .22 / Electrical heating	0.5-1.5 (816-2500)	The heat transfer coefficient increased with an increase in the air velocity and fin spacing, however, it reached its asymptotic value as the fin spacing approached infinity.
66	Pongsoi et al. (2012a)	16.35	2-5	40/35	Crimped spiral	35 / 0.5	6.3	0.43 × 0.48 / Hot water (60-65)	2-6 (4000-13000)	It was found that, the number of tube rows does not affect the Colburn factor and the friction factor beyond a Re number of 2000. This was believed to be due to the shedding of the downstream turbulence eddies, which causes good mixing.
67	Pongsoi et al. (2012b)	16.35	2-4	40/35	Crimped spiral	35 / 0.5	6.3	0.43 × 0.48 / Hot water (60-65)	2-6 (4000-13000)	The effect of the number of tube rows were similar as were found in the previous study [(Pongsoi et al.., 2012a)]. The only different result was the increase in the pressure drop with an increase in the fin diameter.

68	Pongsoi et al. (2012c)	16.35	2	39/35	Crimped spiral	34.8 / 0.4	2.4-6.5	0.43 × 0.48 / Hot water (60-65)	2-6 (4000-13000)	An optimum fin pitch of 4.2 mm was suggested.
69	Pongsoi et al. (2013)	16.85	2	39/35	Spiral Annular	34.8 / 0.4	2.4-4.2	0.43 × 0.48 / Hot water (60-65)	2 (4000-13000)	The Colburn factor was found to be independent of the fin spacing at all *Re*. However, the friction factor increased as the fin pitch was increased for *Re* > 6000, and for *Re* < 6000, the fin pitch did not affect the friction factor.

Table 2.4. Summary of published work on air cooled heat exchanger (numerical).

Sr. No.	**Author/s, Year**	**Computational Domain**						**Thermal BC (Q (W), T (K))**	***Re***	**Grid Size/ Scheme**	**Model / Solution algorithm**	**Remarks**
		Diameter of the tubes, D (mm)	**Number of rows, N_r**	**Tube Pitch (S_t (mm)/ S_l (mm))**	**Type of fins**	**Fin Length or Diameter (mm) / Fin thickness, t_f (mm)**	**Fin Pitch, S_f (mm)**					
1.	Brockmeier et al. (1993)				Plain with DWP			Constant temperature for fin and tube	500-3000, Re_h	140 × 40 × 20		The vortices were observed near the leading edge of the winglet. The fin with DWP allowed a 76% decrease in the heat transfer area as compared to the plain fins.
2.	Biswas et al. (1994)		1		Plain with DWP			Constant temperature for fin and tube	500-1000, Re_s	98 × 14 × 34	/ Marker and Cell (MAC)	The interaction of the longitudinal and transverse vortices led to the periodic flow for the *Re* = 1000.
3.	Fiebig et al. (1995)		1		Plain with DWP			Constant temperature for the tube	250-300, Re_s		/ SIMPLEC	The DWP reduced the heat transfer reversal and enhanced the heat transfer behind the tubes in the wake zone.

4.	Rocha et al. (1997)					Plain						The elliptical arrangement performed better than the circular arrangement with 18 % more efficiency.
5.	Tsai and Sheu (1998)	7.5	2	12.75 / 20.4	Plain and slit fin	25.5 × 20.4 / 0.0575	1.4	Constant temperature at tube (50)	367.28 - 1133.5 94, Re_h	142 × 84 × 54	/ SIMPLE	The horseshoe vortex led to higher heat transfer in the upstream of the tubes. The wake region behind the second row tubes gave rise to heat transfer reversal (HTR).
6.	Chen et al. (1998a)		1		Plain with DWP			Constant temperature for tube	300, Re_s	187 × 52 × 25-152 × 52 × 25 / Upwind Scheme	Laminar / SIMPLE C	The best performance of the delta winglets were observed for an aspect ratio of 2 and an attack angle of 30°.
7.	Chen et al. (1998b)		1		Plain with DWP			Constant temperature for tube	300, Re_s	152 × 60 × 24 / Upwind Scheme	Laminar / SIMPLE C	The heat transfer increased with an increase in the number of rows of delta winglets.
8.	Jang and Yang (1998)	36 × 12.7 (elliptical), 27.2	4	50, 37 / 34, 42	Annular and elliptical	50 × 26.7 (elliptical), 41 / 0.5	3.175	Constant temperature without conjugate heat transfer	20000-80000, Re_p	10 × 12 ×178 - 9 × 11 × 152 / Hybrid Scheme	Laminar / SIMPLE R	The heat transfer per unit pressure drop was 50% higher for the elliptical finned tubes as compared to the circular finned tubes.

9.	Sheu and Tsai (1999)	7.5	2	12.75 / 20.4	Plain and slit	25.5×20.4 / 0.0575	1.4	Constant temperature at tube (50)	367.28 - 1133.594, Re_h	142 × 84 × 54 / QUICK	Laminar / SIMPLE	The heat transfer was higher near the leading edge and upstream of the tubes for both types of fins. The Nu number decreased along the flow direction. The heat transfer and pressure drop were higher for the slit fin as compared to the plate fin.
10.	Tsai et al. (1999)	7.5	2	12.75 / 20.4	Plain and Wavy	25.5×20.4 / 0.0575	1.4	Constant temperature at tube (50)	367.28 - 1133.594, Re_h	142 × 84 × 54, 142 × 84 × 40, QUICK	Laminar / SIMPLE	The heat transfer and pressure drop were higher for the wavy fin as compared to the plate fin.
11.	Chen et al. (2000)		1		Plain			Constant temperature for tube	300, Re_s	152 × 60 × 24	/ SIMPLEC	The staggered arrangement increased the heat transfer by 20% and decreased the pressure drop by 14.6 % as compared to the inline arrangement.
12.	Romero-Mendez et al. (2000)		1					Constant temperature for tube and fin	260-1450			The Nusselt number per unit pressure drop per unit fin spacing was maximum for an optimum fin spacing.
13.	Matos et al. (2001)		4					Constant temperature	300-800, Re_a (based on array length)	5180 (elements), upwind	Laminar /	The elliptical tubes provided 13 % more heat transfer as compared to the circular tubes.

14. Matos et al. (2004a)		4					Constant temperature	300-800, Re_a	5180 (elements), upwind	Laminar /	The elliptical tubes provided more heat transfer for a fixed pressure drop. Dimensionless tube spacing and eccentricity were optimized.
15. Matos et al. (2004b)		4					Constant temperature	300-800, Re_a	5180 (elements), upwind	Laminar /	The optimum value of the parameters [dimensionless tube spacing (0.5), eccentricity (0.5) and dimensionless fin spacing (0.006)] were obtained.
16. Mon and Gross (2004)	24	4	35.33-45.73 / 40.8-52.8	Annular	34 / 0.5	0.7-4	Constant Temperature	8600-43000	50000-90000, upwind	k-ε / PISO	An optimized fin spacing was obtained. The staggered arrangement performed better than the inline arrangement of the tubes.
17. Cheng et al. (2004)	19.1	3	25 / 25	Plain and slit	0.3	2.5	Constant temperature for tube	288-5000	211 × 85 × 24	/ CLEAR	The slit fins performed better than the plain fins, and the increase in the heat transfer was higher than the increase in the pressure drop.
18. Qu et al. (2004)	7.2	2	12.7 / 11.97	Plain and strip	0.105	1.4	Constant temperature for tube	348-3480	136 × 116 × 34	Laminar / CLEAR	The fin with strips in the downstream part performed best for velocity < 2m/s. For u_{fr} > 2 m/s, the whole strip fin performed best.
19. Erek et al. (2005)	0.4064-1 (ellipticity)	1		Plate	35 (length) / 0.3-0.4	3	Constant temperature for tube	2100-13500	4,00,000		The heat transfer increased with an increase in the fin height, decrease in fin pitch, increase in ellipticity, and

											decrease in tube thickness. The pressure drop increased with an increase in the fin spacing.
20.	He et al. (2005)	10	1-4	12-30 / 10-24	Plate	Length =21.65-86.65, Width=12.5 / 0.2	0.5-5	Constant temperature for fin and tube	500-5000	62 × 10 × 10 -158 × 22 ×10	/ SIMPLER	The synergy was worse at the back side of the tube. Therefore improvement measurements were recommended for the backside of the tube.
21.	Lin and Jang (2005)	20	4	34.6 (staggered) 40 (inline) / 40	Plate	Length=138, 140, Width =20 / 0.2	6.25	Constant temperature, 77	1050-10500	246 × 21 × 21, Third order upwind		The heat transfer enhancement by EHD was more effective at low Reynolds number and high applied voltage. The maximum heat transfer was obtained for a Reynolds number of 100 at 16 kV.
22.	Tao et al. (2006)	8.31	2	12.7 / 15.88	Slit fins and Plate	/ 0.114		Constant temperature for tube, 283.15 K	900-2700	143 × 66 × 24, SGSD	/ CLEAR	Three different convergence criterions were discussed. Only one of them was found to give the consistent results.
23.	Jin et al. (2006)	8.31	2	12.7 / 15.88	Slit fins and Plate	/ 0.114		Constant temperature for tube, 283.15 K	900-2700	143 × 66 × 24, SGSD	/ CLEAR	Optimum designs were recommended for the slit fins.
24.	Tao et al. (2007a)	10.55	2	21.65 / 25	Wavy	43.3 × 12.5 / 0.2	2	Constant temperature for tube	500-4000	142 × 22 × 12	Laminar / SIMPLE	The heat transfer coefficient increased and the fin efficiency decreased along the air flow direction. The wavy pattern caused a

											fluctuating Nusselt number distribution.
25.	Tao et al. (2007b)	19.1	3	25 / 25	Slit and Plate	/ 0.3	2.5	Constant temperature , 308	650-4800	211 × 85 × 24, SGSD	Laminar / CLEAR	It was recommended that, the strips should be placed in a way that the thermal resistance of the front and the rear part becomes equal.
26.	Cheng et al. (2007)	8.8-13.6	2	22.4 / 25	Wavy		2-3	Constant temperature for tube, 303	660-7700	114 × 34 × 22, SGSD	Laminar / CLEARER	The synergy angle and heat transfer was minimum for the largest wavy angle.
27.	Cheng et al. (2009)	8.8-13.6	2	22.4 / 25	Wavy		2-3	Constant temperature for tube, 303	660-7700	114 × 34 × 22, SGSD	Laminar / CLEARER	The Nusselt number and friction factor increased with an increase in the wave amplitude, tube diameter, and wave density. However, the increase in the friction factor was higher.
28.	Xie et al. (2009)	16-20	2-7	32-36 / 19-23	Plate		1.5-4.5	Constant temperature for both fin and tube	1310-7700	201 × 62 × 22, Power law scheme	Laminar / SIMPLE	The effect of number of tube rows diminished for $N_r > 6$. The heat transfer increased with a decrease in the tube diameter, fin spacing and with an increase in the tube pitch. The pressure drop increased with a decrease in the fin pitch and the tube diameter.
29.	Ibrahim and Gomaa (2009)	12.7	5	26 / 30					5300-28000, Re_h	30000 nodes, Second order	RNG- k-ε / SIMPLEC	Four criterion for the thermal performance were identified, (1) comparison of the heat transfer and the pressure

									upwind scheme		drop (2) heat transfer per unit pressure drop (3) the area goodness factor (4) the efficiency index. At an angle of attack of 0°, all these factors were maximum.
30. Tian et al. (2009)	10.55	3	21.65 / 25	Wavy with delta winglet	/ 0.2	3.2	Constant wall heat flux	2900-15356	196, 000, Hybrid Scheme	k-ε / SIMPLE	It was observed that the delta winglet generates a main vortex and a corner vortex. The delta winglet augmented the heat transfer and pressure drop.
31. Tang et al. (2009b)	18	6	34 / 42	Plain with VGs	/ 0.3	3.1	Constant temperature for the tube	3870-9677	QUICK	k-ε / SIMPLEC	Before optimization, the slit fin performed better than the plain fin with the DWP at, but after optimizing by Genetic Algorithm, the fin with the DWP performed better than the slit fins.
32. Zeng et al. (2010)	18	6	32-40 / 38-54	Plate with VGs	/ 0.3	2.5-4.5	Constant temperature for the inside tube wall	5300-12500	430 × 28 × 22,QUICK	k-ε / SIMPLEC	The Fin pitch, transverse and longitudinal tube pitch, winglet length and height, and winglet attack angle were the six important factor for the optimization of the heat transfer.
33. Tao et al. (2011)	10.55	2	21.65 / 25	Wavy	43.3 × 12.5 / 0.05-0.42	0.5-4	Constant temperature for tube, 313 K	500-4000	142 × 22 × 12, Power law scheme	Laminar / SIMPLE	The heat transfer increased with an increase in the Reynolds number, the wavy angle, and the fin thickness and with a decrease in the fin pitch and tube transverse

											pitch. For best performance a wavy angle in the range from 10^o to 20^o was suggested.
34. Hou et al. (2011)	219 × 19 (elliptical)			Serpentine	200 × 19 / 0.26	2.30				k-ε /	It was found that the heat transfer increases with an increase in the angle between the fin channel and the air.
35. Lemouedda et al. (2011)	25.4	3	55 / 63.5	Serrated	57.15 / 0.20	2.54	Constant temperature (350 K)	600-2600	8100000, Second Order upwind	Laminar /	It was found that the serrated fin gives 9% more heat transfer as compared to the plain fin with same heat transfer area. However, no data for pressure drop was provided, therefore it is difficult to assess the performance of the serrated fins as compared to the plain fins.
36. Yang et al. (2012)	219 × 19 (elliptical)			Wavy flat	200 × 19 / 0.26	2.30	Constant temperature without conjugate heat transfer, 65	700-14000	230000-253000, Second order upwind	k-ε / SIMPLE	A new type of fin was proposed and its thermal-hydraulic characteristics were studied.
37. Banerjee et al. (2012)	27	4	36.5 / 21.5	Anuular perforated	41 / 0.5	3.5	Constant temperature	700-14500	100000-426500	RNG- k-ε / SIMPLEC	The perforation on the back side or in the wake area of the fin was recommended.

38.	Wang et al. (2015)	16	4	33/38	Plate fin with VGs	138 × 240/0.12	3	Constant temperature	400-2400	2,500,000	Laminar	The new vortex generators enhanced the thermal performance of the heat exchanger as compared to the plane fin and fin with rectangular winglet pair.
39.	Arora et al. (2015)	38.1	3	100/100	Plate fin with VGs	300×50/1	12	Constant temperature	1415-7075	45,70,000	RNG- k-ε/SIMPLE	The corner and longitudinal vortices were observed and found significant in enhancing the heat transfer.
40.	Pathak et al. (2015)	38.1	12	85/204	Annular	64.1/1.22	5.1	Constant temperature		1,85,091	RNG- k-ε/SIMPLE	Correlations were proposed for the Nusselt number and the fin effectiveness.
41.	Talor and Oclon (2014a)	11.82 x 6.35 (elliptical tube)	2	18.5/17	Plate	34×18.5/0.4	1	Constant temperature	1-2.5 (150-400)		SST k-omega	Same as in Table 2.3
42.	Talor and Oclon (2014b)	11.82 x 6.35 (elliptical tube)	2	18.5/17	Plate	34×18.5/0.4	1	Constant temperature	1-2.5 (150-400)		SST k-omega	Same as in Table 2.3
43.	Lopata and Oclon (2015)	36 x 14 (elliptical tube)	2	30/60	Plate	126×60/0.25	2.5	Constant temperature	3/		SST k-omega	A new method of determining the local equivalent heat transfer coefficient accounting fouling effect was proposed.
44.	Sun et al. (2015)	8.4/ 11.01 x 4.94 (elliptical)	2	17.8(elliptical), 22/ 19.05	Plate	/0.125	1.52	Temperature	0.8-2.4		Distribut-ed parameter-r model	A comparison of the performance of various refrigerants was also investigated.

45.	Martinez et al. (2015)	25.4	6	11.43/9.906	Serrated	88.9/1.2	3	Constant Temperature (51.5)	1.5-3.7/9652-23696	65120-468832	RNG- k-ε/	The effect of implementation of the periodic boundary conditions on k and ε was observed on the local physical properties

Table 2.5. summary of published correlations (heat transfer)

Sr. No.	Author and year	Correlation
		Annular fin
1.	Briggs and Young (1963)	$Nu = 0.134Re^{0.681}Pr^{1/3}(\frac{S}{h_f})^{0.2}(\frac{S}{t_f})^{0.1134}$
2.	Nir (1991)	Based on fin diameter: $St\ Pr^{2/3} = 1.0Re_{Df}^{-0.4}W^{-0.266}{R_b}^{-0.4}K_{z,h}$ Based on tube outer diameter: $St\ Pr^{2/3} = 1.0Re_{Df}^{-0.4}W^{-0.266}{R_b}^{-0.4}\left(\frac{D_f}{D}\right)^{-0.4}K_{z,h}$ Where, W: ratio of heat transfer area of a row of tubes to free flow area, $K_{z,h}$: heat transfer correction factor which depends on number of rows.
3.	Watel et al. (2000)	$Nu = 0.446XRe^{0.55}$ Where $X = \left(\frac{t_f}{S}+1\right)^{0.55}\left(1-\frac{K}{\left(\frac{S}{D}\right)^{b1}}Re^{-a1}\right)^{0.55}$ $a1 = 0.07$ For $0.034 \le \frac{S}{D} \le 0.14,\ K = 0.62, b1 = 0.27$

		For $\frac{S}{D} \geq 0.14,\ K = 0.36, b = 0.55$ Valid for $2550 \leq Re \leq 42000$
4.	Pongsoi et al. (2013)	$j = 0.215Re^{-0.4059}$
		Crimped fin
5.	Nuntaphan et al. (2005)	For inline: $j = 3.9048\ \times 10^{-4}Re^{0.0637}\left(\frac{t_f}{S}\right)^{-0.8363}\left(\frac{S_l}{S_t}\right)^{1.9926}\left(\frac{S_t}{D}\right)^{2.2810}\left(\frac{D_f}{D}\right)^{-2.1720}$ For staggered: $j = 0.1970\ Re^{-0.1295}\left(\frac{t_f}{S}\right)^{-0.1452}\left(\frac{S_l}{S_t}\right)^{1.1874}\left(\frac{S_t}{D}\right)^{0.8238}\left(\frac{D_f}{D}\right)^{0.0010}$ Valid for $600 \leq Re \leq 2700$
6.	Naphon and Wongwises (2005a)	For dry conditions: $Nu = 4.0De^{0.464}Pr^{-0.755}$where $200 \leq De(Dean\ number) \geq 3000$, Pr>5. $j = 0.0178Re^{-0.239}$for $Re < 3000$. For wet conditions: $Nu = 19.0De^{0.464}Pr^{-0.755}$where $200 \leq De \geq 3000$, Pr>7. $j = 0.029Re^{-0.202}$for $Re < 3000$.
7.	Nuntaphan et al. (2005b)	$j = 0.1970\ Re^{m}\left(\frac{t_f}{S}\right)^{-2.5950}\left(\frac{S_l}{S_t}\right)^{0.7905}\left(\frac{S_t}{D}\right)^{0.2391}\left(\frac{D_f}{D}\right)^{0.2761}$

		Where $m = -0.2871 + 0.5322 \left(\frac{D}{S_t}\right) - 1.2856 \left(\frac{t_f}{S}\right) + 0.1845 \left(\frac{S_l}{S_t}\right)$ Valid for $600 \leq Re \leq 2700$
8.	Pongsoi et al. (2012)	$j = 0.4132\, Re^{-0.4287}$
		Serrated fin
9.	Nir (1991)	Based on fin diameter: $St\, Pr^{2/3} = 1.0 Re_{Df}^{-0.4} W^{-0.266} R_b{}^{-0.4} K_{z,h}$ Based on tube outer diameter: $St\, Pr^{2/3} = 1.0 Re_{D}^{-0.4} W^{-0.266} R_b{}^{-0.4} \left(\frac{D_f}{D}\right)^{-0.4} K_{z,h}$ Where, W: ratio of heat transfer area of a row of tubes to free flow area, $K_{z,h}$: heat transfer correction factor which depends on number of rows.
10.	Næss (2010)	$Nu = 0.107 Re^{0.65} Pr^{1/3} \left(\frac{S_t}{D_c}\right)^{0.2} \left(\frac{h_f}{D_c}\right)^{-0.13} \left(\frac{h_f}{S}\right)^{-0.14} \left(\frac{S}{D_c}\right)^{-0.2}$ for $\frac{A_t}{A_d} < 1$ $Nu = 0.141 Re^{0.65} Pr^{1/3} \left(0.43 + 9.75 e^{-3.23\left(\frac{A_t}{A_d}\right)}\right) \left(\frac{h_f}{D_c}\right)^{-0.13} \left(\frac{h_f}{S}\right)^{-0.14} \left(\frac{S}{D_c}\right)^{-0.2}$ for $\frac{A_t}{A_d} > 1$ $A_t: transverse\ flow\ area, A_d: diagnol\ flow\ area$ Valid for $2500 \leq Re \leq 50000$
11.	Ma et al. (2012)	$Nu = 0.117 Re^{0.717} Pr^{1/3} \left(0.6 + 0.4 e^{-\frac{250\frac{h_f}{S}}{Re}}\right) \left(\frac{S_t}{S_l}\right)^{0.06}$

		Valid for $4000 \le Re \le 30000, \frac{h_f}{s} = 5 - 5.5, \frac{S_t}{S_l} = 0.75 - 1.30$
		Plain fin
12.	Kayansayan (1993)	$j = 0.15\ Re^{-0.28}\epsilon^{-0.362}$ where $\epsilon = \frac{total\ heat\ transfer\ area}{bare\ tube\ heat\ transfer\ area}$ Valid for $500 \le Re \le 30000$
13.	Wang and Chang (1996)	$j = 0.394\ {Re_c}^{-0.392}\left(\frac{t_f}{D_c}\right)^{-0.0449} N_r^{-0.0897}\left(\frac{S_f}{D_c}\right)^{-0.212}$ Valid for $800 \le Re \le 7500$
14.	Wang et al. (2000)	$j = 0.086\ {Re_c}^{P3} N_r^{P4}\left(\frac{S_f}{D_c}\right)^{P5}\left(\frac{S_f}{D_h}\right)^{P6}\left(\frac{S_f}{S_t}\right)^{-0.93}$ Where: $P3 = -0.361 - \frac{0.042N_r}{\ln(Re_c)} + 0.158ln\left[N_r\left(\frac{S_f}{D_c}\right)^{0.41}\right]$ $P4 = -1.224 - \frac{0.076\left(\frac{S_l}{D_h}\right)^{1.42}}{\ln(Re_c)}$ $P5 = -0.083 + \frac{0.058N_r}{\ln(Re_c)}$ $P6 = -5.735 + 1.211ln\left(\frac{Re_c}{N_r}\right)$ $D_h = 4\frac{A_cL}{A_o}$

		L is the depth of the heat exchanger along the flow direction.
15.	Pirompugd et al. (2005)	$j = 1.49\, Re_c^{0.002061N-0.625} N_r^{-0.0575}(0.00583N_r + 0.825)\varepsilon^{-0.001921N+0.068}$ Where: $\varepsilon = \dfrac{total\ heat\ transfer\ area}{bare\ tube\ heat\ transfer\ area}$
16.	Pirompugd et al. (2007)	For N_r=1, (Fully wet conditions) $j_{1,f} = 0.5284\left(\dfrac{S}{D_c}\right)^{0.5440} Re_c^{\left(0.1001\frac{S}{D_c}-0.6529\frac{S_l}{D_c}-0.06752\frac{S_t}{D_c}-0.3734\right)} \varepsilon^{0.7519}$ For N_r=1, $0.65<\frac{A_w}{A_o}<1$, (Partially wet conditions) $j_{1,p} = j_{1,f}\left(\dfrac{S}{D_c}\right)^{-1.1918} Re_c^{\left(1.0816\frac{S}{D_c}-0.06438\frac{S_l}{D_c}-0.1133\frac{S_t}{D_c}-0.05124\right)} \left(\dfrac{A_w}{A_o}\right)^{-1.1861}$ For N_r>1, (Fully wet conditions) $j_{N,f} = j_{1,f} N^{0.2310}\left(\dfrac{S}{D_c}\right)^{(-0.04426N-0.08561)} Re_c^{\left(0.02940N-0.1308\frac{S}{D_c}+0.03457\frac{S_l}{D_c}+0.04793\frac{P_t}{D_c}-0.1560\right)} \varepsilon^{(-0.1407N-0.08005)}$ For N_r>1, (Partially wet conditions)

		$$j_{N,p} = j_{N,f} N^{-0.07957} \left(\frac{S}{D_c}\right)^{(-0.06148N+0.07271)} Re_c^{\left(-0.00885N+0.06733\frac{S}{D_c}+0.006928\frac{S_l}{D_c}+0.005305\frac{P_t}{D_c}-0.02962\right)} \left(\frac{A_w}{A_o}\right)^{(0.03322N-0.3148)}$$
17.	Xie et al. (2009)	$$Nu = 1.565 Re^{0.3414} \left(N\frac{S_f}{D}\right)^{-0.165} \left(\frac{S_t}{S_l}\right)^{-0.0558}$$ Valid for : $Re = 1000 - 6000$.
18.	Choi et al. (2010)	$$j_{inline} = 0.8692\, N^{-0.0981} Re^{-0.5971} \left(\frac{S}{D}\right)^{0.0996} \left(\frac{F_s}{D}\right)^{-2.1720}$$ $$j_{staggered} = 1.4534\, N^{-0.0681} Re^{-0.6722} \left(\frac{S}{D}\right)^{0.0652} \left(\frac{F_s}{D}\right)^{-0.0058}$$ Valid for: $Re = 500 - 800$. Where F_s is the vertical fin spacing in the paper.
19.	Paeng et al. (2010)	$$Nu_{exp} = 0.049\, Re^{0.784}$$ $$Nu_{num} = 0.097\, Re^{0.671}$$ Valid for: Re= 1082-1649.
		Wavy fin

20.	Mirth and Ramadhyani (1994)	$$Nu = 0.0197 {Re_s}^{0.94} \left(\frac{S_t - D_c}{2S}\right)^{-0.3} \left\{1 + \frac{111,900}{\left[Re_s\left(\frac{L}{2S}\right)\right]^{1.2}}\right\} Pr^{1/3}$$ L is the length of the coil. Valid for: $440 < Re_s < 1680$.
21.	Wang et al. (1997)	$$j = \frac{1.201}{[\ln({Re_s}^{\sigma})]^{2.921}}$$ Valid for: $372 < Re_c < 7456$.
22.	Wang et al. (2000)	$$\frac{(\eta h A_o)_w}{(\eta h A_o)_{plain}} = 1.075 \left(\frac{P_d}{S_f}\right)^{0.1425-0.03884N}$$ P_d is the wave height here. Subscript plain is for plain fin. Valid for: $150 < Re_c < 1800$.
23.	Pirompugd et al. (2006)	$$j = 0.171\, \varepsilon^{0.377N} Re_c^{(-0.0142N-0.478)} \left(\frac{S}{D}\right)^{(0.00412N-0.0217)} \left(\frac{A_o}{A_b}\right)^{(-0.114+0.440)}$$ ε is the fin factor here defined in the paper.
24.	Kuvannarat et al. (2006)	$$j = 0.213262\, N^{0.09891} Re_c^{-0.51507} \left(\frac{t_f}{S_l}\right)^{0.072448} \left(\frac{A_o}{A_b}\right)^{0.600543}$$
25.	Pirompugd et al. (2008)	For N_r=1, (Fully wet and partially wet conditions) $$j_1 = 6.6412 \left(\frac{S_l}{D_c}\right)^{-0.00085} \left(\frac{S_t}{D_c}\right)^{-2.1461} Re_c^{\left(-0.2636\frac{S}{D_c}-0.00091\frac{S_l}{D_c}+0.1558\frac{S_t}{D_c}-0.8865\right)}$$ For N_r>1, (Fully wet conditions)

		$j_{N,f} = j_1 N^{-0.06451}\left(\frac{S}{D_c}\right)^{(-0.1219N+0.7381)} Re_c^{\left(0.03475N+0.1145\frac{S}{D_c}+0.00521\frac{S_l}{D_c}-0.03498\frac{P_t}{D_c}-0.04374\right)} \varepsilon^{(-0.1616N+0.6105)}$ For $N_r>1$, (Partially wet conditions) $j_{N,p} = j_{N,f} N^{-1.7838}\left(\frac{S}{D_c}\right)^{(-0.9459N+3.9329)} Re_c^{\left(-0.1554N+1.1667\frac{S}{D_c}+0.2253\frac{S_l}{D_c}-0.1645\frac{P_t}{D_c}+0.7158\right)} \left(\frac{A_w}{A_o}\right)^{(0.6919N-4.7697)}$ Valid for: $525 < Re_c < 7650$.
		Slit fin
26.	Du and Wang (2000)	$j = 5.98 Re_c^{j1}\left(\frac{S}{D_c}\right)^{j2} N_r^{j3}\left(\frac{S_w}{S_h}\right)^{j4}\left(\frac{S_t}{S_l}\right)^{-0.804}$ Where $j1 = -0.647 + \frac{0.198N}{\ln(Re_c)} - 0.458\left(\frac{S}{D_c}\right) + 0.458\left(\frac{N_r}{Re_c}\right)$ $j2 = 0.116 + \frac{1.125N}{\ln(Re_c)} + 47.6\left(\frac{N_r}{Re_c}\right)$ $j3 = 0.49 + \frac{175\frac{S}{D_c}}{\ln(Re_c)} - \frac{3.08}{\ln(Re_c)}$

		$$j4 = -0.63 + 0.086S_n$$ Valid for: $200 < Re_c < 8000$.
Plain fins with delta winglet		
27.	Tang et al. (2009)	$$j = 43.28Re^{-0.501}(\sin\alpha)^{0.0143}\left(\frac{V_h}{V_l}\right)^{0.04}$$ Valid for: $4000 < Re < 10000$. Where V_h= winglet height, V_l= winglet length, α = winglet attack angle

Table 2.6. Summary of published correlations (pressure drop)

Sr. No.	Author and year	Correlation
		Annular fin
1.	Robinson and Briggs (1966)	$Eu = 18.9Re^{-0.316}(\frac{S_t}{D})^{-0.927}N_r$
2.	Nir (1991)	Based on fin diameter: $f = 2.12Re_{Df}^{-0.25}W^{-0.55}K_{z,P}$ Based on tube outer diameter: $f = 2.12Re_D^{-0.25}W^{-0.55}\left(\frac{D_f}{D}\right)^{-0.25}K_{z,P}$ Where, W: ratio of heat transfer area of a row of tubes to free flow area, $K_{z,P}$: Pressure drop correction factor which depends on number of rows.
3.	Pongsoi et al. (2013)	$f = 0.4852Re_c{}^{-0.2156}\left(\frac{f_p}{D_c}\right)$
		Crimped fin
4.	Nuntaphan et al. (2005a)	For inline: $f = 0.1635\ Re^{-0.4172}\left(\frac{t_f}{S}\right)^{-0.5215}\left(\frac{S_l}{S_t}\right)^{-1.2235}\left(\frac{S_t}{D}\right)^{-0.6334}\left(\frac{D_f}{D}\right)^{1.2000}$ For staggered: $f = 2.1768\ Re^{-0.2679}\left(\frac{t_f}{S}\right)^{-0.2468}\left(\frac{S_l}{S_t}\right)^{1.8680}\left(\frac{S_t}{D}\right)^{0.3011}\left(\frac{D_f}{D}\right)^{-0.4470}$

		Valid for $600 \leq Re \leq 2700$
5.	Nuntaphan et al. (2005b)	$f = 17.02\, Re^{-0.5636} \left(\frac{t_f}{S}\right)^{-0.3728} \left(\frac{S_l}{S_t}\right)^{1.2804} \left(\frac{S_t}{D}\right)^{0.3956} \left(\frac{D_f}{D}\right)^{0.1738}$ Valid for $600 \leq Re \leq 2700$
6.	Pongsoi et al. (2012)	$f = 0.3775\, Re^{-0.1485} \left(\frac{S_f}{D}\right)^{0.4321}$
		Serrated fin
7.	Nir (1991)	Based on fin diameter: $f = 1.24 Re_{Df}^{-0.25} W^{-0.32} K_{z,P}$ Based on tube outer diameter: $f = 1.24 Re_{D}^{-0.25} W^{-0.32} \left(\frac{D_f}{D}\right)^{-0.25} K_{z,P}$ Where, W: ratio of heat transfer area of a row of tubes to free flow area, $K_{z,P}$: Pressure drop correction factor which depends on number of rows.
8.	Kawaguchi et al. (2004)	For spiral annular fin: $f = 18.6\, {Re_h}^{-0.228} \left(\frac{S_f}{t_f}\right)^{-0.872}$ Valid for: $600 \leq Re_h \leq 27000$, $2.95 \leq \frac{S_f}{t_f} \leq 4.39$ For spiral serrated fin: $f = 6.46\, {Re_h}^{-0.179} \left(\frac{S_f}{t_f}\right)^{-0.354}$ Valid for: $3000 \leq Re_h \leq 30000$, $3.07 \leq \frac{S_f}{t_f} \leq 5.07$

9.	Næss (2010)	$$Eu = \left(0.24 + \frac{8.2}{Re^{0.5}}\right) min\left(1, 0.52 + 964.5e^{-3.24\left(\frac{S_t}{S_l}\right)}\right)\left(\frac{h_f}{D_c}\right)^{0.18}\left(\frac{S}{D_c}\right)^{-0.74}$$ Valid for $2500 \leq Re \leq 50000$
10.	Ma et al. (2012)	$$Eu = 1.773\ Re^{-0.184}\left(\frac{h_f}{S}\right)^{0.556}\left(\frac{S_t}{D}\right)^{-0.673}\left(\frac{S_l}{D}\right)^{-0.133}$$ Valid for $4000 \leq Re \leq 30000, \frac{h_f}{S} = 5 - 5.5, \frac{S_t}{D} = 2.3 - 3.2, \frac{S_l}{D} = 2.4 - 3.1.$
		Plain fin
11.	Wang and Chang (1996)	$$f = 1.039\ Re_D{}^{-0.418}\left(\frac{t_f}{D_c}\right)^{-0.104} N_r^{-0.0935}\left(\frac{S_f}{D_c}\right)^{-0.197}$$ Valid for $800 \leq Re \leq 7500$
12.	Wang et al. (2000)	$$f = 0.0267\ Re_c{}^{F1}\left(\frac{S_t}{S_l}\right)^{F2}\left(\frac{S_f}{D_c}\right)^{F3}$$ Where: $$F1 = -0.764 + \frac{0.739S_t}{S_l} + 0.177\frac{S_f}{D_c} - \frac{0.00758}{N_r}$$ $$F2 = -15.689 + \frac{64.021}{\ln(Re_c)}$$ $$F3 = 1.696 - \frac{15.695}{\ln(Re_c)}$$

13.	Xie et al. (2009)	$$f = 20.713Re^{-0.3489}\left(N\frac{S_f}{D}\right)^{-0.1676}\left(\frac{S_t}{S_l}\right)^{-0.6265}$$ Valid for: $U_{fr} = 0.67 - 4.0\frac{m}{s}, Re = 1000 - 6000, D = 16 - 20\ mm, S_f = 2 - 4\ mm, S_t = 38 - 46\ mm, S_l = 32 - 36\ mm$
		Wavy fin
14.	Mirth and Ramadhyani (1994)	For coils 1-3 (refer to the paper): $f = \frac{8.64}{Re_{wh}^{0.457}}\left(\frac{2S}{wh}\right)^{0.473}\left(\frac{L}{wh}\right)^{-0.545}$ For coils 3-5: $f = \frac{0.375}{Re_{wh}^{0.368}}$ Valid for: Valid for: $440 < Re_s < 1680$.
15.	Wang et al. (1997)	$$f = \frac{16.67}{[\ln(Re_s)]^{2.64}}\left(\frac{A_o}{A_t}\right)^{-0.096} N^{0.098}$$ Valid for: $372 < Re_c < 7456$.
16.	Wang et al. (2000)	$$\frac{\Delta P_w}{\Delta P_p} = 0.64Re_c^{P1}\left(\frac{P_d}{S_f}\right)^{p2} N^{p3}\left(\frac{P_d}{D_c}\right)^{-0.6265} RH^{-0.06}$$ Where: $$p1 = -0.18934 + 0.15643exp\left(\frac{P_d}{S_f}\right)^{2.55}\left(\frac{S_f}{D_c}\right)^{0.9}$$ $$p2 = -1.21912 + 0.07457N^4\left(\frac{S_f}{D_c}\right)^3$$

		$$p3 = 0.65154 - 1.1432\left(\frac{P_d}{S_f}\right)^{3.2}\ln(Re_c)^{1.4}\left(\frac{S_f}{D_c}\right)^{1.5}$$ $$p4 = -0.34631\left(\frac{P_d}{S_f}\right)^{1.1}$$
17.	Kuvannarat et al. (2006)	$$f = 64.0542\, N^{-0.5237} Re_c^{-0.69284}\left(\frac{t_f}{S_l}\right)^{-0.98371}\left(\frac{A_o}{A_b}\right)^{-0.54736}$$
	Slit fin	
18.	Du and Wang (2000)	$$f = 0.1851 Re_c^{f1}\left(\frac{S}{D_c}\right)^{f2} N_r^{j-0.046}\left(\frac{S_w}{S_h}\right)^{f3}$$ Where $$f1 = -1.485 + 0.656\frac{S}{D_c} + 0.855\left(\frac{S_t}{S_l}\right)$$ $$f2 = -1.04 - \frac{125}{Re_c}$$ $$f3 = -0.83 + 0.117 S_n$$ Valid for: $200 < Re_c < 8000$.
Plain fins with delta winglet		

19.	Tang et al. (2009)	$$f = 0.9856Re^{-0.571}(\sin\alpha)^{0.0086}\left(\frac{V_h}{V_l}\right)^{0.0014}$$ Valid for: 4000 < Re <10000. Where V_h= winglet height V_l= winglet length α = winglet attack angle

The heat transfer coefficient can be expressed in terms of the heat transfer per unit heat transfer area per unit temperature difference and in terms of the Colburn factor as:

$$h = \frac{Q}{A\,(T_a - T_m)} = \frac{\mu c_p}{Pr^{2/3} D_h} Re\, j \qquad \dots (2.7)$$

$$\text{or } h = \frac{Q}{\beta V\,(T_a - T_m)} \qquad \dots (2.8)$$

The pumping power per unit surface area can be expressed as:

$$P_n = \frac{P_p}{A} = \frac{\mu^3}{2\rho^2 D_h^3} Re^3\, f \qquad \dots (2.9)$$

$$\text{Or } P_p = P_n A = P_n \beta V = \frac{\dot{m}\,\Delta P}{\rho} \qquad \dots (2.10)$$

From the above equations (4-7), it can be observed that a high value of h vs P_n plot indicates a more compact volume of the heat exchanger. However, this method considers a constant heat transfer coefficient throughout the depth of the heat exchanger, which is not the case in reality. Another method to determine the volume goodness factor was developed by Kays and London (1950), which compares the heat transfer per unit heat exchanger volume and per unit temperature difference (Z) with the power provided per unit heat exchanger volume (E).

$$Z = \frac{\eta h A}{L A_{fr}} \qquad \dots (2.11)$$

$$E = \Delta P \left(\frac{\dot{m}}{\rho_m}\right) \frac{1}{L A_{fr}} \qquad \dots (2.12)$$

A high value of Z with respect to E indicates a more compact heat exchanger. The method developed by Kays and London has been used by most of the authors.

In both the volume goodness factors following quantities are kept constant: (1) heat transfer rate, (2) pressure drop, (3) temperature difference between the surface and the fluid, and (4) fluid flow rate.

Therefore, along with the high heat transfer coefficient and lower pressure drop, the area goodness factor and the volume goodness factors are important in order to design a more compact and economical heat exchanger.

2.4.2. Classification based on fin type

In this Section all the previous studies are divided based on the fin types considered in the present review, and these are: (A) annular fins, and (B) plate fins, and each of these are further divided into four types of fins. For annular fins, the fin types are: (1) plane annular fins (2) serrated fins, (3) crimped spiral fins, (4) perforated fins, and for the plate fins, the fin types are (1) plain plate fins, (2) wavy plate fins, (3) plate fins with DWP, and (4) slit and strip fins. The schematic of these fins is given in Figs. 2.2 and 2.3.

2.4.2.1. Annular fins

2.4.2.1.1. Plain annular fins

The annular fins are made up of rectangular plates, which are wrapped around a circular or elliptical tube (Fig. 2.2A). These fins have been used widely in the industry in the air cooling application. Briggs and Young (1963), and Robinson and Briggs (1966) proposed empirical correlations on the heat transfer and pressure drop characteristics of plain circular finned tubes in staggered tube arrangement and are given in Tables 2.5 and 2.6. Webb (1994) provided a survey of published correlations of heat transfer and pressure drop on circular finned-tubes. He concluded that, all the correlations are empirical and they cannot be generalized, therefore, a single correlation could not be recommended for the practical use. Idem et al. (1990, 1993) carried out experiments on the heat transfer and pressure drop for circular finned tubes in inline

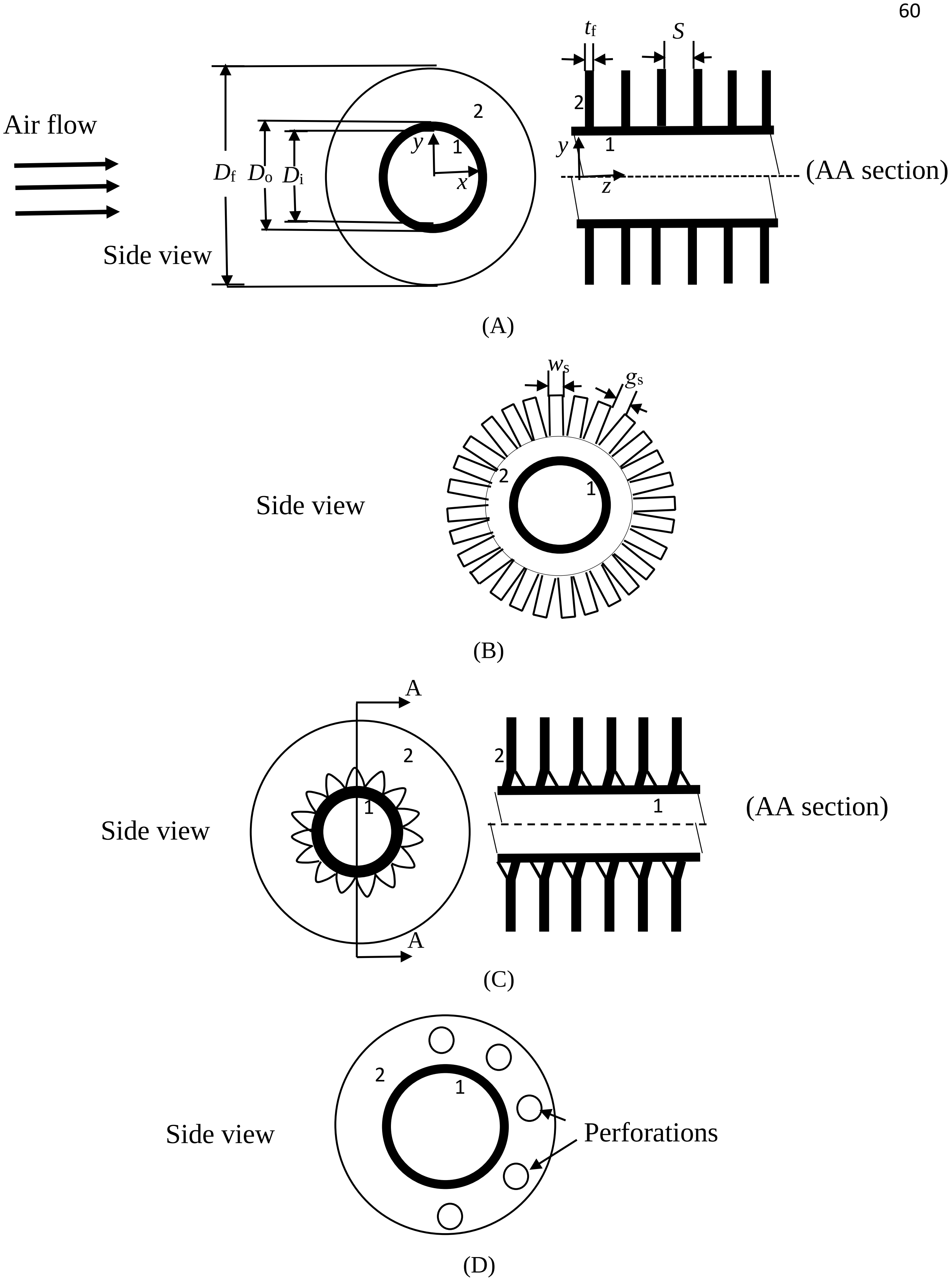

Fig. 2.1. Schematic representation of annular fins, (A) plain annular fin, (B) serrated fin, (C) crimped spiral fin, (D) perforated fin. [(1) tube surface, (2) fin surface]

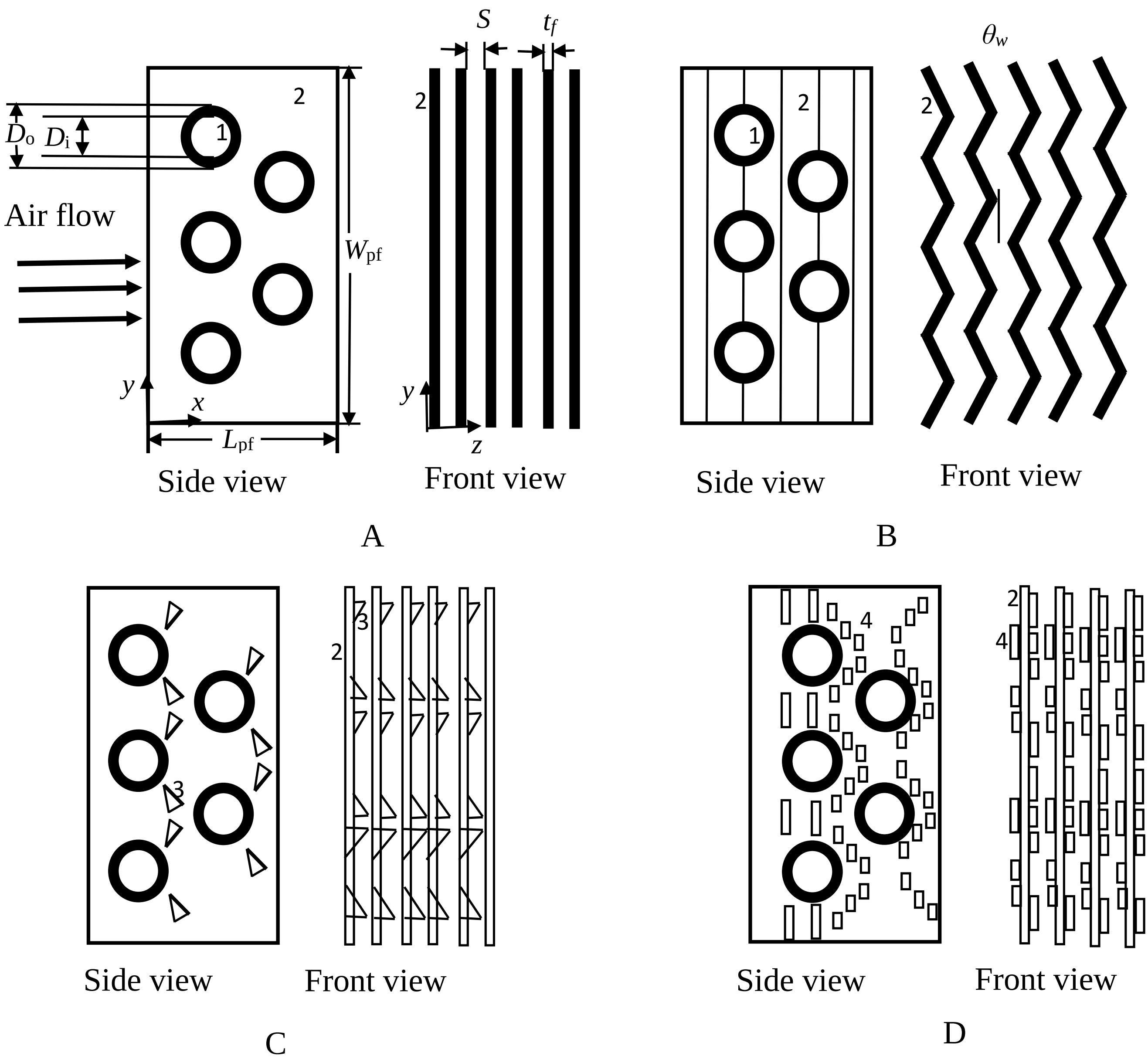

Fig. 2.2. Schematic representation of plate fins, (A) plain plate fin, (B) wavy plate fin, (C) plate fin with delta winglet, (D) plate fin with slits. [(1) tube surface, (2) fin surface, (3) delta winglets, (4) slits]

arrangement. Brauer (1964) was the first one to study elliptical finned tubes in dry conditions. Only few experimental studies were carried out on elliptical tubes in dry conditions prior to 1990s.

The Correlations available in the literature prior to 1990s for annular finned tubes were based on the assumption of uniform convective heat transfer coefficient on the fin surface, and the local flow phenomenon was not understood. Hu and Jacobi (1993) performed experiments on 1-row annular-finned tube using the naphthalene sublimation technique to understand the flow physics. *Sh* distribution on the fin surface was measured, and then, the heat and mass transfer analogy was used to obtain the heat transfer and the fin efficiency.

Jang and Yang (1998) performed experimental as well as numerical studies in both the dry and the wet conditions for the annular circular and elliptical finned tubes. The heat transfer coefficient was found to be larger for the wet coils as compared to the dry coils for the circular as well as for the elliptical tubes. The heat transfer per unit pressure drop was 50% higher for the elliptical tubes as compared to the circular tubes.

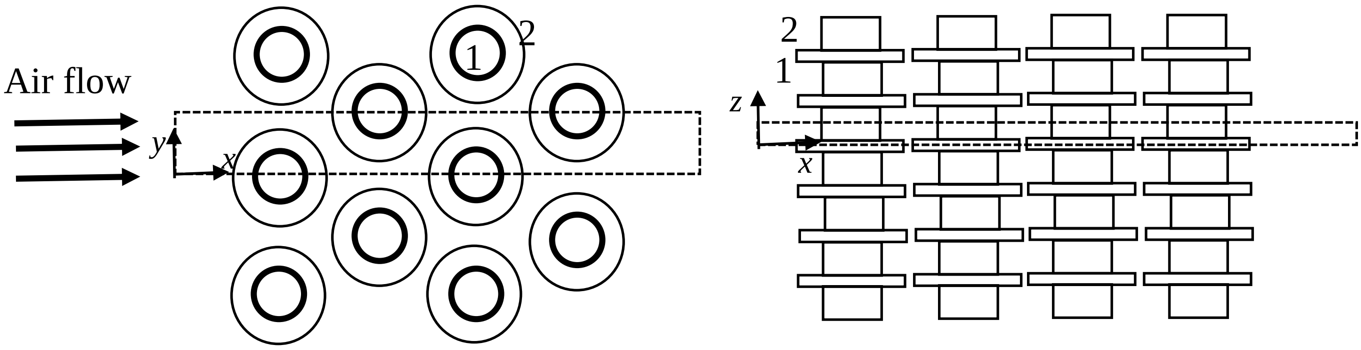

Fig. 2.3. Computational domain of (Mon and Gross, 2003).

In the studies of Hu and Jacobi (1993) and Jang and Yang (1998), the effect of fin spacing and other parameters was not investigated. This motivated Watel et al. (1999) to perform the experiments to study the effect of fin spacing and Reynolds number on the *Nu* of the annular finned tube. The *Nu* increased with an increase in the fin spacing, because at larger fin spacing, there was no interaction between the boundary layers developed at two fin surfaces. After studying the effect of the fin spacing on the convective heat transfer, Watel et al. (2000a) and Watel et al. (2000b) performed experiments to study the heat transfer from a rotating annular fin subjected to an external air flow and concentrated only on the forced convection part.

To incorporate the fin efficiency, Mon and Gross (2004) performed numerical study to investigate the thermal-hydraulic performance of the annular-finned tubes for a range of $8.6 \times 10^3 \leq Re \leq 4.3 \times 10^4$. The numerical domain is shown in Fig. 2.4 (similar type of computational domain has been used by other authors as well). They observed that, the hydrodynamic boundary layer starts developing from the leading edge of the fin, and reaches a maximum thickness at the fin-tube junction. A maxima in the heat transfer coefficient was found at particular fin spacing. Chen and Hsu (2008) developed a finite difference method in conjunction with the least square method and the temperature measurements to predict the temperature distribution and the local heat transfer coefficient on the fin surface. It was observed that, the heat transfer coefficient was highest on the bottom part of the fin as compared to the top portion of the fin (approximately 9 times). The heat transfer coefficient increased and the fin efficiency (η) decreased with the fin spacing. Pongsoi et al. (2013) performed experiments to study the air side performance of the L-footed spiral annular fins. The effect of the fin spacing was studied on the air side performance of the heat exchangers. The average heat transfer rate and the average pressure drop increased with a decrease in the fin spacing. Pathak et al. (2015) carried out numerical and experimental investigation on a sodium to air heat exchanger. Correlations were proposed for the Nusselt number and the fin effectiveness.

2.4.2.1.2. Serrated fins

The serrated fins are made up by cutting the tip of the plain annular fins into many segments or by attaching segments on the rectangular strip. Fig. 2.1B shows the schematic of the serrated fins, the front view (AA section) of the serrated fin is similar to the front view of the plain annular fin and is not given. Further, only segment parameters are shown in the Fig. 2.1B (fin-tube parameters are similar to that of the plain annular fin). The boundary layer breakup by these segments is the attractive feature of the serrated fins, which enhance mixing and heat transfer, however, it gives rise to more pressure drop as well. Previous studies on the serrated fins focus mostly on its heat transfer per unit pressure drop performance as compared to the plain annular fin. Nir (1991) argued that the published correlation for the heat transfer and pressure drop characteristics of the finned-tube banks have been formulated based only on the data, and the understanding of the flow patterns has not been considered. Therefore, they tried to modify the previous correlations based on the understanding of the flow patterns and proposed new correlations for the plain and segmented annular fins. Hashizume et al. (2002) carried out analytical and experimental investigation to study the fin efficiency of the serrated fins. The analytical model was developed based on two assumptions: (1) uniform heat transfer coefficient on the fin surface, and (2) no heat transfer from the tip of the fins. The comparison of heat transfer and pressure drop characteristics of the spiral annular fins and serrated fins was first presented by Kawaguchi et al. (2004). For a fin pitch of 5 mm, for the serrated fins, the friction factor was found to be 1.15 times the friction factor for the spiral fins. The turbulence generated by the serrated fins was believed to be the reason for this increase in the friction factor. Næss (2010) performed experiments on the serrated-finned-tube heat exchangers to study the effect of the tube bundle layout, the tube and the fin geometry. It was found that, *Nu* shows a maxima when the flow areas in the transverse and diagonal directions become equal.

Martinez et al. (2010) performed experiments to study the heat transfer and pressure drop characteristics of helically segmented-finned-tube heat exchangers and compared the results with the correlations of Weierman (1976), Weierman et al. (1978), Nir (1991), Ganapathy (2003) and Kawaguchi et al. (2004). The correlation of Kawaguchi et al. (2004) was recommended for the heat transfer design of the compact heat exchanger. In the cases where the finned tube geometry and fluid conditions were outside the range of Kawaguchi's correlations, the Weierman's correlation was recommended.

The experimental investigations on the serrated fins gives its thermal-hydraulic performance, however to obtain the 3D flow pattern, 3D numerical simulations are required. For this purpose, Lemouedda et al. (2011) performed numerical investigation It was found that the serrated fin gives 9% more heat transfer as compared to the plain fin with same heat transfer area. However, with the same height the plain fin and serrated fin performed equally well.

Further, the segments were twisted from 0° to 25° and it was found that the heat transfer performance increases up to an angle of 15° and then it decreases. Ma et al. (2012) carried out experimental investigation to study the effect of fin spacing, fin height, tube pitches on the heat transfer and the pressure drop characteristics of the serrated finned tubes. A critical *Re* was found, above which the effect of the h_f/S ratio on the heat transfer was negligible. The transverse tube pitch had negligible effects on the heat transfer, whereas, the heat transfer was affected by the longitudinal tube pitch. The correlations were given for *Nu* and *Eu*. Martinez et al. (2015) performed numerical simulations to study the turbulent flow over a finned-tube bundle with periodic boundary conditions. The effect of implementation of the periodic boundary conditions on k and ε was observed on the local physical properties. The numerical results were in good agreement with the experimental data and correlations from the literature.

2.4.2.1.3. Crimped spiral fins

The crimped spiral fins are shown in Fig. 2.2C, and the geometrical parameters are same as shown for the plain annular fin and are not shown. These fins are designed to produces more disturbance in the air flow as compared to the plain annular fins, which should enhance the turbulence and mixing in the flow and hence is expected to enhance the heat transfer. However, the design of the fin must be optimized to minimize the increase in the pressure loss due to more resistance to the flow. In the literature prior to 2004, only plane annular fins were studied and the first study on crimped spiral fins was performed by Nuntaphan et al. (2005a). They investigated the effects of fin spacing, tube diameter, and fin height and tube arrangement on the heat transfer and pressure drop of the exchanger. For both inline and staggered arrangements, it was observed that, the pressure drop increases and the heat transfer coefficient decreases with an increase in the tube diameter. In a similar manner, Nuntaphan et al. (2005b) investigated 10 samples of crimped spiral-finned-tube heat exchangers in the dehumidifying conditions. It was found that, the heat transfer coefficient for a wet surface was lower as compared to the dry surface for *Re* < 2000. At smaller fin spacing, the heat transfer rate was lower, this was due to the enhanced resistance offered by the condensate, therefore leading to more airflow bypass.

Naphon and Wongwises (2005) presented the inside and outside heat transfer coefficients for the spirally coiled finned tube heat exchanger under dry and wet surface conditions. The heat transfer coefficient increased rapidly with an increase in the air mass flow rate but was unaffected by the T_{ai}. Correlations were proposed for *Nu* and the Colburn factor for the dry and the wet surface conditions. Wongwises and Naphon (2006a) extended their study on the spirally-coiled-finned-tube heat exchangers and performed experiments under wet-surface conditions. Similar to the study in the wet surface conditions Wongwises and Naphon (2006b) performed experiments in the dry surface condition. The effect of the air mass flow rate was significant on the heat exchanger effectiveness and heat transfer, whereas, the effect of the water mass flow rate on these quantities was negligible.

Earlier in this section, we have discussed the study performed by Nuntaphan et al.. (2005a) on the effect of fin pitch on the air side heat transfer coefficient for spiral-finned-tube heat exchanger. However, the frontal velocity was in the range of $0.5 \leq U_{fr} \leq 1.5$ m/s, which has been considered to be low for the commercial applications. This motivated Pongsoi et al. (2011) to perform the experimental study to investigate the effect of fin pitch, Reynolds number, fin material and number of tube rows on the air side performance of the spiral-finned-tube heat exchanger for a frontal velocity range of $2 \leq U_{fr} \leq 6$ m/s . They argued that the effect of fin pitch was very small on the Colburn factor due to high value of *Re* in their study. Pongsoi et al. (2012a) studied the effect of number of tube rows on the performance of the crimped spiral-finned-tube heat exchanger with multipass semi-parallel-and-counter current flow configuration. It was found that the number of tube rows does not affect the Colburn factor and the friction factor beyond a Re > 2000. The reason was believed to be the shedding of the downstream turbulence eddies, which causes good mixing. In the similar study on the same experimental setup Pongsoi et al. (2012b) studied the effect of number of tube rows along with the variation in the fin height. After performing the studies on the effect of the fin spacing, number of tube rows and fin height on the air side heat transfer, Pongsoi et al. (2012c) tried to optimize the heat exchanger with respect to the fin spacing for a crimped-spiral-finned-tube heat exchanger.

2.4.2.1.4. Perforated fins

The plain annular fin has been investigated by many researchers in the past as we have discussed in Section 2.3.1.1. Banerjee et al. (2012) modified the plain annular fins with perforations on the fin (Fig. 2.2D). The heat transfer and pressure drop characteristics were studied with different locations of the perforations using numerical simulations. The $Q/\Delta P$ ratio was found to be 1.23 and 1.05 for two particular perforation locations with respect to the solid fins. The non-uniform fin spacing was also found to be beneficial and for two different cases, and the pressure drop was found be lower than the uniform fin spacing case.

2.4.2.2. Plate fins

2.4.2.2.1. Plain plate fins

Plain plate fins are used extensively in the air cooled heat exchangers (Fig. 2.2A) (now onwards in the paper plain plate fin will be referred as plain fin). Rich (1973) provided a survey of the published work relating to the heat transfer of multi-row plate finned-tube heat exchangers in the form of average heat transfer coefficients. The quantitative data on the heat transfer for 2-rows plate-finned-tube heat exchanger was not known prior to 1975. This motivated Saboya and Sparrow (1976) to apply the heat and mass transfer analogy in conjunction with the naphthalene sublimation technique to investigate the heat transfer for a two row plate-finned-tube heat exchanger for a range of $211 \leq Re_{\mathrm{h}} \leq 1089$. Rich (1973, 1975) examined the effects of fin spacing, and number of tube rows ($2 \leq N_{\mathrm{r}} \leq 6$) for heat exchangers.

Elmahdy and Biggs (1979) determined the m exponent of Reynolds number for $200 \leq Re \leq 2000$. McQuiston (1981) developed a simple correlation for the Colburn factor for four row staggered bank of plain fins for $100 \leq Re \leq 4000$. In all these previous studies, the range of the Reynolds number was very small. Therefore, to consider a larger range of Reynolds number ($100 \leq Re \leq 30000$), Kayansayan (1993) performed experiments with 10 samples of heat exchangers. The Colburn factor was presented with respect to the varying Finning factor (ratio of total heat transfer area to the tube outside area) and the Colburn factor decreased as the Reynolds number was increased. Rocha et al. (1997) performed 2D numerical simulations to study 1-row and 2-row circular and elliptical plate-finned-tube heat exchangers for range of $299 \leq Re_h \leq 1576$. It was found that the elliptical arrangement with $e = 0.5$ and two rows of tubes was the most efficient arrangement, and the efficiency of the elliptical arrangement was 18 % higher than the circular arrangement.

In HVAC&R applications, the use of smaller diameter tubes has been very popular. Wang et al. (1996) focused their study on the smaller diameter tubes ($D = 9.52$ mm) and carried out experiments in an open wind tunnel with 15 samples of heat exchangers. The effect of fin spacing on the Colburn factor and the friction factor was negligible. Wang and Chi (2000) and Wang et al. (2000a) carried forward the study on smaller diameter tubes (7 mm $\leq D \leq$ 9.52 mm) and investigated 18 samples of heat exchangers (1.22 mm $\leq f_p \leq$ 2.3 mm, $2 \leq N_r \leq 4$). The effect of fin pitch on the Colburn factor was negligible for $N_r > 4$ and $Re > 2000$. The effect of different geometrical parameters on the heat transfer performance of the air-cooled heat exchangers has been studied by many researchers as we have discussed in previous sections, however, in some studies, the results contradict. For example in similar studies, Rich (1973) and Wang et al. (1996) argued that the effect of fin pitch was negligible for plain-finned-tube heat exchangers. However when the data of Wang et al. (1996), Kayansayan (1993), McQuiston (1978a), and Seshimo and Fuji (1991) was plotted together by Wang et al. (2000b), then the effect of the fin spacing could be clearly seen on the Colburn factor. To study the deviation in the results, Wang et al. (2000b) carried out a theoretical study on the data reduction method for air-cooled heat exchangers.

The main conclusions of the study were:

(1) The energy balance in the experiments for the air side and the tube side should be less than 5%, and for better accuracy for the water side heat transfer rate, the temperature drop on the water side should be larger than 2℃.

(2) ε-NTU correlation must be used carefully for the data reduction according to the circuitry design.

Ay et al. (2002) introduced the use of Infrared thermography to determine the heat transfer coefficient for the plate-finned-tube heat exchangers in inline and staggered arrangement of tube. The heat transfer coefficient was found to be larger for the staggered arrangement as compared to the inline arrangement. Matos et al. (2004a, 2004b) carried out numerical simulations and experimental investigation to optimize the staggered circular and elliptical finned tubes in a fixed volume. Pirompugd et al. (2005) investigated the performance of the plate-finned-tube heat exchanger in the dehumidifying conditions experimentally for a range of $525 \leq Re \leq 7650$. Also, they developed a tube to tube reduction method from the method of Threkeld (1970) to analyze the performance of the heat exchanger. Erek et al. (2005) performed 3D numerical simulations to study the heat transfer and pressure drop characteristics of plate fins with varying geometrical parameters (tube center location, fin height, tube thickness, tube ellipticity and fin pitch). Various researchers have performed studies on the performance of the air cooled heat exchangers with respect to the parameters like, Reynolds number, fin spacing, number of tube rows, fin pitch. However to present a common essence for the variation of heat transfer with these parameters, He et al. (2005) performed numerical simulations and the results were explained according the field synergy principle. The synergy is defined as the angle between the velocity and the temperature gradient. The synergy principle states that the heat transfer properties of the finned geometry depend on the intersection angle between the velocity and the temperature gradient, and by minimizing this angle we can maximize the heat transfer.. The synergy and *Nu* increased with an increase in the number of tube rows, however, they did not show any significant variation for $N_r > 3$. Therefore, row number less than 3 were recommended for the practical purpose.

One way to improve the thermo-hydraulic performance is the use of electro hydrodynamic (EHD) wire electrodes. The EHD electrodes generated a high electric field in the fluid resulting in the ionization, and the ions are then driven by Coulomb force. In their path, they transfer momentum to the fluid and disturb the flow. The effect of the electro-magnetic forces on the heat transfer and friction factor has been studied for a tube, channel and tube bundles in the past. Yabe et al. (1978), Yabe et al. (1987),Yabe et al. (1991), Kulacki et al. (1983), Poulter and Allen (1986), Nelson et al. (1991), Ohadi et al. (1991), Ishiguro et al. (1991), Ogata et al. (1992), Wangnippanto et al. (2001), but Lin and Jang (2005) were the first to apply the EHD electrodes on a finned-tube heat exchanger. They studied the effects of different arrangements of electrodes, applied voltage and tube pitch on the streamline, pressure and temperature profile for a finned tube heat exchanger. As the Reynolds number was increased, the effect of EHD on the heat transfer and pressure drop decreased due to the dominance of the forced convection.

Few studies have been reported to measure the distribution of local heat transfer coefficient over a finned surface. Chen et al. (2005) developed a finite difference method in conjunction with the least square method and the temperature measurements to predict the local heat transfer coefficient on the fin surface. It was found that the distribution of the temperature and the heat transfer coefficient was not symmetric on both sides of the tube. The upstream region had higher heat transfer coefficient than the downstream side of the fin and a wake region was found to exist at the back side of the tube. Therefore, the improvements measures were recommended for the back side of the tube to enhance the heat transfer performance. In the similar manner Chen et al. (2007) applied the same method to predict the temperature distribution and average heat transfer coefficient of square fins for different air speeds and fin spacing.

Pirompugd et al. (2007a) developed a finite circular fin method (FCFM) and applied it on a plain-finned-tube heat exchanger to study the heat and mass transfer characteristics. It was observed that the fin efficiency obtained for the partial wet surface was higher as compared to the fin efficiency for the fully wet surface and was lower than the fin efficiency for the fully dry surface and the fin efficiency decreased with an increase in the relative humidity. Pirompugd et al. (2009) presented a review on the reduction methods for the heat and mass transfer of the finned-tube heat exchangers under dehumidifying conditions. It was observed that, the models based on the lumped approach (Threlkeld, EDT) were unable to predict the heat and mass transfer characteristics of the partially wet surfaces. Huang et al. (2009) applied the SDM (steepest descent method) developed by Huang et al. (2003) with commercial code CFX 4.4 to study the temperature distribution and convective heat transfer coefficient and to check the validity of the SDM. The heat transfer coefficient for the staggered arrangement was higher than the inline arrangement.

Xie et al. (2009) argued that no study had been performed for large number of rows (more than 4) with larger diameter of the tubes (greater than 13 mm). Therefore, it motivated them to perform numerical simulations to study the effect of number of tube rows, diameter of the tubes, tube pitch, and fin pitch on the thermo-flow characteristics of the larger diameter finned tubes for a range of $1310 \leq Re \leq 7700$. Choi et al. (2010) carried out experimental investigation to study the heat transfer and pressure drop characteristics of the discrete-plate-finned tubes for larger fin pitch (f_p > 8 mm). The Colburn factor for the discrete plate finned-tubes was found to be 6-11 % higher than the continuous plate-finned-tube heat exchanger for 7.5 mm ≤ f_p ≤ 15 mm. Paeng et al. (2010) carried out numerical simulations and experiments to study the convective heat transfer coefficient for the plate fins and results were compared with the results of the Kays and London (1955), Wang et al. (2000a), Gray and Webb (1986), and Kim et al. (1999). Chen and Lai (2012) applied the inverse scheme of the finite difference method in conjunction with the least square method to predict the temperature distribution and average heat transfer coefficient of two row plate finned-tube heat exchanger for different air speed and fin spacing. Taler and Oclan (2014a, 2014b) performed experiments and numerical simulations to study the gas side heat transfer coefficient of a plate-fin oval tube heat exchanger. Based on the numerical results, the correlations for the Nusselt number were obtained were validated with the experimental measurements. Similarly, Lopata and Oclon (2015) studied the effect of fouling on the local heat transfer conditions in a fin-and-tube heat exchanger using 3D numerical simulations. They proposed a new method of determining the local equivalent heat transfer coefficient. Korzen and Talor (2015) proposed a set of equations for predicting the transient thermal performance of a finned-tube heat exchanger. Sun et al. (2015) observed that heat transfer was 8.3 – 30.9% higher and the pressure drop was 20-27.3% lower for the elliptical tubes as compared to the circular tubes.

2.4.2.2.2. Wavy fins

Wavy fin pattern (Fig. 2.2B) provides a longer airflow path with boundary layer breakage at the crest of the fin, and therefore, increases the heat transfer rate. Beecher and Fagan (1987) tested 27 fin-and-tube heat exchangers, 21 of them having wavy fin geometry with three rows in staggered arrangement. Webb (1990) used a multiple regression technique to correlate Beecher and Fagan's data. Webb's correlation was able to predict 88% of the wavy fin data within ±5%, and 96% of the data was correlated within ±10%. The effect of dehumidifying conditions on the heat transfer and pressure drop characteristics of air cooled heat exchangers has been studied by many researchers in the past. For some of the researchers like Bettanini (1970), Guillory and McQuiston (1973), Myers (1967), Elmahdy (1975), Eckels and Rabas (1987), Yoshii et al. (1983) and McQuiston (1978a, 1978b), the heat transfer coefficient was higher in the wet conditions as compared to the dry conditions. On the other hand for Tree and Helmer (1976), the heat transfer characteristics obtained under dry and wet conditions were same, and for Jacobi and Goldshmidt (1990), the heat transfer coefficient was lower for the wet surface as compared to the dry surface. Mirth and Ramadhyani (1993) tried to clarify this discrepancy by performing experiments on different samples of the wavy-finned-tube heat exchangers under wet conditions for a range of $300 \leq Re \leq 1700$. A model was developed in order to evaluate the heat transfer performance by discretizing the heat exchanger coil into many segments. The results for the wet coil were compared with the correlations for the dry coils, and the results indicated that the wet surface Nu showed some deviation with the correlation for dry coils. The extent of discrepancy was different for different coils and no conclusion could be drawn from that. To resolve the issue, the sensitivity analysis was carried out. In the similar study, Mirth and Ramadhyani (1994) presented the Nusselt number data for the dry surface and wet surface and presented the correlation for Nu in the dry conditions. Wang et al. (1997) performed experiments to study the heat transfer and pressure drop characteristics for 18 samples of the wavy-finned-tube heat exchangers. Madi et al. (1998) considered 28 samples of heat exchangers consisting of the plain and the wavy fin and studied the effect of fin spacing, number of tube rows, fin thickness and tube pitch on the thermal-hydraulic performance of the heat exchangers. They proposed the correlations for the Colburn factor and the friction factor. The effect of the waffle height (h_w = 1.18 mm and 1.58 mm) on the thermal-hydraulic performance of herringbone wavy fins under dehumidifying condition was first investigated by Wang et al. (2000c). The heat transfer was found to be a strong function of the fin pitch for larger waffle height.

Wongwises and Chokeman (2003) were the first one to study the effect of fin thickness ($0.115 \leq t_f \leq 0.250$ mm) for the wavy fins for a range of $900 \leq Re \leq 5400$. It was found that for $N_r = 2$, the Colburn factor increases with an increase in the fin thickness due to the occurrence of the horseshoe vortices at the leading edge, and the friction factor also increased with the fin thickness for $f_p = 1.41$ mm and 1.81 mm, however, for $f_p = 2.54$ mm, the effect of the fin thickness on the friction factor was negligible. Wongwises and Chokeman (2005) continued their research on the wavy fin and studied the effect of fin pitch and number of tube rows on the thermal-hydraulic characteristics of the wavy-finned-tube heat exchanger. Chokeman and Wongwises (2005) performed experiments to study the effects of fin pattern and edge corrugation on the thermal-hydraulic characteristics of the wavy-finned-tube heat exchanger and performed experiments for a range of $1400 \leq Re \leq 5600$. As we have discussed in the Section 2.4.2.2.2, Pirompugd et al. (2005) performed experiments on the plain-finned-tube heat exchangers in the dehumidifying conditions. In the similar manner, Pirompugd et al. (2006) carried out experiments on the wavy-finned-tube heat exchangers in the dehumidifying conditions. Kuvannarat et al. (2006) carried forward the research of Wongwises and Chokeman (2003) in the dehumidifying conditions. It was observed that for small fin pitch ($f_p = 1.41$ mm), the heat transfer coefficient for $t_f = 0.25$ mm was 5-50% higher than for $t_f = 0.115$ mm, and the corresponding pressure drop was 5-20% higher for $t_f = 0.25$ mm. Tao et al. (2007a) carried forward the study of He et al. (2005) (discussed in Section 2.3.2.2.1) and performed the 3D numerical simulation to study the thermal-hydraulic characteristics of the wavy fin for varying wavy angle ($0° \leq \theta \leq 20°$) (Fig. 2.2B). Nu was found to be higher on the front side and lower on the back side of the tube and it decreased along the flow direction. An increase in the fin area on the front side and decrease in area on the back side of the tube was recommended for better performance of the heat exchanger.

Cheng et al. (2007) investigated the wavy fin and tube heat exchanger numerically. The main aim of the study was to simulate the heat exchanger with larger number of tube rows and to use the synergy principle to explain the results. In section 2.3.2.2.1, we discussed the finite circular fin method developed by Pirompugd et al. (2007) for a plain fin. Pirompugd et al. (2008) applied the same method on the wavy-finned-tube heat exchanger for a range of $500 \leq Re \leq 5000$. Cheng et al. (2009) carried forward their previous study [Cheng et al. (2007)] on the wavy fin and tube heat exchanger. Both *Nu* and the friction factor were higher for a larger diameter of the tube (D = 13.36 mm), however, the increase in the friction factor was higher than the increase in *Nu.* The friction factor for four waves was very large as compared to the friction factor for one and two waves, similar effect was observed for *Nu*. Tao et al. (2011) performed numerical simulations to study the effect of various parameters (Reynolds number, fin pitch, wavy angle, fin thickness, transverse tube pitch) on the heat transfer and pressure drop characteristics of the wavy-finned-tube heat exchanger. An optimized wavy angle $10° \leq \theta_w \leq 20°$ and an optimum value of fin pitch between 1.2 mm and 2 mm was recommended for the practical use.

2.4.2.2.3. Fins with vortex generators

In this section, we are going to discuss about the thermal-hydraulic properties of the fins with vortex generators (Fig. 2.3C). Four types of vortex generators (VGs) (DW= delta wing, RW= rectangular wing, RWP= rectangular winglet pair, DWP= delta winglet pair) are shown in Fig. 2.5A and in Fig. 2.5B, we have shown the dimensions of the delta winglet (c = length, $b1$ = span of the delta winglet, α = attack angle). The vortex generators produce longitudinal and transverse vortices which enhances the heat transfer on the air side. Brockmeier et al. (1993) performed numerical simulations to compare the performance of the fin with delta wings with the plain fin, off-strip fin, and louvered fins for a range of 500 ≤ *Re* ≤ 3000. It was found that, the fin with delta wing performs best out of all fin configurations.

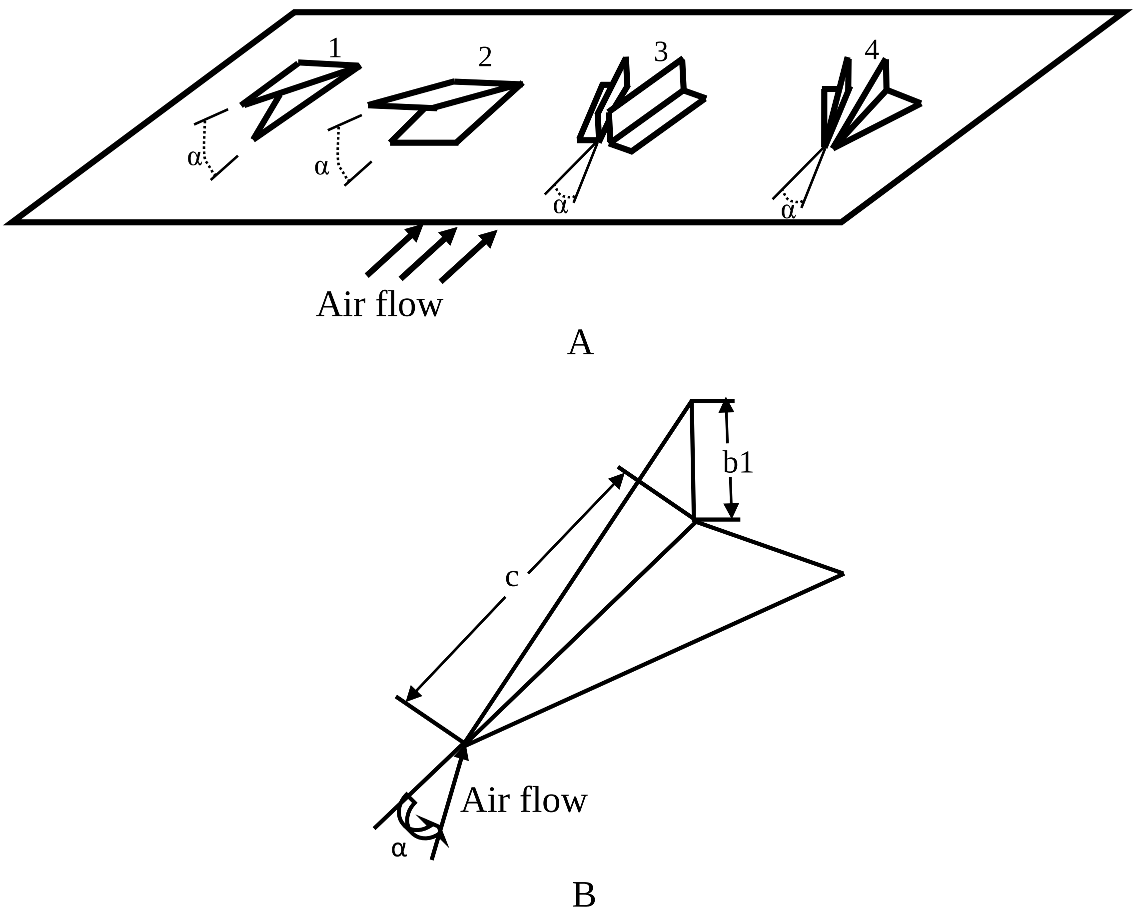

Fig. 2.4. Schematic of (A) Vortex generators, (1) delta wing, (2) rectangular wing, (3) rectangular winglet pair (4) delta winglet pair, (B) Delta winglet, c=length, b=span, α=attack angle.

Fiebig et al. (1993) performed experiments on the inline and staggered bank of finned tubes with delta winglets to study the heat transfer and pressure drop characteristics. With the VG, for the inline arrangement, the increment in *Nu* and friction factor was 55-60 % and 20-45 %, respectively, while for the staggered arrangement, the increment in the *Nu* and friction factor was 9% and 3%, respectively. Previous two studies focused on the heat transfer enhancement by the longitudinal vortices, however, the effect of the transverse vortices produced by the VGs was not considered. To study the interaction between the longitudinal and the transverse vortices, Biswas et al. (1994) performed numerical simulations in a rectangular channel with tube and winglet type vortex generator (DWP) for a range of $500 \leq Re \leq 1000$. Fiebig et al. (1994) performed the experimental investigation to study the heat transfer and pressure drop characteristics of the plate-finned-flat-tubes with DWP, and the results were compared with the results of plate-finned-round-tubes with DWP. It was observed that, the flat tubes with the DWP provided two times the heat transfer and half the friction factor as compared to the round tubes with the DWP. Tigglebeck et al. (1994) continued their work and compared the thermal hydraulic performance of a plate fin with four types of vortex generators e.g., DW, RW, DWP and RWP. DWP performed best out of all the VGs considered in the study. Fiebig et al. (1995) performed numerical investigation to study the effect of the DWP on the heat transfer and the heat transfer reversal for a plate-fin-tube heat exchanger for a range of $250 \leq Re \leq 500$.

Jacobi and Shah (1995) presented a review on the use of the longitudinal vortices as a method of the heat transfer enhancements. They reviewed the active and passive vortex methods for the enhancement of the heat transfer. Chen et al. (1998a) performed numerical investigation to study the effect of the DWP on the thermal-hydraulic characteristics of the finned oval tubes for different attack angles (α in Fig. 2.4B) and aspect ratio (AR) of the DWP. The best performance of the DWP was observed for an *AR* of 2 and an attack angle of 20°. Fiebig (1998) presented a survey on the delta and the rectangular vortex generators. The formation of the longitudinal and transverse vortices and their effect on the heat transfer enhancement was given in detail. The comparison of the rectangular and triangular vortex generators was also provided. Global heat transfer enhancement of more than 100 % over 40 times the vortex generator area could be achieved.

From all the previous studies discussed, it can be observed that the heat transfer increases as the number of rows of the DWP increases. To find out the reason behind this, Chen et al. (1998b) carried out numerical investigation to study the heat transfer enhancement due to the number of rows (3 rows in inline arrangement) of the DWP for a *Re* of 300. The interaction of the longitudinal vortices from the DWP of the first row with the longitudinal vortices caused by the DWP of the downstream rows was also explained. After studying the inline arrangement of the DWP, Chen et al. (2000) studied the staggered arrangement of the DWP. The heat transfer by the staggered arrangement was 20% more with 14.6% lower pressure drop penalty as compared to the inline arrangement. Torii et al. (2002) changed the common flow down configuration to common flow up configuration (Fig. 2.5) and studied the heat transfer and pressure drop characteristics of the new configuration for a range of $350 \leq Re_{lw} \leq 2100$. The common flow up configuration resulted in an enhancement in the heat transfer by 30 - 10% for the staggered arrangement, and 20 – 10 % for the inline arrangement, and the corresponding decrement in the pressure drop was 55-34% for the staggered arrangement and 15-8 % for the inline arrangement.

Kwak et al. (2002) carried out experimental investigation to study the effect of the DWP on the heat transfer enhancement and flow characteristics of a plate-finned-tube heat

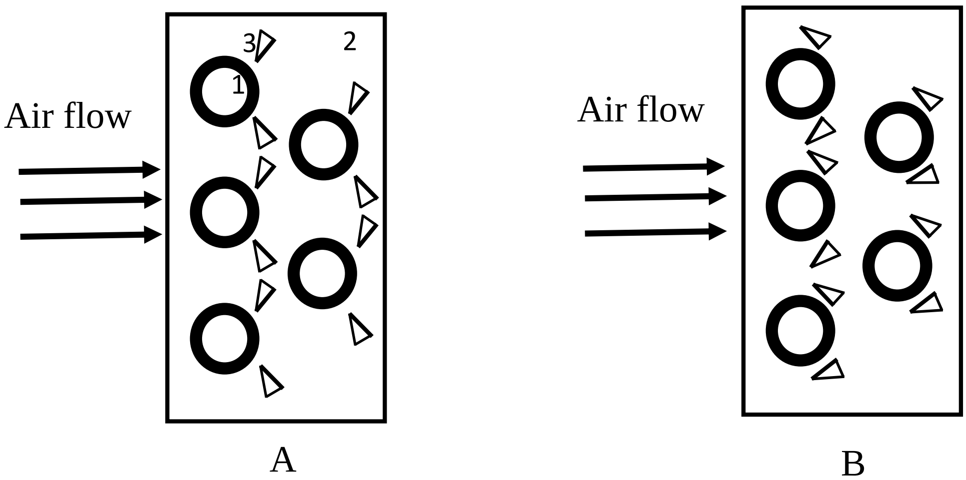

Fig. 2.5. Delta winglet pair configurations, (A) common flow down, (1) tube surface, (2) plate fin surface, (3) delta winglet, (B) common flow up.

exchanger. It was found that the inline arrangement performed better than the staggered arrangement and due to this reason, the DWPs were included in the inline arrangement. An increment of 10-25% in the heat transfer and 20-30% in the pressure drop was found with DWP included.

ElSherbini et al. (2002) argued that, in all the previous studies prior to 2002, real size heat exchangers were not used because of the experimental limitations, geometrical considerations and other restrictions. Therefore, ElSherbini et al. (2002) performed experiments to determine the effects of two sizes of delta wings on the thermal-hydraulic performance of the plate-finned-tube heat exchangers for a range of $700 < Re_{\mathrm{h}} < 2300$. Kwak et al. (2003) continued their work and performed another experimental investigation to study the effect of number of tube rows ($2 \leq N_r \leq 5$) on the heat transfer and pressure drop of plain-finned-tube heat exchanger with one row of DWP in common flow up configuration. The three row coil was found to be perform best with a 30-10% augmentation in heat transfer and a reduction of 55-34 % in the pressure drop for Reynolds number ranging from 350-2100. Kwak et al. (2005) carried forward their study and performed experiments to study the common flow up configuration of the DWP with two rows of DWP placed in a three row plate-finned-tube heat exchanger. It was concluded that the common flow up configuration performed better for the inline arrangement.

Pesteei et al. (2005) performed experiments to study the best location of the DWP for the plain-finned-tube heat exchanger and the best location for the winglet was at $\Delta x = 0.5D$ and $\Delta y = 0.5D$, where Δx and Δy were the streamwise and cross-stream distances. Joardar and Jacobi (2008) performed experimental investigation to study the effects of one row and multi rows of DWP on the thermal-hydraulic performance of the plain-fin-tube heat exchanger. The use of the DWP was restricted to the plain fins only, until Tian et al. (2009) studied the heat transfer and pressure drop characteristics of the wavy fin with the DWP in the inline and the staggered arrangements. The maximum heat transfer was observed to be 80% and 95% for the inline and staggered arrangements, respectively, as compared to the case where no DWP was present. A study which includes all the geometrical parameters for a complete optimization with small number of tubes and small diameter tubes was first performed by Zeng et al. (2010). All the parameters, fin pitch (2.5 mm $\leq f_p \leq$4.5 mm), fin thickness (0.2 mm $\leq t_f \leq$ 0.4 mm), transverse tube pitch (38 mm $\leq S_t \leq$ 54 mm), longitudinal tube pitch (32 mm $\leq S_l \leq$ 40 mm), vortex generator height (1.7 $\leq b1/2 \leq$ 2.5 mm), length (4 mm $\leq c \leq$ 6 mm) and attack angle (30° $\leq \alpha \leq$ 60°) were optimized in the study using Taguchi method (1989, 1991). Wang et al. (2015) performed numerical simulations to study the thermal-hydraulic characteristics of a novel combined winglet pairs (NCWPs) in common flow up configuration. It was observed that NCWPs provide better mixing and heat transfer per unit pressure loss as compared to the RWPs.

2.4.2.2.4. Slit fins

The slit fins are shown in Fig. 2.2D. The basic understanding of the slit fins was presented by Mullisen and Loehrke (1986), Mochizuki et al. (1987), Dejong and Jacobi (1997), and Zhang et al. (1997). Some of the studies on the slit fins were performed by comparing the performance of slit fins with the other fins, therefore, we have presented those studies in Section 2.4.2.2.5. The lack of the experiment methodology in determining the local conjugate heat transfer coefficient between the fin and tube motivated Tsai and Sheu (1998) to perform the numerical simulations to determine the local conjugate heat transfer and pressure drop for the plain and slit fins for a range of 367 $\leq Re_\mathrm{h} \leq$ 1133. The flow structure on the plain-finned-tubes was explained in details. Sheu and Tsai (1999) performed numerical simulations to determine the local conjugate heat transfer for plate and slit fins. The computational domain and numerical method was similar to the previous study [Tsai and Sheu, 1998)]. Most of the results were similar to the results of Tsai and Sheu (1998). In another study, Tsai et al. (1999)

performed numerical simulations to study the local conjugate heat transfer and pressure drop for the wavy slit fin.

Kang and Kim (1999) investigated the thermal-hydraulic characteristics of the strip fins and the effect of the location of the strips, and compared its performance with the plain fin. The recommended fin pattern is shown in Fig (2.6).

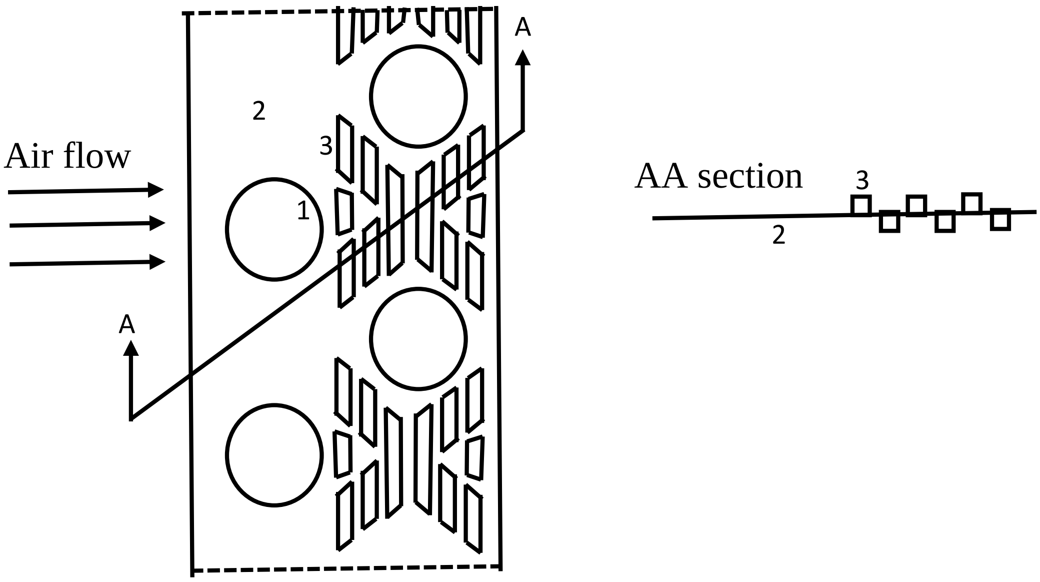

Fig. 2.6. Strip patterns recommended by Kang and Kim (1999), (1) tube surface, (2) plate fin surface, (3) slits,

Nakayama and Xu (1983) presented the heat transfer and friction factor correlations from the test performed on the three samples of slit-finned-tube heat exchangers. However, the applicability of these was very limited. Wang et al. (1999) also provided the correlations for the air-side performance of the slit-finned-tube heat exchangers. Du and Wang (2000) conducted experiments to provide an updated correlation for the air-side performance of the slit-finned-tube heat exchangers. Yun and Lee (2000) performed experiments to study the various parameters affecting the performance of the slit-fin heat exchanger using the Taguchi method. It was found that the effect of four factors, fin pitch (39%), angle of slit pattern (28%), slit length (20%), slit height (9%) among the seven factors was significant on the performance of the heat exchanger. Cheng et al. (2004) performed numerical simulations and applied the field synergy principle (explained in Section 2.3.2.2.1) to different patterns of the slotted fin surface and compared the results with the plain fin. Under the same pressure drop and same pumping power conditions, slit fin 1 (Fig. 2.7) showed a better *j*/*f* ratio as compared to the other fins.

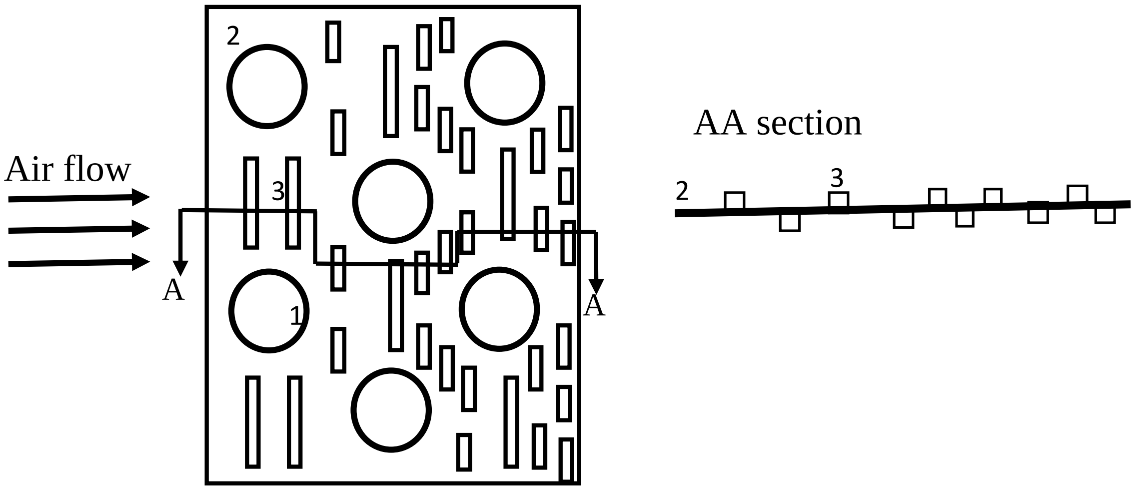

Fig. 2.7. Strip patterns recommended by Cheng et al. (2004), (1) tube surface, (2) plate fin surface, (3) slits.

Qu et al. (2004) performed numerical simulations to determine the most effective location of the strips in the plain-finned-tube heat exchanger for a range of $348 \leq Re \leq 3480$. Four different configurations of fins were used, (A) whole plain fin, (B) strips in the upstream of the fin, (C) strips in the downstream of the fin, and (D) whole strip fin. The synergy between the velocity and temperature gradient was minimum for fin D, and the fin C showed better synergy than fin B. Based on the goodness factor, the fin C (Fig. 2.8) performed best than the others for $U_{fr} <$ 2 m/s, and above this frontal velocity, fin D performed best. The studies presented so far discuss about the strip fin configuration in 'front coarse and rear dense'. Tao et al. (2006) used numerical methods to investigate the effect of strip number, strip length, strip location, and strip distribution style on the heat transfer and pressure drop characteristics of finned-tube heat exchanger. Three different convergence criteria were discussed, and it was found that only one of them gives consistent results.

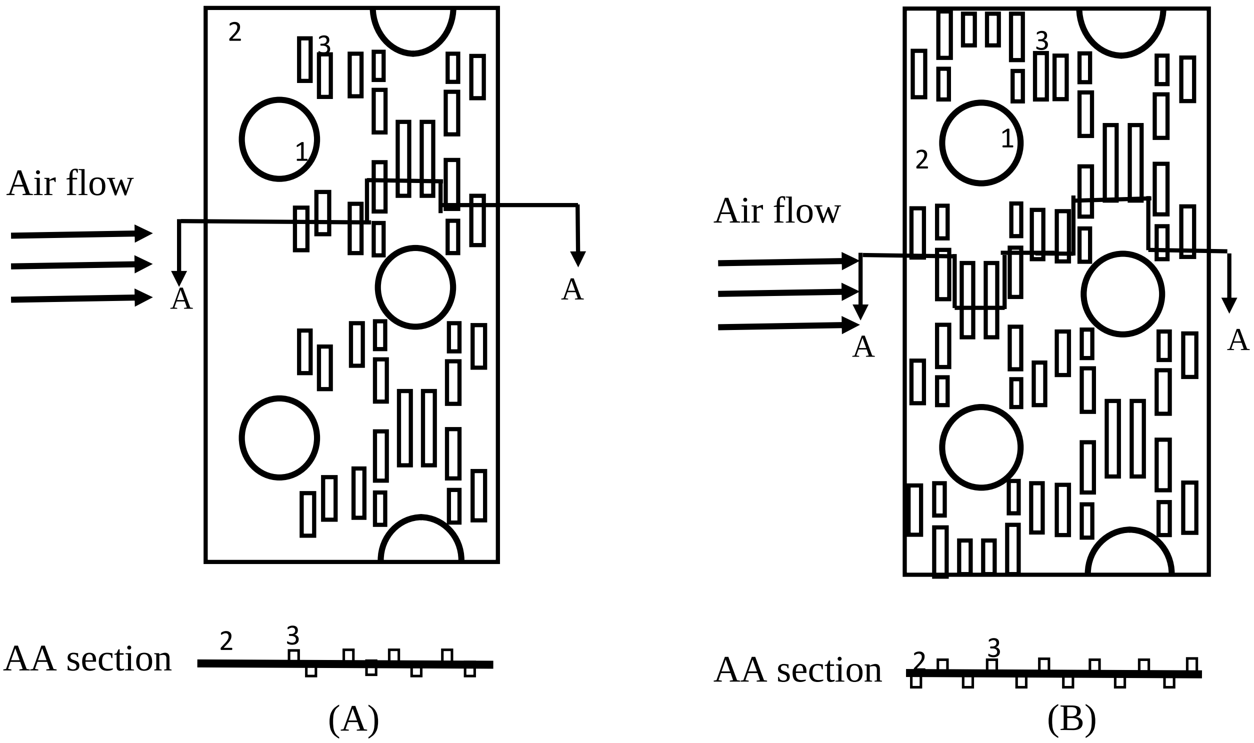

Fig. 2.8. Slit patterns recommended by Qu et al (2004), (A) fin C, (B) fin D. [(1) tube surface, (2) plate fin surface, (3) slits].

Jin et al. (2006) continued the work started by Tao et al. (2006), and presented the heat transfer and pressure drop characteristics data for all the slotted fins. The results were also explained with the help of the synergy principle. The recommended design of the slit fins (A1-3 and slit fin 3) is shown in Fig. 2.9. The location of the slits was found to be the most prominent factor, which affects the performance of the heat exchanger, and after that strip length and strip number were the important factors. Tao et al. (2007b) performed numerical simulations to study the heat transfer and pressure drop characteristics of the slotted fins. The slit fin 3 (Fig. 2.10) showed the highest *Nu* among all the slit fins.

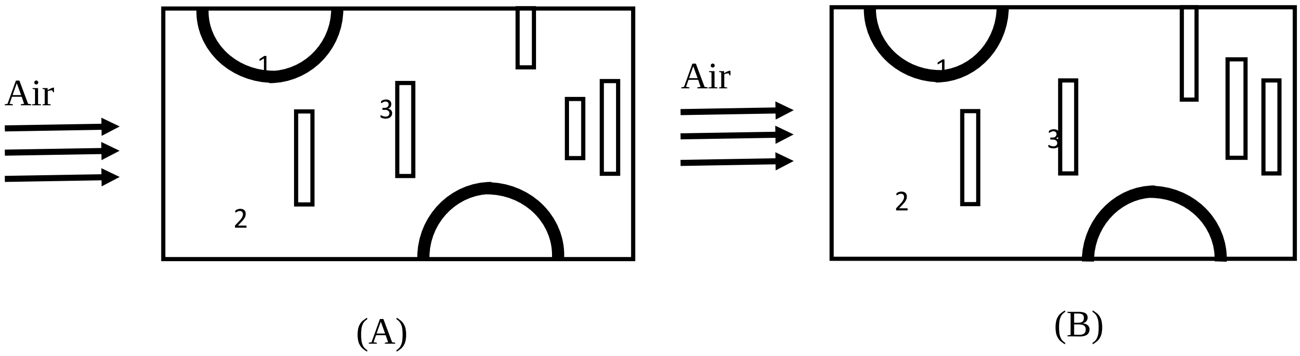

Fig. 2.9. Slit patterns recommended by Jin et al (2006), (A) fin A1-3,(B) slit fin 3. [(1) tube surface, (2) plate fin surface, (3) slits].

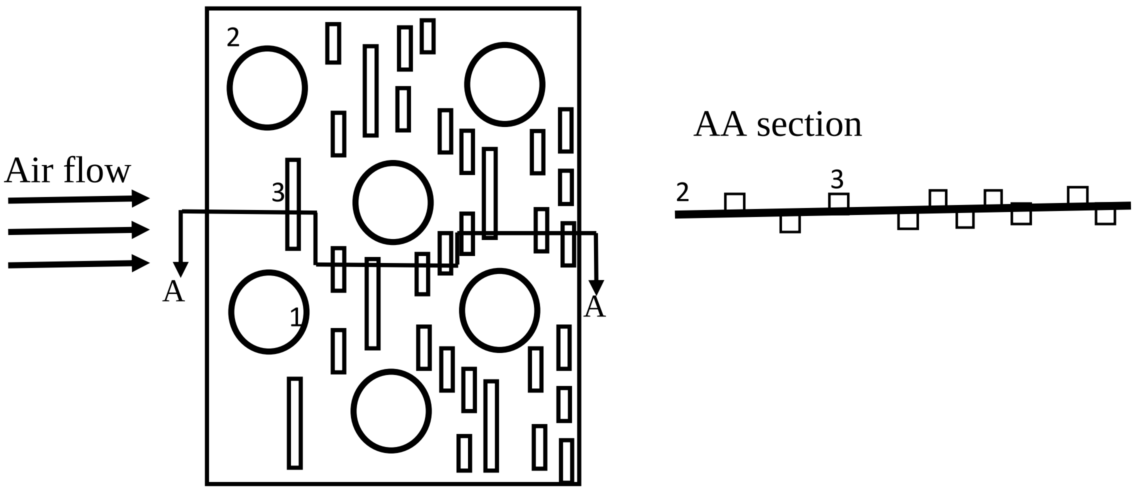

Fig. 2.10. Slit patterns recommended by Tao et al (2007b), (1) tube surface, (2) plate fin surface, (3) slits.

2.4.2.3. Studies on the comparison of fins

In earlier sections, we have discussed the studies which focus on only one type of fin. In this section, we are going to discuss the studies in which a comparison of different types of fins is given. Yun and Lee (1999) performed experimental investigation to study the thermal-hydraulic properties of different slit and louver type fins. The effect of different slit patterns on the heat transfer coefficient was negligible, however, the effect on the pressure drop was quite significant. Yan and Sheen (2000) performed experiments on 36 samples including 12 plain, 12 wavy, and 12 louver finned-tube heat exchangers were tested for a range of 300 ≤ *Re* ≤

2000. For a fixed fan power, the heat transfer was maximum and the required heat transfer area was minimum for the louver fin. Tang et al. (2009a) focused on the larger diameter tubes and studied the heat transfer and pressure drop characteristics of the finned tubes with plain fins, slit fins, and fins with DWP. It was concluded that the slit fin performs better, and the fin with the DWP must be designed carefully. Tang et al. (2009b) extended their previous study to crimped spiral fins, plain fins, slit fins, fin with DWP, and mixed fins (DWPs in front and slits in rear). After optimization, it was found that the DWP could perform better than the slit fin. The correlations for the Colburn factor and the friction factor were developed for the fin with DWP.

2.4.3. Effects of different parameters

2.4.3.1. Reynolds number

The Reynolds number is the most common parameter which has been studied by various researchers. However, the basis for the calculation of Reynolds number has been divided mainly in three categories. First is the tube outer diameter or tube collar diameter, second is the hydraulic diameter of the finned tubes, and third is the fin spacing. We have discussed the basis for the calculation of Reynolds number in detail in Section 2.4.1. The heat transfer performance of the heat exchangers depends on the behavior of the boundary layer, formation of vortices and eddies, and generation of turbulence. For the plain fin, at low Reynolds number (Re_h = 211), the enhancement in the heat or mass transfer is due to the boundary layer growth [Saboya and Sparrow (1976)], and at higher Reynolds number the enhancement is mainly due to the formation of the vortices. The effect of the other geometrical parameters like fin pitch and number of tube rows depends on the value of the Reynolds number, and from the literature, it has been observed that the effect of these geometrical parameters diminishes above a Re > 2000. For the fins with DWP, the formation of the longitudinal and transverse vortices is important, and with the increase in the Reynolds number, these vortices get stronger. The increment in the heat transfer with an increase in Reynolds number has been found to be higher for the fins with DWP as compared to the plain fins (Tigglebeck et al. 1994). The geometrical configuration of the winglet affects the transitional Reynolds number value and the formation of the vortices. For wavy-finned-tube, Wang and Chang (1996) found that the downstream turbulence shedding starts at Re = 900 for staggered arrangement, and at Re = 2000 for the inline arrangement. These results could be extended to other type of finned-tubes as well. For the annular fin, the effect of the Reynolds number has been found similar to the effect of Reynolds number on the plain fin. For the off-strip fins [Jin et al. (2006)], the effect of the strip number was significant on the heat transfer and pressure drop, however, at high Reynolds number (Re > 2250), the effect of the strip number diminished, and all the four slotted fins performed equally well.

On the basis of the foregoing discussion, we can conclude that, beyond a value of Reynolds number the effect of the other geometrical parameters (example: fin pitch, number of tube rows, and number of strips in strip fin) on the heat transfer coefficient and friction factor tends to diminish. The main reasons being the downstream vortex shedding and turbulence generated at higher Reynolds number (Re > 5000).

2.4.3.2. Fin Pitch

The fin pitch is the second most important parameter which affects the performance of the finned-tube heat exchangers. In Section 2.4.2.2.1, we discussed the importance of the boundary layer growth at the fin surface and the formation of the horseshoe vortices at the tube surface with the variation in Re. The fin pitch affects both of these physical phenomena. At a constant Re, as the fin pitch is varied, the interaction between the boundary layers on the two fin surfaces gets affected, which results in a variation in the heat transfer. The effect of fin pitch on the heat transfer and pressure drop is mainly dependent on three other parameters, Reynolds number, number of tube rows and condensate formation on the heat transfer surface (for wet surface conditions). The effect of fin pitch is also different for different fins. For the plain fin, Wang and Chang (1996) did not observe any significant effect of the fin pitch on the Colburn factor and the friction factor but in their another study [Wang and Chi (2000)] found that for one and two rows coils, the heat transfer increases by almost 30-50% with a decrease in the fin pitch (1.19 mm $\leq f_p \leq$ 3.31 mm) for a Re < 5000. Similar results were obtained by Yan and Sheen (2000) for heat transfer (50% higher heat transfer at lower fin pitch) for a fin pitch of 1.4-2 mm, however, the friction factor was found to increase with a decrease in the fin pitch. Chen et al. (2005), Huang et al. (2009) and Choi et al. (2010) varied the fin pitch in a larger range (5 mm $\leq f_p \leq$ 30 mm), and found that the heat transfer coefficient increases (by 20-100 %) with an increase in the fin pitch. Wang and Chi (2000) argued that, at lower fin pitch, the flow can be kept as laminar and vortex behind the tube is suppressed, however, they did not explain the effect of the boundary layer interaction between the fins and horseshoe vortices on the heat transfer. Choi et al. (2010) attributed the increase in the heat transfer with an increase in the fin spacing to the delay in the boundary layer interaction at larger fin spacing. Romero-Méndez et al. (1997), He et al. (2005) and Liu et al. (2010) observed that the heat transfer coefficient increases upto a value of the fin pitch, and after that, it decreases. The reason was again the delay in the boundary layer interaction at larger fin pitch, however, beyond a certain value of the fin pitch, the flow bypassed the finned surface area, and heat transfer between the fins was inefficient. The maxima was found at S/D = 0.167 (tube OD not given) by Romero-Mendez, at S/D = 0.06 (D =10 mm) by He et al., and at S/D = 0.152 (D =16.68 mm) by Liu et al.. The occurrence of the maxima at different S/D ratio can be caused by the different values of the tube diameter, which affects the size of the horseshoe vortices and ineffective area behind the tube. In the dehumidifying conditions, the effect of fin pitch on the heat transfer was negligible due to the turbulence generated by the condensate. In all the studies for plain fin, the friction factor or pressure drop decreased with an increase in the fin pitch except for Liu et al., where the pressure drop increased with an increase in the fin pitch due to more accumulation of condensate at larger fin pitch. For wavy fin, Wang et al. (1997) and Wongwises and Chokeman (2005) did not find any significant effect of the fin pitch on the heat transfer. At lower Reynolds number (*Re* < 4000), Pirompugd et al. (2005), Pirompugd et al. (2008), and Cheng et al. (2009) found that the heat transfer was higher (30-50%) for the smaller fin pitch ($1.2 \leq f_p \leq 3.5$), and the reason was believed to be the laminar flow and suppressing of the vortex region behind the tube at smaller fin pitch [similar to the Wang and Chi (2000)]. Tao et al. (2011) found a maxima in the heat transfer for a fin pitch of $1.2 \leq f_p \leq 2$ mm. The results were analogues to the other authors as Tao et al. kept the Reynolds number below 4000. The friction factor was found to be higher for the smaller fin spacing in all the studies. For annular fin, Watel et al. (2000a) and Chen and Hsu (2008) found that, *Nu* increases with an increase in the fin pitch ($2 \leq f_p \leq 40$ mm) (10-20% for Chen and Hsu and 100 % for Watel et al.). Mon and Gross (2004) found a maxima in the *Nu* at $S/D = 0.0875$, and they concluded that, with an increase in the fin pitch, the horseshoe vortices get stronger and the thermal boundary layer becomes thinner resulting in an increase in the heat transfer (20-30 %). Pongsoi et al. (2013) found that, the Colburn factor was independent of the fin pitch (2.4 mm $\leq f_p \leq$ 4.2 mm) for all Reynolds number considered in the study, however, the friction factor increased (20-40 %) as the fin pitch was increased for *Re* > 6000, and for *Re* < 6000, the fin pitch did not affect the friction factor. For the crimped spiral fin Kawaguchi et al. (2004) found that the effect of the fin pitch depends on the transverse tube pitch and bypass flow rate. For inline arrangement, at higher tube pitch ($S_t = 71.4$ mm), the increment in the fin pitch did not affect the pressure drop as flow bypassed the finned region. However, for a smaller tube pitch ($S_t = 40$ mm), the friction factor increased (80 % for 2.4 mm $\leq f_p \leq$ 4.2 mm) for with a decrease in the fin pitch. The heat transfer in both the cases increased with an increase in the fin pitch and the reason was thought to be the decrease in the bypass flow rate with an increase in the fin pitch, however, the role of the horseshoe vortices was not explained in the study. Similarly, for the staggered arrangement at higher transverse tube pitch, the heat transfer decreased at lower fin pitch due to bypassing of the flow. For lower tube pitch, the heat transfer was independent of the fin pitch, as the phenomenon of bypass flow was not so significant. Pongsoi et al. (2011) and Pongsoi et al. (2012c) found that the heat transfer becomes independent of the fin pitch for a transverse tube pitch of 40 mm, and the reason was attributed to the high Reynolds number ($4000 \leq Re \leq 13000$). However, an optimum fin pitch of 4.2 mm was suggested. Kawaguchi et al. (2004) observed that the friction factor for serrated fins was 1.15 times the friction factor for the annular fins at $f_p = 5$ mm, and it reduced to 1.1 times at $f_p = 3.3$ mm. This shows that the increase in the friction factor with the fin pitch was larger for the plain annular fins. It was believed that the turbulence generated by the segmentations increases the friction factor for the serrated fins. However, smaller force requirement for changing the flow direction across the fins for serrated fins and entrainment of the flow in the wake region due to the turbulence generated by the serrated fins were believed to be the two factors, which limited the friction factor for the serrated fins. The effect of fin pitch on the heat transfer was found to be negligible for serrated fins. Ma et al. (2012) observed that, Nu decreased in the range of 11 -0% as the fin pitch was decreased from 4.2 mm to 3.9 mm in the Reynolds number range of $4000 \leq Re \leq 30000$. A critical Reynolds number was found, above which the effect of h_f/S ratio on the heat transfer was negligible. The Euler number increased by 8%, when the fin pitch was decreased from 4.2 mm to 3.9 mm. For slit fins, Yun and Lee (2000) proposed an optimized fin pitch of 3.6 mm.

From all these previous studies, it can be concluded that, the effect of fin pitch depends on the fin type. However, most of the authors have obtained maxima in the heat transfer for a particular fin pitch, and this optimum value of fin pitch depends on the other parameters like tube diameter, wet or dry surface conditions and Reynolds number. This optimum value lies between 1.2-4 mm for a $Re > 3000$ for almost all types of finned-tubes with $D > 8$ mm. However, some of the authors have obtained the heat transfer coefficient as an increasing or a decreasing function of the fin pitch. Therefore, further studies are required to capture the flow physics and effect of the fin pitch on the thermal-hydraulic performance of the finned-tube-heat exchangers. Further, in the dehumidifying conditions, the effect of the fin pitch varies due to the presence of the condensate. Therefore, in the dehumidifying conditions, the fin pitch must be optimized carefully.

2.4.3.3. Effect of fin thickness

For plain fin, Wang and Chang (1996) studied the effect of the fin thickness, and observed that, it does not affect the heat transfer or pressure drop. Madi et al. (1998) found that fin with a thickness of 0.12 mm performed better than the fin with thickness of 0.13 mm. For wavy fin, Wongwises and Chokeman (2005) found that, the effect of fin thickness depends upon the number of tube rows. For 2 row coil, as the fin thickness was increased from 0.115 mm to 0.250 mm, then the horseshoe vortices became stronger, and the heat transfer enhancement due to the horseshoe vortices dominated over the heat transfer decrement due to the wake region behind the tubes. However, for 4 row coil, the wake region behind the tubes dominated over the formation of horseshoe vortices, and the Colburn factor decreased with an increase in the fin thickness at $Re < 1800$. For $Re > 1800$, the horseshoe vortices became stronger than the wake region behind the tubes. The friction factor also increased with an increase in the fin thickness. Tao et al. (2011) varied the fin thickness in the range of $0.05 \leq t_f \leq 0.42$ mm, and they observed that, Nu and friction factor both increase with an increase in the fin thickness. This was due to the consideration of same frontal velocity for all the cases, due to which, at larger fin thickness, the fin spacing decreased and the maximum velocity between the fins increased, resulting in an increase in the heat transfer and pressure drop. For fins with delta winglet, Zeng et al. (2010) observed that the effect of the fin thickness was negligible and hence was neglected. However, similar to the case of Tao et al. (2011), the effect of the fin thickness was observed at the same frontal velocity and a fin thickness of 0.1-0.12 mm was suggested. In wet conditions, Kuvannarat et al. (2006) observed that, for 2 row coil and small fin pitch (1.41 mm), the heat transfer coefficient for t_f = 0.25 mm was 5-50 % higher than for t_f = 0.115 mm, and the corresponding pressure drop was 5-20 % higher for t_f = 0.25 mm. At lower fin spacing, the droplet size was found to be comparable to the fin spacing, and it produced swirling motion and vortices which helped in better mixing in the main flow. However, at higher fin spacing, the mixing was not pronounced and the effect of the fin thickness was negligible. At larger number of tube rows (N_r = 6), the effect of the fin thickness and spacing reduced and became negligible.

From this section, we can conclude that at a constant frontal velocity, when the fin thickness is varied, then it results in an increase in the maximum velocity, which enhances the heat transfer and pressure drop. An optimized fin thickness of 0.1-0.2 mm can be suggested from this discussion.

2.4.3.4. Effect of fin height

The increment in the fin height increases the heat transfer area, due to this the heat transfer rate gets enhanced, however, the pressure drop also increases due to more friction and blockage provided to the flow. The effect of fin height on the heat transfer coefficient, however, depends on the type of fin and dry or wet conditions. For crimped spiral fins, Nuntaphan et al. (2005a) found that for the inline arrangement, increase in the fin height from 10-15 mm results in an increase in the pressure drop upto 100% and it decreased the heat transfer coefficient by 50% at lower frontal velocity (0.7 m/s) and by 90% for U_{fr} = 1.5 m/s. This was believed that the flow bypasses the high resistive fin regions (for larger diameter fin) and do not participate in the heat transfer. For staggered arrangement, the effect of fin height was not significant on the pressure drop, because most of the pressure drop was caused by the staggered arrangement of the tubes. In the similar study in wet conditions Nuntaphan et al. (2005b) found that the condensate resistance dominates over the effect of fin height on the heat transfer coefficient resulting in a negligible effect of the fin height on heat transfer coefficient, whereas, the pressure drop increased with an increase in the fin height. For serrated fin, Næss (2010) observed that the heat transfer coefficient increases with an increase in the fin height ($8.61 \leq h_f \leq 11.38$ mm), whereas, the effect of fin height on the pressure drop was found to be negligible. This result was found to be different from the prediction by other correlations and it was thought that, the earlier correlations were based on the performance of the assumption of similar behavior of serrated fin and plain annular. However, this assumption does not hold true, because the fluid may not penetrate as efficiently to the fin root of plain annular fin as to the fin root of the serrated fin, which results in more mixing for the serrated finned tubes. Therefore, the correlations should be developed on the basis of the performance of the serrated fin.

Overall it can be concluded that, the increase in fin height results in an increase in the average heat transfer and pressure drop. However, the heat transfer coefficient decreases with an increase in the fin diameter beyond a certain value. Therefore, fin height should be optimized to obtain the maximum heat transfer at the lowest total cost of the heat exchanger, and for that purpose, the capital cost of the heat exchanger, the area goodness factor and the volume goodness factor must be considered. For annular fins, a fin height of 5-10 mm can be suggested for better performance.

2.4.3.5. Effect of tube diameter

For plain fin, Wang and Chi (2000) observed that the heat transfer coefficient was higher for lower tube diameter (D = 8.5 mm) as compared to the larger tube diameter (D = 10.23 mm) due to the increase in the ineffective area behind the tubes for larger diameter tubes. For 1-row coil, the heat transfer coefficient was higher for the larger tube diameter (as the increase in the ineffective area for 1-row was smaller). The total heat transfer rate and pressure drop were higher for the larger tube diameter. Similar results for plain fin were obtained by Xie et al. (2009). For crimped spiral fin, Nuntaphan et al. (2005a) found similar results to those obtained by Wang and Chi (2000) for the plain fin. Cheng et al. (2009) presented the results in terms of *Nu* and pressure drop for the wavy fin and observed that, *Nu* was 21% higher for D =11.2 mm and 33% higher for D =13.6 mm as compared to that for D = 8.8 mm. The friction factor was found to be 33% higher for D =11.2 mm and 83% higher for D =13.6 mm as compared to that for D = 8.8 mm. The high *Nu* did not represent the high heat transfer, as the heat transfer coefficient is a ratio of *Nu* to the diameter of the tube, hence the heat transfer coefficient was higher for the tube with D = 8.8 mm.

From all of these studies it can be concluded that, the increase in the tube diameter results in a decrease in the heat transfer coefficient and increase in the pressure drop irrespective of the fin type. Therefore, the use of smaller tubes with *OD* ranging from 7 to 10 mm should be preferred. However, as we decreases the tube diameter, the pressure drop on the tube side gets enhanced, therefore, that part should be taken into consideration while designing the air cooled heat exchangers.

2.4.3.6. Tube pitch

The variation in the transverse tube pitch results in a variation in the flow area between the tubes. The effect on the heat transfer and pressure drop depends on whether the system is operated at a constant frontal velocity or at a constant Reynolds number (based on the maximum velocity). For plain fin, He et al. (2005) and Xie et al. (2009) observed that, for a fixed inlet velocity, the heat transfer and pressure drop decrease with an increase in the transverse tube pitch. For serrated fins, Kawaguchi et al. (2004) found that the heat transfer and pressure drop were independent of the tube pitch (40 mm ≤ S_t ≤ 45 mm, 30 mm ≤ S_l ≤ 40 mm). Naess et al. (2010) observed that, the transverse tube pitch had significant effect on the heat transfer for $S_t/D_f = 2$. Ma et al. (2012) found that the transverse tube pitch has negligible effects on the heat transfer (less than 3%), whereas, the heat transfer gets affected by the longitudinal tube pitch. Further, they observed that, the heat transfer remains independent of the transverse tube pitch for a tube pitch to fin diameter ratio ($1.2 \leq S_t/D_f \leq 1.7$) for their study and for $1.2 \leq S_t/D_f \leq 1.5$ for Kawaguchi et al. (2004). It was concluded that, there should be an optimum transverse to longitudinal pitch ratio for a specific transverse tube pitch. *Eu* was found to decrease by 20 % with an increase in the transverse tube pitch from 88 mm to 120 mm, whereas, the effect of the longitudinal tube pitch on the Euler number was negligible.

It can be concluded that, the effect of transverse tube pitch depends on the fin type. For serrated fins, it affects the heat transfer results above a certain value of S_t/D_f ratio (0.2). For plain fin, the heat transfer and pressure drop decrease with an increase in the transverse tube pitch, however, for the better performance, the transverse to longitudinal pitch ratio should be optimized.

2.4.3.7. Tube type

The flow separation at the tube surface and the formation of the wake region is very prominent for the circular tubes. It results in an ineffective area behind the tube, which in turn decreases the heat transfer coefficient. The form drag for the circular tubes is also high and results in a larger pressure drop as compared to the elliptical and oval tubes. The elliptical and oval tubes have less ineffective area behind the tubes and lesser form drag. Various studies have been carried out to compare the performance of the circular and elliptical tubes (or oval tubes). For plain finned tubes, Rocha et al. (1997) found that maximum fin efficiency is obtained with an ellipticity (e) of 0.5. Saboya and Saboya (2001) recommended the elliptical tube, as it provided a better fin efficiency. Erek et al. (2005) observed that, the elliptical tubes give more heat transfer coefficient and lesser pressure drop as compared to the circular tubes.

Ibrahim and Gomaa (2009) studied the elliptical tubes at different attack angle with respect to the incoming air flow. They found that at an angle of attack of 0°, the heat transfer per unit pressure drop, area goodness factor and efficiency index were maximum. The average *Nu* was larger for the larger angle of attack and was maximum for 90°, and was 19% greater than the circular tubes. However, the friction factor was also increased with an increase in the angle of attack, and it was maximum at 90°, and was 65% greater than the circular tubes. For annular fins, Jang and Yang (1998) observed that, the heat transfer per unit pressure drop was 50% higher for the elliptical tubes as compared to the circular tubes. Fiebig et al. (1994) put DWP with the round and the flat tubes, and observed that the circular tubes perform better than the flat tubes without DWP, but the flat tubes with DWP gave two times the heat transfer and half the friction factor as compared to the round tubes with DWP. The physical reason behind this was believed to be the absence of the horseshoe vortices for the flat tubes without DWP, because the flat tubes were placed near the fin edge, and hence heat transfer was less for the flat tubes as compared to the round tubes. As the DWP was put, they generated vortices and *Nu* for the flat tubes with DWP became higher as compared to the *Nu* for the round tubes with DWPs.

Overall it can be concluded that the heat transfer per unit pressure drop is always higher for the elliptical and flat tubes as compared to the circular tubes and they are recommended for the practical purpose. However, the area goodness factor and the volume goodness factor should also be optimized for an economical design.

2.4.3.8. Number of tube rows

The effect of number of tube rows depends mainly on the tube arrangement, value of the Reynolds number and wet or dry conditions. For plain fin, Wang and Chang (1996) and Wang and Chi (2000) found that, the heat transfer coefficient decreases with an increase in the number of tube rows (maximum 6) for $Re < 3000$, and the effect of tube rows on the friction factor was found to be negligible. Beyond $Re > 3000$, the effect of number of tube rows diminished due to better mixing at high Re. He et al. (2005) recommended a maximum 3 rows of the tubes for the practical purpose. Xie et al. (2009) and Choi et al. (2010) found that, both the heat transfer coefficient and friction factor decrease with an increase in the number of tubes rows, and for $N_r > 6$, the effect of tube rows diminishes. Liu et al. (2010) studied plain fin in wet conditions and observed that the effect of tube rows depends on the fin pitch and Reynolds number. For $Re > 4000$, the Colburn factor was found to decrease with an increase in the number of tube rows ($2 \leq N_r \leq 8$). They argued that this was associated with the condensate blow off phenomenon (at lower Reynolds number the condensate is more prone to adhere to the surface of the fin, and it provides more mixing in the flow which makes the effect of tube rows negligible). At larger fin spacing also the effect of tube row number diminished because large condensate was prone to suspending between fins at larger fin spacing. For wavy fin, Wang et al. (1997) found that, for the staggered arrangement, the heat transfer coefficient decreases with an increase in the row number for $Re < 900$, and beyond that a slight increase in the heat transfer coefficient was observed with an increase in the row number. For the inline arrangement, the heat transfer coefficient decreased with an increase in the row number for $Re < 2000$, and above this Re, the effect of tube rows diminished. Wongwises and Chokeman (2005) observed that the Colburn effect and friction factor decrease with an increase in the row number for $Re < 4000$, and for $Re > 4000$, no effect of tube row number on the Colburn factor and friction factor was observed. Similar results were obtained for the slit fin by Du and Wang (2000), and the effect of tube rows on the heat transfer and pressure drop performance became negligible for $Re > 2000$. Tang et al. (2009) studied slit fin, plain fin and fin with DWPs and observed that the heat transfer coefficient and friction factor were independent of number of tube rows ($6 \leq N_r \leq 12$). For fin with DWPs, Kwak et al. (2003) varied the tube rows in the range of $2 \leq N_r \leq 5$, and observed that the Colburn factor was maximum for 2 rows and decreased as the row number was increased. The friction factor was minimum for 3 rows and beyond Re > 1000, the effect of row number on the friction factor diminished. Overall, the three row coil performed best with a 30-10% augmentation in the heat transfer and a reduction of 55-34% in the pressure drop for $350 \leq Re \leq 2100$. The lower pressure drop penalty for 3 row coil was explained as: The flow gets accelerated between the DWP and the tube surface, and it reduces the wake region for downstream rows and brings separation delay. The form drag reduces per unit length as we go downstream. However, the effect of DWP does not reach upto 4 and 5 rows and hence the pressure drop increases for 4 and 5 row coil.

Overall it can be concluded that a row number of 3 has been recommended by various authors and the effect of row number diminishes for $N_r > 6$, and $Re > 3000$.

2.4.3.9. Effect of dehumidifying conditions

There are two major effects of water condensate, one is the turbulence generated by the droplets which enhances the heat transfer and the other is the water film resistance which degrades the heat transfer. The effect of water condensate also depends on other parameters, for example above a certain value of Reynolds number, the turbulence becomes dominant over the film resistance. Along with the effects on the heat transfer, the condensate affects the pressure drop as well, by providing more resistance to the flow. The turbulence generated by the condensate also influences the effect of other geometrical parameters on the heat transfer and pressure drop. For plain fin, Pirompugd et al. (2005) observed that, the effect of fin spacing on the heat transfer diminishes because of the presence of the condensate, which enhances the mixing by roughening the surface. The effect of number of tube rows was also affected by the condensate. Pirompugd et al. (2007) observed that, the fin efficiency obtained for the partial wet surface was higher than the efficiency for the fully wet surface and was lower than the efficiency for the fully dry surface. The fin efficiency decreased with an increase in the relative humidity. For wavy fin, Wang et al. (2000c) found that the pressure drop in wet conditions was higher for the wavy fins due to the generation of the swirling flow behind the droplets. This effect was more prominent for larger waffle height and smaller fin spacing. Pirompugd et al. (2006) observed that, at lower fin spacing, the increase in the inlet humidity gives rise to a lower mass transfer because of the condensate retention phenomenon, however, if Reynolds number is increased above 1000 (at inlet humidity of 50%), then the mass transfer increases because of the blow-off of condensate by the flow inertia. Kuvannarat et al. (2006) observed that at higher fin pitch (f_p = 2.54 mm), the effect of water condensate mixing was not significant.

Therefore, it can be concluded that the presence of the water condensate at low Reynolds number degrades the heat transfer because of the thermal resistance provided by the condensate, however, as the Reynolds number is increased (Re > 1000) then the swirling motion provided by the condensate helps in mixing in the flow and it improves the heat transfer. The presence of condensate always leads to more pressure drop.

2.4.4. Conclusions and gap areas

(1) From all the studies discussed in this review, it may be noted that, most of the studies focus on the thermal-hydraulic performance of the heat exchangers. However, none of the studies have focused on the optimization of the heat exchangers with respect to the cost of the heat exchanger. The capital cost of the condenser can be optimized by maximizing the heat transfer coefficient, and hence minimizing the heat transfer area. However, the associated pressure drop must be minimized for obtaining a minimum operating cost. Various studies have discussed the optimization of these factors, however, the real cost of the heat exchangers have not been discussed in these studies. The other costs include the cost associated with the space required, for this purpose, one need to design a very compact heat exchanger. For this purpose, the area goodness factor and volume goodness factor have to be optimized, however, only few studies

have focused on the optimization of these factors, and in these studies also, the cost associated with the required space have not been discussed.

(2) A review has been presented on the thermal-hydraulic performance of the air cooled heat exchangers. The experimental studies have been performed by many researchers during the last 50-60 years. The experimental studies mostly lack in determining the 3D flow patterns, temperature contours and velocity vectors.

(3) A great improvement in the numerical methodologies and computational capability has led us to understand the 3D flow patterns around the finned tubes. However, some of the fins are very complex to model (example: serrated fin, crimped spiral fins), and the numerical studies on these fins have been very limited. Therefore, more numerical studies are needed for these types of fins. Further, in all the studies only two or three fins are taken in the computational domain and a periodic boundary condition is assumed to model the whole length of the tube. However, it has been observed that by varying the fin pitch along the length of the tube, the thermal-hydraulic performance can be improved. Therefore, more of 3D numerical studies should be performed to model the whole length of the tube by varying the fin spacing along the length.

(4) From the discussion in Section 2.4.2 and 2.4.3, it is clear that the estimation of heat loss in the published literature has been addressed using two types of approaches: (1) development of empirical correlations and (2) use of CFD. The latter approach permits the understanding of physics of the system through the insights in (a) fluid mechanics and (b) the relationship between the fluid mechanics and design objectives such as heat losses. Secondly, during the past 25 years, CFD is being increasingly used because of the development in computational power as well as numerical techniques. Joshi and Ranade (2003) have given an overview of opportunities and scope of CFD. Ranade et al. (1989, 1990, 1992), Murthy et al. (2008), Ekambra et al. (2005), and Joshi et al. (2011a, 2011b) have given the details pertaining to

governing equation, method of solution and appropriate precautions for the implementation of CFD. Further, some examples of relationship between the fluid mechanics and design objectives have been described in the published literature. For instance, heat transfer [Thakre et al. (1999)], mixing [Patwardhan and Joshi (1999), Nere et al. (2003), Kumaresan and Joshi (2006), Joshi and Sharma (1978), Joshi and Shah (1981)], solid suspension [Rao et al. (1988), Rewatkar and Joshi (1991), Murthy et al. (2007)] and the rate of gas induction [Murthy et al. (2007), Joshi and Sharma (1977)]. Similar methodology needs to be employed in the future work for the estimation of heat losses and pressure drop. In particular, LES (and if possible DNS) simulations need to be undertaken for developing better insight.

(5) For better understanding of transport phenomenon, the future work should include the identification and dynamics of flow structures. [Joshi and Sharma (1976), Shnip et al. (1992), Thorat et al. (1998, 2004), Kulkarni et al. (2001, 2007), Bhole et al. (2008), Joshi et al. (2009), and Mathpati et al. (2009). Additional work is also needed to understand the relationship between the structure dynamics and heat transfer as well as pressure drop.

(6) A comparison of various correlations for the annular fin with the experimental results of Pongsoi et al. (2013) is shown in Fig. 2.11. It can be observed that the correlations show a deviation of 5%-50% with the experimental results. Therefore, it can be concluded that the validity of the empirical correlations is limited and can lead to underdesign or overdesign of the air cooled heat exchangers. Thus, the use of 3D numerical simulations must be emphasize in the commercial design procedures.

(7) For crimped spiral fins, all the studies have been experimental and empirical correlations have been developed. The visualization of flow pattern, development and breaking of the boundary layer has been missing from the literature. Therefore, it is recommended to perform numerical simulation to understand the flow physics for the crimped spiral-finned-tube heat exchangers.

(8) For serrated fins as well, the flow physics has not been investigated extensively and only one numerical study by Lemouedda et al. (2011) has been reported. In that study also, the pressure drop across the finned-tube heat exchanger was not presented, therefore the performance of the serrated fins as compared to the plain annular fin could not be determined. Therefore, more of the numerical studies are recommended in this case also.

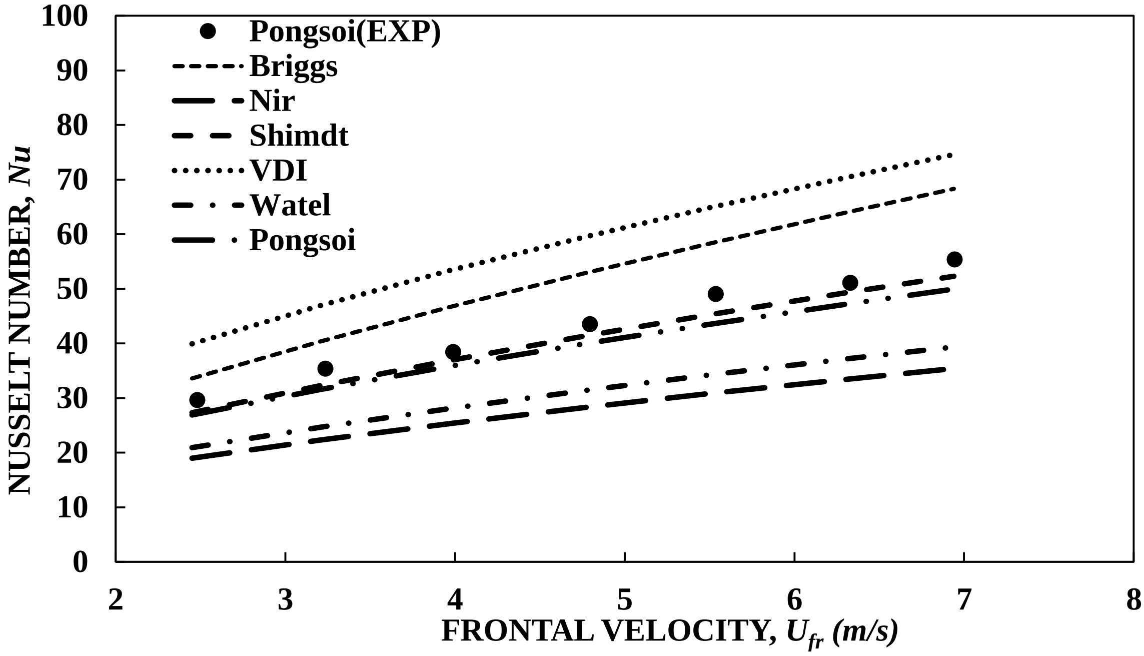

Fig. 2.11: A comparison of correlations for the annular-finned-tube with the experimental results of Pongsoi et al. (2013).

(9) Banerjee et al. (2012) modified the annular fin into perforated fins and they obtained excellent results for the perforations in the wake region. These type of fins enhance the heat transfer in the wake region, however, only one study is available on this kind of fin. Therefore, more studies should be performed in order to optimize these kind of fins for commercial use.

(10) Banerjee et al. (2012) performed 2D numerical study, in which they varied the fin pitch along the length of the finned tube, and they observed a reduction in the pressure drop. However the effect on the heat transfer was unknown. Therefore it is recommended to perform 3D

numerical study by varying the fin spacing along the length of the tube to determine the thermal-hydraulic performance of the heat exchangers.

(11) For the slit fins, most of the studies are performed with the circular tubes, further studies can be performed to compare the performance of slit fins with the Elliptical or flat tubes.

(12) From Section 2.4.2.3, it may be noted that, only few studies are present which compares the performance of the different fins. From these studies it can be concluded that out of crimped spiral fins, plain fins, slit fins, and fins with vortex generators (VG), and mixed fins (VGs in front and slits in rear), the slit fins and fins with VGs perform better. However, more studies in this direction should be performed to make the results more applicable for the commercial purpose.

(13) In the heat exchangers, a combination of fins can be used and the combinations of the fins can be optimized by analyzing the flow structure and dynamics in the heat exchangers. For that purpose 3D numerical simulations are required, so far, only one has been reported by Tang et al. (2009b), which considered a combination of VGs and the slit fins. More combination of this sort can be studied for the practical purpose.

Chapter 3
Introduction to Computational Fluid Dynamics (CFD)

3.1. Introduction

Fluid flows occur in microscopic to macroscopic systems, e.g., flows through micro channels, air flow around the air crafts, water flows in oceans etc. The understanding of fluid flows and heat transfer is very important for many of the commercial applications. In case of power plants, the heat from nuclear fission reaction is taken by the cooling fluid and used to rotate the turbines, which further drives the electrical generators to produce electricity. The flow through the reactor core and pipes is often in turbulent region and is complex, therefore, a good understanding of the flow patterns is needed. All fluid flows can be described by Navier Stokes equations, which forms the basis of computational fluid dynamics. These equations are first simplified using some assumptions and then are solved numerically. The Navier Stokes equation for momentum is given below:

$$\frac{D\rho v}{\partial t} = -v(\nabla . \rho v) - (\nabla . \tau) - (\nabla p) + \rho g \qquad \ldots (3.1)$$

3.2. Numerical Solution

3.2.1. Pre-processing

The geometry generation and meshing was performed by using GMSH 2.3. In most of the cases non-uniform structured grid was used.

3.2.2. Governing equations

In the present work various turbulence models have been used based on the application and flow conditions. The equations corresponding to (1) Laminar model, (2) standard k- ε, (3) SST k-omega, (4) Re-normalization group (RNG) k- ε, (5) Launder Sharma k- ε are given below:

(1) Laminar model

When the value of Reynolds number or Rayleigh number is low (Re<3000, Ra<10^9) the flow is considered to be in the laminar region. In those cases, the laminar model is used for the simulations. The governing equations for laminar model are continuity equation, momentum equation and energy equation and are given as:

$$\frac{D\rho}{\partial t} + (\nabla . \rho v) = 0 \qquad \dots (3.2)$$

$$\frac{D\rho v}{\partial t} = -v(\nabla . \rho v) - (\nabla . \tau) - (\nabla p) + \rho g \qquad \dots (3.3)$$

$$\rho C_p \frac{DT}{\partial t} = (\nabla p) + \nabla . (\mathrm{k}\nabla T) \qquad \dots (3.4)$$

For incompressible flows, the continuity equation becomes:

$$\frac{\partial u_j}{\partial x_j} = 0 \qquad \dots (3.5)$$

In buoyancy driven flows, the equations are simplified by ignoring density difference except in the terms where gravity is involved. This is called Boussinesq approximation and it transforms the momentum equation for incompressible flows to:

$$\frac{\partial u_i}{\partial t} + \frac{\partial (u_j u_i)}{\partial x_j} - \frac{\partial}{\partial x_j}\left\{ v \left[\left(\frac{\partial u_i}{\partial x_j} + \frac{\partial u_j}{\partial x_i} \right) \right] \right\} = -\frac{\partial p}{\partial x_i} + g_i \left[1 - \beta (T - T_o) \right] \qquad \dots (3.6)$$

Also, the energy equation for incompressible flows transforms to:

$$\frac{\partial T}{\partial t} + \frac{\partial (T u_i)}{\partial x_j} = \frac{\partial}{\partial x_k}\left[\left(\frac{v}{Pr} \right) \frac{\partial T}{\partial x_k} \right] \qquad \dots (3.7)$$

Where, T, p, and u represent the mean temperature, pressure and mean flow velocity respectively and T_o represents the bulk mean temperature. υ, β, and g_are the kinematic viscosity, thermal expansion coefficients and gravitational acceleration constant.

(2) Standard k- ε model

Standard k- ε model uses wall functions to account for the influence of wall (relation between Reynolds stresses with the mean velocity gradients and turbulent viscosity) on the mean flow and therefore first grid needs to be placed in the log layer or $Y^+ > 20$. The governing equations for the 3D unsteady natural convection are continuity, momentum, turbulence kinetic energy (k), turbulence energy dissipation rate (ε) equations, and energy equation, which are given as:

$$\frac{\partial \overline{u_j}}{\partial x_j} = 0 \qquad \dots (3.8)$$

$$\frac{\partial \overline{u_i}}{\partial t} + \frac{\partial(\overline{u_j u_i})}{\partial x_j} - \frac{\partial}{\partial x_j}\left\{\upsilon_{eff}\left[\left(\frac{\partial \overline{u_i}}{\partial x_j} + \frac{\partial \overline{u_j}}{\partial x_i}\right) - \frac{2}{3}\left(\frac{\partial \overline{u_i}}{\partial x_j}\right)\delta_{ij}\right]\right\} = -\frac{\partial \bar{p}}{\partial x_i} + g_i\left[1 - \beta(\bar{T} - T_o)\right] \qquad \dots (2)$$

$$\frac{\partial \rho k}{\partial t} + \overline{u_j}\frac{\partial \rho k}{\partial x_j} - \frac{\partial}{\partial x_j}\left\{\left(\mu + \frac{\mu_t}{\sigma_k}\right)\frac{\partial k}{\partial x_j}\right\} = -\rho\mu_t\frac{\partial \overline{u_i}}{\partial x_j}\left(\frac{\partial \overline{u_i}}{\partial x_j} + \frac{\partial \overline{u_j}}{\partial x_i}\right) - \rho\varepsilon \qquad \dots (3.9)$$

$$\frac{\partial \rho \varepsilon}{\partial t} + \overline{u_j}\frac{\partial \rho \varepsilon}{\partial x_j} - \frac{\partial}{\partial x_j}\left\{\left(\mu + \frac{\mu_t}{\sigma_\varepsilon}\right)\frac{\partial \varepsilon}{\partial x_j}\right\} = -C_{1\varepsilon}\frac{\varepsilon}{k}\rho\mu_t\frac{\partial \overline{u_i}}{\partial x_j}\left(\frac{\partial \overline{u_i}}{\partial x_j} + \frac{\partial \overline{u_j}}{\partial x_i}\right) - C_{2\varepsilon}\rho\frac{\varepsilon^2}{k} \dots (3.10)$$

$$\frac{\partial \bar{T}}{\partial t} + \frac{\partial(\bar{T}\overline{u_j})}{\partial x_j} = \frac{\partial}{\partial x_k}\left[\left(\frac{\upsilon_t}{Pr_t} + \frac{\upsilon_o}{Pr}\right)\frac{\partial \bar{T}}{\partial x_k}\right] \qquad \dots (3.11)$$

For steady forced convection (neglecting gravity), the equations (1), (2), (3) and (4) become:

$$\frac{\partial \overline{u_j}}{\partial x_j} = 0 \qquad \dots (3.12)$$

$$\frac{\partial(\overline{u_j u_i})}{\partial x_j} - \frac{\partial}{\partial x_j}\left\{\upsilon_{eff}\left[\left(\frac{\partial \overline{u_i}}{\partial x_j} + \frac{\partial \overline{u_j}}{\partial x_i}\right) - \frac{2}{3}\left(\frac{\partial \overline{u_i}}{\partial x_j}\right)\delta_{ij}\right]\right\} = -\frac{\partial \bar{p}}{\partial x_i} \qquad \dots (3.13)$$

$$\overline{u_j}\frac{\partial \rho k}{\partial x_j} - \frac{\partial}{\partial x_j}\left\{\left(\mu + \frac{\mu_t}{\sigma_k}\right)\frac{\partial k}{\partial x_j}\right\} = -\rho\mu_t\frac{\partial \overline{u_i}}{\partial x_j}\left(\frac{\partial \overline{u_i}}{\partial x_j} + \frac{\partial \overline{u_j}}{\partial x_i}\right) - \rho\varepsilon \qquad \dots (3.14)$$

$$\frac{\partial \rho \varepsilon}{\partial t} + \overline{u_j}\frac{\partial \rho \varepsilon}{\partial x_j} - \frac{\partial}{\partial x_j}\left\{\left(\mu + \frac{\mu_t}{\sigma_\varepsilon}\right)\frac{\partial \varepsilon}{\partial x_j}\right\} = -\,C_{1\varepsilon}\frac{\varepsilon}{k}\rho\mu_t\frac{\partial \overline{u_i}}{\partial x_j}\left(\frac{\partial \overline{u_i}}{\partial x_j} + \frac{\partial \overline{u_j}}{\partial x_i}\right) - C_{2\varepsilon}\rho\frac{\varepsilon^2}{k} \quad \ldots (3.15)$$

$$\frac{\partial(\bar{T}\overline{u_j})}{\partial x_j} = \frac{\partial}{\partial x_k}\left[\left(\frac{\upsilon_t}{Pr_t} + \frac{\upsilon_o}{Pr}\right)\frac{\partial \bar{T}}{\partial x_k}\right] \quad \ldots (3.16)$$

Where, $\bar{T}$, $\bar{p}$, and $\bar{u}$ represent the mean temperature, pressure and mean flow velocity respectively and T_o represents the bulk mean temperature. υ, β, μ_t and g are the kinematic viscosity, thermal expansion coefficients, turbulent viscosity and gravitational acceleration constant, respectively.

The other coefficients are given as:

$$\mu_t = \rho C_\mu \frac{k^2}{\varepsilon} \quad \ldots (3.17)$$

C_μ=0.09, σ_k=1.00, σ_ε=1.30, $C_{1\varepsilon}$=1.44, $C_{2\varepsilon}$=1.92

The thermal coefficients are calculated at the mean temperature of the tube and the ambient. The value of the Prandtl number, *Pr*, is taken as 0.7.

(3) SST k-omega

SST k-omega model uses wall functions at high Reynolds number (turbulent range) and shifts to low Reynolds number formulation at low *Re*. For this case the first grid should be placed in the viscous layer or at $Y^+ < 5$. The governing equations for continuity, momentum and energy are same as for Standard k- ε model. For turbulence kinetic energy (*k*), and specific dissipation rate (ω), the equations are:

$$\frac{\partial k}{\partial t} + U_j\frac{\partial k}{\partial x_j} = P_k - \beta^* k\omega + \frac{\partial}{\partial x_j}\left[(\nu + \sigma_k \nu_t)\frac{\partial k}{\partial x_j}\right] \quad \ldots (3.18)$$

$$\nu_t = \frac{a_{1k}}{max(a_{1\omega,}, SF_2)}$$

$$\frac{\partial \omega}{\partial t} + U_j\frac{\partial \omega}{\partial x_j} = \alpha S^2 - \beta\omega^2 + \frac{\partial}{\partial x_j}\left[(\nu + \sigma_\omega \nu_T)\frac{\partial \omega}{\partial x_j}\right] + 2(1 - F_1)\sigma_{\omega 2} \quad \ldots (3.19)$$

The constants are given as:

$$F_2 = \tanh\left[\left[max\left(\frac{2\sqrt{k}}{\beta^* y\omega}, \frac{500\nu}{y^2\omega}\right)\right]^2\right]$$

$$P_k = \ min\left(\tau_{ij}\frac{\partial U_i}{\partial x_j}, 10\beta^* k\omega\right)$$

$$F_1 = \tanh\left\{\left\{min\left[max\left(\frac{\sqrt{k}}{\beta^* y\omega}, \frac{500\nu}{y^2\omega}\right), \frac{4\sigma_{\omega 2}k}{CD_{k\omega}y^2}\right]\right\}^4\right\}$$

$$CD_{k\omega} = max\left(2\rho\sigma_{\omega 2}\frac{1}{\omega}\frac{\partial k}{\partial x_i}\frac{\partial \omega}{\partial x_i}, 10^{-10}\right)$$

$$\phi = \phi_1 F_1 + \phi_2(1 - F_1)$$

$$\alpha_1 = \frac{5}{9}, \alpha_2 = 0.44$$

$$\beta_1 = \frac{3}{40}, \beta_2 = 0.0828\ , \beta^* = \frac{9}{100}, \sigma_{k1} = 0.85, \sigma_{k2} = 1, \sigma_{\omega 1} = 0.5, \sigma_{\omega 2} = 0.856$$

(4) Re-normalization group (RNG) k- ε model

RNG k- ε model is derived from standard k- ε model to improve the accuracy for swirling flows, rapidly strained flows and also can handle low *Re* problems quite well. RNG k- ε model contains an analytical derivation for effective viscosity, due to which the near wall formulation for RNG k- ε differs from standard k- ε. A grid resolution of $Y^+ < 5$ is considered for this model also. The governing equations are same as for Standard k- ε model except one modification in the equation of turbulence energy dissipation rate (ε), and is given as:

$$\overline{u_j}\frac{\partial \rho\varepsilon}{\partial x_j} - \frac{\partial}{\partial x_j}\left\{\left(\mu + \frac{\mu_t}{\sigma_\varepsilon}\right)\frac{\partial \varepsilon}{\partial x_j}\right\} = -\ C_{1\varepsilon}\frac{\varepsilon}{k}\rho\mu_t\frac{\partial \overline{u_i}}{\partial x_j}\left(\frac{\partial \overline{u_i}}{\partial x_j} + \frac{\partial \overline{u_j}}{\partial x_i}\right) - C_{2\epsilon}^*\rho\frac{\varepsilon^2}{k} \qquad \ldots (3.20)$$

The coefficients are given as:

$$\mu_t = \rho C_\mu \frac{k^2}{\varepsilon} \qquad \ldots (3.21)$$

$$C_{2\epsilon}^{*}=C_{2\varepsilon}+\frac{C_{\mu}\eta^{3}(1-\frac{\eta}{\eta_0})}{1+\beta\eta^{3}} \quad \text{... (3.22)}$$

C_{μ}=0.0845, σ_k=0.719, σ_{ε}=0.719, $C_{1\varepsilon}$=1.42, $C_{2\varepsilon}$=1.68, $\eta = Sk/\varepsilon$, $S = (2S_{ij}S_{ij})^{1/2}$

(5) Launder Sharma k- ε model

Launder Sharma k- ε model is a low *Re* model and requires very fine meshing around the tube walls ($Y^{+} < 1$) and does not involve the use of wall functions. The equations for turbulence kinetic energy (*k*), and turbulence energy dissipation rate (ε) can be given as:

$$\frac{\partial\rho k}{\partial t}+\frac{\partial}{\partial x_j}\left\{\rho k\overline{u_j}-\left(\mu+\frac{\mu_t}{\sigma_k}\right)\frac{\partial k}{\partial x_j}\right\}=P-\rho\varepsilon-\ \rho D \quad \text{… (3.23)}$$

$$\frac{\partial\rho\varepsilon}{\partial t}+\frac{\partial}{\partial x_j}\left\{\rho\varepsilon\overline{u_j}-\left(\mu+\frac{\mu_t}{\sigma_\varepsilon}\right)\frac{\partial\varepsilon}{\partial x_j}\right\}=(C_{1\varepsilon}f_1P-C_{2\varepsilon}f_2\rho\varepsilon)\frac{\varepsilon}{k}\ +\rho E \quad \text{… (3.24)}$$

The coefficients are:

$$\mu_t=\rho C_\mu f_\mu\frac{k^2}{\varepsilon}$$

$$\mathrm{P}{=}-\rho\mu_t\frac{\partial\overline{u_i}}{\partial x_j}\left(\frac{\partial\overline{u_i}}{\partial x_j}+\frac{\partial\overline{u_j}}{\partial x_i}\right)$$

C_{μ}=0.09, σ_k=1.00, σ_{ε}=1.30, $C_{1\varepsilon}$=1.44, $C_{2\varepsilon}$=1.92

$$f_\mu=\exp\frac{-3.4}{(1+R_t/50)^2}\,,\ f_1=1,\ f_2=1-0.3exp-Re_t^2$$

$$Re_t=\frac{k^2}{\nu\varepsilon}=\frac{u^{*}y}{\nu}$$

3.2.3. Boundary condition

There are multiple type of boundary conditions depending on the type of problem. For heater, either constant heat flux or constant temperature boundary condition is used. For velocity field, fixed value of velocity or Neumann type boundary condition is used. The Neumann boundary condition sets the normal derivative of velocity to a constant value. For pressure also, a fixed value or Neumann boundary condition is used. Detailed boundary conditions are explained for each case in next chapters.

3.2.4. Method of solution

All the computational work was carried out using the software OpenFOAM-2.2, which is based on finite volume approach. In all the cases considered in the present work, QUICK scheme was used to discretize the divergence terms, which is a third order accurate scheme and the diffusion terms were discretized using the central difference scheme, which is a second order accurate scheme. All the discretized equations were solved in a segregated manner with the SIMPLE (Pressure Implicit with Splitting of Operators) algorithm for steady state problems and using PIMPLE (Combination of PISO and SIMPLE) for unsteady problems. In SIMPLE or PIMPLE algorithms, the equations are solved using initial guess values of flow variables, and then the values are corrected in each iteration. The iterative process continues until the convergence criterion is satisfied. The convergence criterion was based on the scaled residuals of the velocity, when the residuals reached below 10^{-5}, the solution was considered to be fully converged. For example consider the unsteady 1D convection-diffusion equation without any source term:

$$\frac{\partial(\rho\phi)}{\partial x} + \nabla(\rho u\phi) = \nabla(\upsilon\nabla\phi) \qquad \dots (3.25)$$

In the momentum equation ϕ can be replaced by *u*.

Consider the discretized one dimensional space (Fig. 3.1) in which control volume is shown around a node P. The node E and W are the neighbouring nodes around P, and e and w are the faces of the control volume.

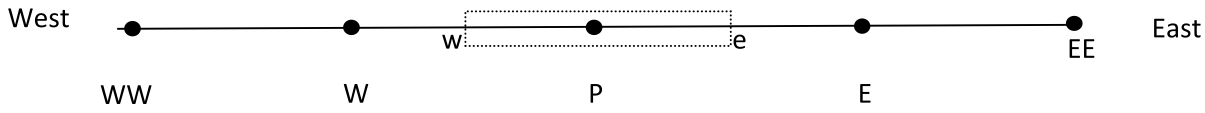

Fig. 3.1

By integrating the equation 4 over this control volume and over a time interval of t to t+Δt gives us:

$$\int_t^{t+\Delta t}\int_w^e \frac{\partial(\rho\phi)}{\partial x}dVdt + \int_t^{t+\Delta t}\int_w^e \nabla(\rho u\phi)dVdt = \int_t^{t+\Delta t}\int_w^e \nabla(\nu\nabla\phi)dVdt$$

The transient term on L.H.S can be written as:

$$\int_t^{t+\Delta t}\int_w^e \frac{\partial(\rho\phi)}{\partial x}dVdt = \rho(\phi_P - \phi_P^o)\Delta V \qquad \ldots (3.26)$$

Here ϕ_P^o is the value of the parameter at t=0, and $\phi_P$at $t+\Delta t$.

The diffusion term on R.H.S. can be discretized using central difference scheme and can be written as:

$$\int_t^{t+\Delta t}\int_w^e \nabla(\nu\nabla\phi)dVdt = \int_t^{t+\Delta t}\left[\left(\nu A\frac{d\phi}{dx}\right)_e - \left(\nu A\frac{d\phi}{dx}\right)_w\right]dt$$

Or it may be re-written as

$$\int_t^{t+\Delta t}\left[\nu_e A_e\left(\frac{\phi_E - \phi_P}{\delta x_{\mathrm{PE}}}\right) - \nu_w A_w\left(\frac{\phi_P - \phi_W}{\delta x_{\mathrm{WP}}}\right)\right]dt \qquad \ldots (3.27)$$

For convection terms, the QUICK scheme is used,

$$\int_t^{t+\Delta t}\int_w^e \nabla(\rho u\phi)dVdt$$

In QUICK scheme, the properties at point P are calculated using three nodes in both directions, for example, for west face, ϕ can be expressed as (the fluid is assumed to be flowing from west to east and higher order terms are neglected):

$$\phi_w = \phi_W + \frac{\Delta x}{2}\left(\frac{\partial \phi}{\partial x}\right)_W + \frac{\left(\frac{\Delta x}{2}\right)^2}{2!}\left(\frac{\partial^2 \phi}{\partial x^2}\right)_W$$

After rearranging, we can write

$\phi_w = \frac{6}{8}\phi_W + \frac{3}{8}\phi_P - \frac{1}{8}\phi_{WW}$

Similarly for the east node, we can write

$\phi_e = \frac{6}{8}\phi_P + \frac{3}{8}\phi_E - \frac{1}{8}\phi_W$

We can write the convection term as

$\int_t^{t+\Delta t}\left[\rho_e u_e\left(\frac{6}{8}\phi_P + \frac{3}{8}\phi_E - \frac{1}{8}\phi_W\right) - \rho_w u_w\left(\frac{6}{8}\phi_W + \frac{3}{8}\phi_P - \frac{1}{8}\phi_{WW}\right)\right]dt$

Substituting all the discretized terms in equation 3.26, we obtain:

$\rho(\phi_P - \phi_P^o)\Delta x + \int_t^{t+\Delta t}\left[\rho_e u_e\left(\frac{6}{8}\phi_P + \frac{3}{8}\phi_E - \frac{1}{8}\phi_W\right) - \rho_w u_w\left(\frac{6}{8}\phi_W + \frac{3}{8}\phi_P - \frac{1}{8}\phi_{WW}\right)\right]dt$

$= \int_t^{t+\Delta t}\left[\nu_e A_e\left(\frac{\phi_E - \phi_P}{\delta x_{\mathrm{PE}}}\right) - \nu_w A_w\left(\frac{\phi_P - \phi_W}{\delta x_{\mathrm{WP}}}\right)\right]dt$ … (3.28)

To evaluate the parameter ϕ with time, we introduce a weighing parameter θ, and write the integrals as:

$I_T = \int_t^{t+\Delta t}\phi_P dt = [\theta\phi_P + (1-\theta)\phi_P^o]\Delta t$

Using this, the eqn (3.28) becomes:

$\rho(\phi_P - \phi_P^o)\Delta x + \theta\left[\rho_e u_e\left(\frac{6}{8}\phi_P + \frac{3}{8}\phi_E - \frac{1}{8}\phi_W\right) - \rho_w u_w\left(\frac{6}{8}\phi_W + \frac{3}{8}\phi_P - \frac{1}{8}\phi_{WW}\right)\right]\Delta t + (1 - \theta)\left[\rho_e u_e\left(\frac{6}{8}\phi_P^o + \frac{3}{8}\phi_E^o - \frac{1}{8}\phi_W^o\right) - \rho_w u_w\left(\frac{6}{8}\phi_W^o + \frac{3}{8}\phi_P^o - \frac{1}{8}\phi_{WW}^o\right)\right]\Delta t = \theta\left[\nu_e\left(\frac{\phi_E - \phi_P}{\delta x_{\mathrm{PE}}}\right) - \nu_w\left(\frac{\phi_P - \phi_W}{\delta x_{\mathrm{WP}}}\right)\right]\Delta t + (1-\theta)\left[\nu_e\left(\frac{\phi_E^o - \phi_P^o}{\delta x_{\mathrm{PE}}}\right) - \nu_w\left(\frac{\phi_P^o - \phi_W^o}{\delta x_{\mathrm{WP}}}\right)\right]\Delta t$

By rearranging,

$$\left(\rho\frac{\Delta x}{\Delta t}+\frac{6}{8}\rho_e u_e-\frac{3}{8}\rho_w u_w+\frac{\nu_e}{\delta x_{\mathrm{PE}}}+\frac{\nu_W}{\delta x_{\mathrm{WP}}}\right)\phi_P=\left(\frac{\nu_e}{\delta x_{\mathrm{PE}}}-\frac{3}{8}\rho_e u_e\right)[\theta\phi_E+(1-\theta)\phi_E^o]+\left(\frac{\nu_w}{\delta x_{\mathrm{WP}}}+\frac{1}{8}\rho_e u_e+\frac{6}{8}\rho_w u_w\right)[\theta\phi_W+(1-\theta)\phi_W^o]-\left(\frac{1}{8}\rho_w u_w\right)[\theta\phi_{WW}+(1-\theta)\phi_{WW}^o]+\left(\rho\frac{\Delta x}{\Delta t}-\frac{6}{8}(1-\theta)\rho_e u_e+\frac{3}{8}(1-\theta)\rho_w u_w-(1-\theta)\frac{\nu_e}{\delta x_{\mathrm{PE}}}-(1-\theta)\frac{\nu_W}{\delta x_{\mathrm{WP}}}\right)\phi_P^o \quad (12)$$

This is the obtained discretized equation using QUICK scheme, which can be solved for any property ϕ_P. The same procedure can be extended to 3D for equations (1), (2) and (3).

3.2.5. Grid independence

Grid independence has been carried out for each of the case considered. The general idea has been to change the grid density in high gradient regions and observe the change in the heat transfer coefficient under same boundary conditions. In the present work, the grid independence was considered to be established when the variation in the heat transfer coefficient became lower than 2-5% for all the cases.

3.3. Natural and forced convection air cooled condensers

This section focus on the difference between the forced convection air cooled condensers and natural convection air cooled condensers and how numerical methodology varies for both. We will shortly explain why we have considered natural convection around bare and finned tubes in chapter 4 and 5 and why we shifted to forced convection air cooled condensers in chapter 6 and 7. In chapters 4 and 5, we discussed natural convection around bare tubes and finned tubes. The results obtained are important when we consider the natural air cooled condensers. However, currently most of the power plants employ forced draft air cooled condenser. Therefore, it is important to study the thermal-hydraulic characteristics of finned-tubes under forced flow conditions in greater detail.

The importance and requirements of natural and forced convection air cooled condensers differs for each to some extent.

A general comparison of forced and natural convection air cooled condenser is given below:

- Forced draft air cooled condensers use blowers, which run on the external power, whereas in the natural air cooled condensers the flow is generated in the chimney.
- The regulation of air flow rate is easier in the forced convection air cooled condensers due to external blower, which is helpful in load variation situations.
- Higher flow rates can be achieved using blowers (forced convection condensers) as compared to the flow rates generated by the buoyancy (natural convection condensers). This causes higher heat removal capacity of forced convection air cooled condensers per unit volume of the condensers as compared to the natural convection air cooled condensers. This also results in lower capital cost of the forced draft condensers.
- Despite more compact design of the forced convection condensers, they require external power to remove the heat which adds to the operating cost of the condensers. Therefore, natural convection condensers are more economical as far as operating cost is concerned.
- In case of any accident causing station black out in nuclear power plants, the natural convection condensers are safer because of their ability to operate without any external power.

Requirements for the numerical analysis of forced and natural convection condensers:

A typical forced convection air cooled condenser unit is shown in Fig. 1.2. Forced convection air cooled condenser are placed in arrays with certain number of blowers or fans in the power plants shown in Fig. 3.2.

Fig. 3.2. Array of air-cooled condensers

For computational analysis, it is considered that the flow is uniform throughout the array of the condensers and therefore, the computational domain can be considered one cross section on any side of A frame (shown in Fig. 3.2) with symmetry or periodic boundary conditions.

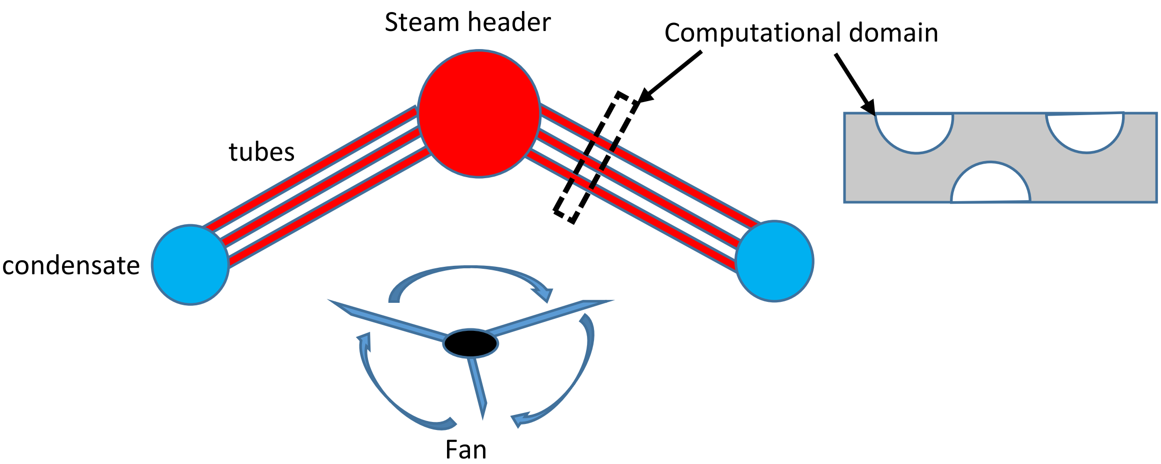

Fig. 3.3. Typical computational domain

This way, the performance of whole array of the condensers is investigated. This reduces the computational domain size and the computational time.

On the other hand, a natural convection air cooled condenser for a large power plant (500 MWe or larger) involves a chimney of approximately 100 m diameter and 150-200 m height (shown in Fig. 3.4.). For the computational model, the chimney must be considered along with the finned tube condensers placed at the bottom, which makes the computational domain large and increases the computational time significantly, which is not feasible.

Chapter 4 presents 3D numerical simulations for natural convection around bare tubes in cavities. This gives us a deeper understanding of the 3D natural convection around circular tubes. To study the natural convection air cooled condenser, 3D numerical simulations have been performed for a single finned tube with a small chimney (upto 1 m height) and presented in chapter 5. The reason for selecting the smaller chimney is the large computational time taken for natural convection studies around finned-tubes (for reaching 200 s, it takes more than 10 days). However, even in small scale geometry the importance of fin parameters (fin spacing, fin diameter etc.) on the heat transfer can be studied, which can be used in large scale commercial natural air cooled condensers. Therefore, studies on natural convection condensers have been restricted to smaller computational domains.

Forced convection air cooled condensers have been studied in larger detail as compared to the natural convection condensers in the present thesis due to smaller computational time larger commercial application. Chapter 6 presents a comparison of various types of fins under forced convection conditions. It should be noted that fin type affects the heat transfer significantly under both natural and forced convection conditions. However, studying various types of fins under natural convection conditions would have taken a very large amount of computational time. Therefore, the comparison of fins has been restricted to only forced convection conditions. Similarly, chapter 7 presents the thermal-hydraulic optimization of the forced convection air cooled condensers. The optimization methodology requires output from many numerical simulations because of the involvement of many geometrical parameters (fin spacing, fin diameter, number of tube rows, tube diameter etc.). Therefore, optimization has also been considered for forced convection air cooled condenser only to reduce the computational time.

Chapter 4
Natural convection in cavities

4.1. Introduction

The phenomena of natural convection occurs in many applications, for example, heat exchangers, cooling towers, air condensers, automobile industry, power plants, cooling of electronic equipment, solar collectors, cooling of buildings, etc. The better reliability of natural convection cooling makes it advantageous compared to the forced convection cooling. In the nuclear power plants, the safety has been a major issue for a long time. Therefore, to minimize the risk and improve the safety, the use of passive systems has been receiving increasing attention. The natural air convection is used in containment cooling, decay heat removal systems, pressure vessel cooling, etc., in the nuclear power plants.

The subject of natural convection of air on a circular cylinder enclosed in a cavity or in a box has been studied by many researchers experimentally as well as numerically. However, all of the numerical investigations performed so far, have been 2D only. The experimental studies were performed with the help of PIV (Particle Image Velocimetry), holographic interferometry, and smoke visualization. The location of the cylinder and the value of Rayleigh number have been the two main parameters in the previous studies. The details pertaining to previous work have been given in Chapter 2 (Section 2.2). The system details for the experiments and numerical simulations of the previous studies are given in Table 2.1 and Table 2.2, respectively.

From the literature survey discussed in Chapter 2 (Section 2.2), it may be noted that the 2D numerical simulations for the natural convection of air on a horizontal circular cylinder have been performed in cavities having a wide range of geometrical configurations. However, scant information is available on the 3D numerical simulations. The flow in the case of a finite circular cylinder can become three dimensional and oscillatory as shown by Koizumi and

Hosokawa (1996) depending on the *H*/D* ratio. This behaviour is difficult to capture quantitatively by 2D simulations. Further, *H*/D* ratio is an important parameter in the analysis of an air cooled condenser due to its compact configuration and formation of 3D vortices (presented in later chapters). Therefore, it was thought desirable to undertake systematic investigations in two steps: (a) to compare the published experimental data and the 2D numerical simulations published with the 2D simulations of the present work (b) to perform 3D simulations and present a comprehensive comparison with the experimental data and to bring out the difference between the 2D and 3D simulations.

4.2. Numerical solution

4.2.1. Preamble

From the discussion in Section 4.2, it is clear that the estimation of heat loss in the published literature has been addressed using two types of approaches: (1) development of empirical correlations and (2) use of CFD. The latter approach permits the understanding of physics of the system through the insights in (a) fluid mechanics and (b) the relationship between the fluid mechanics and design objectives such as heat losses. Secondly, during the past 25 years, CFD is being increasingly used because of the development in computational power as well as numerical techniques. Joshi and Ranade (2003) have given an overview of opportunities and scope of CFD. Ranade et al., (1989, 1990, 1992), Murthy et al., (2008) and Gandhi et al., (2011, 2013) have given the details pertaining to governing equation, method of solution and appropriate precautions for the implementation of CFD. Further, some examples of relationship between the fluid mechanics and design objectives have been described in the published literature. For instance, heat transfer [Thakre and Joshi (2000), Dhotre and Joshi (2004), Joshi et al., (1980)], mixing [Patwardhan and Joshi (1999), Nere et al., (2003), Kumaresan and Joshi (2006), Joshi and Sharma (1978), Kulkarni et al., (2001)], solid suspension [Murthy et al., (2007), Raghav Rao et al., (1988), Rewatkar and Joshi (1991)] and the rate of gas induction [Murthy et al., (2007), Joshi and Sharma (1977)]. Similar methodology has been employed in the present work for the estimation of heat losses.

4.2.2. Geometry

The system under consideration comprises of a box of dimensions 1000 mm × 600 mm × 1200 mm, and a circular cylinder of diameter 76.2 mm and length 560 mm (Fig. 4.1A). The half symmetry of the box is used for the 3D simulations (dotted box) as shown in Fig. 4.1B and for 2D simulations only the cross-section (*x*-*z* plane) of the geometry is used. The cylinder is

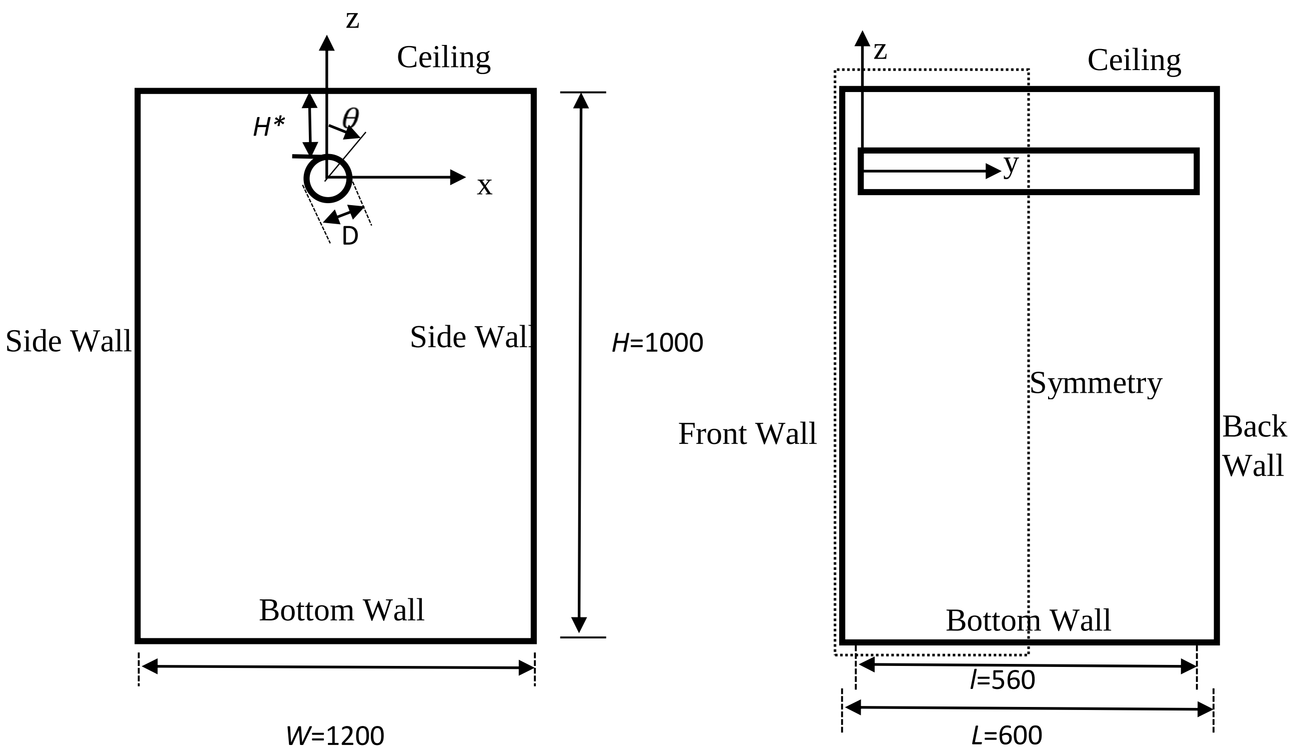

Fig. 4.1. Schematic of the physical model (a) front view (*x*-*z* plane), (b) side view (*y*-*z* plane), and the dotted box is showing the considered computational domain.

kept horizontally inside the box and the position of the cylinder is changed vertically with respect to the ceiling for a range of $0.2 \leq H^*/D \leq 2.3$. The working fluid in the enclosure is air and is kept at an initial temperature of 300 K. The geometry generation and meshing are performed using Gmsh 2.3 [Geuzaine and Remacle (2009)].

4.2.3. Governing equations and model assumptions

The problem under consideration is unsteady 3D natural convection of air inside a cuboidal enclosure. The assumptions in the computational model are the following:

1. Flow is Newtonian and incompressible.
2. Boussinesq approximation is valid i.e., density difference is only important in producing buoyancy.
3. Constant fluid properties except in the formulations of buoyancy term.

The Rayleigh number is 1.3×10^6, therefore, the flow is considered in the laminar region. The governing equations for the 3D unsteady natural convection are continuity, momentum and energy equations have been given in Chapter 3 (Eqns. 3.5-3.7)

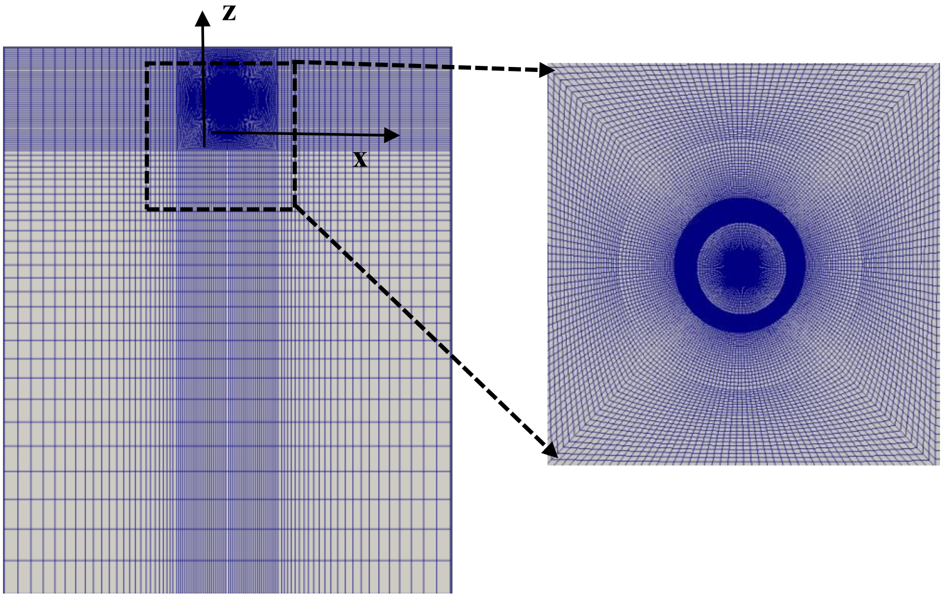

Fig. 4.2. Computational grid with closer view of the mesh around the cylinder.

The thermal coefficients are calculated at the mean temperature of the cylinder and ambient. The value of the Prandtl number, *Pr*, is taken as 0.7. The local heat transfer coefficient at any point on the cylinder or the enclosure wall is calculated using the temperature predictions from the numerical simulations and is defined as:

$$h = \frac{k}{\Delta T} \frac{\partial T}{\partial x}\bigg|_{surface} \qquad \dots (4.1)$$

The length average heat transfer coefficient for the cylinder is calculated by integrating h over the length of the cylinder and is given as:

$$h_l = \int_0^l \frac{k}{\Delta T}\frac{\partial T}{\partial x} dy \qquad \dots (4.2)$$

The circumferential average heat transfer coefficient is obtained by integrating the h over the periphery of the cylinder and is given as:

$$h_\theta = \int_0^\theta \frac{k}{\Delta T}\frac{\partial T}{\partial x} d\theta \qquad \dots (4.3)$$

In the present case angle θ is 0° at the top of the cylinder and it increases as we move along the periphery (clockwise) of the cylinder and at the lowest point of the cylinder (stagnation point), it becomes 180° (Fig. 4.1A).

The total surface area averaged heat transfer coefficient for the cylinder is obtained by integrating h_l over the periphery of the cylinder and is given as:

$$h_{avg} = \int_0^\theta h_l \, d\theta \qquad \dots (4.4)$$

where ΔT is the temperature difference between the cylinder surface and isothermal wall. For 2D numerical simulations, h is equivalent to the h_l.

Nusselt number can be obtained for all the above definitions of heat transfer coefficient using the relation,

$$Nu = \frac{hD}{k}$$

4.2.4. Boundary condition

The walls of the box are specified as adiabatic boundary condition except the ceiling, which is conducting and is set at a constant temperature of 300 K. The cylinder is assumed to be at a constant temperature of 340 K. The no slip boundary condition is used at the cylinder surface and cuboidal box surface. The details pertaining to the boundary conditions are given in Table 4.1.

4.2.5. Method of solution

In the present work, simulations are performed under unsteady conditions. All the computational work is carried out using the software OpenFOAM-2.2, which is based on finite volume approach. The transient terms are discretized by using the second order implicit scheme. QUICK scheme is used to discretize the divergence terms, which is a third order

Table 4.1. Boundary conditions for the present case.

	Temperature	Velocity	Pressure
Cylinder	T_c	$U = 0$	Atmospheric
Ceiling	T_w	$U = 0$	Atmospheric
Side Walls	$\frac{\partial T}{\partial x} = 0$	$U = 0$	Atmospheric
Bottom Wall	$\frac{\partial T}{\partial x} = 0$	$U = 0$	Atmospheric
Front Wall	$\frac{\partial T}{\partial x} = 0$	$U = 0$	Atmospheric
Symmetry	$\frac{\partial T}{\partial x} = 0$	$\frac{\partial U}{\partial x} = 0$	$\frac{\partial p}{\partial x} = 0$

scheme and the diffusion terms are discretized using the central difference method, which is a second accurate scheme. All the discretized equations are solved in a segregated manner with the PISO (Pressure Implicit with Splitting of Operators) algorithm. In PISO algorithm, the equations are solved using initial guess values of flow variables, and then the values are corrected in each iteration. The iterative process continues until the convergence criterion is satisfied. The convergence criterion was based on the scaled residuals of the velocity, when the residuals reached below 10^{-5}, the solution was considered to be fully converged.

4.2.6 Grid independence

A structured hexahedaral non-uniform mesh was generated using Gmsh 2.3. A fine mesh was generated around the cylinder to capture the high velocity and temperature gradients. A grid resolution of 500000, 700000, and 900000 was used to carry out the grid senstivity. The difference in the h_{avg}, was within 1 % for the three cases. Finally a grid of 700000 cells was used for all the cases.

4.3. Results and discussions

The validation of present code with the experimental based correlations is given in the Section 4.4.1. Further, a comparison between the experimental and 2D numerical results of Cesini et al., (1999) and Newport et al., (2001) with the present 2D and 3D numerical simulations results is given in Sections 4.3.2 and 4.3.3, respectively. The detailed results of the present study in terms of 3D velocity vectors, temperature contours and heat transfer coefficient are presented in Section 4.4.5.

4.3.1. Validation

The first validation has been done by comparing the surface averaged Nusselt number, Nu_{avg} of the cylinder kept at the center of the box (with adiabatic walls) with the correlations given by Churchill and Chou (1975) and Morgan (1975) and is shown in Fig. 4.3A. We can observe that the numerical model is in a good agreement with the correlations. The second validation is given with the local temperature measurements by Koizumi and Hosokawa (1996) for H^*/D =0.2 and is shown in Fig. 4.3B. For the temperature measurements, Koizumi and Hosokawa (1996) placed the thermocouples between the cylinder and the ceiling at equal distance from the mid-point of the cylinder. The distance between the thermocouples was varied in order to take the measurements at different locations along the length, and then the mean of both the thermocouples was taken. In the present CFD simulations, we have considered the symmetry at the mid-plane along the length, therefore the temperature measurement comparison is considered in one half of the box. Small deviations were observed

(4% - 11%) between the CFD predictions and the experimental measurements, and the reason is explained in Section 4.3.4.2.

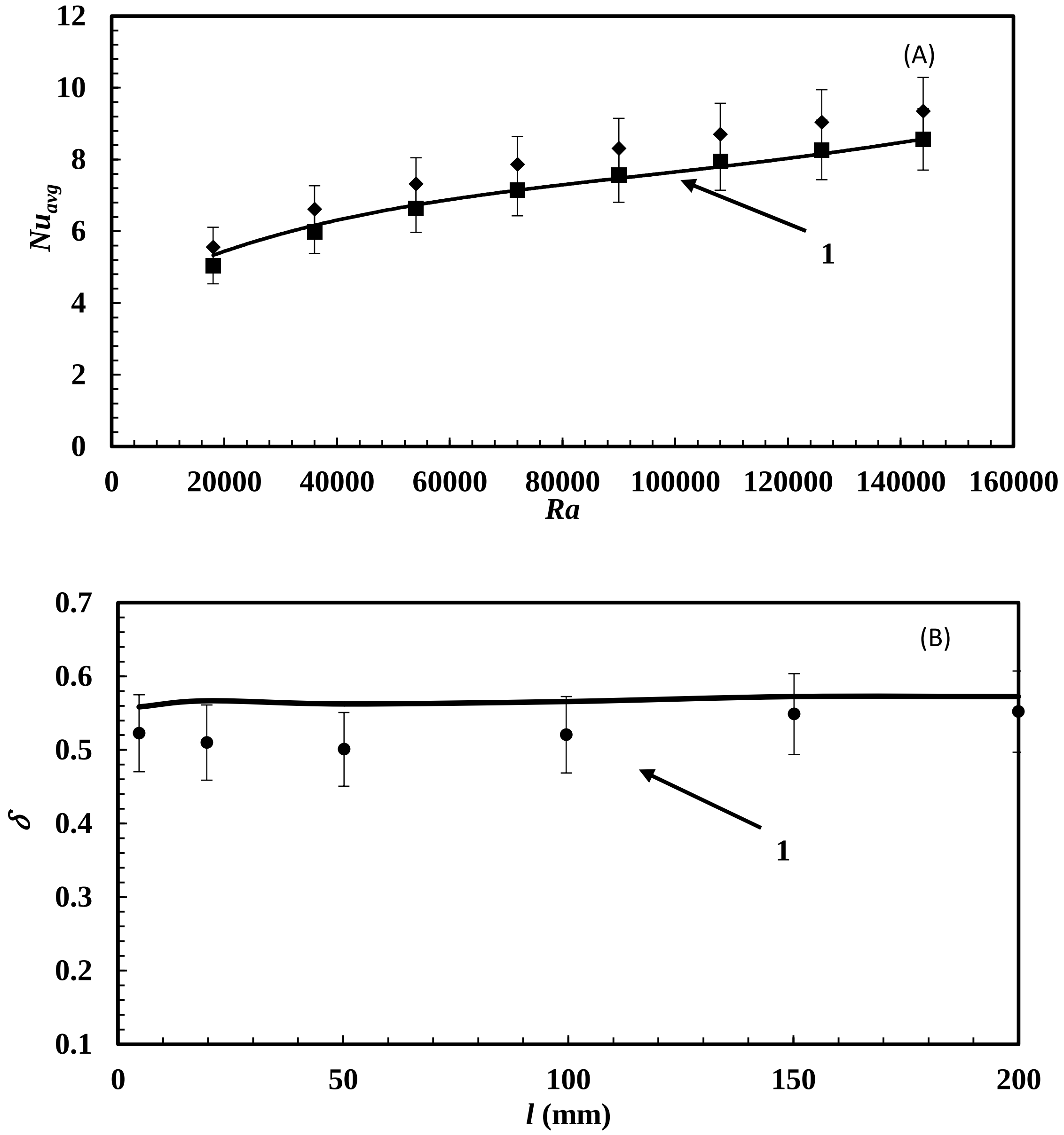

Fig. 4.3. Code Validations (A) Comparison of surface averaged Nusselt number predicted by numerical simulations for cylinder kept at the centre of the box with the correlations proposed by (■)Churchill and Chou (1975) and (♦)Morgan, (B) Comparison of local temperature predicted by CFD with (●)Koizumi (1996) for the case of H^*/D = 0.2. (1) CFD predictions

4.3.2. Analysis of the work of Cesini et al. (1999)

In Section 2.2 (Chapter 2), we have explained the study performed by Cesini et al., (1999). For comparison, initially we performed 2D numerical simulations of their physical model with a cavity aspect ratio, *AR* of 2.1 at *Ra* = 1300, 2400, 3400. The numerical method is given in Section 4.3, and the boundary conditions are the same as used in the study of Cesini et al., (1999) (Table 4.3). A good agreement between present results and the results of Cesini et al., (1999) can be observed in Table 4.4 for 2D numerical simulations. Proceeding further,

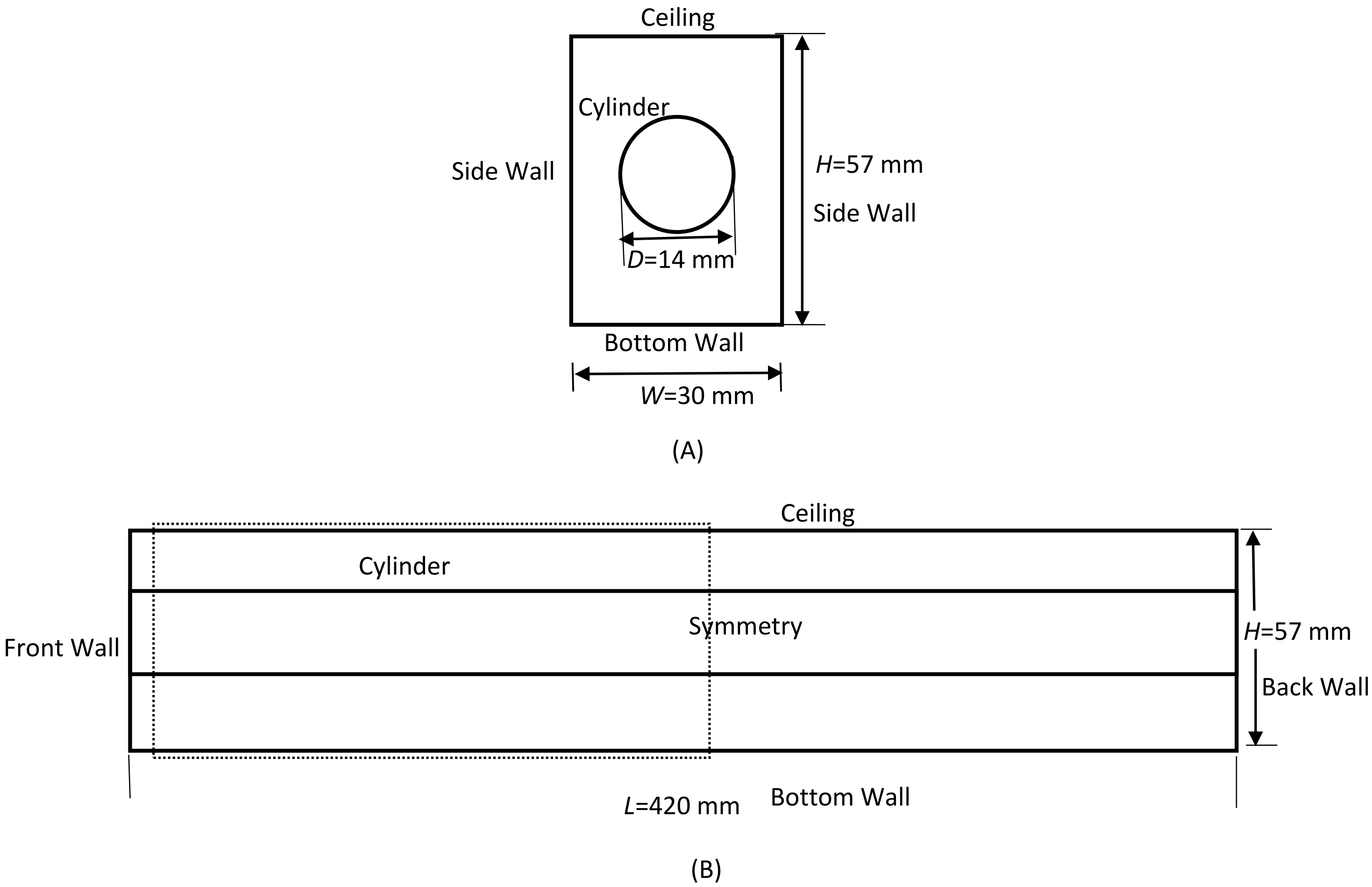

Fig. 4.4. Schematic of the physical model of (Cesini et al., (1999)) (A) front view (x-z plane), (B) side view (y-z plane), and the dotted box is showing the computational domain.

we performed the 3D numerical simulations by considering symmetry at half-length of the cavity (Fig. 4.4, dotted box shows the computational domain). The number of cells was varied from 720000 to 950000, and the difference in h_{avg} was negligible, therefore a mesh size of 844000 was used in the study. It was found that the h_{avg} value (present work) was 13-20 % higher than the surface averaged heat transfer coefficient obtained by their 2D numerical simulations and approximately 10 % higher from their experimental heat transfer coefficient (Table 4.5). We tried to find the reason behind this discrepancy and analyzed the 3D velocity vectors and the temperature contours, which are shown in Figs. 4.5 and 4.6. In Fig. 4.5, the velocity vectors and temperature contours are shown in the *x*-*z* plane, it was difficult to select a particular location to observe the velocity vectors and temperature contours because the flow was not uniform along the length of the cavity as can be seen in Fig. 4.6. Therefore, a plane was chosen where the main circulation eddies were present in the *x*-*z* plane for all the cases (at y = 0.1186 m). In *x*-*z* plane, it can be observed that the fluid inside the cavity is heated at the cylinder surface and moves upward due to the density

Table 4.2. Boundary conditions for Cesini et al. (1999)

	Temperature	Velocity	Pressure
Cylinder	T_c	$U = 0$	Atmospheric
Ceiling	$\frac{\partial T}{\partial x} = h(T - T_a)$	$U = 0$	Atmospheric
Side Walls	T_w	$U = 0$	Atmospheric
Bottom Wall	$\frac{\partial T}{\partial x} = 0$	$U = 0$	Atmospheric
Front Walls	$\frac{\partial T}{\partial x} = 0$	$U = 0$	Atmospheric
Symmetry	$\frac{\partial T}{\partial x} = 0$	$\frac{\partial U}{\partial x} = 0$	$\frac{\partial p}{\partial x} = 0$

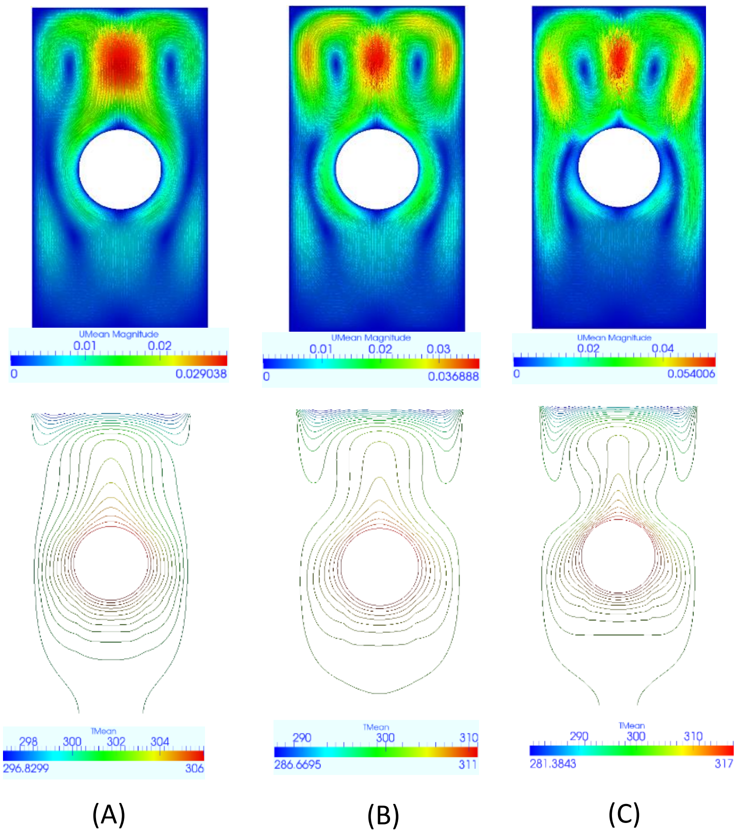

Fig. 4.5. Velocity vectors and temperature contours in *x*-*z* plane at *y*=0.1186 m, (A) *Ra*=1300, (B) *Ra*=2400, (C) *Ra*=3600.

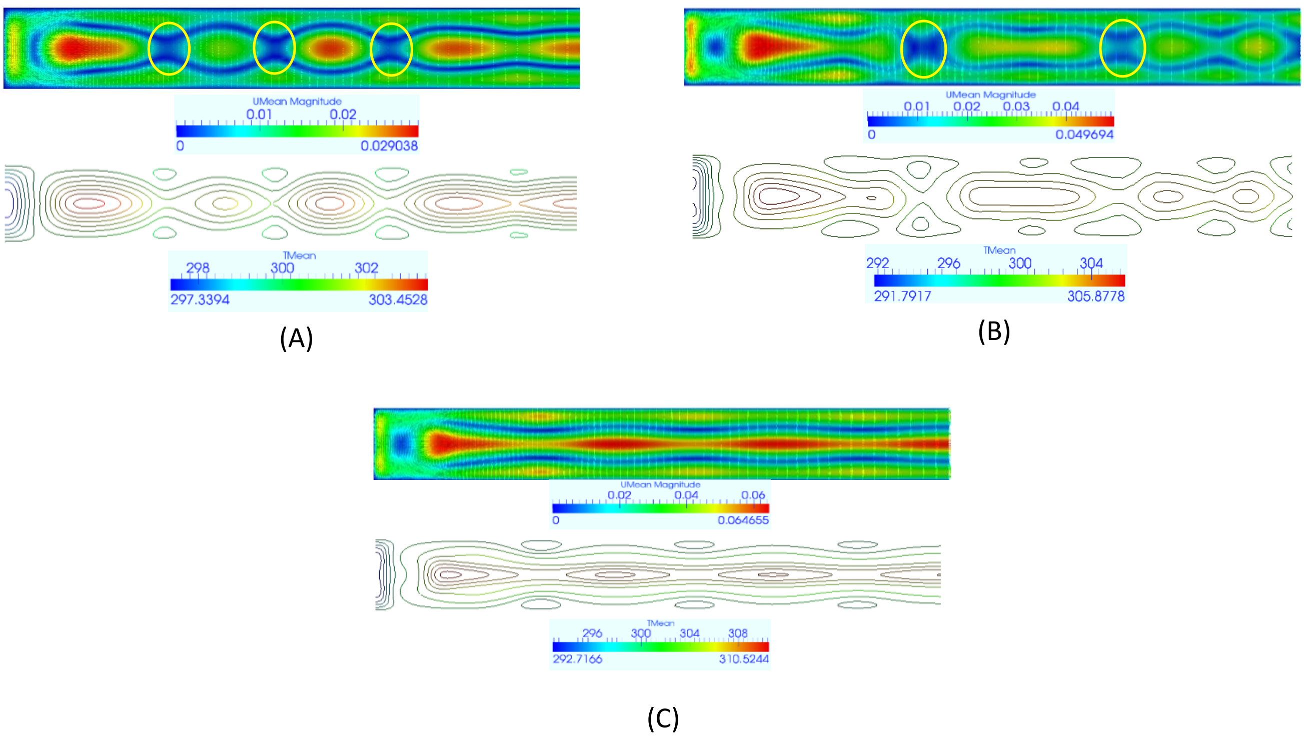

Fig. 4.6. Velocity vectors in *x*-*y* plane at *z*=0.017 m and in *y*-*z* plane at *x*=0, (A) *Ra*=1300, (B) *Ra*=2400, (C) *Ra*=3600.

difference caused by the heating. The fluid transfers heat to the ambient through the ceiling, and moves along the ceiling and side walls and reaches to the lower part of the cavity and then move upwards. Further, it gets again heated at the cylinder surface. This way two large recirculating eddies are formed inside the cavity in the *x*-*z* plane. It can also be observed that as the Rayleigh number is increased from 1300 to 3400, the circulation flow velocity increases in the cavity. The temperature contours are smooth and relaxed at low Rayleigh number. Moreover, these become distorted and denser in the vicinity of the cylinder and the ceiling with an increase in the Rayleigh number. This indicates that the temperature gradient near the conducting cylinder and the ceiling increases, leading to a thinner thermal boundary layer which enhances the convective heat transfer rate. This type of flow behavior has also been explained by Kim et al., (2008) in the 2D natural convection of air inside a square cavity. However, 2D natural convection does not consider the flow variation along the length of the cavity. Therefore, we have given the velocity vectors and temperature contours along the length of the cavity in Fig. 4.6. In the *x*-*y* plane (Fig. 4.6A), for $Ra = 1300$, we observe that the flow is not uniform along the length of the cavity and the two main recirculation cells which are observed in Fig. 4.5 (in the *x*-*z* plane) merge with each other at some locations (the yellow circles show the merging locations) leading to a division of the flow into several smaller plumes. The temperature contours indicate a non-uniform distribution of heat transfer along the length of the cavity and regions of low temperature gradient (low heat transfer) are seen at the merging locations of the recirculating eddies. As the front wall of the cavity is approached, a very complex flow is seen to be emerging with a secondary recirculating eddy in the *y*-*z* plane (not presented), which can be caused by the interaction of the front wall, ceiling, bottom wall and cylinder. A location of maximum velocity can be observed near this region, which can be a resultant of the flow velocities of main recirculating eddies and the secondary recirculating eddy. The temperature contours are very dense in this region, which indicates a large heat transfer rate near the front wall of the cavity. The non-uniformity in the flow profile and temperature contours is symmetric on both sides of the centre-line of the cavity. For *Ra* = 2400 (Fig. 4.6B), the flow behaves similar to the case of *Ra* =1300. The flow is non-uniform and symmetric along the length of the cavity, and a secondary recirculating eddy is observed near the front wall of the cavity. The merging locations for the recirculating eddies are fewer in this case and the temperature contours are almost symmetric and non-uniform along the length with

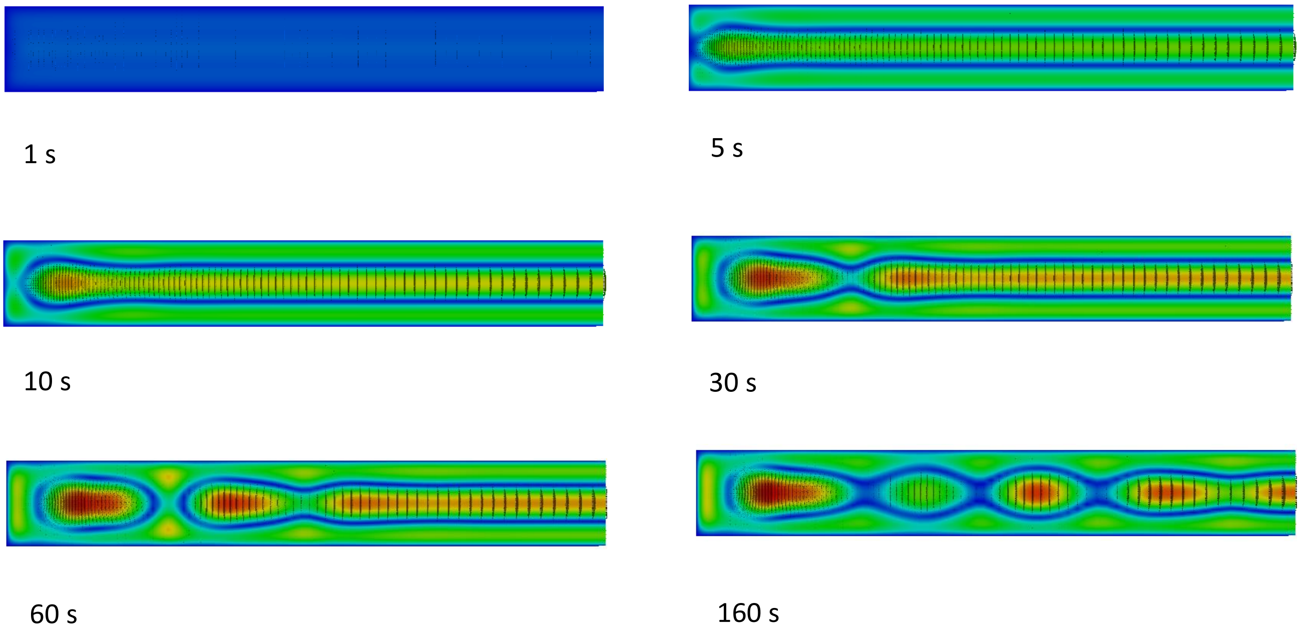

Fig. 4.7. Flow development with time for *Ra*= 1300.

Table 4.3. Comparison of h_{avg} obtained in present 3D numerical simulations with Cesini et al., (1999).

Rayleigh number	Cesini et al. (2D)	Present results (2D)	Cesini et al. (Experimental)	Present Results (3D)
1300	4.46	4.38	4.65	5.12
2400	4.93	4.91	5.29	5.85
3400	5.23	5.21	5.80	6.46

low temperature gradient in the merging locations. It can also be observed that the temperature contours are more distorted in this case as compared to those for *Ra* = 1300 and the flow is thus divided into several plumes as was observed for the case of *Ra* = 1300. For *Ra* = 3400 (Fig. 4.6C), we observe that the main recirculating eddies do not merge with each other, however, they are still unstable. This results in a 3D, unstable and oscillating flow along the length of the cavity and the secondary recirculating eddy is present in this case as well. The temperature contours are not distorted in this case, however, they are very dense and oscillating. In Fig. 4.7, we have given the flow development in the cavity with time for *Ra* = 1300 in the *x-y* plane, which shows that between *t* = 0-5 sec the flow starts developing in the cavity. Initially the main recirculating eddies and the secondary eddies are formed and as the time progresses the recirculating eddies start merging with each other (*t* = 30 s). From *t* = 60 s to *t* = 160 s, the flow reaches a steady state with the merging of recirculating eddies at some location and the flow is divided into several separate plumes. Yu et al. (2011) have given the time varying average Nusselt number for the case of 2D natural convection by a heated cylinder inside a triangular enclosure. In their study, the flow reached a steady state or oscillatory state in a time duration of approximately 15 s. In the present case, it can be observed that the flow reaches a steady state in about 160 s, which is very large as compared to the time duration of 15 s for Yu et al., (2011). Therefore, we can conclude that due to the complexity of the 3D natural convection, the flow takes a larger time to reach the steady state. From these results, we find that the flow in the cavity is 3D, unstable, complex and oscillating which leads to a variation in Nusselt number along the length of the cavity. Therefore, this type of flow behavior cannot be captured by 2D numerical simulations or by some of the experimental techniques (e.g., holographic interferometer), which gives the flow pattern only in 2D. Therefore, 3D numerical simulations must be performed to capture the complexity of the flow in the 3D natural convection.

4.3.3 Analysis of the work of Newport et al. (2001)

As explained in Section 2.2, Newport et al., (2001) studied the natural convection of air around a circular cylinder kept in a cubical box. We have carried out 2D and 3D simulations for two of their cases and compared the results with their experimental and numerical results. Their Rayleigh number range was from 6800 to 21800 and for comparison we have chosen the lowest and highest values of Rayleigh number (6800 and 21800). In Fig. 4.8, we have shown the physical model, and the computational domain is enclosed by the dotted lines, which is half symmetry (along the length) of the physical model. The numerical model has already been explained in Section 4.3, and the boundary conditions are similar to the boundary conditions

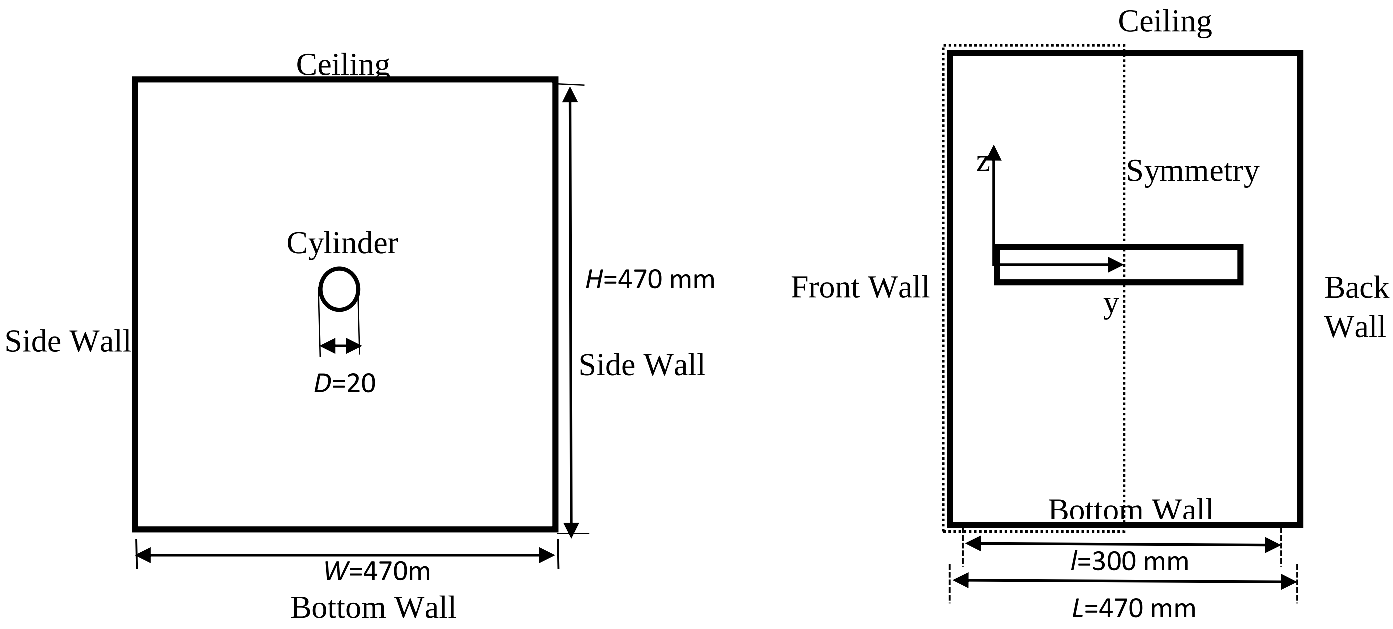

(A) (B)

Fig. 4.8. Schematic of the physical model of (Newport et al., (2001)) (A) front view (x-z plane), (B) side view (y-z plane), and the dotted box is showing the computational domain.

of Newport et al., (2001) (Table 4.5). A grid independence in the results was observed for a range of cell number from 550000 to 700000 and then a mesh of 640000 number of cells was used in the study. In Figs. 4.9A, 4.9B and 4.9C, the velocity vectors and temperature contours can be seen in all the three planes for *Ra* = 21800. The flow was found to be mostly in the *x-z* plane and the end effects were negligible. In Fig. 4.9A, we have given the closer view for the flow in upper right part of the domain. It can be clearly seen that the hot plume rising from the hot cylinder surface moves up, takes a turn at the ceiling and moves horizontally along the cooled ceiling. Then, it turns downwards and moves along the side walls. It may be pointed out that the main circulation is present only near the walls unlike the case of the cavity (Section 4.3.2). In the bulk, only small recirculating flow is present and the temperature contours are denser near the cylinder and enclosure walls. Therefore, it indicates that the heat transfer and mixing is poor in the bulk, and most of the heat transfer occurs in the vicinity of cylinder and walls. In Figs. 9B

Table 4.4. Boundary conditions for Newport et al. (2002)

	Temperature	Velocity	Pressure
Cylinder	T_c	$U = 0$	Atmospheric
Ceiling	T_w	$U = 0$	Atmospheric
Side Walls	T_w	$U = 0$	Atmospheric
Bottom Wall	T_w	$U = 0$	Atmospheric
Front Walls	$\frac{\partial T}{\partial x} = 0$	$U = 0$	Atmospheric
Symmetry	$\frac{\partial T}{\partial x} = 0$	$\frac{\partial U}{\partial x} = 0$	$\frac{\partial p}{\partial x} = 0$

and 9C, the velocity vectors are straight and parallel, therefore no 3D effects are observed in this case. The temperature contours also indicate a 2D and stable flow. In Figs. 10A and 10B, a comparison is given between the heat transfer coefficient (h_l for cylinder and h for ceiling) obtained from the present 2D and 3D numerical simulations and the numerical and experimental results of Newport et al., (2001) for the cylinder and ceiling respectively. It can

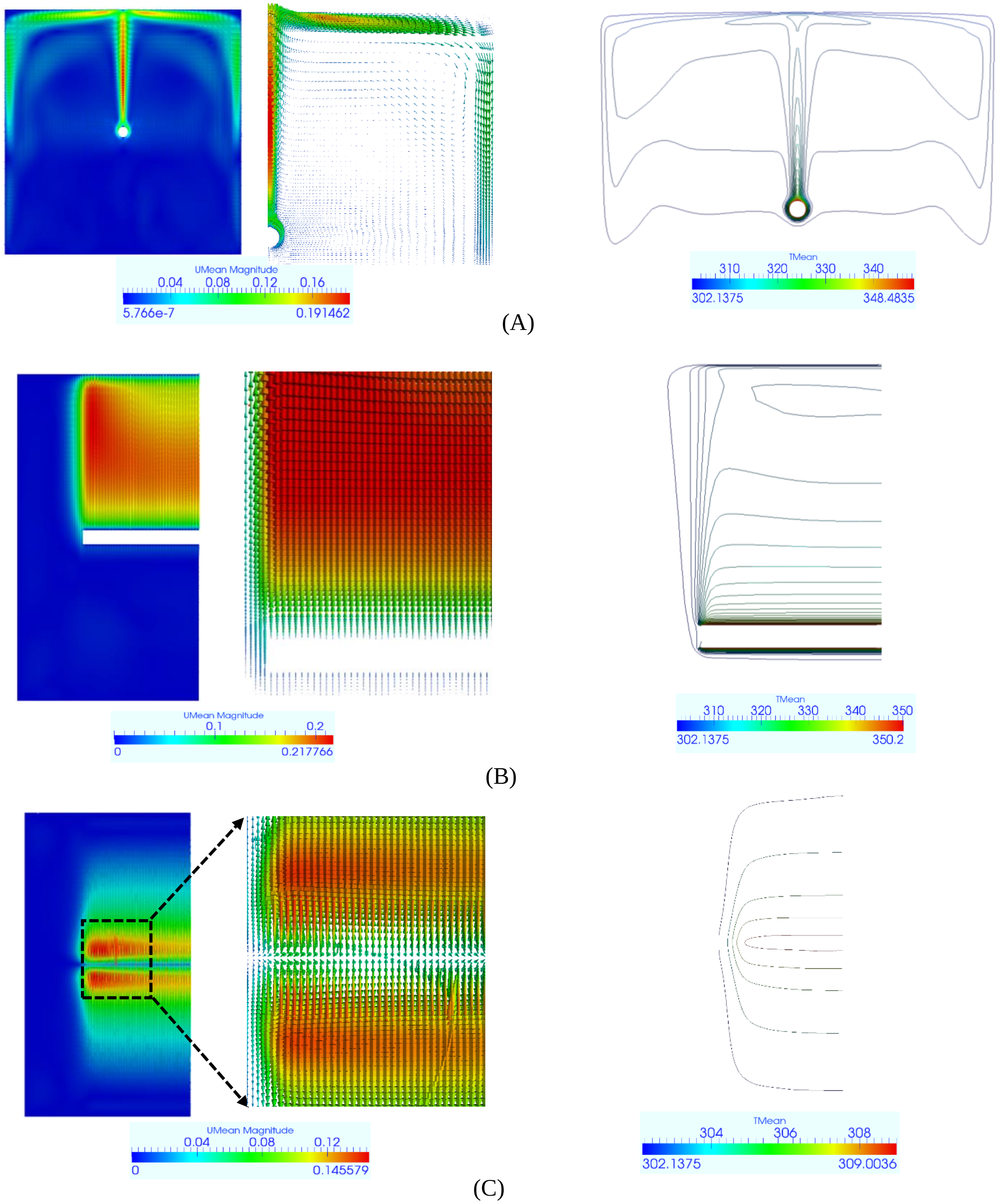

Fig. 4.9. 3D Velocity vectors and temperature contours for *Ra*=21800, (A) *x*-*z* plane at *y*=0.15, (B) *x*-*y* plane at *z*=0.233, (C) *y*-*z* plane at *x*= 0.

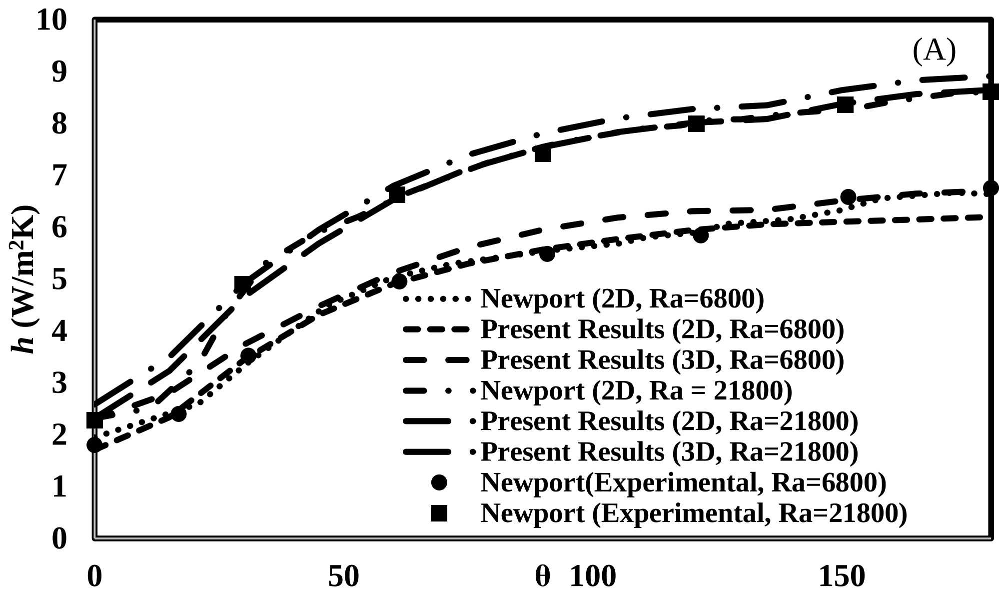

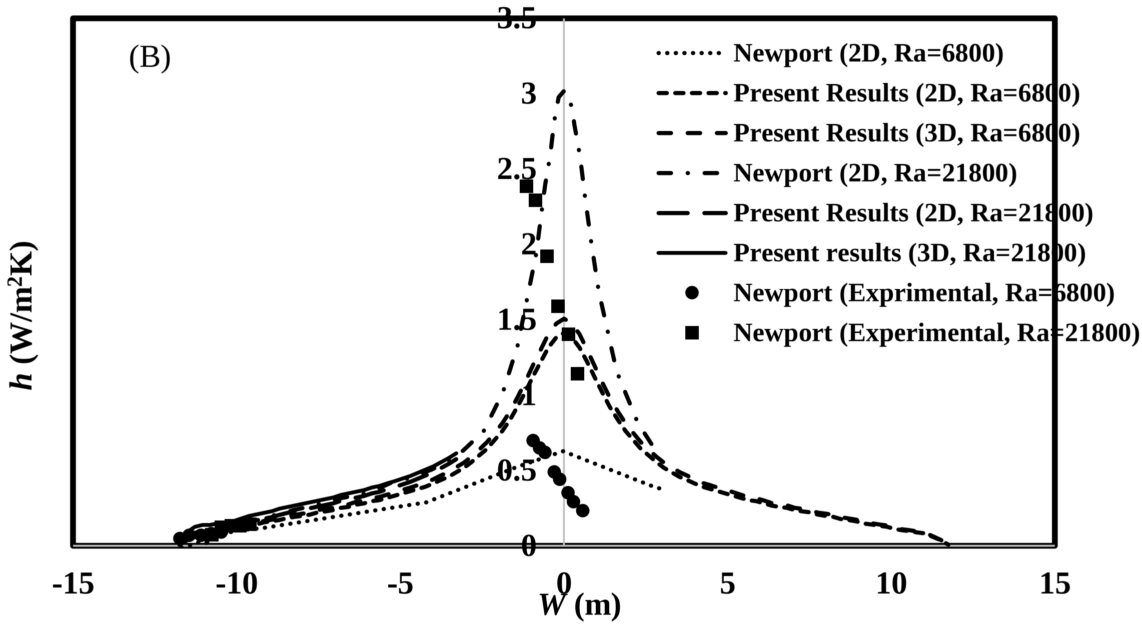

Fig. 4.10. Heat transfer coefficient comparison of present results and Newport et al (2001), (A) Distribution of h_l for the cylinder, (●) Newport (experimental, *Ra*=6800), (■) Newport (experimental, *Ra*=21800),
(B) Distribution of *h* for the ceiling, (●) Newport (experimental, *Ra*=6800), (■) Newport (experimental, *Ra*=21800).

be observed that for the cylinder, present results for 2D and 3D numerical simulations are very close to the experimental and numerical results of Newport et al. (2001) for both the Rayleigh numbers. However, for the ceiling, the present numerical results show a higher *h* than the experimental and numerical results of Newport et al. (2001) at *Ra* = 6800. At *Ra* = 21800, present numerical results slightly underpredict their experimental results and largely underpredict their 2D numerical results. Newport et al. (2001) stated that their 2D numerical results overpredict the experimental results due to the presence of 3D effects near the ceiling, which seems contradicting statement as 3D vortices should enhance the heat transfer. Still, we carried out detailed analysis of the flow we could not find any 3D effects near the ceiling. Further, present 2D and 3D numerical results are closer to the experimental results of Newport et al. (2001). Therefore, the discprency between the numerical and experimental results of Newport et al., (2001) is still unknown to us. From these results, it can be concluded that, when the cylinder is kept at the centre of the enclosure and aspect ratio is large enough to avoid cylinder-wall interaction, then the flow is 2D and stable in the enclosure.

4.3.4. Heat transfer and flow patterns for the present study

The heat transfer coefficient is presented for 2D and 3D numerical simulations and is compared with the experimental results of Koizumi and Hosokawa (1996) (experimental results were available only for H^*/D = 0.2 and 1), while the flow patterns are shown only for the 3D numerical simulations. The velocity profile over a line or plane may not give the overall view of the 3D nature of the flow, therefore, we have given the velocity profiles (for H^*/D = 0.2 only) at five different locations along the length of the cylinder in the *y-z* plane.

4.3.4.1. Flow patterns

Fig. 4.11 shows, the velocity vectors and temperature contours in the *x-z* plane. It can be seen from Fig. 4.11 that, for the smallest H^*/D ratio (0.2), two vortices appear in the gap between the ceiling and the cylinder, and the vortices rotate in opposite directions. The flow separates at about 30° (zero degree being on the top) from the surface of the cylinder and the flow is symmetric on both sides of the cylinder. The main flow recirculation is present only in the upper part of the enclosure and there is negligible mixing and heat transfer in the rest of the

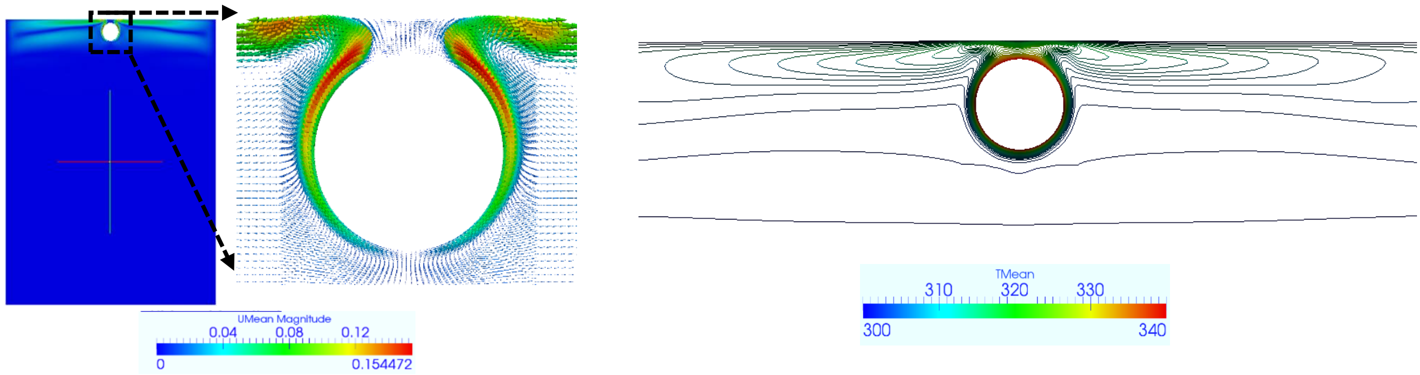

(A)

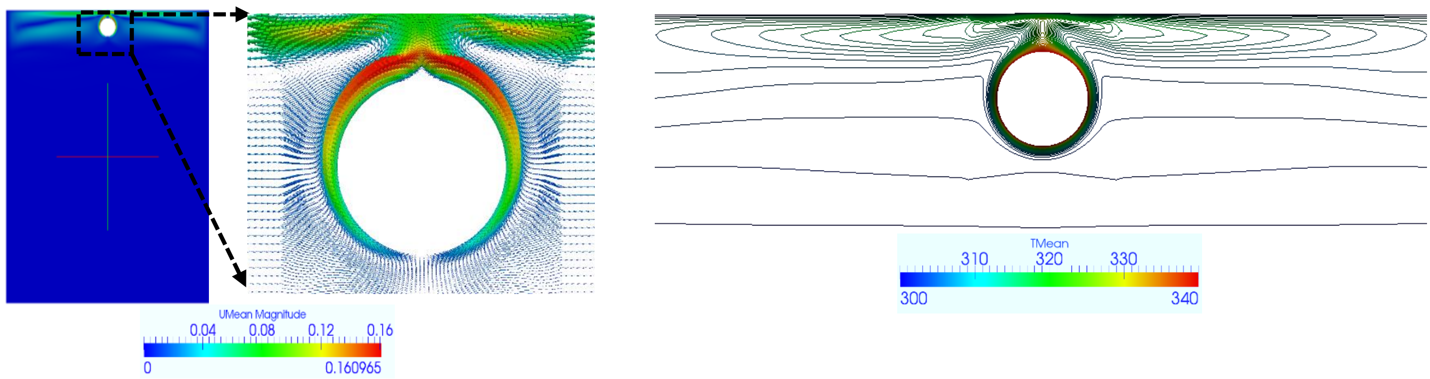

(B)

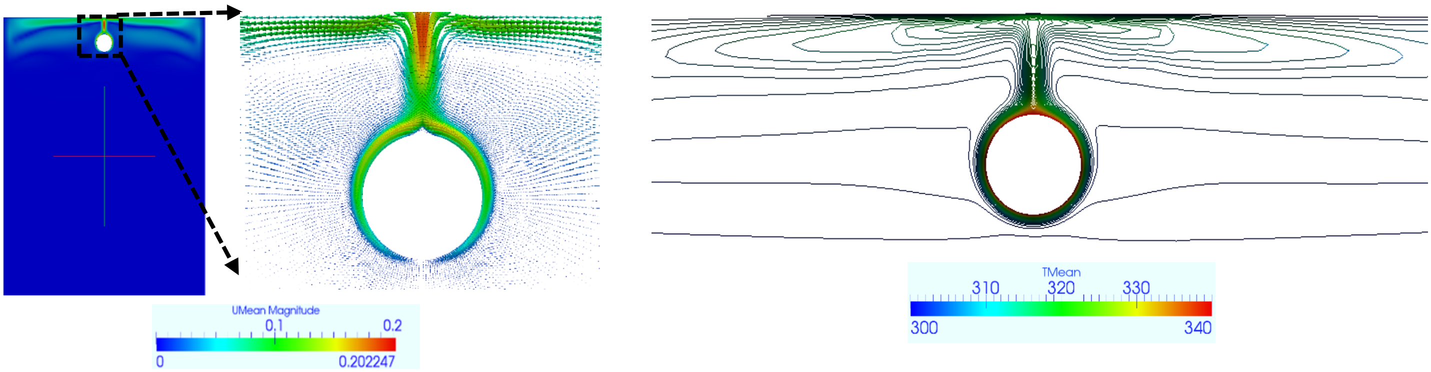

(C)

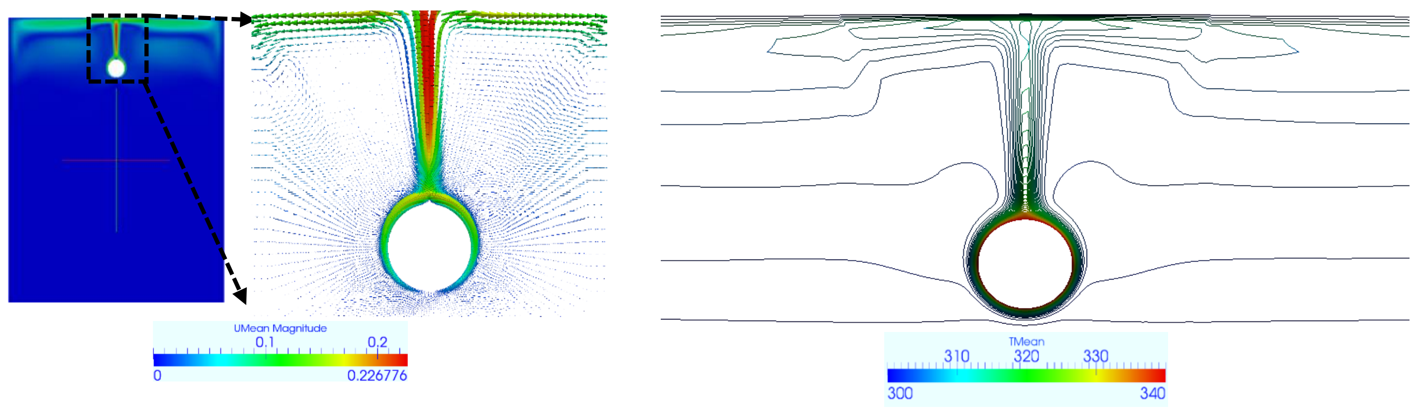

(D)

Fig. 4.11. Velocity vectors and temperature contours in *x-z* plane at *y* =0.16 m for (a) *H*/D*= 0.2, (b) *H*/D*=0.4, (c) *H*/D*=1, and (d) *H*/D*= 2.3

bulk. As the *H*/D* ratio is increased to 0.4, we find that the two vortices disappear. In this case the flow emerging from two sides of the cylinder meet and form a single plume, which separates only at the ceiling. As the *H*/D* ratio is increased to 1, we observe that the flow behaves like the case of *H*/D = 0.4*, and it separates at the ceiling and moves along the ceiling and side walls. The main flow recirculation is present in a larger part of the enclosure as compared to the case *of H*/D* = 0.2 and 0.4. For *H*/D* = 2.3, the plume rising from the cylinder separates before it reaches the ceiling. This type of flow profile was also observed by Koizumi and Hosokawa (1996), and was described as oscillating flow. In this case, a larger flow recirculation is observed in the upper part of the enclosure and hence the mixing and heat transfer is enhanced. Also, as the distance between the ceiling and cylinder is increased, the buoyancy effects increase, which leads to a higher value of maximum velocity for larger *H*/D* ratio. For *H*/D = 0.2*, the temperature contours are very dense in the vicinity of the cylinder and are symmetric on both sides of the cylinder, and as the distance between the ceiling and cylinder is increased (*H*/D=0.4, 1, 2.3*), the contours become more relaxed in the region between the cylinder and the ceiling. This indicates a lower temperature gradient with an increase in the ceiling-cylinder distance. Similar predictions in the *x-z* plane can be seen in the experimental results of Koizumi and Hosokawa (1996), and *2D* numerical simulations of Kim et al. (2008), and Hussain and Hussein (2010). However, previous numerical studies did not consider the flow profile and temperature contours in the other two planes. Therefore, we analyzed the flow profile and temperature contours in the *y-z* and *x-y* planes. Fig. 4.12, shows velocity vectors and temperature contours in the *y-z* plane (mid plane at *x=0*) for all the cases. For *H*/D* = 0.2, we observe that the flow is wavy and complex, which

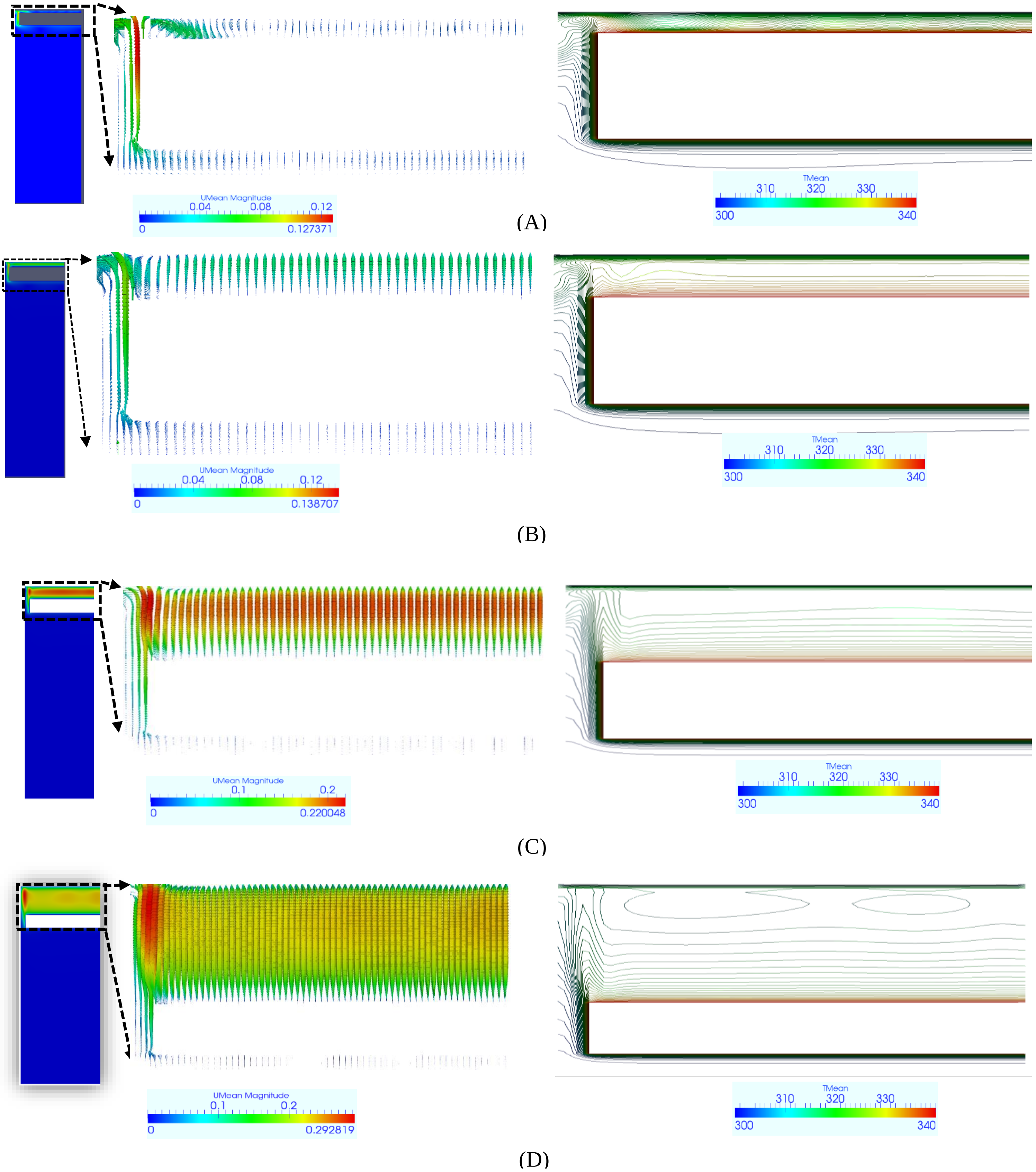

Fig. 4.12. Velocity vectors and temperature contours in *y-z* plane at *x*=0 for (a) *H*/D*= 0.2, (b) *H*/D*=0.4, (c) *H*/D*=1, and (d) *H*/D*= 2.3.

clearly indicates a 3D fluid flow between the cylinder and the ceiling. As the *H*/D* ratio is increased to 0.4, 1 and 2.3, the flow becomes 2D and moves in the *z* direction only. It can also be observed that, the temperature contours are very dense and wavy for *H*/D =0.2*. The wavy temperature contours are caused by the complex flow pattern between the cylinder and the ceiling for this case. As the *H*/D* ratio is increased to 0.4, 1 and 2.3, the contours become relaxed and almost straight, which indicates a less temperature gradient and presence of a 2D flow between the cylinder and ceiling. Fig. 4.13 gives the flow profile and temperature contours in the *x-y* plane. For *H*/D* = 0.2, similar to the *y-z* plane, the flow is very complex and unstable, in addition, vortices are present in this plane, which are helping in mixing of the two plumes originating from both sides of the cylinder. As the *H*/D* ratio is increased to 0.4, 1 and 2.3, the flow becomes 2D and velocity vectors are almost straight (except near the ends due to the interaction of the cylinder end and enclosure wall). The temperature contours are wavy for the case of *H*/D = 0.2*, and the small circular temperature contours show the presence of the vortices in this plane. Therefore, there is a significant heat transfer in the region between the cylinder and the ceiling for the case of *H*/D = 0.2*. As the *H*/D* ratio is increased to 0.4, 1 and 2.3, 2D flow profile and relaxed contours are observed. In all the cases, the interaction of the cylinder end and enclosure wall causes some complexity near the cylinder end and due to this, the flow near the ends of the cylinder shows a 3D nature.

Further, to capture the 3D nature of the flow for *H*/D = 0.2*, Fig. 4.14 shows velocity profile at five different locations in the enclosure. For $\theta = 0°$ (Fig. 4.14A), it can be observed that, near the end of the cylinder, the velocity is larger in the *y* and *z* directions as compared to the velocity in *x* direction, and as the mid region of the cylinder is approached, the three components become comparable due to the presence of the 3D vortices at this location. As we move away from the centerline ($\theta = 20°$, Fig. 4.14B), the mean velocity decreases in the *y* direction and the *x* component of the velocity increases. This location is closer to the location

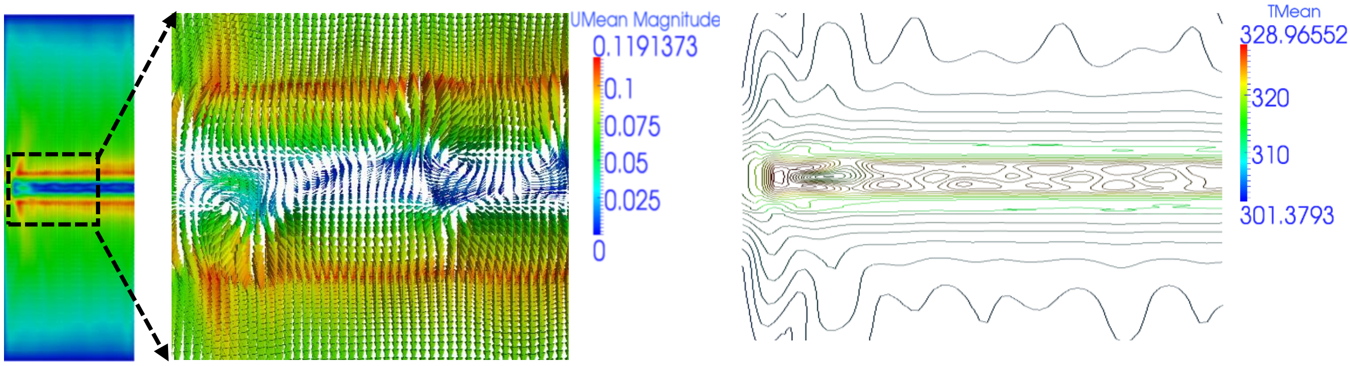

(A)

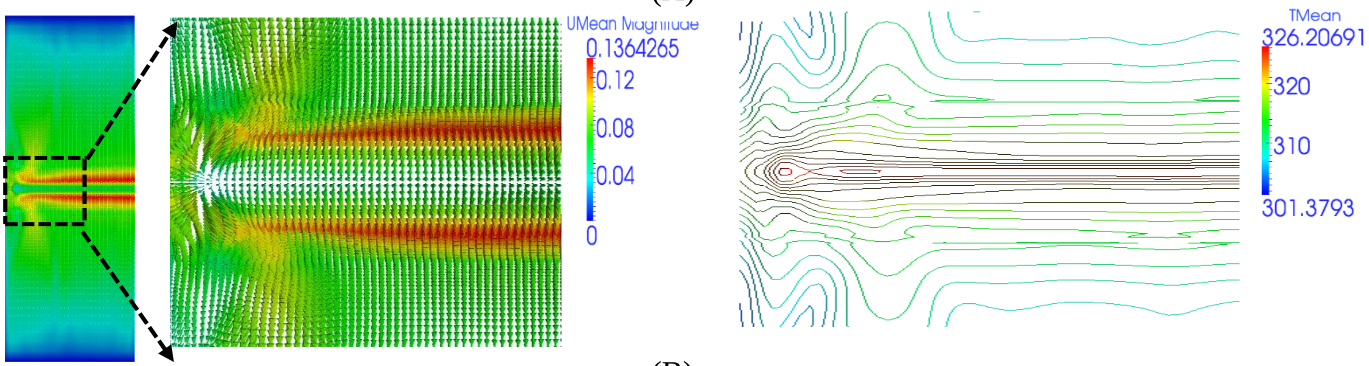

(B)

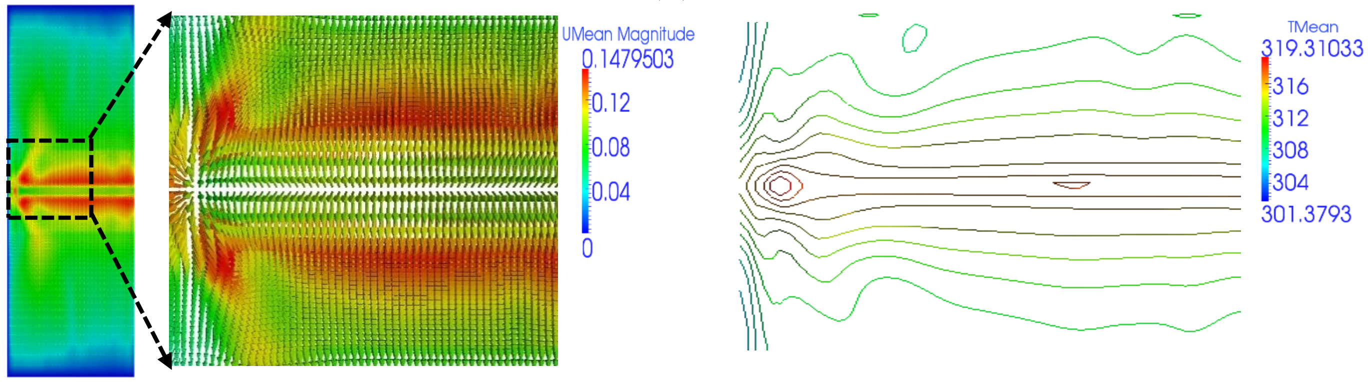

(C)

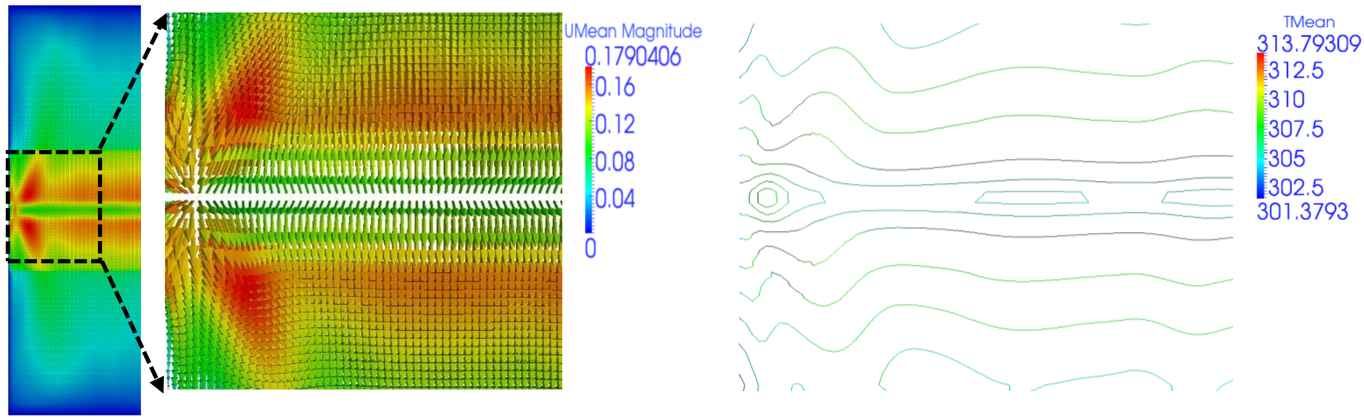

(D)

Fig. 4.13. Velocity vectors and temperature contours in *x*-*y* plane at 0.00762 m below the ceiling for (a) H^*/D= 0.2, (b) H^*/D=0.4, (c) H^*/D=1, and (d) H^*/D= 2.3.

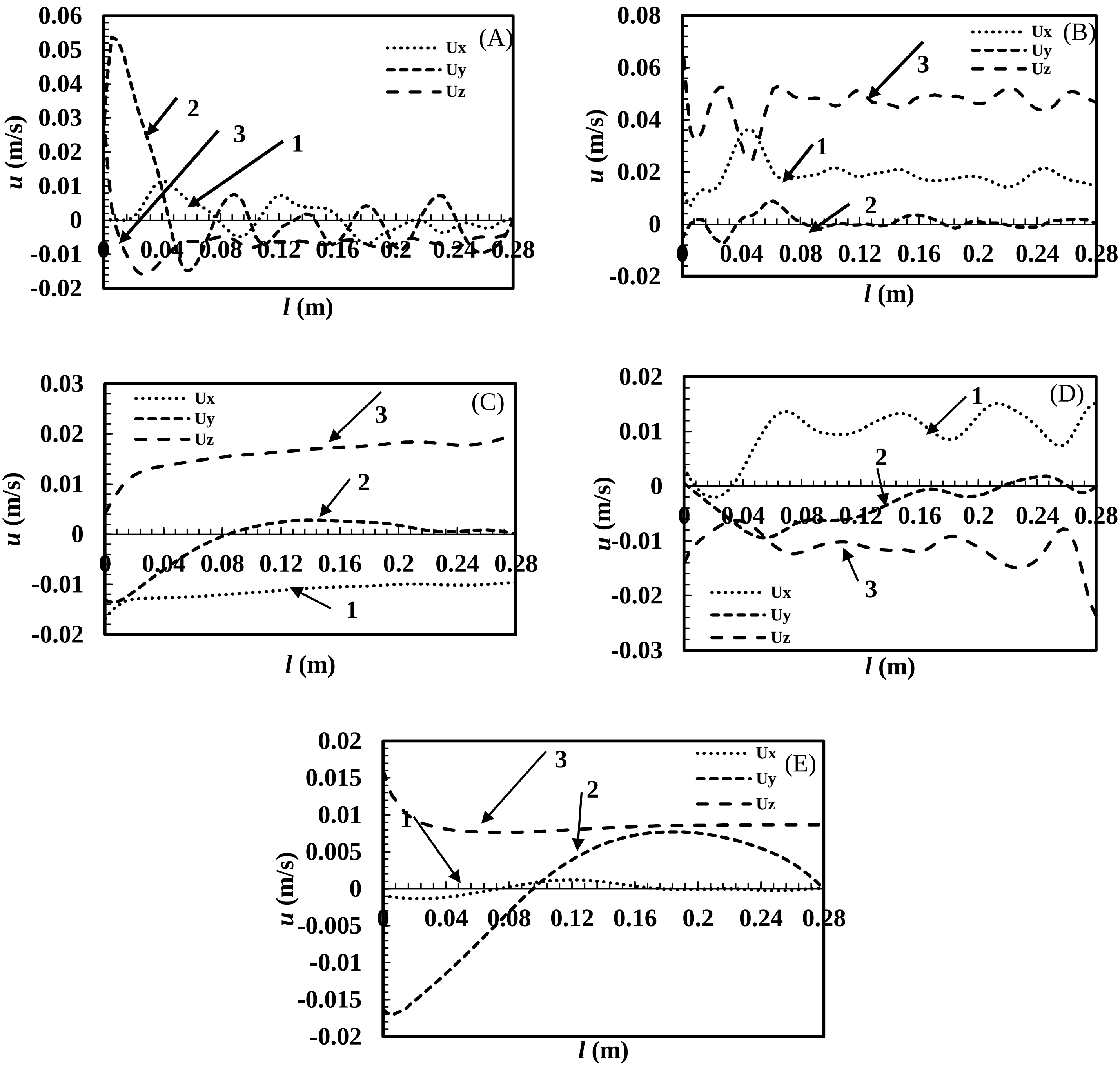

Fig. 4.14. Mean velocity plots for H^*/D = 0.2 (3D), in axial direction for z = 0.04572; (a) $\theta= 0^0$, z= 0.050, (b) $\theta= 20^0$, x= 0.01710, z = 0.04698, (c) $\theta = 90^0$, x = 0.05, z=0, (d) $\theta = 90^0$, x = 0.45, z= 0, (e) $\theta = 180^0$, x =0, z= -0.050.

of the separation of plume, and indicates that the plume goes in the x direction. For θ = 90°, x =0.05, in the vicinity of the cylinder (Fig. 4.14C), we find that the flow is mostly in the x and z directions, at this location the flow recirculating in the upper part of the enclosure joins the main plume originating from the cylinder. Far away from the cylinder for θ = 90°, x =0.45 (Fig. 4.14D), we find that the y component of the velocity is finite and negative due to mixing of the flow originating near the ends of the cylinder with the bulk of the fluid as can be observed in Fig. 4.13. In Fig. 4.14E, after reaching the stagnation point (θ = 90°), the flow moves along the periphery of the cylinder (z direction) as well as some flow moves along the length of the cylinder (y direction). In Fig. 4.14, we have observed that, at most of the locations in the enclosure, the flow shows a 3D nature. It has also been observed that, the velocity fluctuations are present between y = 0 to y =0.07 for all the cases, which are due to the complex flow pattern at the ends of the cylinder. Therefore, it shows that the 2D numerical simulations are not sufficient to predict the 3D flow behavior in the enclosure, especially at some locations.

4.3.4.2. Heat transfer

The dimensionless heat transfer coefficient, h_l^*, is plotted in Fig. 4.15 for H^*/D = 0.2, 0.4, 1, and 2.3. h_l^* for H^*/D = 0.2 and 1 is compared with the experimental h_l^* obtained by Koizumi and Hosokawa [4]. The CFD predictions do not agree with the experimental h_l^* obtained by Koizumi and Hosokawa (1996) for θ = 0° to 100° (with an error of 10% - 60%). For the case of H^*/D = 0.2, h_l^* is maximum at the stagnation point (θ = 180°) and it decreases as we move along the periphery of the cylinder due to the increase in the thickness of the thermal boundary layer. However, it attains a minima at around θ = 30° (where the plume separates from the cylinder) and then it increases to a second highest value (45-50% of the value at stagnation point) at the uppermost point (θ = 0°). The rise in the h_l^* in the upper part of the cylinder is due to the presence of the *3D* vortices. Kim et al., (2008) obtained similar results (δ = 0.2) with a dip in the h_l^* distribution around the periphery of the cylinder. The value of the minima in the case of Kim et al., (2008) and present results is very prominent (30 % of the maximum value at the stagnation point), however, in the experimental results of Koizumi and Hosokawa (1996), the dip in the h_l^* distribution was not significant with the value of the minima being 70 % of the maximum value at the stagnation point. As the cylinder is lowered (*H*/D* = 0.4), we observe that the h_l^* distribution does not show any minima due to the disappearance of the 3D vortices from the upper part of the cylinder. In this case, the variation in h_l^* depends only on the behavior of the thermal boundary layer and it decreases as we move from the stagnation point to the upper most point of the cylinder. As the distance between the cylinder and ceiling is increased further (*H*/D* = 1 and 2.3), we obtain a

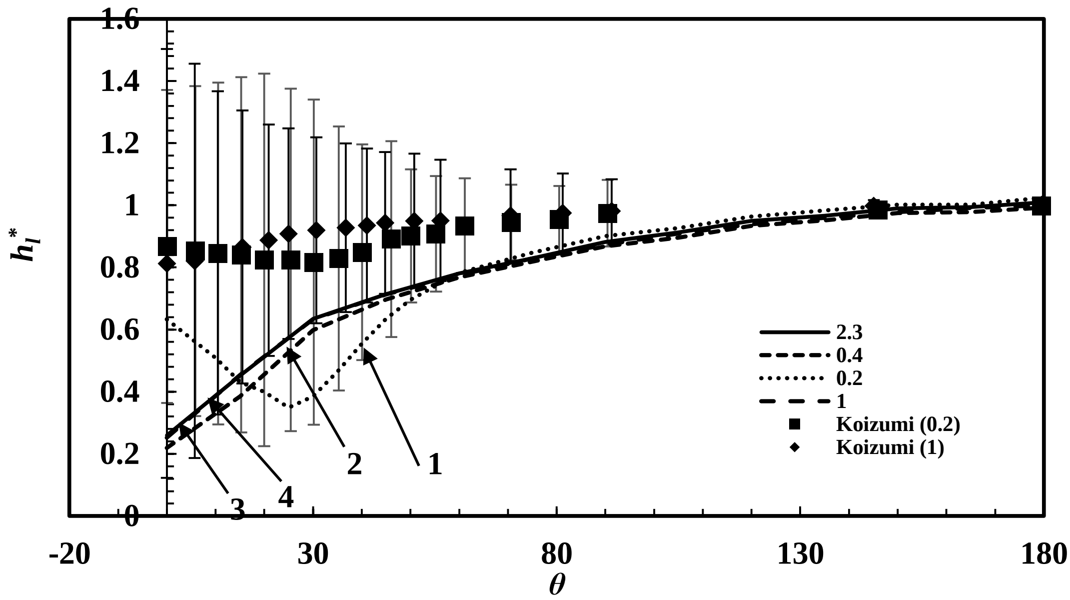

Fig. 4.15. Dimensionless heat transfer coefficient distribution along the periphery of the cylinder for (1) *H*/D*=0.2 (2) *H*/D*=0.4, (3) *H*/D*=1, (4) *H*/D*=2.3, (■)Experiment by Koizumi and Hosokawa for *H*/D*=0.2, and (♦)Experiment by Koizumi and Hosokawa for *H*/D*=1

similar h_l^* distribution as that for *H*/D* = 0.4. For the case of *H*/D* =1, Koizumi and Hosokawa (1996) obtained a very high value of h_l^* (80 % of the maximum value at the stagnation point) in the upper part of the cylinder, which seems to be an unusual value because 3D vortices are not present in the upper region. In the present case, for *H*/D* = 1 and 2.3, at θ = 0°, the Nu_l^* drops down to 20 % of the maximum value at the stagnation point. Similar results were obtained in Section 4.3.3, where we compared our CFD predictions of h_l^* distribution along the periphery of the cylinder with the results of Newport et al., (2001) (Fig. 4.10A). These predictions agree with the predictions of Cesini et al., (1999) as well. In Table 4.6, we have given h_{avg} for each case and it is compared with the correlations of Churchill and Chou (1975) and Morgan (1975). It is found that h_{avg} is lower as compared to h_{avg} obtained from the correlations of Churchill and Chou (1975) and Morgan (1975). The discrepancy between the present predictions and the correlations of Churchill and Chou (1975) and Morgan (1975) is

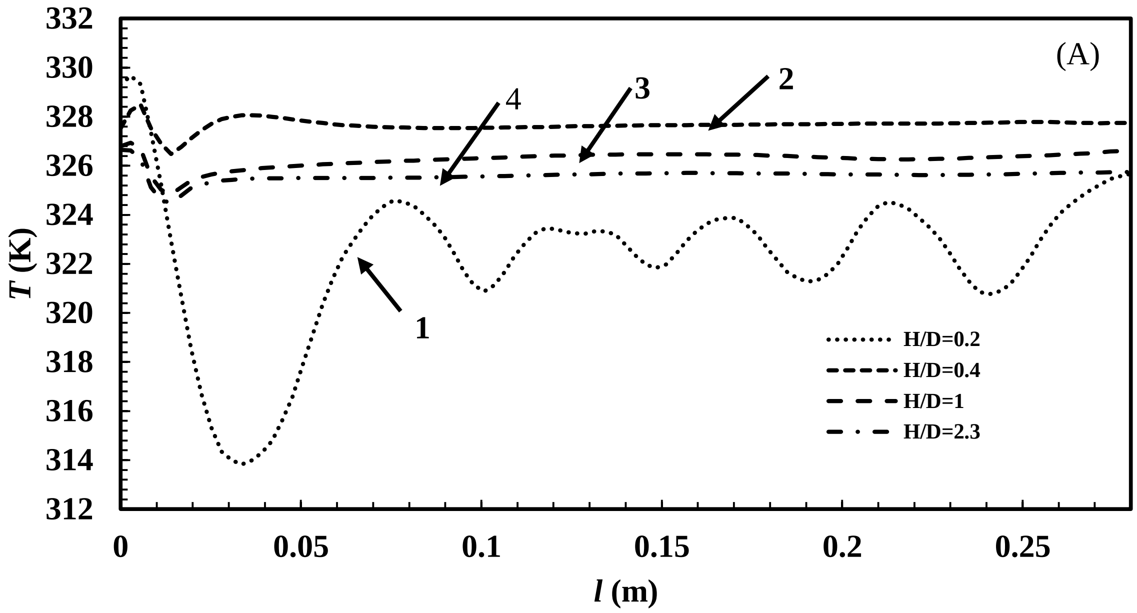

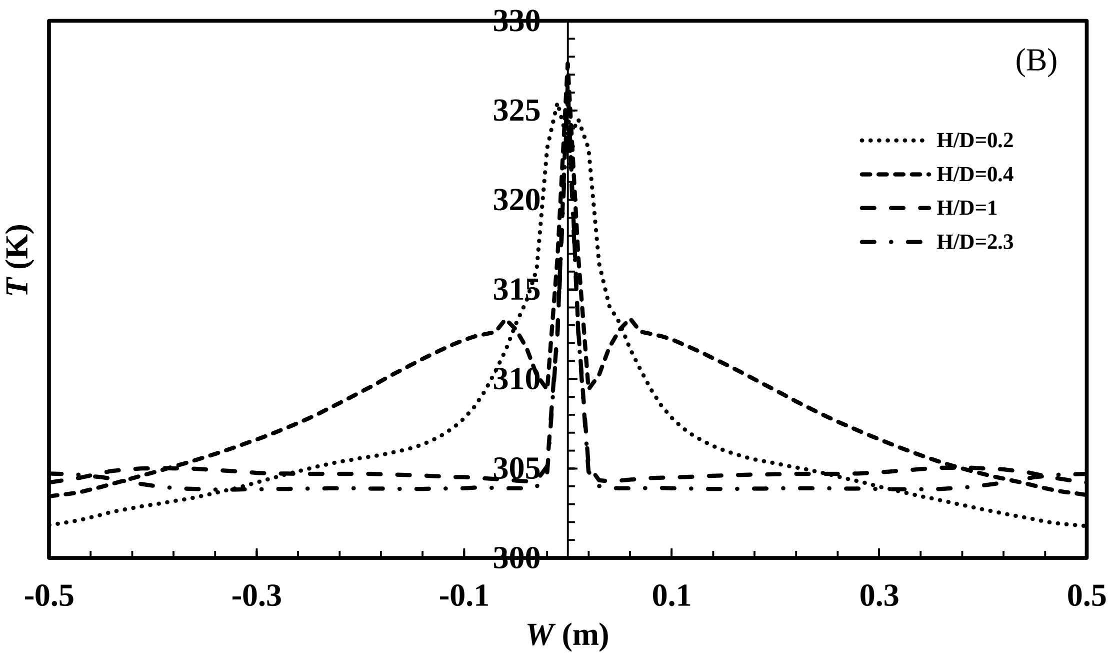

Fig. 4.16. Temperature profile; (a) Axial direction along the length of the cylinder, at $\theta = 0^0$, at x=0, z=0.05 m, (1) H^*/D = 0.2, (2) H^*/D = 0.4, (3) H^*/D = 1, (4) H^*/D = 2.3. (b) Tranverse direction across the length of the cylinder, at y =0.15 m, z=0.05 m, (1) H^*/D = 0.2, (2) H^*/D = 0.4, (3) H^*/D = 1, (4) H^*/D = 2.3.

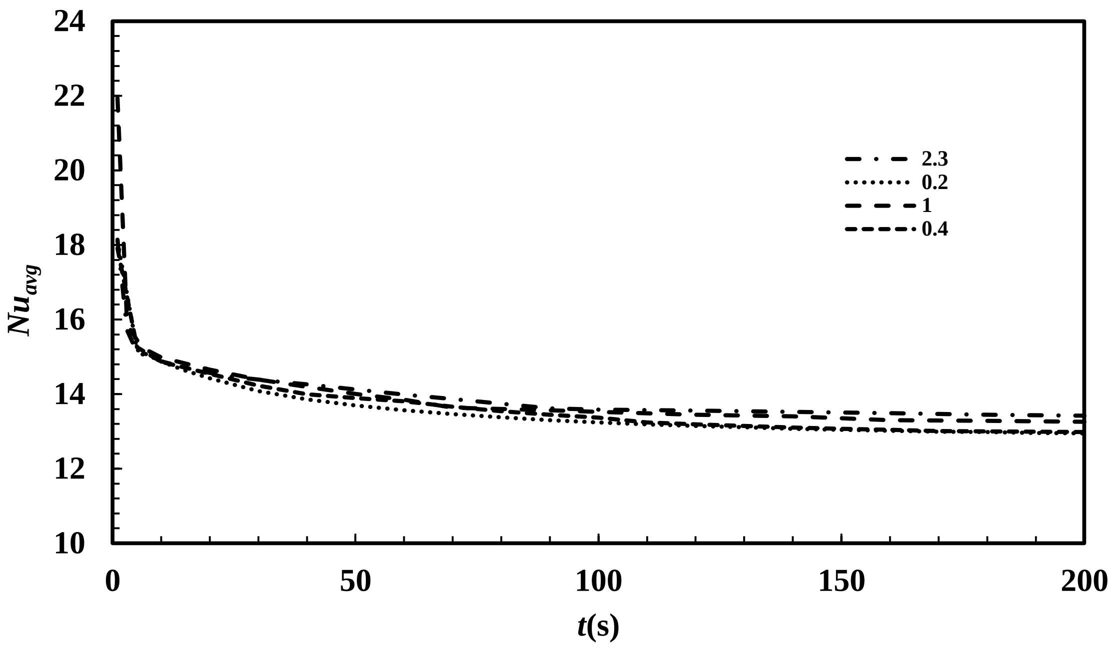

Fig. 4.17. Variation of surface averaged Nusselt number with the time.

Table 4.5. Comparison of h_{avg} for the present case with the literature.

Case	Present Results (3D)	Present Results (2D)	Churchill and Chou	Morgan
H/D=0.2	4.53	4.27		
H/D=0.4	4.54	4.43		
H/D=1	4.64	4.41	5.35	5.56
H/D=2.3	4.69	4.53		

because these correlations were obtained by considering the bare tube at the center of a large enclosure (open space or large room) where wall-cylinder interaction is negligible. That is why as the distance between the cylinder and the ceiling is increased, h_{avg} also increases and comes closer to the values obtained by both the correlations mentioned above. Butler et al., (2013) reported similar results, and found that the interaction between the conducting wall and the cylinder affects the value of heat transfer coefficient. It can be noted that, h_{avg} obtained from

3D numerical simulations is always higher as compared to h_{avg} obtained from 2D numerical simulations. This indicates that the 3D nature of the flow (for all the cases) and 3D vortices (for H^*/D = 0.2) enhances the heat transfer rate for the natural convection of air. The maximum and the minimum difference in h_{avg} was found to be 6.1 % (for H^*/D = 0.2) and 2.5 % (for H^*/D = 0.4) respectively between 2D and 3D numerical simulations, which might not be so significant. However, to capture the effect of the 3D vortices, 3D flow profile and interaction between cylinder and the enclosure walls it is important to perform the 3D numerical simulations.

In Fig. 4.16A, the temperature profiles are given along the length of the cylinder at θ = 0° and at 11.9 mm above the cylinder surface. It is observed that the temperature prediction is lowest in the case of H^*/D = 0.2, the reason being the absence of main plume above the cylinder because the flow separates before coming into this region and vortices are formed, as can be seen from the velocity vector and temperature contour plots (Fig. 4.11). The wavy profile of the temperature is caused by the presence of vortices above the cylinder in the *x-y* plane. As the distance between the cylinder and the wall is increased, the temperature increases for H^*/D = 0.4, because unlike the case of H^*/D = 0.2, the plume is formed in the upper region of the cylinder and vortices are absent. As distance is increased to H^*/D = 1 and 2.3, the temperature drops down slightly. Across the length in the *x* direction (Fig. 4.16B), we observe two peaks for H^*/D = 0.2 due to the presence of two vortices in the *x-z* plane, and the maximum temperature is lower than the other cases because of the 3D vortices and absence of the main plume. As we move away from the centerline, the temperature decreases for all the cases, however, it remains higher for H^*/D = 0.2 and 0.4 because the main plume is present at this location for these cases, but for H^*/D = 1 and 2.3, the main plume is present above this distance near the top wall.

4.3.5. Time varying behavior of Nu_{avg}

The simulations were performed for 200 seconds and the variation of Nu_{avg} with time is given in Fig. 4.17. Initially, it can be observed that Nu_{avg} is very high for all the *H*/D* ratios. This is because the temperature of the air is low initially in the vicinity of the cylinder resulting in a higher heat transfer rate. As the time increases, the temperature of air increases in the vicinity, and hence Nu_{avg} is decreased. We can observe that, Nu_{avg} gradually decreases up to 140-150 s, after 150 s the variation in Nu_{avg} is less than 1% and we can assume that steady state is reached. As explained in Section 4.3.2, Yu et al., (2011) reached steady state within a time duration of 15 s for 2D natural convection in a cavity. The difference in the time to reach steady state for the present case and Yu et al., (2011) is believed to be because of the larger aspect ratio (*AR* = 13) of the geometry and 3D nature of the natural convection in the present case as compared to the smaller *AR* of 3 and 2D natural convection for Yu et al., (2011). Therefore, in order to reach steady state for larger *AR* geometries with 3D natural convection and smaller AR geometries with 3D, complex, unstable and oscillatory flows (Section 4.3.2), the flow takes a larger time as compared to the geometries with smaller *AR* with 2D natural convection. It can also be noted that after reaching steady state also, the nature of flow predicted by 2D and 3D numerical simulations is quite different as discussed in previous sections.

4.4. Conclusion

By analyzing the study of Cesini et al., (1999), it was found that the small aspect ratio of the cavity causes the wall-cylinder interaction, which results in a 3D, unstable, oscillatory and complex flow. The merging of the primary recirculating eddies and formation of secondary eddies was observed along the length of the cavity. By performing the 3D numerical simulations, the surface averaged heat transfer coefficient was increased by 20% as compared to the 2D numerical simulations performed by Cesini et al. (1999), and by 10 % as compared to the experimental results of Cesini et al., (1999). The augmentation in the heat transfer was due to the presence of 3D vortices and 3D nature of the natural convection. Therefore, the 3D numerical simulations are required to estimate the accurate rate of heat transfer by natural convection of air in this type of complex flow.

From the 3D numerical simulations of Newport et al., (2001), the flow was found to be 2D around the cylinder and in the vicinity of the enclosure walls. In the case of Newport et al. (2001), the cylinder was kept at the center of the enclosure and the distance between the walls and cylinder was found to be sufficient enough to eliminate the wall-cylinder interaction leading to a 2D stable flow.

The investigation of natural convection of air on a finite circular cylinder was carried out using transient 3D numerical simulations. It was found that the distance between the cylinder and the top wall is an important parameter which affects the nature of the flow. 3D vortices were observed when the H^*/D ratio was 0.2 and these vortices helped in enhancing the heat transfer in the region between the cylinder and the ceiling as was shown in the comparison between the 3D and 2D numerical simulations. For H^*/D = 0.4, 1, and 2.3, the difference between the results of 2D and 3D numerical simulations was very small, and hence the flow could be treated as 2D.

From all the simulations performed (Cesini et al., (1999), Newport et al., (2001) and present case) in the present work, it can be concluded that the interaction of enclosure walls and cylinder can lead to a 3D, oscillating, and complex fluid flow. This is important in the analysis of natural and forced convection of an air-cooled condenser because of the formation of 3D vortices by various types of fins. Therefore, it can be concluded that the 3D numerical simulations must be performed to capture the 3D flow phenomenon which can affect the performance of an air cooled condenser significantly.

Chapter 5
Natural convection around finned-tube heat exchangers

5.1. Introduction

The air cooling technology is used in a variety of applications, for example automobile industry, power plants, computer systems, air conditioners, etc. In the power plants, the air cooling is used in the air cooled condensers, and dry and wet cooling towers. The A-type air-cooled condensers are used to condense the exhaust steam from the turbine, whereas the dry and wet cooling towers are used to remove the heat from the secondary water loop by forced or natural draft of air. The research on the air-cooled heat exchangers and condensers has been ongoing for more than 50 years. The performance of the air-cooled heat condensers depends upon many geometrical parameters, like fin type, fin spacing, number of tube rows, tube pitch, etc. The ambient parameters like wind, humidity, etc., are also very important in determining the efficiency of the air-cooled heat condensers. One of the major problems with the air cooling technology is the low value of heat transfer coefficient, which results in a large heat transfer area of the heat condensers, and therefore, a high associated capital cost as compared to the water cooled heat condensers. In the power plants, the air-cooled condensers are gaining increasing attention due to non-availability of the water in many areas. The annular fins are widely used in practice to increase the heat transfer area on the air side and the role of suchfinshas been investigated by many researchers in natural and focred convection,experimentally as well as numerically. However, all of the numerical investigations have considered one or two fins and assumes a uniform air flow over the whole length of the finned-tube. Previous experimental studies on the natural convection over a finned tube were performed by measuring temperature on the surface of finned tube and in ambient using thermocouples.

Most of the currently employed air-cooled condensers use external power for the blower, however, in the case of a station black out (e.g., Fukushima nuclear accident), it can cause various safety concerns (e.g., core melt). Therefore, the use of a natural air-cooled condenser should be considered in the power plants. However, the cost associated with a natural air-cooled condenser should be comparable to the forced air-cooled condenser. In the present work, an effort has been made to understand the flow physics of natural draft of air over a finned-tube kept under a chimney and to incorporate these finding in the commercial natural air cooled condenser. The details pertaining to the previous work have been given in the chapter 2 (section 2.3) and from that discussion it can be noted that all the experimental studies on the natural convection of air around finned tube have been performed in a closed system. The numerical studies have also been performed in the similar manner and only one or two fins are considered in the numerical domain and the flow is assumed to be uniform along the length of the tube. However, no 3D numerical simulations have been reported in the published literature on a system where finned-tube heat exchanger is placed under a chimney to generate a natural draft. In this type of system, the numerical domain must consider the whole system, to take into account the chimney effect and the heat transfer from all the fins. Therefore, in the present work, 3D numerical simulations have been performed to characterize the natural draft of air over a finned-tube and to study the effect of fin spacing, fin diameter, number of fins and chimney height on the heat transfer and driving force of the chimney.

5.2. Numerical Solution

5.2.1 Geometry

The system under consideration comprises of a chimney and an annular-finned circular tube of diameter 24.9 mm and length 610 mm (Fig. 5.1). The half symmetry of the box is used for the 3D numerical simulations. The tube is kept horizontally inside the chimney with eight annular fins on the tube. The fin spacing is varied from 2 mm to 12 mm and the fin diameter is varied from 35 mm to 50 mm, and the corresponding S/D_f ratio varied in the range of 0.057 mm ≤ S/D_f ≤ 0.24 mm. The chimney height is varied from 400 mm to 1000mmand the difference between the surface to ambient temperature is varied from 10 K to 65 K. The working fluid in the chimney is air with an inlet temperature of 300 K. The numerical simulations were performed for 120 s, and it was observed that the steady state in the domain reaches after 60-80 s. The grid generation and meshing were executed using Gmsh2.3 (2009).

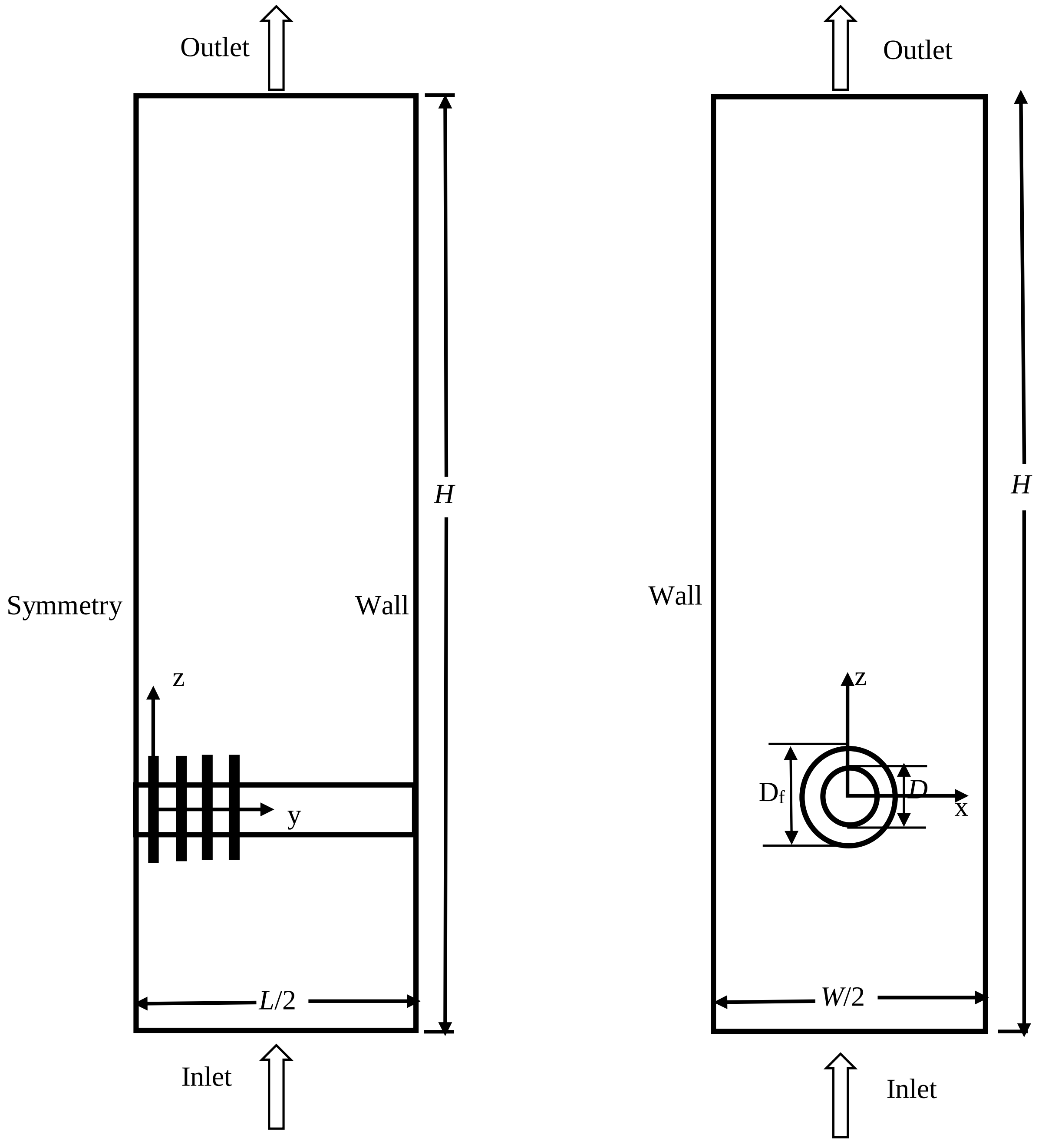

Fig. 5.1. Schematic of the computational model (A) y-z plane, (B) x-z plane.

5.2.2 Governing equations and model assumptions

The problem under consideration is unsteady 3D natural convection of air inside a cuboidal enclosure. The assumptions in the computational model are the following:

4. Flow is Newtonian and incompressible.
5. Boussinesq approximation is valid i.e., density difference is only important in producing buoyancy.
6. Constant fluid properties except in the formulations of buoyancy term.

In no flow condition the Rayleigh number is found to be 3.8 x 10^4, therefore, the flow is considered in the laminar region. The governing equations for the 3D unsteady natural convection are continuity, momentum and energy equations, which are given as:

$$\frac{\partial u_j}{\partial x_j} = 0 \qquad \dots (5.1)$$

$$\frac{\partial u_i}{\partial t} + \frac{\partial (u_j u_i)}{\partial x_j} - \frac{\partial}{\partial x_j}\left\{\upsilon\left[\left(\frac{\partial u_i}{\partial x_j} + \frac{\partial u_j}{\partial x_i}\right)\right]\right\} = -\frac{\partial p}{\partial x_i} + g_i\,[1 - \beta(T - T_o\,)] \qquad \dots (5.2)$$

$$\frac{\partial T}{\partial t} + \frac{\partial (T u_i)}{\partial x_j} = \frac{\partial}{\partial x_k}\left[\left(\frac{\upsilon}{Pr}\right)\frac{\partial T}{\partial x_k}\right] \qquad \dots (5.3)$$

Where, T, p, and u represent the mean temperature, pressure and mean flow velocity respectively and $T_o$represents the bulk mean temperature. υ, β, and g are the kinematic viscosity, thermal expansion coefficients and gravitational acceleration constant. The thermal coefficients are calculated at the mean temperature of the tube and the ambient. The value of the Prandtl number, *Pr*, is taken as 0.7.

The heat transfer coefficient is averaged over the finned-tube surface area and is calculated using the following equation,

$$h = \frac{k}{\Delta T}\frac{dT}{dn}\bigg|_{surface} \qquad \dots (5.4)$$

Where$k$ is the thermal conductivity andΔT is the temperature difference between the finned-tube surface and the ambient.

5.2.3 Boundary condition

The walls of the chimney are specified as adiabatic boundaries. The tubeand fins are assumed to be at a constant temperature (310 K $\leq T_s \leq$ 365 K). The assumption of the constant

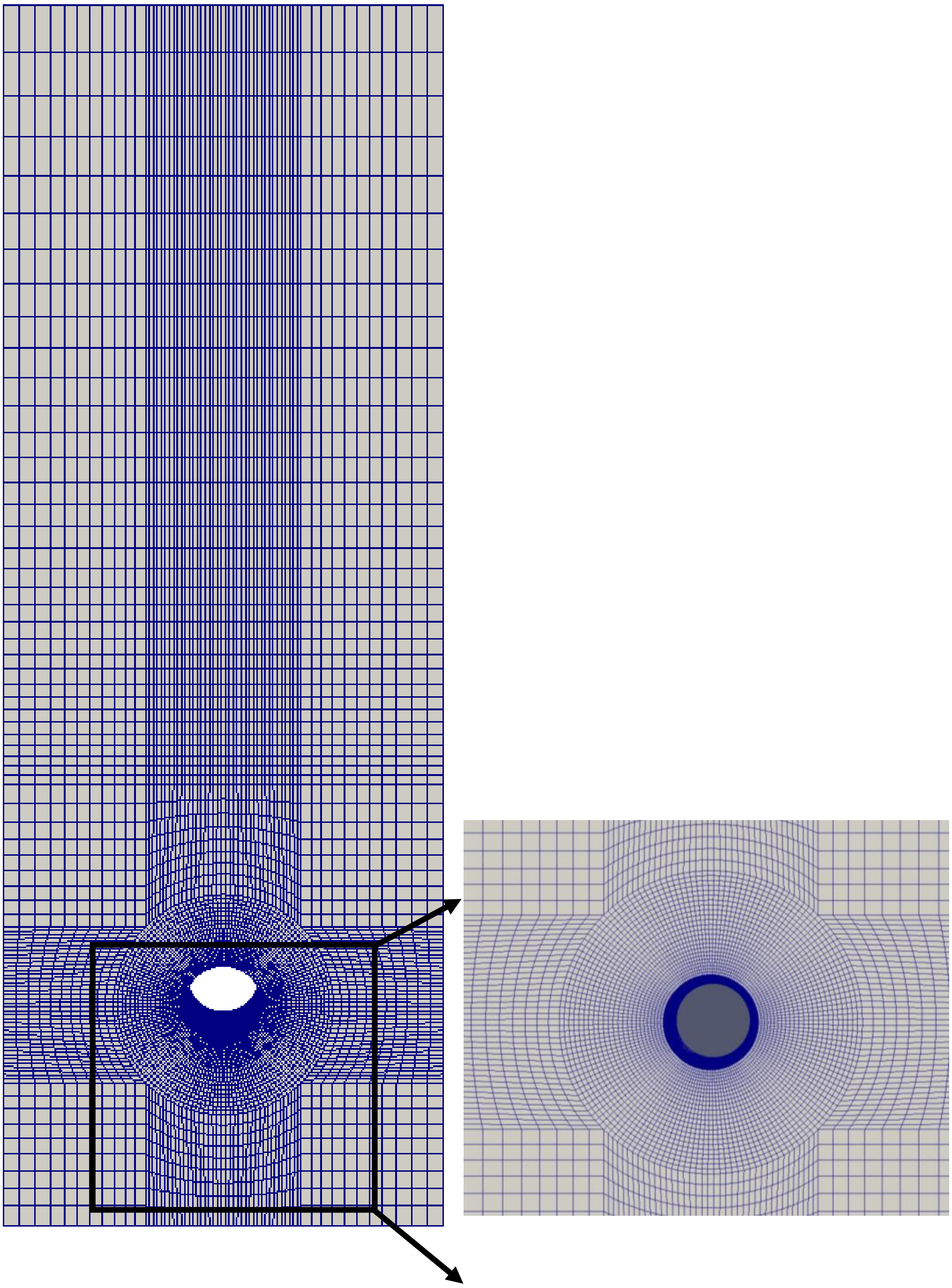

Fig. 5.2. Computational grid.

temperature boundary condition for the fin is because, the model considered in the present study is well validated with earlier experimental data in Chapter 4. The model considers an incompressible fluid flow of air, for which the conjugate type of boundary condition is not present in Openfoam 2.2 so far. The conjugate type of boundary condition is present only for compressible fluid flows, which has not been considered in the present work, because of the low Mach number. The no slip boundary condition is used at the cylinder surface and chimney wall. At the inlet, a zero fixed velocity is provided with a total pressure boundary condition and at the outlet the Neumann boundary condition is used for velocity and the pressure is set to atmospheric.

5.2.4 Method of solution

In the present work, simulations were performed under unsteady conditions. All the computational work was carried out using the software OpenFOAM-2.2, which is based on finite volume approach. For the discretization of the unsteady terms, the first order implicit scheme was used, for diffusion terms and pressure gradient term, the central difference scheme is applied, and for the convective terms, the QUICK scheme is applied.

Table 5.1: Results for various convergence criteria

Fin spacing (mm)	**convergence criterion =1e-05 [*h* (W/m^{2}K)]**	**convergence criterion =1e-06 [*h* (W/m^{2}K)]**
2	5.88	5.90
4	9.60	9.63
8	10.64	10.68

All the obtained discretized equation are solved using the algorithm PIMPLE given in Openfoam. Which is an unsteady solver and a merged form of PISO and SIMPLE. In PIMPLE algorithm, the equations are solved using initial guess values of flow variables, and then the values are corrected in each iteration. The iterative process continues until the convergence criterion is satisfied. The convergence criterion was based on the scaled residual of the velocity, when the residuals reached below 10^{-5}, the solution was considered to be fully converged. The value of the convergence criterion is chosen based on the accuracy in the results and the computational time. A convergence criterion of 1e-06 has been kept for S = 2, 4 and 8 mm at D_f = 41 mm. The difference in the previous results (convergence criterion 1e-05) and the

Table 5.2. Grid size independence results

Fin spacing (mm)	**Grid size= 300000 [h (W/m^{2}K)]**	**Grid size= 500000 [h (W/m^{2}K)]**	**Grid size= 600000 [h (W/m^{2}K)]**	**Grid size= 1000000 [h (W/m^{2}K)]**
2	5.98	5.88	6.01	5.94
4	9.51	9.60	9.71	9.65
8	10.76	10.64	10.73	10.70

present results is negligible as can be seen in Table 5.1. However, when the convergence criterion is chosen to be 1e-06, the computational time increases and hence, a convergence criterion of 1e-05 is chosen.

5.2.5 Grid independence and time step independence

A structured hexahedaral non-uniform mesh was generated using Gmsh 2.3. A fine mesh was generated around the cylinder to capture the high velocity and temperature gradients. A grid resolution of 300000, 450000, 600000 and 1000000 was used to carry out the grid senstivity for the cases of S = 2, 4, 8 mm at D_f= 41 mm. The difference in the heat transfer coefficient was within 2% for the four cases (Table 5.2). Finally a grid of 400000-500000 (higher grid number was used for the larger fin spacing) cells was used for all the cases to opbtain the maximum accuracy with optimized comuptational time. (The computaional time for a grid size > 600000 takes more than 50 days to reach a time of 120 sec). The grid geometry has been schematically shown in Fig. 5.2. A time step independence study was also performed for various time steps (1e-4, 5e-05, 1e-05, 1e-06). The difference in the results was negligble (within 2%) as can be observed in Table 5.3 (simulations were performed for 40 sec in this case due to large computational time for larger time steps).

Table 5.3. Time step independence results (at t = 40 s)

Time step: 1e-04 **[*h* (W/m^{2}K)]**	**Time step: 5e-05** **[*h* (W/m^{2}K)]**	**Time step: 1e-05** **[*h* (W/m^{2}K)]**	**Time step: 5e-06** **[*h* (W/m^{2}K)]**
9.94	9.87	10.05	9.95

5.3. Results and discussions

In Chapter 4, a detailed comparison was shown between the present code and the previous experimental results on the natural convection of air. It was found that, the numerical results agree well with practically all the previous experimental results published in the literature. For further validation with finned-tube, the numerical results have been compared with the experimental results of Yaghoubi and Mahdavi (2013) for one of their cases. Yaghoubi and Mahdavi (2013) performed experiments and numerical simulations to study the heat transfer and fluid flow around a single circular finned-tube kept in a test room. The tube diameter was 25.4 mm, the fin diameter was 56 mm, the fin spacing was 2 mm and the fin thickness was 0.4 mm. In the numerical domain, two half fins were considered with a fixed fin spacing using symmetric boundary conditions on both the sides. The tube temperature has been kept at 281℃, 285℃, and 288℃, the ambient air temperature is fixed at 295 ℃ and the enclosure temperature is kept at 294.5℃. It can be observed that, numerical results agree with the experimental measurements within 80-90% accuracy. For local temperature validation, the temperature measurements were not given in the work of Yaghoubi and Mahdavi (2013). In the literature, as well, we could not find any paper on the natural convection around circular finned-tubes,

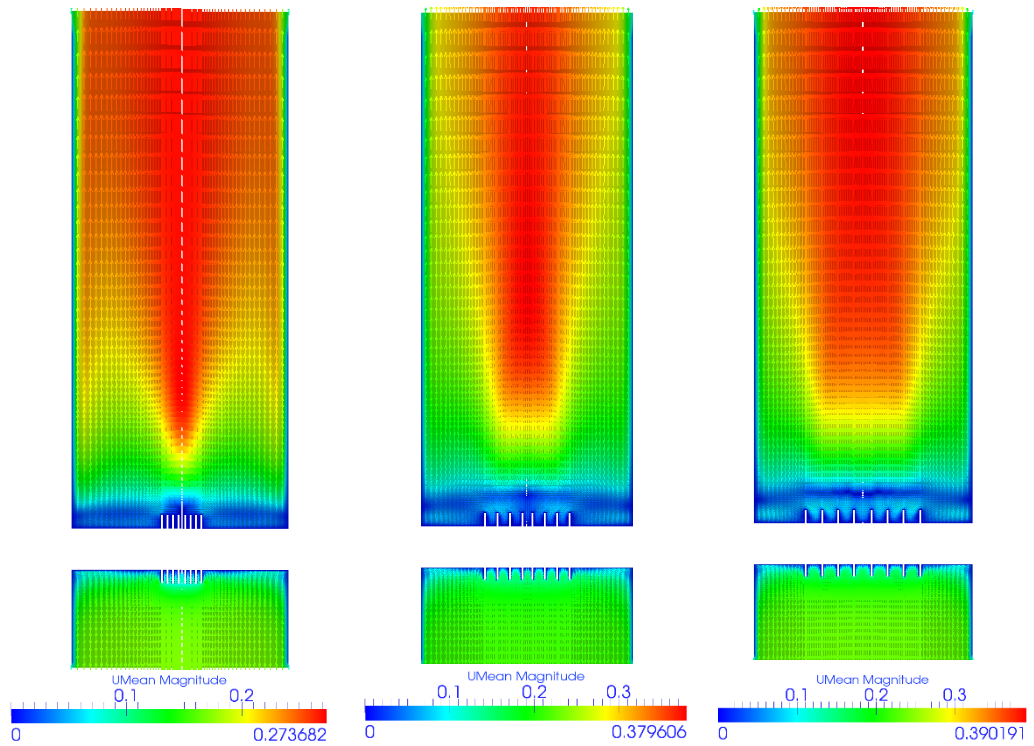

(A)

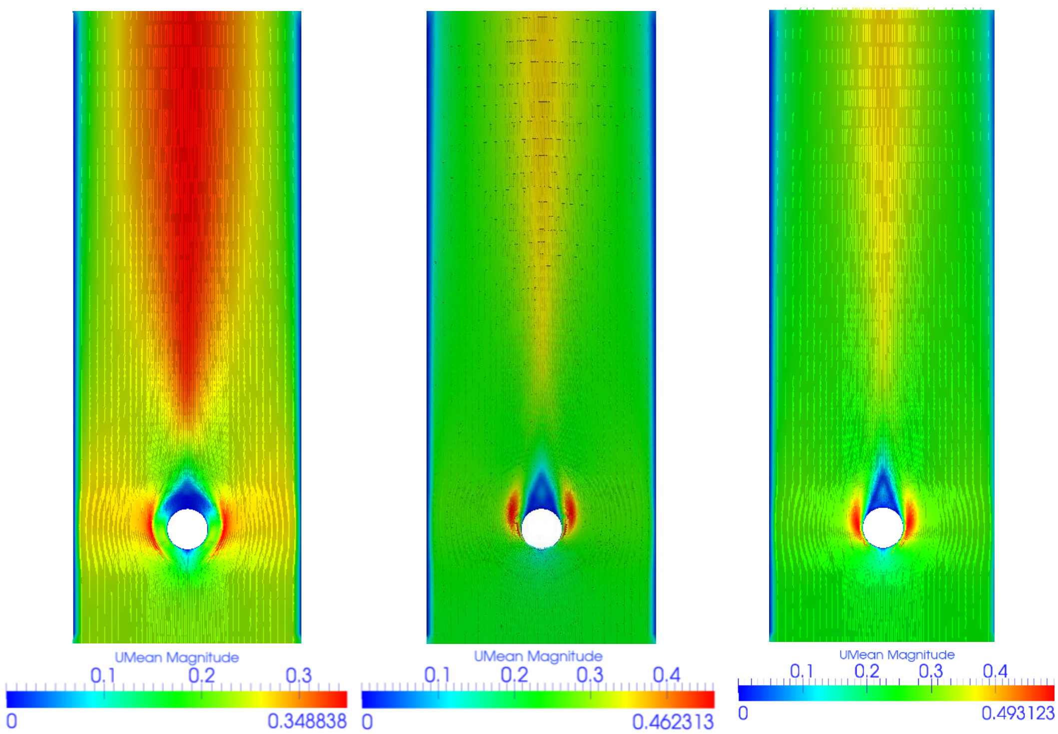

(B)

Fig. 5.3. Velocity vectors for S = 2 mm, 6 mm and 8 mm, and H = 400 mm (A) y-z plane, x = 0 m, (B) x-z plane, at 1 mm away from the fin surface.

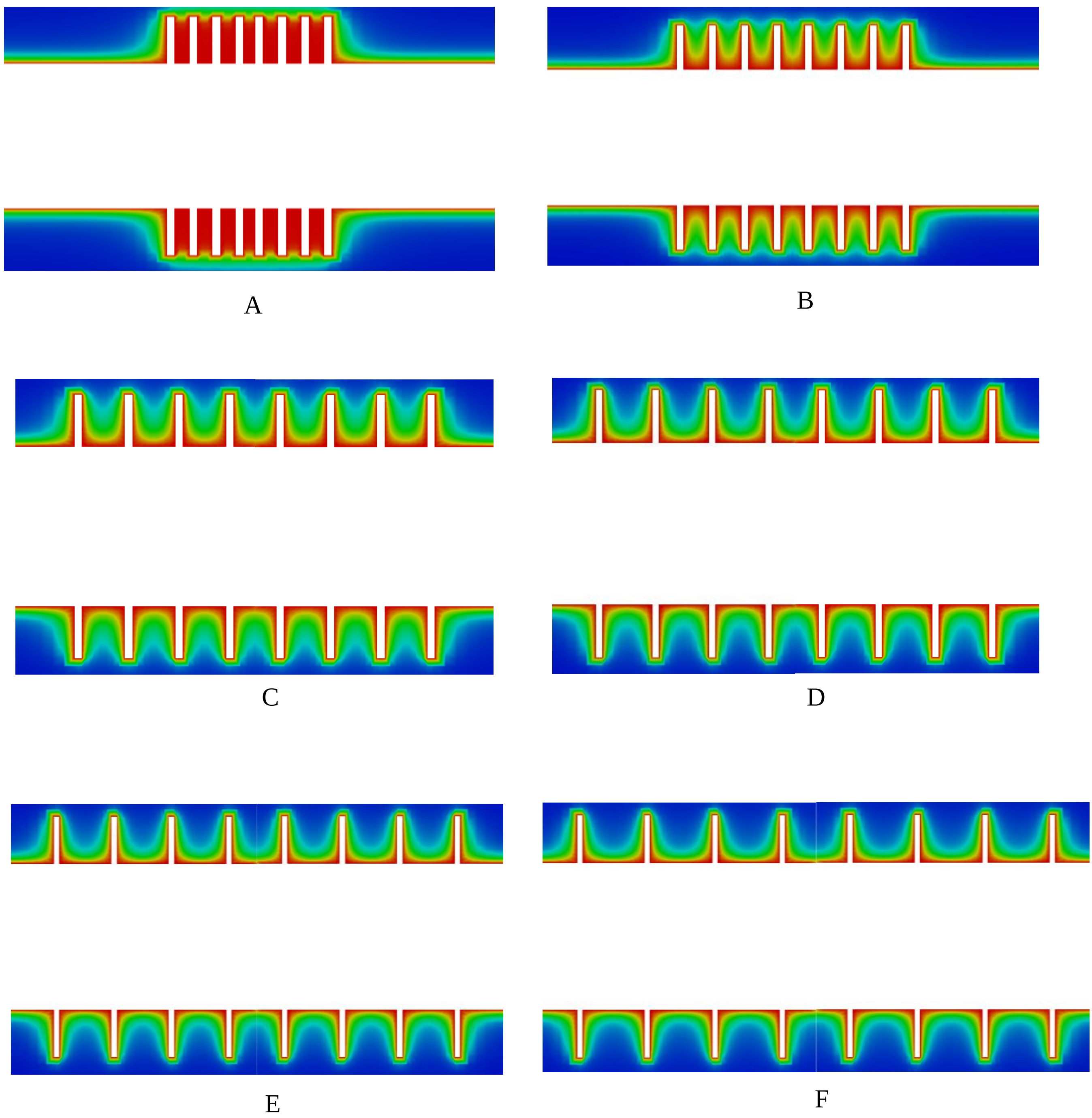

Fig. 5.4. Temperature contours showing thermal boundary growth for varying fin spacing in the *y*-*z* plane at $x = 0$ mm. (A) $S = 2$ mm (B) $S = 4$ mm (C) $S = 6$ mm (D) $S = 8$ mm (E) $S = 10$ mm (F) $S = 12$ mm.

which provides temperature profile in the mean flow. Therefore, the temperature predictions could not be compared. Overall, the code shows a good validation with the experimental results. Therefore, such a validated code has been used in the present study. Theresults are presented in the form of temperature contours, velocity vectors, heat transfer coefficient and pressure drop in Sections 5.3.1 to 5.3.7.

5.3.1 Effect of fin spacing

Fig. 5.3 shows the velocity vectors generated for the case of *S*=2 mm, 4 mm,8 mm and 10 mm in the*y-z* and the *x-z* plane for D_f= 41 mm. In Fig. 5.3A, we can observe that a good natural draft of air is generated in the chimney, and the value of the maximum velocity in the domain is larger for the larger fin spacing due to less resistance to the flow. In Fig. 5.3B, the velocity vectors are given in the finned region of the tube, for *S*=2 mm, and it can be observed that the maximum velocity of the fluid occurs at the tip of the fins and the flow is not able to penetrate between the fins unlike the other cases, where the flow is able to penetrate between the fins and the maximum velocity occurs between the fins. This is due to the larger thermal resistance provided to the air by fins at lower fin spacing, and as the fin spacing is increased, the resistance decreases resulting in relatively more intense velocity field between the fins. In

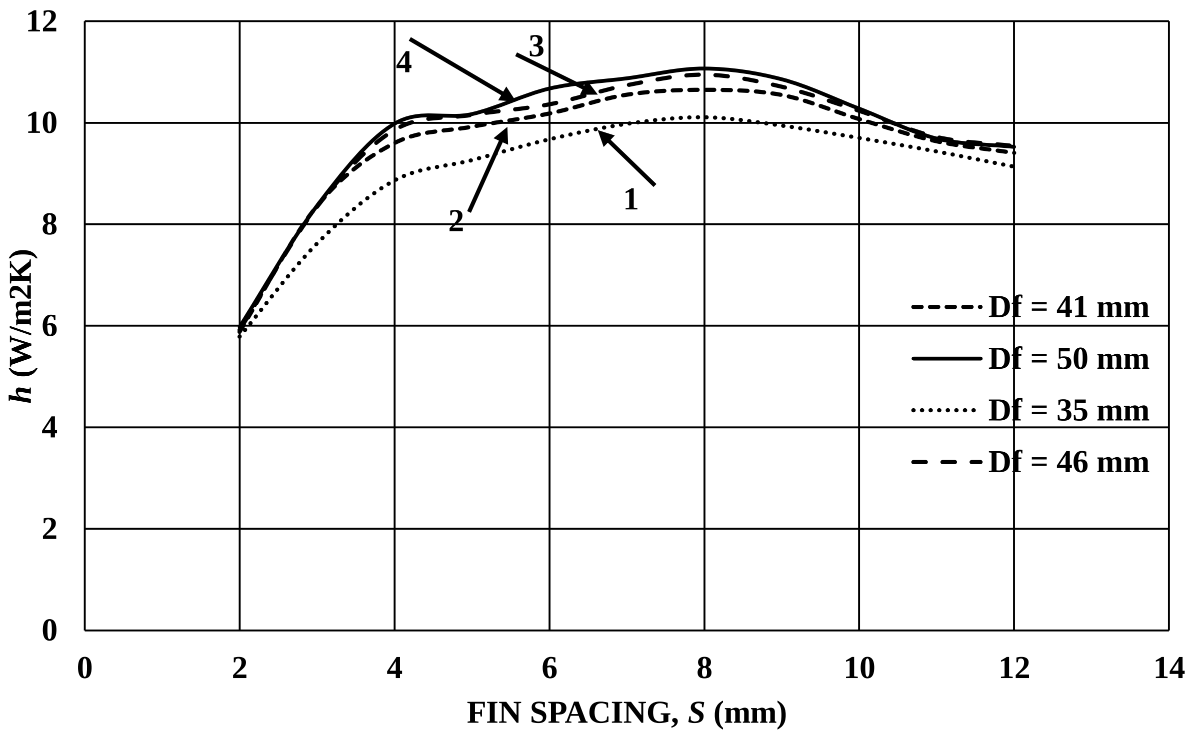

Fig. 5.5. Heat transfer coefficient for varying fin spacing to fin diameter ratio (1) D_f = 35 mm, (2) D_f = 41 mm, (3) D_f = 46 mm, (4) D_f = 50 mm.

Fig. 5.4, the thermal boundary layer is shown for S = 2, 4, 6, 8, 10, 12 mm for D_f = 41 mm, at lowest fin spacing, S = 2 mm, the boundary layers at the surface of the fins merge with each other, and the boundary layers increasingly separates from each other with an increase in the fin spacing. Similar velocity vectors and temperature profiles are obtained for the case of D_f = 35 mm, 46 mm and 50 mm (not shown). Fig. 5.5 shows the heat transfer coefficient variation with respect to the fin spacing for D_f = 35, 41, 46, and 50 mm. For all the cases, it can be observed that, at lower fin spacing, S = 2 mm, the heat transfer coefficient is very low and as the fin spacing is increased, the heat transfer coefficient increases and attains a maxima. The merging of the thermal boundary layers in the finned region for S = 2 mm causes the decrease in the heat transfer coefficient, and it also causes the flow to pass over the tip of the fins without penetrating the finned region, as is observed in Fig 3B (shown only for one case). As the fin spacing is increased, the boundary layers start separating and horseshoe vortices are formed at the fin-tube junction, which enhances the heat transfer coefficient. However, at a particular fin spacing (S = 8 mm) the heat transfer coefficient attains a maxima and then again starts decreasing. The value of the maximum heat transfer coefficient varies from 55-60% as compared to its lowest value at S = 2mm for all the cases. This peculiar role of fin spacing ratio is mainly because, as the fin spacing is increased beyond 8 mm, the heat is not transferred very effectively between the fin surfaces and the flow rate at the central region of the fin spacing gets bypassed resulting into inefficient heat transfer rate. Romero-Méndez et al., (1997) and Liu et al., (2010) have observed the maxima in the heat transfer coefficient for a particular fin pitch and the bypass flow phenomenon. However, they have not analysed the effect of fin spacing on the flow field. To understand the bypass flow phenomenon with varying fin spacing, we have shown the velocity plot along the length of the tube for D_f = 41 mm in Fig. 5.6. It can be seen that the velocity attains maxima in the region between the fins, and for S = 2 mm, the maxima is very low due to the merging of the thermal boundary layers, and as the fin spacing is increased to S = 8 mm, the maximum velocity increases. However, for S = 10 and 12 mm, it can be observed that the value of the maximum velocity comes down and it shows a different behavior with a local minima in the region between the fins. Similar results were observed for the other cases, D_f= 35 mm, 41 mm, and 50 mm, but have not been shown to keep the number of Figures less. However, the value of the fin spacing at which the maxima occurs for different cases is same (shown in Fig. 5.5 also). Therefore, it can be concluded that beyond a value of the fin spacing, the heat transfer from the finned-tube to air is not efficient and air stream at the centre of the fin spacing bypasses the finned region with a poor heat transfer. Dogan et al., (2012) observed an optimum fin spacing of 8.7 mm for a range of fin diameter (35 mm $<D_f<$ 160 mm). Similar value of optimum fin spacing is obtained with the present detailed 3D analysis of the flow.

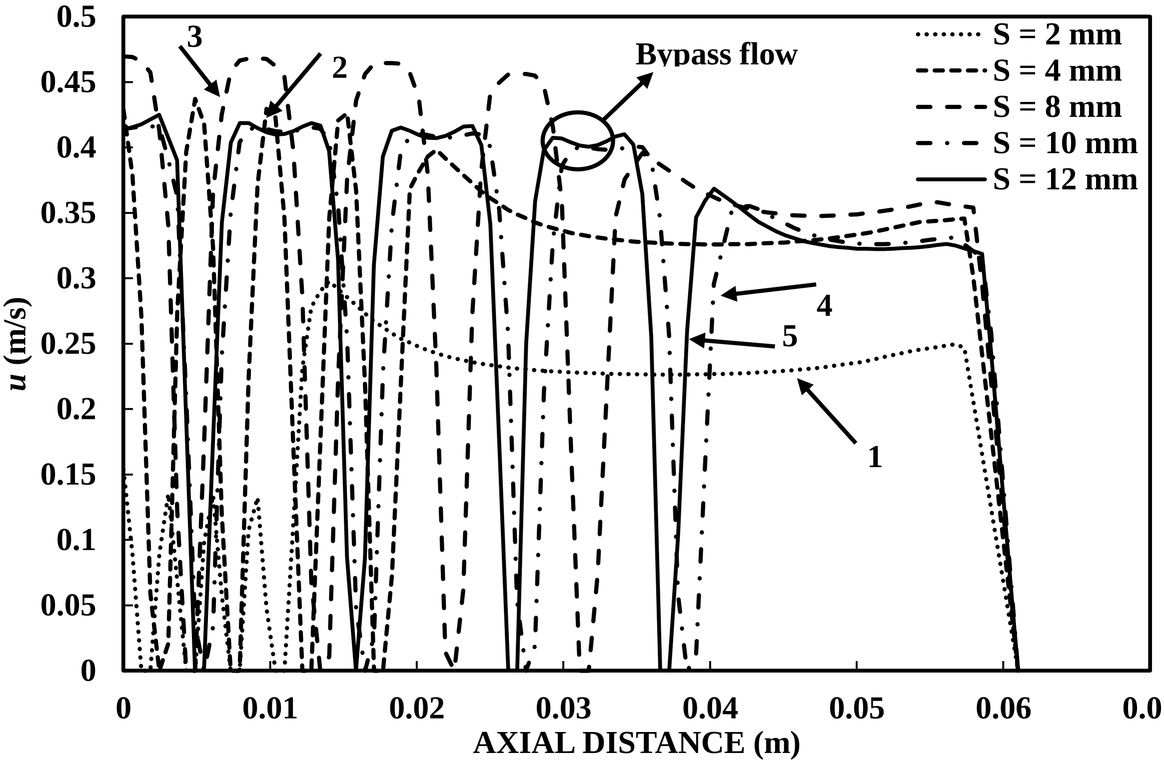

Fig. 5.6. Velocity profile along the length of the tube at x = 0.015 m, z = 0 mm, (1) S = 2 mm, (2) S = 4 mm, (3) S = 8 mm, (4) S = 10 mm, (5) S = 12 mm.

5.3.2. Effect of fin diameter

The individual role of the fin diameter in the heat transfer performance can also be evaluated from Fig. 5.5. The heat transfer coefficient is the highest for D_f=50 mm and the lowest for D_f= 35 mm. As the fin diameter is increased from 35 mm to 41 mm, the heat transfer area increases by 42%, and the heat transfer coefficient increases by 50%. As the fin diameter is increased further to 46 mm, the increase in the heat transfer area is 29%, however the increase in the heat transfer coefficient reduces to 27%. Similarly, as the fin diameter is increased from 46 mm to 50 mm, the increase in the heat transfer area is 20%, and the increase in the heat transfer coefficient is just 11%. We can observe that, as the fin diameter is increased, the increase in the heat transfer coefficient per unit heat transfer area reduces. For the detailed analysis of the role of the fin diameter, the heat transfer rate, the driving force and velocity plot along the length of the finned-tube are given in Fig. 5.7 at a fixed fin spacing of surface is shown in Fig. 5.8. In Fig. 5.7A, when the fin diameter is increased from 35 mm to 50 mm, the buoyancy force or the driving force increases in the domain due to larger heat transfer area provided by the larger fins. Also, it can be observed that the increase in the driving force is sharper from D_f= 35 mm to D_f= 41 mm, and beyond D_f= 41 mm, the rate of increase reduces. Overall, the increase in the driving force results in an increase in the heat transfer coefficient. However, it can also be observed in Fig. 5.8, that the behavior of the thermal boundary layer is almost similar for the case of D_f= 35 mm and 41 mm and hence the sharper increase in the driving force dominates and results in a larger increase in the heat transfer coefficient. However, as the fin diameter is increased further to 46 mm and 50 mm, the thermal boundary layer grows thicker for most of the fin surface area and it overcomes the effect of the increase in the driving force, which results in a reduction of rate of increase in the heat transfer coefficient. Therefore, we can conclude that the buoyancy force dominates over the increase in the thickness of the thermal boundary layer as the fin diameter is increased from 35 mm to 41 mm, and for D_f> 41 mm, the increase in the thermal boundary layer dominates resulting in a lower increase in the heat transfer coefficient.

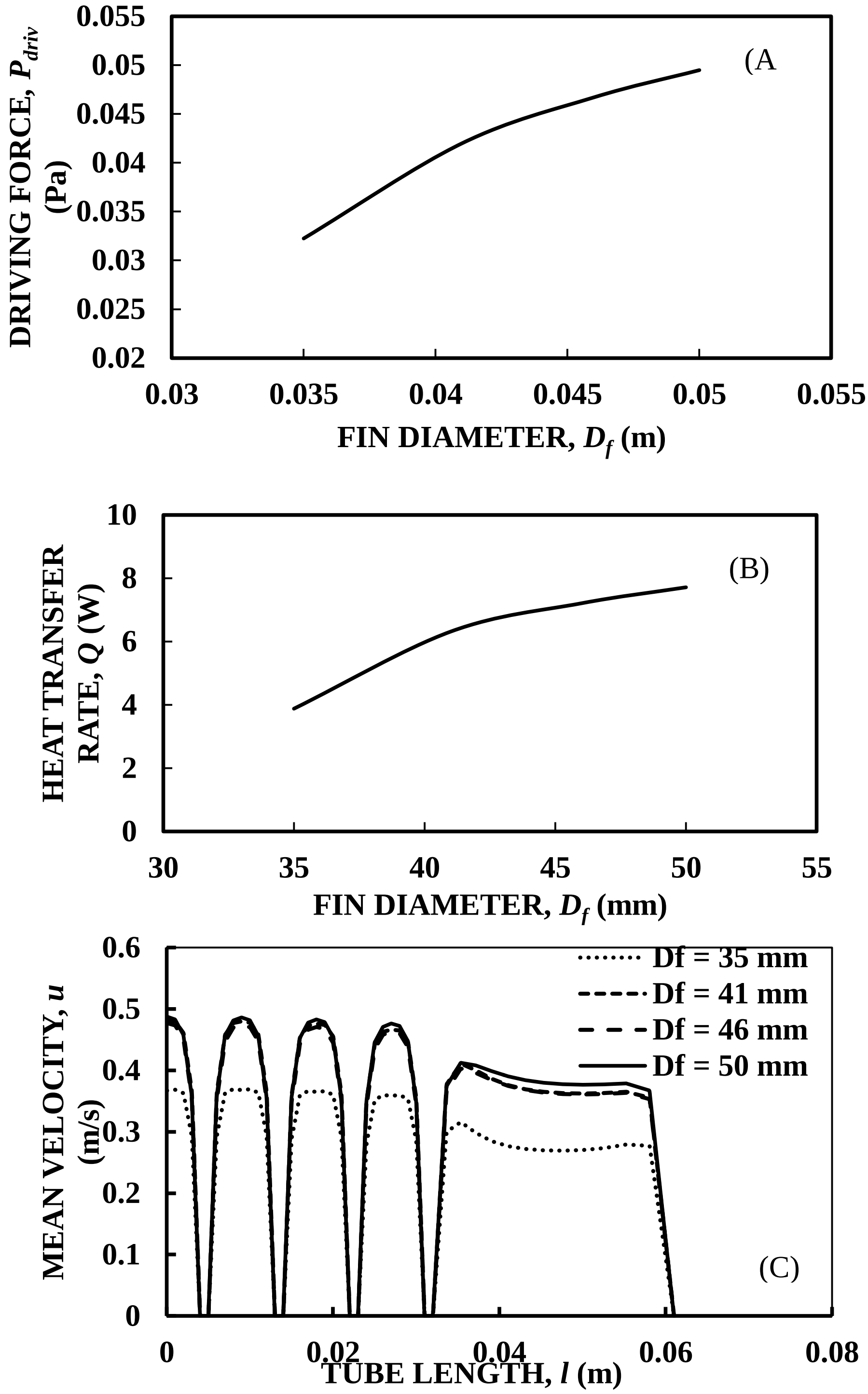

Fig. 5.7. At S = 8 mm for varying fin diameter, (A) Heat transfer rate (B) Driving force and (C) velocity profile along the length of the tube at x = 0.015 m, z = 0 mm, (1) D_f = 35 mm, (2) D_f = 41 mm, (3) D_f = 46 mm, (4) D_f = 50 mm.

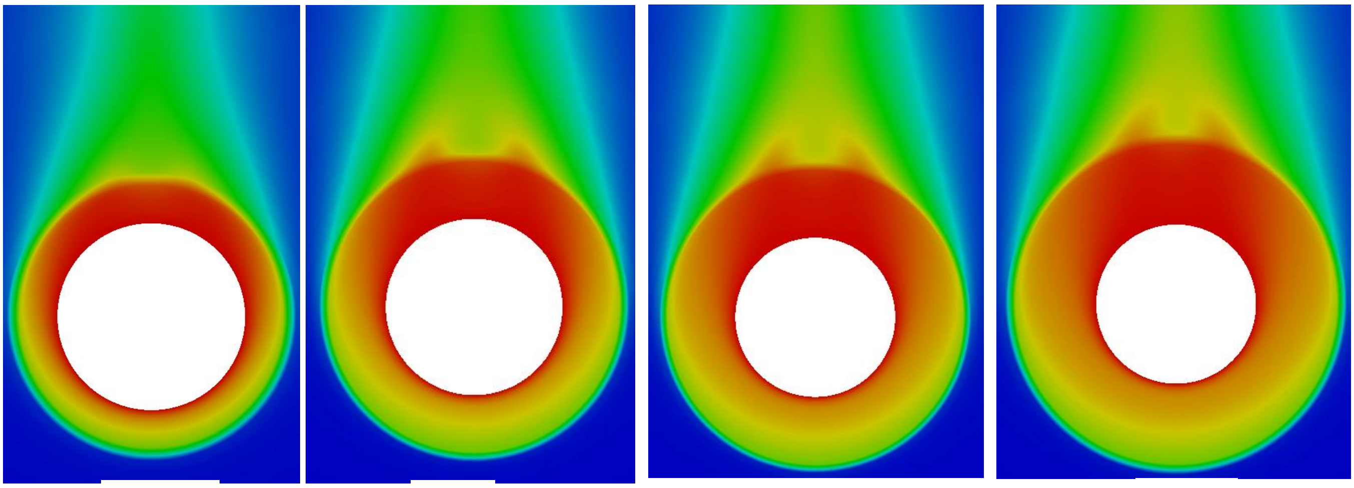

Fig. 5.8. Temperature contours showing thermal boundary growth for (A) D_f = 35 mm, (B) D_f = 41 mm, (C) D_f = 46 mm, (D) D_f = 50 mm for S = 8 mm.

5.3.3. Effect of chimney height

Similar to the effect of the fin diameter, the effect of the chimney has been studied in two parts. In the first part, the chimney height was increased from 400 mm to 500 mm for the fin spacing

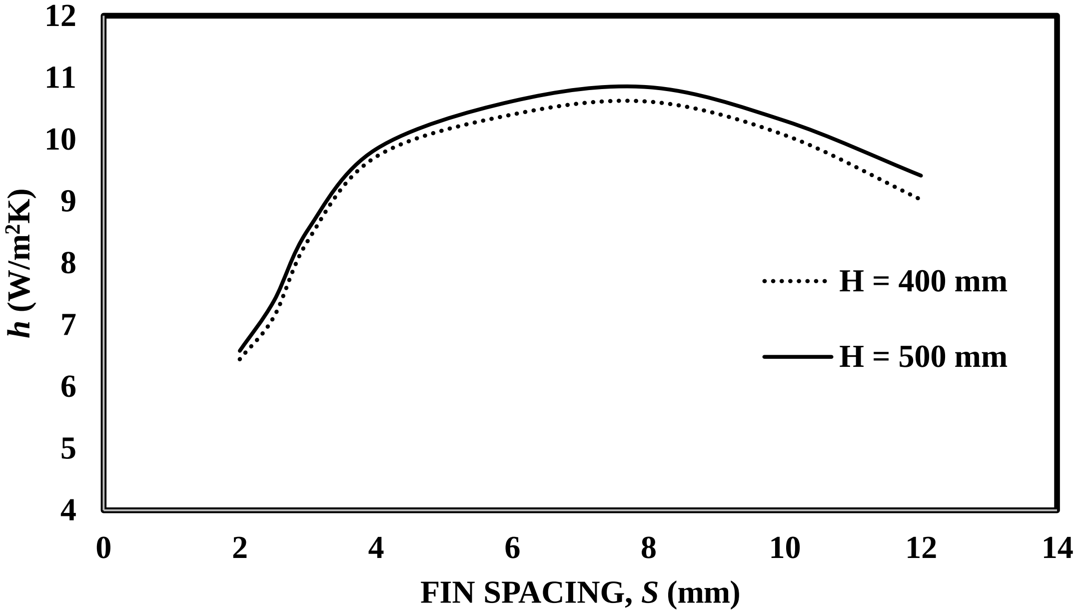

Fig. 5.9. Heat transfer coefficient for the varying chimney height at S = 2, 4, 6 and 8 mm and D_f = 41 mm.

of 2, 4, 6 and 8 mm. Fig. 5.9 shows the heat transfer coefficient, and it can be observed that, as the chimney height is increased the heat transfer coefficient increases. There are two major effects of chimney height on the thermal-hydraulic performance of the heat exchanger. First effect is the increase in the driving force with an increase in the chimney height, and the second effect is a decrease in the air outlet temperature with an increase in the chimney height. Figs. 10A and 10B show the driving force, P_{driv}, and the outlet temperature of the air, T_{out}, respectively. It can be observed that at a fin spacing of 2 mm the effect of chimney height on

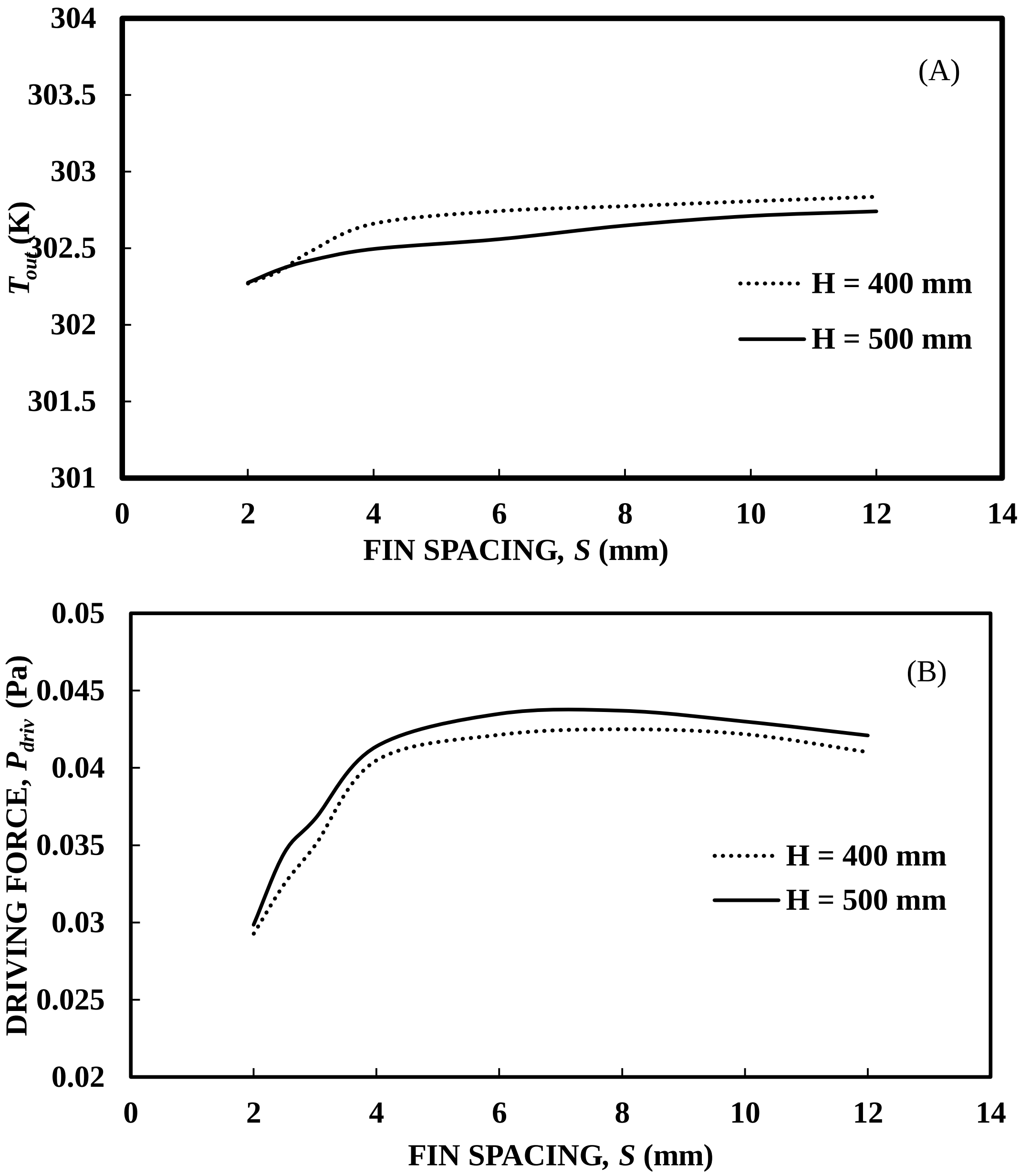

Fig. 5.10. (A) Air outlet temperature for the varying chimney height at S = 2, 4, 6 and 8 mm, (1) H = 400 mm, (2) H = 500 mm. (B) Driving force for the varying chimney height at S = 2, 4, 6 and 8 mm, (1) H = 400 mm, (2) H = 500 mm.

T_{out}, and P_{driv}, is negligible, this is because the heat transfer is very poor at a fin spacing of 2 mm as we have seen in Section 5.4.1, therefore, the effect of the chimney height becomes unimportant. However, at larger fin spacing, P_{driv} increases with an increase in the chimney height, and T_{out} decreases. In the second part of the study, the chimney height was increased

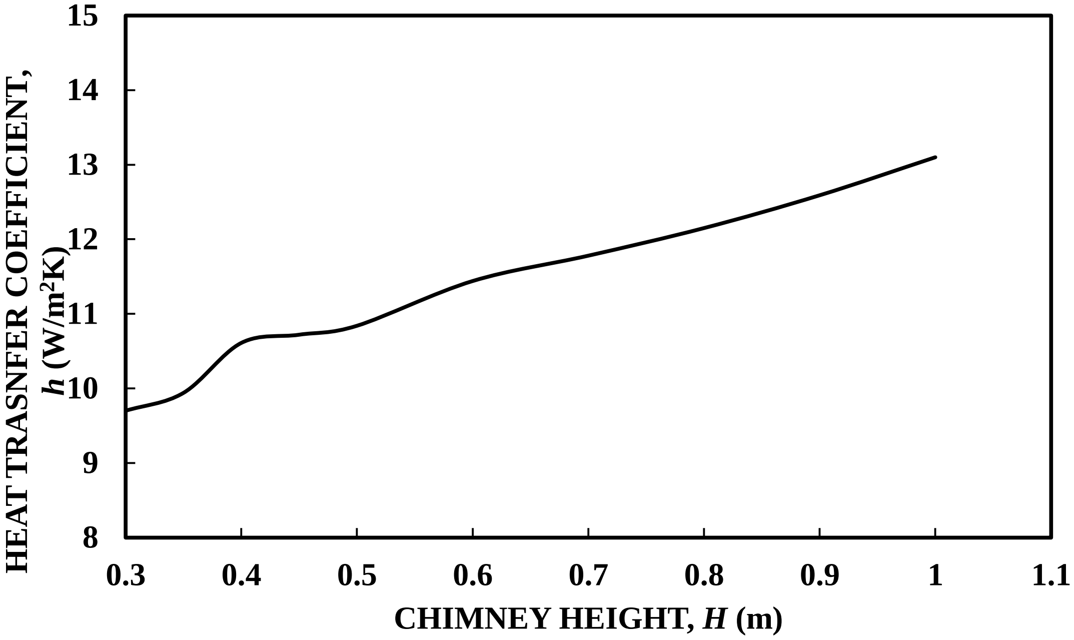

Fig. 5.11. Heat transfer coefficient for the varying chimney height at S = 8 mm, and D_f = 41 mm.

from 300 mm to 1000 mm for an optimized fin spacing of 8 mm. Fig. 5.11 shows the heat transfer coefficient variation as a function of the chimney height. It can be observed that the heat transfer coefficient increases as the chimney height is increased. This is because as the chimney height is increased; the driving force in the chimney increases, leading to a higher air flow rate and as a result, the heat transfer coefficient increases. Figs. 12A and 12B show the driving force, P_{driv}, and the outlet temperature of the air, T_{out}, respectively. A continuous decrease in the air outlet temperature and an increase in the driving force is observed with an increase in the chimney height.

5.3.4. Effect of base to ambient temperature difference

The temperature of the finned-tube surface was varied from 310 K to 365 K to study the effect of the base to ambient temperature difference on the growth of the thermal-boundary layer and heat transfer. For the natural convection, Kayansayan (1993), Yildiz and Yuncu (2004) and Yaghoubi and Mahadevi (2013) have studied the effect of the base to ambient temperature difference. In these previous studies, it has been observed that the incr (A) the base to ambient temperature difference increases the heat transfer coefficient. Similar variation of the heat transfer coefficient can be observed for the present study in Fig. 5.13. In Fig. 5.14A, the growth of the boundary layer is shown on the fin surface in *x*-*z* plane, and it

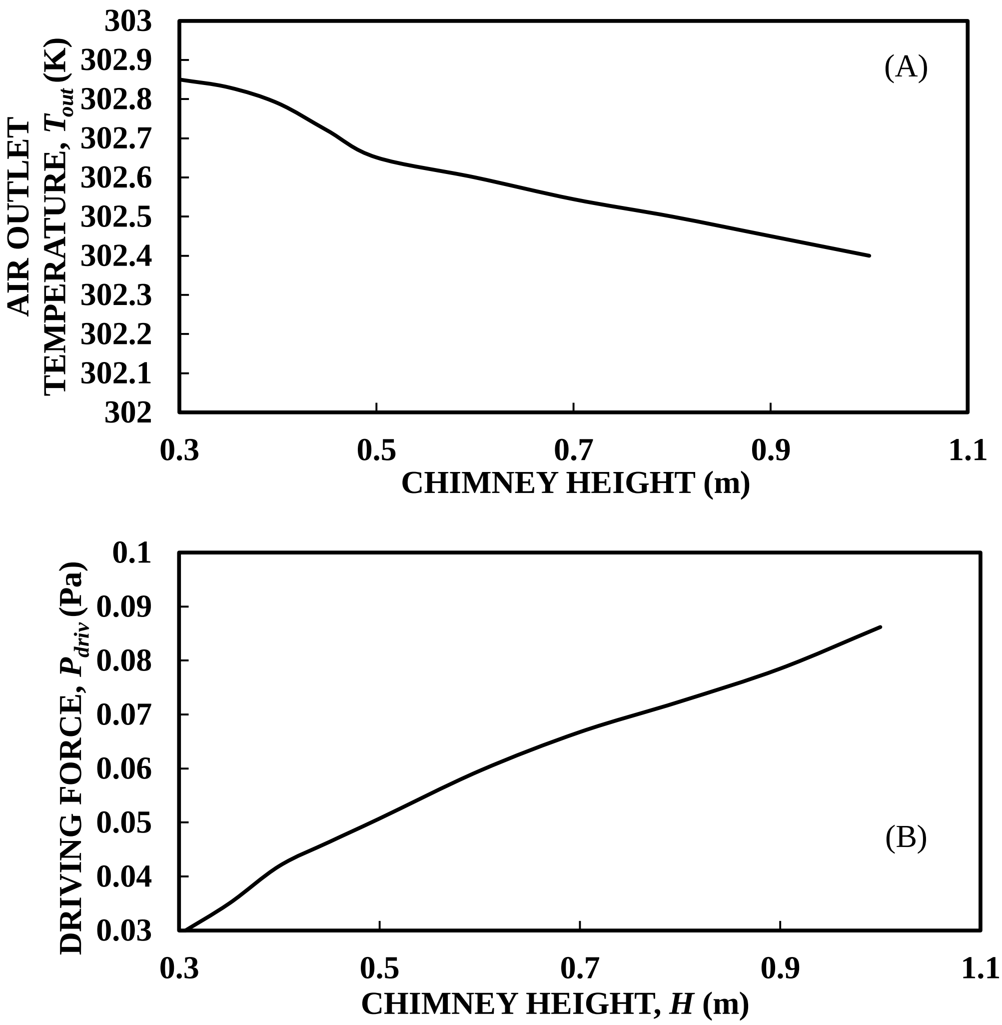

Fig. 5.12. (A) Air outlet temperature for the varying chimney height at S = 8 mm and D_f = 41 mm, (B) Driving force for the varying chimney height at S = 8 mm and D_f = 41 mm.

can be observed that the boundary layers get thinner for most of the fin surface as the base to ambient temperature increases. Similarly in the *y-z* plane (Fig. 5.14B), the thickness of the boundary layer on the fin and tube surface can be seen to be decreasing with an increase in the base to ambient temperature difference. As a result, the heat transfer coefficient increases as the base to ambient temperature difference increases.

5.3.5. Ratio of fin to tube heat transfer

For a finned-tube, the heat transfer coefficient is a combination of heat transfer coefficient provided by fins and by the tube. The major role of the fins is to enhance the heat transfer area, which results in an increase in the heat transfer rate. However, it may not always enhance the heat transfer coefficient. Therefore, to analyse this, a comparison is given for the

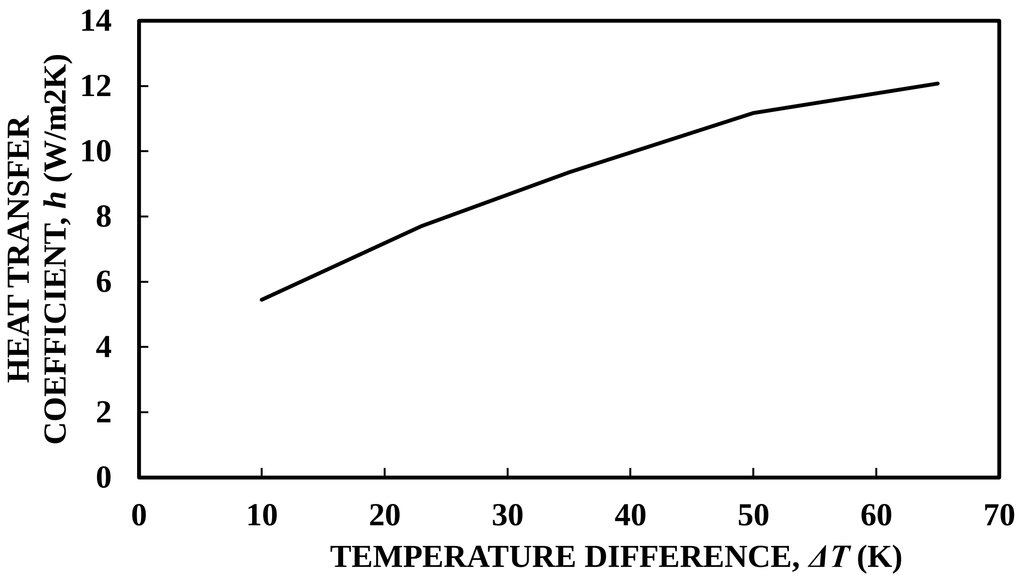

Fig. 5.13. For S = 8 mm and D_f = 41 mm, Variation of heat transfer coefficient with base to ambient temperature difference.

heat transfer coefficient provided by fins and by tube for the cases of D_f= 41 mm and D_f = 50 mm at various fin spacing in Fig. 5.15. For both the fin diameters, the heat transfer coefficient for the fins is very poor at low fin spacing, due to the merging of the thermal boundary layers between the fins, and as the fin spacing is increased, the heat transfer coefficient increases for the fins. As a result the total heat transfer coefficient also increases. The tube heat transfer coefficient remains constant for all the fin spacing at a particular fin diameter. However, the heat transfer coefficient for the tube is lower for D_f = 50 mm as compared to D_f = 41 mm for

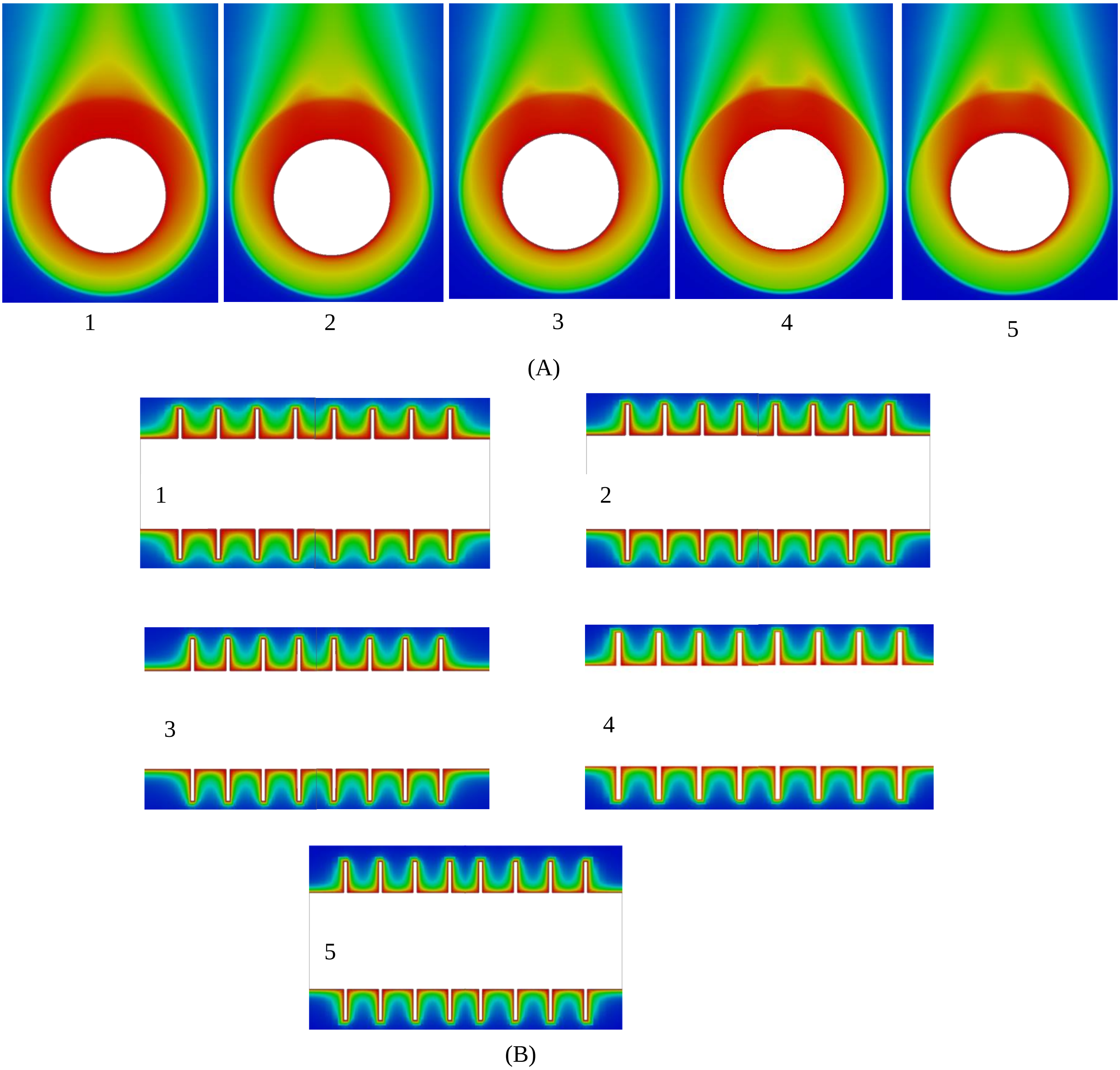

Fig. 5.14. Growth of thermal boundary layer in (A) *x-z* plane, (B) *y-z* plane [(1) ΔT = 10 K, (2) ΔT = 23 K, (3) ΔT = 35 K, (4) ΔT = 50 K, (5) ΔT = 65 K].

all the fin spacing. This can be due to the increase in the temperature of the air reaching the tubes for larger fin diameter, which results in a lower heat transfer coefficient for the tube.

5.3.6. A comparison of various bare tube designs

In the forced convection, many authors [Rocha et al., (1997), Saboya et al., (2001), Erek et al., (2005), Ibrahim and Gomaa (2009) and Jang and Yang (1998)] have compared the thermal-hydraulic performance of the circular and elliptical tubes. In the present study, the thermal-hydraulic performance of various circular and elliptical tube designs have been investigated. The diameter of the circular tubes has been varied from 7 mm to 24 mm, and for elliptical tubes, the cross-section has been varied from 30 x 10 mm to 30 x 20 mm. The fins have not been considered in this case, and plain tubes in the chimney are cosidered. The

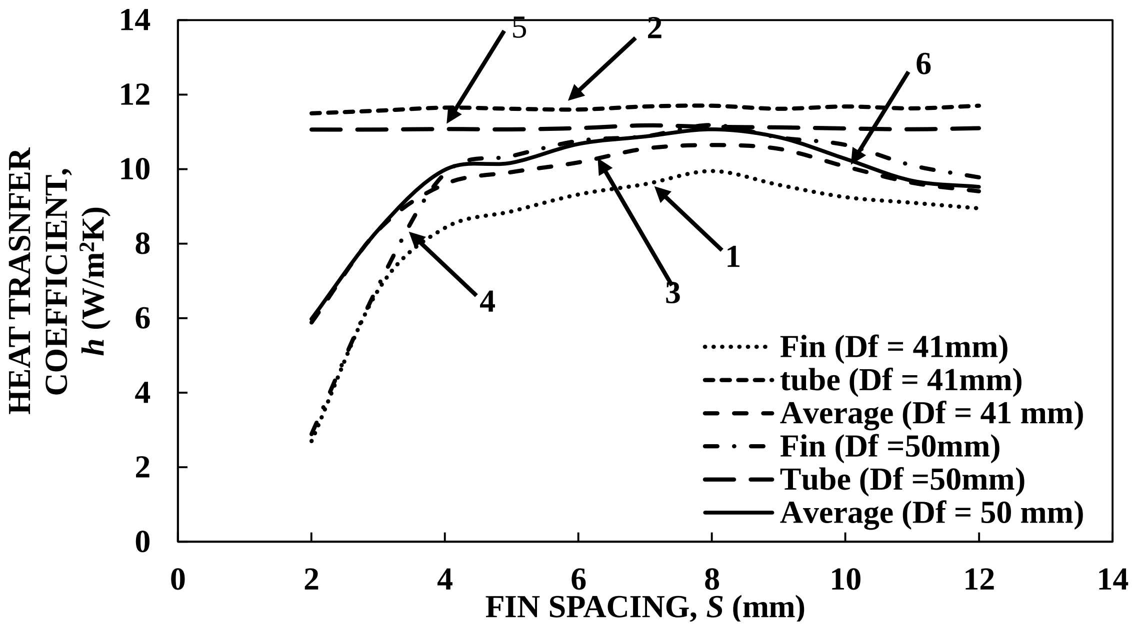

Fig. 5.15. heat transfer coefficient for fin and tube

boundary condition is similar to the finned-tube case, with tube temperature at 350 K. In Table 5, the heat transfer coefficient are given for various tube designs. It can be observed that, the designs with larger diameter. Similarly, the elliptical tube (30 × 10 mm) with smallest ellipticty (b/a) performs better than the other elliptical tube designs. Overall, the elliptical tube of dimensions 30 × 10 mm performs better than the other circular and elliptical tube designs. In Figs. 16A, 16B, 16C, the velocity vectors are shown around the tubes. It can be region circular

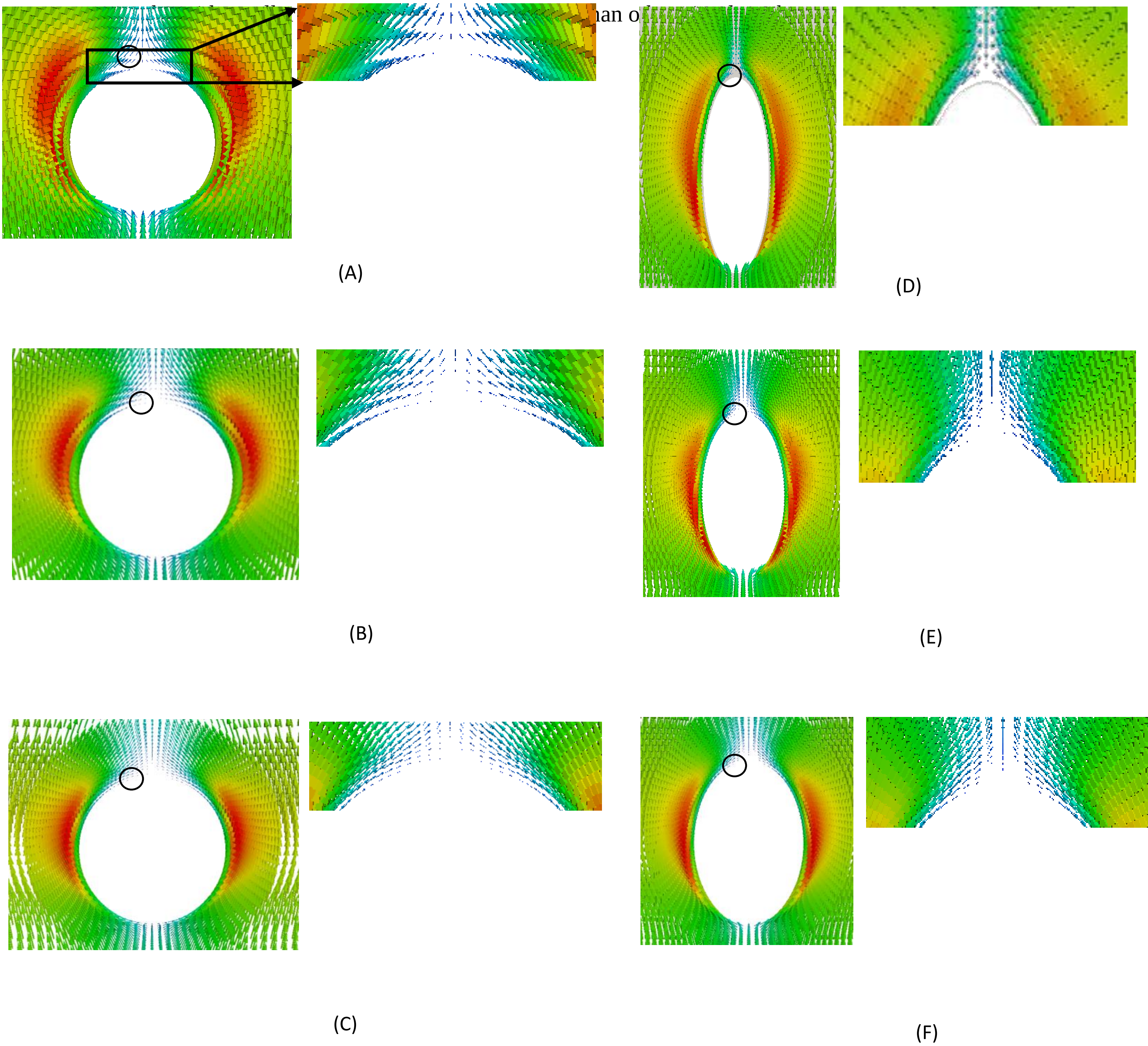

Fig. 5.16. Flow separation and wake region formation for various tube designs (black circles show the separation point). (A) Circular tube, D = 7mm, (B) Circular tube, D = 14 mm, (C) Circular tube, D = 24 mm, (D) Elliptical tube, D = 30 × 10 mm, e = 0.33, (E) Elliptical tube, D = 30 × 15 mm, e = 0.5, (F) Elliptical tube, D = 30 × 20 mm, e = 0.66

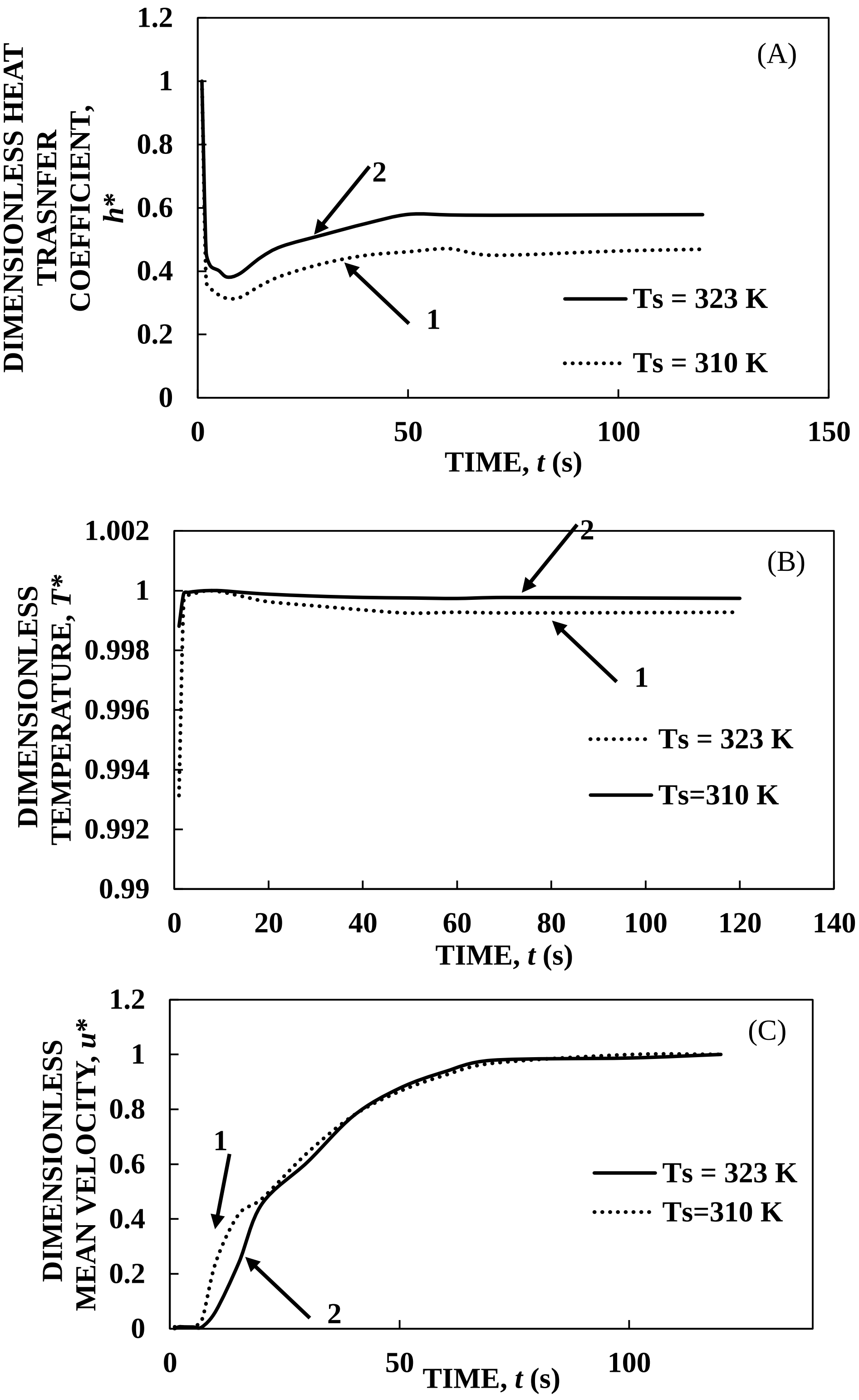

Fig. 5.17. Time varying behavior of (A) dimensionless heat transfer coefficient, (B) dimensionless temperature at z = 0, (C) dimensionless mean velocity at z = 0. (1) T_s= 310 K, (2) T_s=323K.

increases, and the flow separation starts early, leading to a weak flow behind the tube. Hence the heat trasnfer coefficient is highest for the smallest diameter circular tube for circular tube designs. Similarly for elliptical tubes, (16D, 16E, 16F), the tube with cross-section 30 x 10 mm has the minimum wake region and strongest flow behind the tubes, leading to a higher heat trasnfer coefficient. The flow separation is not prominent in the case of elliptical tubes with smaller ellipticity, hence the tube with e= 0.33 performs better than the other elliptical tubes. However as the ellipticity increases, the flow separation starts and heat trasnfer coefficient decreases. Overall, the performance of the elliptical tubes is better than the circular tubes.

5.3.7. *Transient behavior of the natural convection in the chimney*

In our previous chapter, we have given the time varying behavior of the heat transfer coefficient, and showed that h decreases with an increase in the time. However, it reaches steady state after a certain time period (depending on the size of the cavity). In the present case also, we have studied the transient behavior of the dimensionless heat transfer coefficient [h_{max} = 11.21 W m^{-2} K^{-1}(at T_s = 310 K) and 12.7 W m^{-2} K^{-1}(at T_s = 323 K)] and is shown in Fig. 5.17A. We can observe that the heat transfer coefficient is high for the initial time period; however, it takes a dip as the time increases and then starts increasing again. This behavior is different from the case of the closed cavity (Chapter 4), where h decreases continuously. We tried to analyze the reason, and studied the mean velocity and temperature (in the conduction layer near the finned-tube surface) in the domain close the finned-tube. The dimensionless temperature [T_{max} = 309.84 K (at T_s = 310 K) and 324.54 K (at T_s = 323 K)] and dimensionless velocity [u_{max} = 0.09825 m/s (at T_s = 310 K) and 0.162 m/s (at T_s = 323 K)] variation with time is shown in Figs. 17B and 17C for two cases of surface temperature (T_s = 310 K and 323 K) for S = 8 mm and D_f = 41 mm. For both the cases, we can observe that, the temperature increases initially and then starts decreasing and becomes constant for t> 60 s. This is because, initially, the velocity and temperature are very low in the domain, however as the time progresses, the velocity increases negligibly (for $0 < t < 7$ sec) for both the cases and the fluid is almost stationary, but the heat transfer and temperature rise for the fluid in the conduction layer is high. Further, with an increase in time (7 s $<t<$ 20 s), the velocity increases significantly, and therefore, the fluid in the conduction layer is replaced by fresh colder fluid (from the inlet) and hence the temperature drops down. As time increases further, the heat transfer in the whole domain increases and temperature in the conduction layer tends to reach the steady state. The major difference between the closed cavity case and the present case is the replacement of the hot fluid by the cold fluid coming from the inlet, unlike the closed cavity, in which the same hot fluid recirculates around the heated surface. The heat transfer coefficient is directly proportional to the temperature difference between the finned-tube surface and conduction layer [see eqn. (5.4)]. Therefore, the heat transfer coefficient decreases initially and takes a dip and then starts increasing and reaches steady state for $t>$ 60 s. Therefore, we can conclude that the transient behavior of the heat transfer coefficient for the flows with inner circulations differs from the transient behavior of h for the flows with the inlet and outlet.

5.4. Conclusion and suggestion for future work

The effect of the fin spacing, the fin diameter, the chimney height, the base to ambient temperature difference, various tube designs on the thermal-hydraulic characteristics of a single finned tube inside a chimney has been studied numerically. It is found that, with an increase in the fin spacing for a particular fin diameter, the heat transfer coefficient increases due to the separation of the thermal boundary layers between the finned surfaces and formation of horseshoe vortices. However, as the fin spacing is increased beyond a certain value, the heat transfer coefficient decreases due to the bypass flow stream between the fins. The optimum value of the fin spacing has been found to be 8 mm. The increase in the fin diameter from 35 mm to 41 mm at a fixed fin spacing leads to an increase in heat transfer coefficient due to the dominance of the increase in the buoyancy force over the increase in the thermal boundary layer thickness, however, as the fin diameter is increased from 41 mm to 50 mm, the increase in thermal boundary layer thickness dominates over the increase in the buoyancy force and it leads to a decrease in the heat transfer coefficient. The heat transfer coefficient increases with an increase in the chimney due to larger air flow generated by a taller chimney. The effect of the chimney height has been found a combined effect of the air outlet temperature and the driving force generated by the chimney. The heat transfer coefficient has been found to increase with an increase in the base to ambient temperature difference due to the thinning of the thermal boundary layer at higher base to ambient temperature difference. In the last section the heat transfer performance of various tube designs was investigated. It was observed that the elliptical tube with dimensions of 30 × 10 mm performs better than the other circular and elliptical tubes. Out of three circular tubes considered, the tube with smallest diameter provided maximum heat transfer coefficient. The transient behavior of the heat transfer coefficient shows different behavior than the transient behavior of h for closed systems.

We propose to extend the present work for the case of tube bundles and large chimneys. In this case, there is a possibility of occurrence of multiple circulation loops in the chimney [Lee and Korpella (1983), Joshi and Sharma (1976, 1978), Joshi (1981) and Joshi and Shah (1981)]. We wish to address this problem using the theory of linear stability [Shnip et al., (1992) and Thorat and Joshi (2004)].

Chapter 6
A comparison of performance of various fins

6.1. Introduction

Due to lower heat transfer coefficient provided by air, the use of extended surface has been a necessity in the design of air cooled heat exchangers. Longitudinal and transverse types of fins have been used for the extended surface on bare tubes. Due to thermal-hydraulic advantages of transverse fins over longitudinal fins, the use of the transverse fins has been more common. The transverse fins can be divided mainly into two categories, (1) annular fins and (2) plate fins. Further, annular fins can be divided into plain annular fins, crimped spiral fins, and serrated fins. The plate fins can also be divided into plain plate fins, wavy fins, fin with delta winglets and slit fins. Substantial amount of research work has been published on the air-cooled condensers (or heat exchangers) in the past 50 years. The performance of the air-cooled heat exchangers depends upon many geometrical parameters, like tube type, fin type, fin spacing, number of tube rows, tube pitch, etc. A detailed review of the thermal-hydraulic performance of the air-cooled heat exchangers in forced convection is given in Chapter 2 (Section 2.4).

From all the studies discussed in that review, it may be noted that, plain circular fin, plain plate fin, wavy fin and fin with vortex generators have been investigated extensively using experimental and numerical methods. The serrated fin and crimped spiral fin have been studied mostly by experiments. Only one numerical study by Lemouedda et al. (2011) has been reported on serrated fins, whereas, no numerical study has been performed on the crimped spiral fins. These fins generate 3D vortices in the flow and promotes turbulence, therefore, it is important to analyse the flow patterns and design the fins accordingly. Also, no work has been reported on the comparison of thermal-hydrualic performance of various fins. Therefore, in

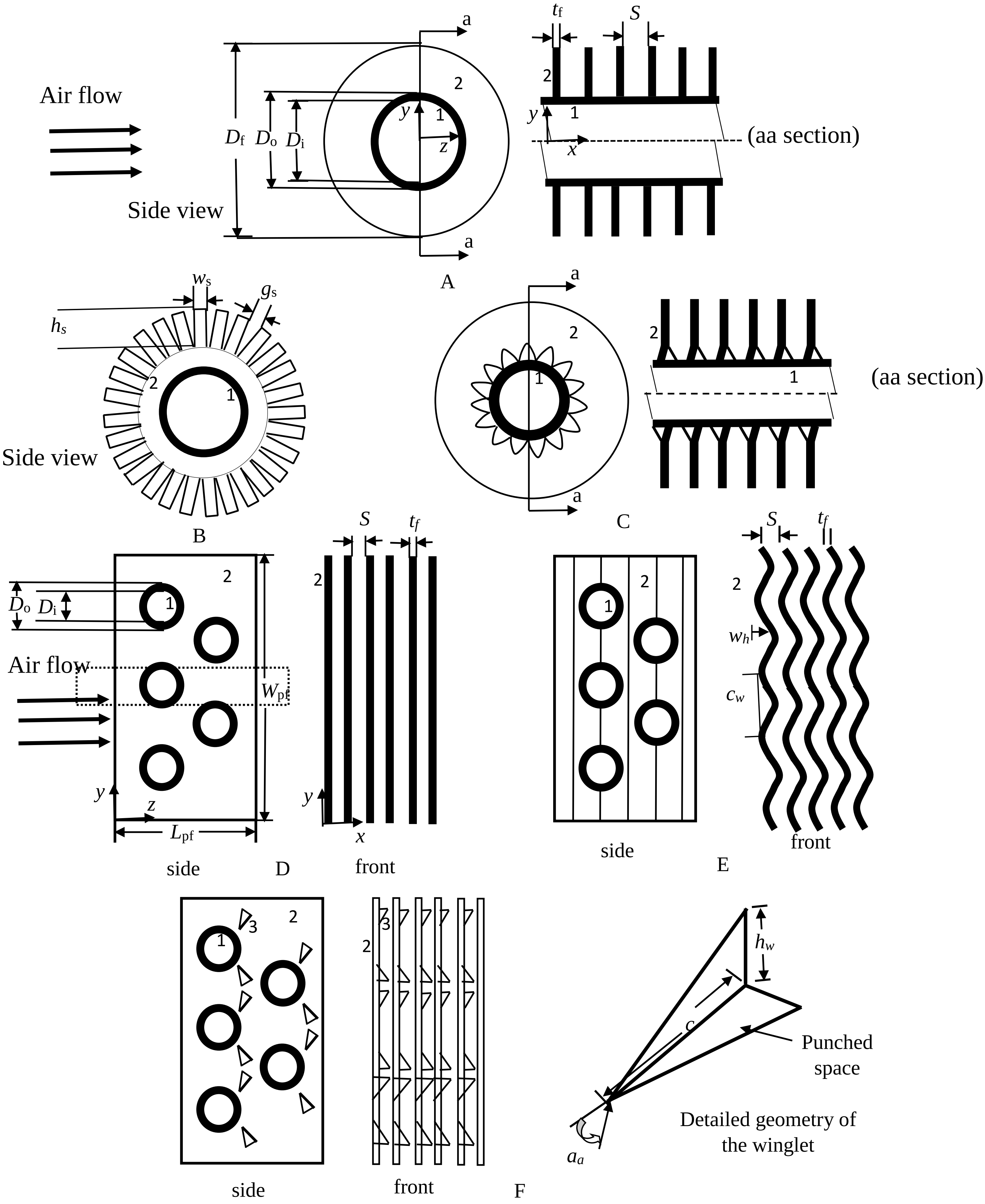

Fig. 6.1. Schematic of the finned-tubes considered, (A) plain circular fin, (B) serrated fin, (C) crimped fin, (D) plain plate fin with computational domain (E) wavy fin and (F) plain fin with punched delta winglet pair (DWP). (1) tube, (2) fin (3) DWPs

Table 6.1: Geometry of the finned tubes

Fin type	Tube diameter (mm)	Fin spacing (mm)	Fin height (mm)	Number of rows (mm)	Transverse tube pitch (mm)	Longitudinal tube pitch (mm)	Segment width (mm)	Segment height (mm)	Winglet height (mm)	Winglet span (mm)
Plain Annular	7	3-6	5	2	23	18				
Plain plate	7	3-6	5	2	23	18				
Wavy fin	7	3-6	5	2	23	18				
Fin with DWP	7	3-6	5	2	23	18			1.5	5
Serrated fin	7	3-6	5	2	23	18	4	2.5		
Crimped spiral fin	7	3-6	5	2	23	18				

6.2. Numerical Solution

6.2.1. Geometry

The system under consideration comprises of six finned-tube patterns (Fig. 6.1). The geometry of various finned tubes is given in Table 6.1. The computational domain and grid generation is shown in Fig. 6.2. The temperature of the inner surface of the tube is kept at 323 K (TPP steam temperature). The geometry of the fins considered are based on the optimization studies performed by various researchers in the past. For example, the location and size of the delta winglet pair (DWP) has determined based on the recommendations by Zeng et al. (2010), the geometry of the serrated fin has been decided based on the study of Lemoudda et al. (2011), in which a moderate number of segments were observed to be better. The geometrical modelling of the crimped fins has been based on the design currently used in the industry. The grid generation and meshing were executed using Gmsh 2.3 (2009).

6.2.2. Governing equations and model assumptions

The problem under consideration is steady 3D forced convection of air around annular-finned tubes. The assumptions in the computational model are the following:

1. Flow is considered to be compressible.
2. The buoyancy is neglected in the domain and flow is assumed to be solely under forced convection conditions.

For the finned-tube case, under natural convection conditions for a temperature difference of 15 K between ambient and the tube surface, the value of the heat transfer coefficient lies in the range of 6-8 W/m^{2}K. Whereas, *h* varies in the range of 50-100 W/m^{2}K for forced convection conditions (for present work). Also, the Richardson number (*Ri*) is in the range of 10^{-4}. Therefore, simplification of the numerical problem by neglecting buoyancy is fairly justified.

The value of the *Re* is 3500-5500, therefore, the flow is considered to be in the turbulent region. At this value of *Re*, the air flow can be treated as incompressible. However, in Openfoam 2.2., the conjugate solvers are present for compressible flows only. The consideration of air flow as compressible is also justified, as the numerical results agree well with the published experimental results (see Section 6.3.2). Therefore, the flow is treated to be compressible. The governing equations for the 3D steady forced convection are continuity, momentum, turbulence kinetic energy (k), turbulence energy dissipation rate (ε) equations, and energy equation are given in Chapter 3 (Section 3.2.2 for RNG k-epsilon model):

The thermal coefficients are calculated at the mean temperature of the tube and the ambient. The value of the Prandtl number, *Pr*, is taken as 0.7.

The heat transfer rate is calculated using the following equations:

$$Q = \dot{m} c_p \Delta T \qquad \dots (6.1)$$

$\dot{m}$is the mass flow rate through the finned tube heat exchanger and is calculated at the minimum flow area, A_c [as recommended in Chapter 2), of the finned heat exchanger and is given by,

$$\dot{m} = \rho A_c u_{max} \qquad \dots (6.2)$$

Where u_{max} is the maximum velocity occurring at the minimum flow area, A_c.

After calculating Q, the heat transfer coefficient is obtained by using the following equation:

$$h = \frac{Q}{A \Delta T_{LMTD}} \qquad \dots (6.3)$$

Where ΔT_{LMTD} is the logarithmic is mean temperature difference and is given by,

$$\Delta T_{LMTD} = \frac{(T_{in} - T_{tube}) - (T_{out} - T_{tube})}{ln\left[\frac{(T_{in} - T_{tube})}{(T_{out} - T_{tube})}\right]} \qquad \dots (6.4)$$

The pumping power (QPP) has been calculated by using the following equation:

Q_{pp}=ΔP ×Volumetric flow rate through finned tubes

The Reynolds number based on the hydraulic diameter is calculated using the expression:

$$Re_h = \frac{\rho U_{fr} D_h}{\mu}$$

Where D_h is the hydraulic diameter and is calculated as: $D_h = 4 \times \frac{A_c}{p_w}$

Table 6.2: Boundary conditions

Physical Surface	Temperature	Velocity	Pressure
Inlet	Fixed Value (323 K)	Fixed Velocity	$\frac{\partial p}{\partial x} = 0$
Outlet	$\frac{\partial T}{\partial x} = 0$	$\frac{\partial u}{\partial x} = 0$	Atmospheric
Tube (inner wall)	Fixed Value (323 K)	No slip	Calculated
Symmetry	$\frac{\partial T}{\partial x} = 0$	$\frac{\partial u}{\partial x} = 0$	$\frac{\partial p}{\partial x} = 0$

6.2.3. Boundary condition

The inner tube wall is given a constant temperature boundary condition. The problem is solved as conjugate heat transfer, and the conduction through the tube wall and the fin is considered. The no slip boundary condition is used at the tube and fin surface. At the inlet a fixed velocity and at the outlet the Neumann boundary condition is used for the velocity and the pressure is set to atmospheric. Additional details pertaining to the boundary conditions are given in Table 6.2.

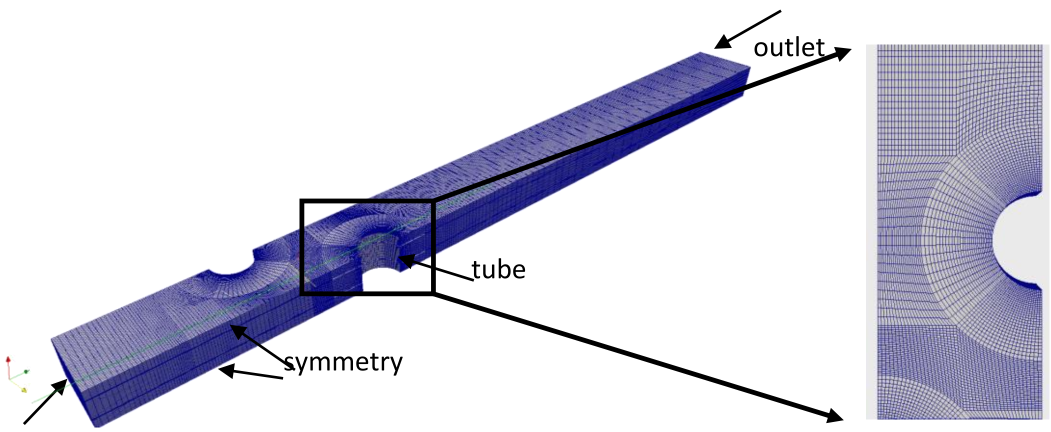

Fig. 6.2. Computational domain and grid generation

6.2.4. Method of solution

In the present work, simulations were performed under steady conditions. All the computational work was carried out using the software OpenFOAM-2.2, which is based on finite volume approach. QUICK scheme was used to discretize the divergence terms, which is a third order accurate scheme and the diffusion terms are discretized using the central difference scheme, which is a second order accurate scheme. All the discretized equations were solved in a segregated manner with the SIMPLE (Pressure Implicit with Splitting of Operators) algorithm. In SIMPLE algorithm, the equations are solved using initial guess values of flow variables, and then the values are corrected in each iteration. The iterative process continues until the convergence criterion is satisfied. The convergence criterion was based on the scaled residuals of the velocity, when the residuals reached below 10^{-5}, the solution was considered to be fully converged.

6.2.5. Grid independence

A structured hexahedaral non-uniform mesh was generated using Gmsh 2.3. A fine mesh was generated around the tube and fins to capture the high velocity and temperature gradients (average value of y^+ was 2 to 3). All the grid independence studies were performed for 3D simulations for serrated fin, crimped fin and fin with DWP. These fins have complex geometries and require careful mesh generation method and therefore are chosen for the grid independence studies. A grid resolution of 650000, 800000, 1000000 and 1500000 was used to understand the grid senstivity for a 2 rows coil (S = 4 and 5 mm) at U_{fr}= 6.32 m/s. The difference in the heat transfer coefficient was within 1-3% for the grid of 1000000 and 1500000 (Table 6.3). Finally a grid of 1000000-1400000 (higher grid number was used for the larger fin spacing and fin with DWP) cells was used for all the cases.

6.3. **Results and discussions**

6.3.1. Comparison of various turbulence models

A study has been performed for the comparison of various turbulence models. The computational models considered are standard k- ε (used presently), SST k-omega, Re-normalization group (RNG) k- ε, laminar and Launder Sharma k- ε. The resolution of the mesh in the vicinity of walls depends on the model used for the study. Standard k- ε model uses wall functions to account for the influence of wall (relation between Reynolds stresses with the mean velocity gradients and turbulent viscosity) on the mean flow and therefore first grid needs to be placed in the log layer or $Y^+ > 20$. SST k-omega model uses wall functions at high Reynolds number (turbulent range) and shifts to low Reynolds number formulation at low *Re*. For this case the first grid should be placed in the viscous layer or at $Y^+ < 5$. RNG k- ε model is derived from standard k- ε model to improve the accuracy for swirling flows, rapidly strained flows and also can handle low *Re* problems quite well. RNG k- ε model contains an analytical derivation for effective viscosity, due to which the near wall formulation for RNG k- ε differs from standard k- ε. A grid resolution of $Y^+ < 5$ is considered for this model also. Launder Sharma k- ε model is a low *Re* model and requires very fine meshing around the tube walls ($Y^+ < 1$) and does not involve the use of wall functions. Therefore, depending on the requirement of the models, the grid sizes have been chosen and given in Table 6.4. The comparison of models has been done with the experimental results of Pongsoi et al. (2012) at U_{fr} = 2.45 m/s, 4.76 m/s and 6.32 m/s for S = 3 mm and N_r = 2. The results for the heat transfer coefficient are shown in Table 6.5. It can be observed that, all the turbulence models overpredicts the experimental results by 9-27%. RNG k- ε model predicts the experimental results with a

Table 6.3: Grid size independence results

Fin spacing (mm)	Serrated fin			Crimped fin			Fin with DWP		
	Grids: 800000	Grids: 1000000	Grids: 1300000	Grids: 800000	Grids: 1000000	Grids: 1300000	Grids: 1000000	Grids: 1200000	Grids: 1500000
4	113.54	118.40	120.05	114.26	119.03	121.023	84.76	87.70	88.95
5	120.32	124.83	125.43	119.84	123.26	124.65	87.98	91.19	92.67

Table 6.4. Number of grid cells for various models considered in the present study.

	RNG k- ε model	**SST k-omega**	**Standard k- ε model**	**Laminar**	**Launder Sharma k- ε model**
Grid cells	360000	360000	240000	300000	400000

Table 6.5. Comparison of various turbulence models with the experimental results of Pongsoi et al. (2012)

U_{fr} **(m/s)**	**Experimental [h (W/m^{2}K)]**	**RNG k- ε model [h (W/m^{2}K)]**	**SST k-omega [h (W/m^{2}K)]**	**Standard k- ε model [h (W/m^{2}K)]**	**Laminar [h (W/m^{2}K)]**	**Launder Sharma k- ε model [h (W/m^{2}K)]**
2.45	46.44	51.54	52.45	54.32	63.50	54.52
4.76	68.22	78.76	77.53	79.75	86.76	79.54
6.32	80.07	88.45	89.96	91.80	95.60	89.21

Table 6.6. Code validation for plate and wavy fin

Plate fin					*Wavy fin*				
U_{fr} (m/s)	h (W/m^{2}K) [Wang and Chi (2000)]	h (W/m^{2}K) (Present work)	ΔP (Pa) [Wang and Chi (2000)]	ΔP (Pa) (Present work)	*Re*	j [Wang et al. (1997)]	j (Present work)	f [Wang et al. (1997)]	f (Present work)
0.3	37.74	42.54	1.57	1.23	348.81	0.034	0.037	0.10	0.095
0.7	43.84	48.65	3.53	3.05	608.34	0.026	0.028	0.088	0.084
1.5	55.44	62.44	9.74	8.65	1051.19	0.020	0.023	0.081	0.078
2.6	67.22	72.54	20.68	17.8	1702.29	0.017	0.020	0.073	0.069
4.7	86.58	93.53	53.24	46.34	2968.89	0.014	0.017	0.066	0.062
6.7	101.88	109.58	94.88	88.45					

deviation of 9-13%, SST k-omega model deviates by 10-12%, Launder Sharma k- ε overpredicts by 10-15%, standard k- ε model deviates by 12-15% and the laminar model provides the maximum error of 16-27%. Overall, RNG k- ε and SST k-omega model provides slightly better accuracy than other models (Launder Sharma k- ε and standard k- ε model), however, Launder Sharma k- ε and standard k- ε model also perform with a good accuracy. The grid requirement for RNG k- ε and SST k-omega model is higher (about 35% for the present case) than the standard k- ε model, which results in a larger computational cost, thus, results in pros and cons for each choice of turbulence model. Therefore, any of the turbulent model can be chosen for the practical purpose and in the present study we have chosen RNG k- ε model.

Table 6.7. Code validation for serrated, crimped fin and fin with DWP

Serrated fin			Crimped fin					Fin with DWP		
Re_h	Friction factor, f [Kawaguchi et al. (2000)]	Friction factor, f (Present work)	U_{fr} (m/s)	h (W/m^{2}K) [Nuntaphan et al. (2005)]	h (W/m^{2}K) (Present work)	ΔP (Pa) [Nuntaphan et al. (2000)]	ΔP (Pa) (Present work)	Re_h	h (W/m^{2}K) [Joardar and Jacobi (2008)]	h(W/m^{2}K) [Joardar and Jacobi (2008)]
1685.84	0.81	0.86	0.6	13.56	17.2	2.35	2.89	172	17.48	18.5
2206.64	0.80	0.85	0.85	18.36	22.54	3.52	3.9	520	26.39	28.2
2691.98	0.77	0.84	1.15	25.31	29.5	6.03	6.51	795	34.46	35.97
3246.36	0.76	0.83	1.4	31.93	36.42	9.89	10.65	1088	41.97	44.28
3735.11	0.73	0.81	1.7	38.38	45.65	12.40	13.54			
			0.6	13.56	17.2	2.35	2.89			

6.3.2 Code Validation

The code validation has been performed for plain annular fin, plate fin, crimped fin, serrated fin and wavy fin. For plain annular fin, the code is validated with the experimental data of Pongsoi et al. (2012). In Fig. 6.3A, the heat transfer results are shown and in Fig. 6.3B, the results for the pressure drop are shown. It can be observed that, the heat transfer results agree well with the experimental data. For plate fin, the numerical results are compared with the experimental results of Wang and Chi (2000). Wang and Chi (2000) performed experiments on 18 samples of heat exchangers. The results are shown in Table. 6.6 for the case of D = 8.51 mm, f_p = 3.85 mm, h_f = 10 mm, and N_r = 2. For crimped fin, the numerical are compared with the experimental results of Nuntaphan et al. (2000) for the case of D = 21.7 mm, S = 3.85 mm, h_f = 10 mm, P_t = 50 mm and P_l = 50 mm and the results are given in Table. 6.7. For serrated fin, experimental results of Kawaguchi et al. (2004) (D = 17.3 mm, f_p = 3.3 mm, h_f = 9 mm, P_t = 40 mm and P_l = 35 mm and N_r = 3) have been compared with the present numerical results (Table 6.7). The frontal velocity was calculated based on the Reynolds number and air flow rate provided by Kawaguchi et al. (2004) for the boundary condition in numerical simulations. For the wavy fin, the numerical results are compared with the experimental results of Wang et al. (1997) (D = 10.3 mm, f_p = 3.53 mm, P_t = 25.4 mm and P_l = 19.05 mm and N_r = 3). For all the fins, the numerical results deviate from the experimental results in the range of 3-20%. The deviation between the CFD results and the experimental results is due to the assumptions considered in the computational model. Also, in the present case the contact resistance between the fin and tube has been ignored, which might affect the results for the CFD simulations. However, with turbulence models based on RANS (Reynolds averaging Navier-Stokes equations) approach, the error of 10-20% can be considered to be reasonable due to assumptions involved. Therefore, with an error of 10-20%, the CFD simulations (RANS based) can be considered to be reliable for the real cases. For more accurate solution, performing Large Eddy Simulations (LES) or Direct Numerical Simulations (DNS) are preferred. However, LES requires a large computational time as compared to RANS models and DNS is yet to be performed for commercial purpose systems.

6.3.3. Comparison of various fins

In this section, the thermal-hydraulic performance of various fins have been compared for a range of $2500 \leq Re_h \leq 4000$ at a constant fin spacing of 5 mm. The Reynolds number

Table 6.8: Reynolds number and frontal velocity

Reynolds number (Re_h)	Plain circular fin		Crimped fin		Serrated fin		Plain plate fin		Wavy fin		Plate fin with DWP	
	D_h(mm)	U_{fr} (m/s)	D_h(mm)	U_{fr} (m/s)	D_h(mm)	U_{fr} (m/s)	D_h(mm)	U_{fr} (m/s)	D_h(mm)	U_{fr} (m/s)	D_h(mm)	U_{fr} (m/s)
2500	10.685	3.37	10.685	3.37	10.82	3.33	7.62	4.72	7.62	4.72	7.62	4.72
3000	10.685	4.04	10.685	4.04	10.82	3.99	7.62	5.67	7.62	5.67	7.62	5.67
3500	10.685	4.72	10.685	4.72	10.82	4.66	7.62	6.61	7.62	6.61	7.62	6.61
4000	10.685	5.39	10.685	5.39	10.82	5.32	7.62	7.56	7.62	7.56	7.62	7.56

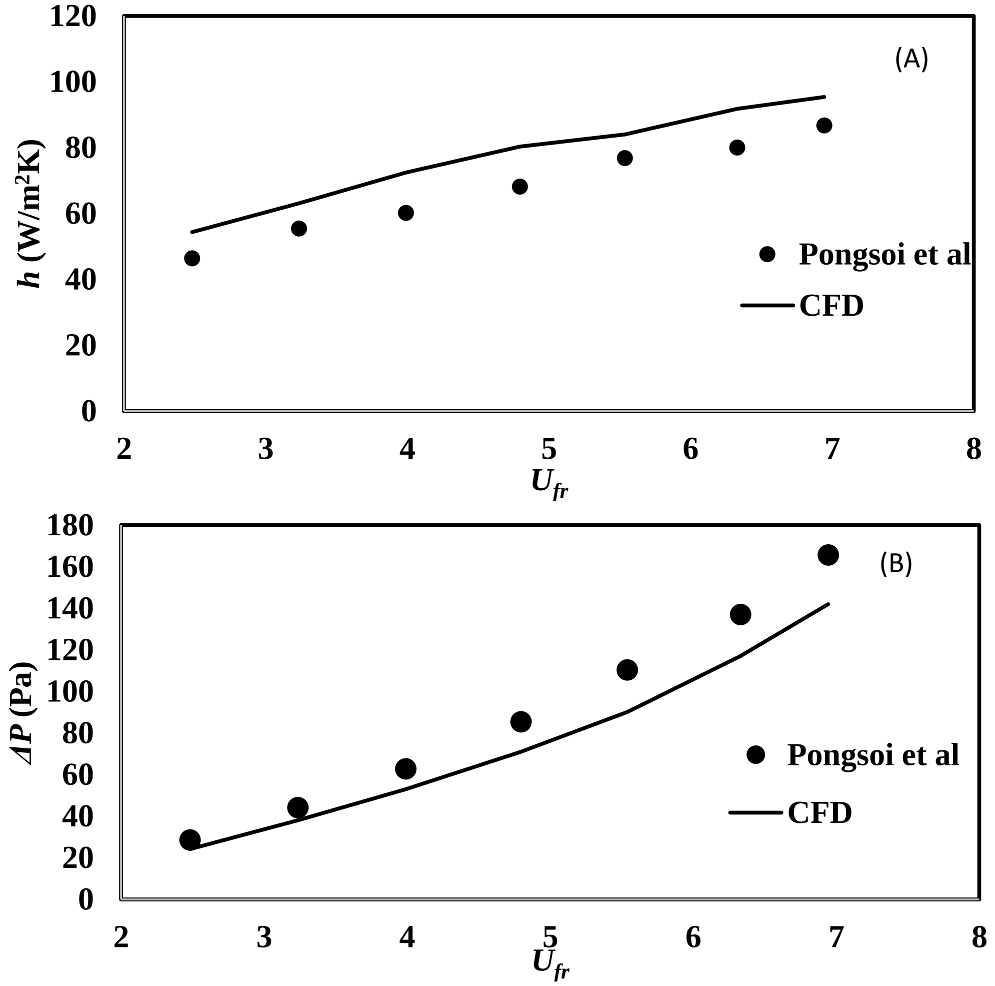

Fig. 6.3. Validation of the code with Pongsoi et al. (2012), (A) heat transfer coefficient (1) CFD, (B) Pressure drop

based on the hydraulic diameter of the finned-tube heat exchanger has been chosen as the basis for the comparison. To obtain same Re_h for different fins, the frontal velocity has to be varied at a constant fin spacing (S = 5 mm). The values of frontal velocity, hydraulic diameter (computational domain) and Reynolds number for various fins have been provided in Table. 6.8. Fig. 6.4 shows the variation in the heat transfer coefficient, pressure drop and heat transfer per unit pumping power with respect to the Re_h. In Fig. 6.4A, it can be observed that, the heat transfer coefficient increases by 25-35% for all the fins with an increase in Re_h from 2500 to 4000. Of the annular fins, crimped and serrated fins provide 18-21% and 12-14% higher heat transfer coefficient as compared to the plain annular fin, respectively. This is due to the enhanced mixing and turbulence by complex geometries of crimped and serrated fin (detail discussion in Section 6.3.4). Similarly, among the plate fins, wavy fin and the fin with DWP provide 12-15% and 5-10% higher heat transfer coefficient as compared to the plain plate fin because of their tendency to promote mixing in the flow. If we compare all the fins, then crimped and serrated fins turn out to be the best in terms of heat transfer coefficient. Fig. 6.4B compares the pressure drop for all the fins, and we can observe that, of the plate fins, the wavy fin produces higher pressure drop penalty (60-90% and 35-80% higher as compared to plain plate and fin with DWP, respectively). The fin with DWP results in a bit higher pressure drop as compared to the plain plate fin due to the presence of the winglet, on the other hand, wavy fin provides a much complex and longer air flow path resulting in a very high pressure drop. Of the circular fins, crimped fin produces highest pressure drop as compared to the plain circular (60-100% higher) and serrated fin (20-70% higher). Comparing performances based on heat transfer coefficient and pressure drop separately is not enough, therefore, heat transfer per unit pumping power has also been compared, which is important for industrial purpose. In Fig. 6.4C, we can observe that, plain circular fin provides higher heat transfer rate per unit pumping power among the circular fins (25-40% and 8-13% higher as compared to the crimped

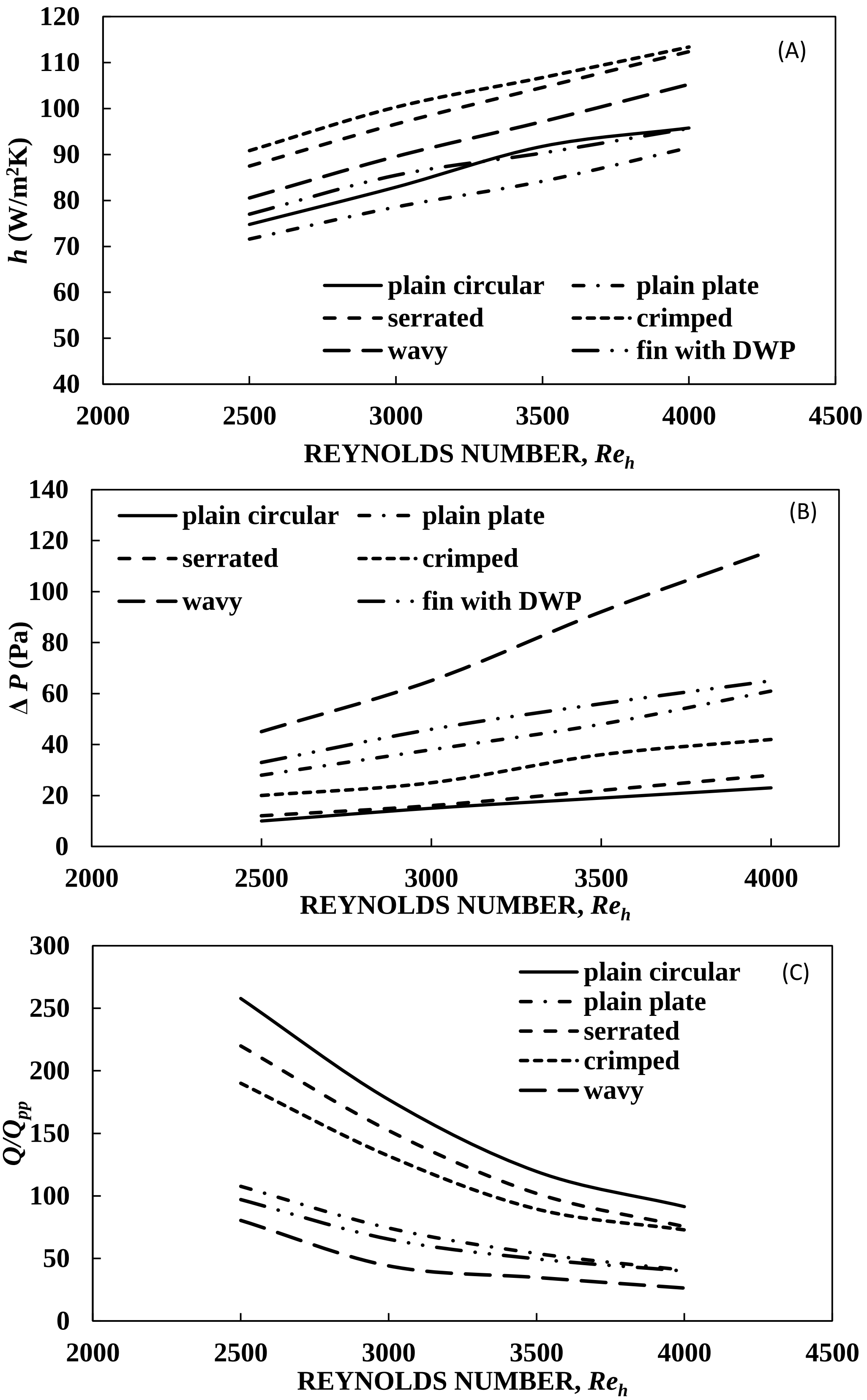

Fig. 6.4. Comparison of fins at varying Reynolds number for S = 5 mm, (A) heat transfer coefficient, (B) pressure drop, and (c) heat transfer per unit pumping power.

and serrated fin, respectively). Of the plate fins, the plain plate fin provides a highest heat transfer rate per unit pumping power. If we compare the circular and plate fins, then it can be observed that circular fins produce a higher heat transfer coefficient (except plain circular) as compared to all the plate fins. Also, due to longer flow path and continuous development of boundary layer, plate fins result in higher pressure drop as compare to the circular fins, which results in a 75-140% higher heat transfer rate per unit pumping power for circular fins as compared to the plate fins. With an increase in the Reynolds number, the heat transfer per unit

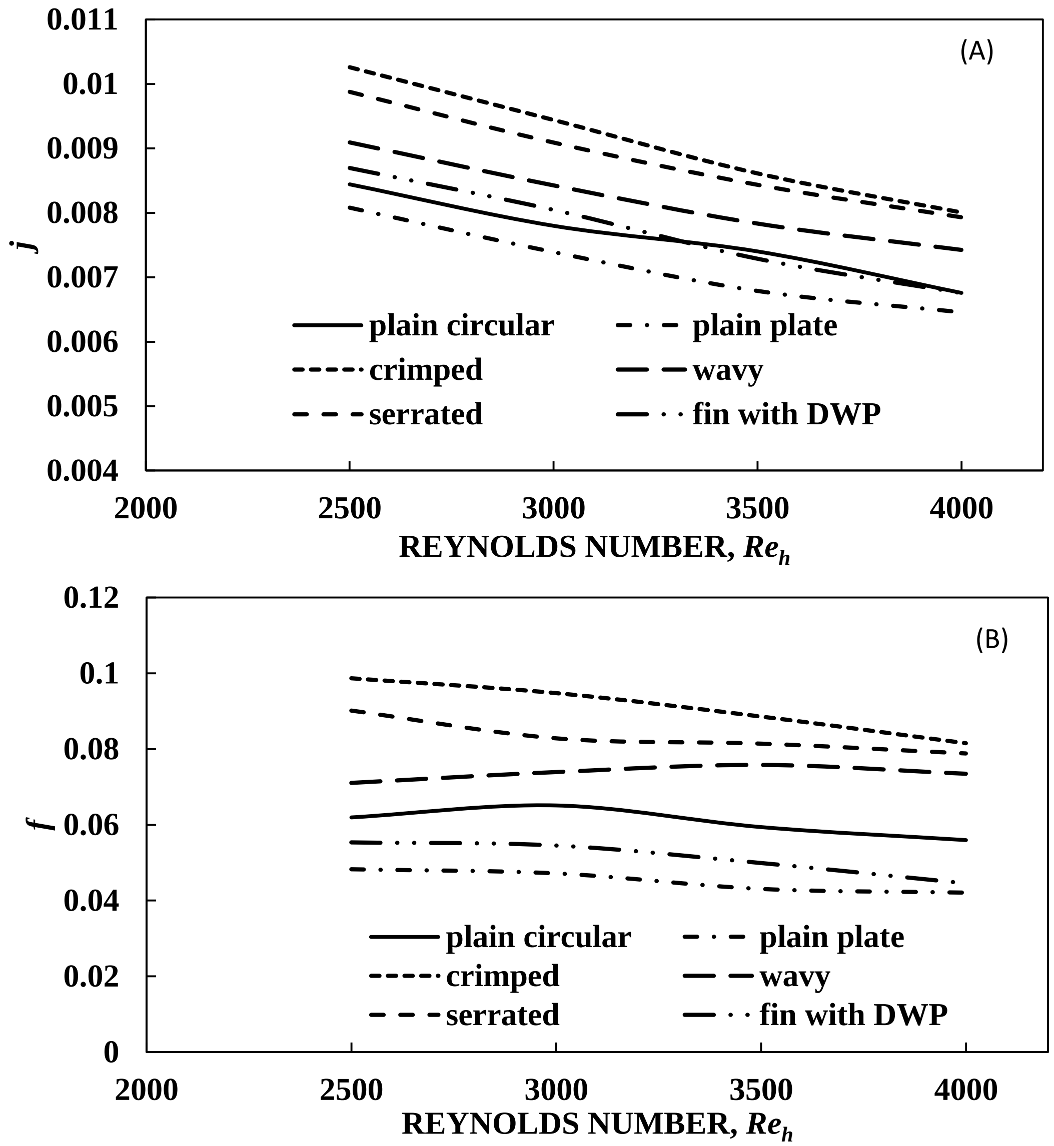

Fig. 6.5. Comparison of fins at varying Reynolds number for S = 5 mm, (A) Colburn factor (j), (B) friction factor (f).

for all the fins for a range of $2500 \leq Re_h \leq 4000$. We can observe that *j* decreases by 15-25% pumping power decreases for all the fin patterns. It is always important to analyze thermal-hydraulic performance in terms of dimensionless numbers, therefore, in Fig. 6.5, we have shown the Colburn factor and friction factor. The definition of Colburn factor and friction factor is given by:

$$\text{Colburn factor } (j) = \frac{Nu}{Re_h Pr^{\frac{1}{3}}} \qquad \ldots (6.5)$$

$$\text{friction factor } (f) = \frac{2\Delta P \rho_m}{G_c^2}\left(\frac{A_c}{A}\right) \qquad \ldots (6.6)$$

The Colburn factor and friction factor relates the heat transfer and pressure drop to the operating conditions and geometry of the heat exchanger. Fig. 6.5A shows the Colburn factor with an increase in the Reynolds number from 2500 to 4000. Of the circular fins, *j* is highest for the crimped fin and lowest for the plain annular fin, the reason is same as for the heat transfer coefficient in Fig. 6.4A. Similarly, for the plate fins, the wavy fin produces highest Colburn factor. The force requires to sustain a certain mean flow is measured by friction factor. Fig. 6.5B shows the friction factor for various fin patterns and unlike pressure drop, *f* decreases with an increase in Reynolds number for most of the fins. This is because it is a ratio of pressure to the square of the mass flux. As Re_h increases, the mass flux also increases in the domain, and hence a combine effect of pressure drop and mass flux affects the friction factor. We can observe that crimped fin provides 45-60% and 5-14% higher friction factor than the plain circular and serrated fins, respectively. Among the plate fins, wavy fin provides 45-74% and 28-60% higher friction factor as compared to the plain plate and fin with DWP, respectively. It is interesting to note that wavy fin and fin with DWP produces maximum pressure loss penalty (Fig. 6.4B), however, the friction factor is highest for the crimped fin. Serrated fin also provides a higher friction factor (as compared to the wavy fin). This shows that if crimped fin and wavy fin have the equivalent surface area, then the pressure drop would be larger for the crimped fin. This is due to shape of the crimped fin, which leads to a larger friction factor indicating more disturbance in the flow. Similar reason can be attributed to the high friction factor for the serrated fin. Despite of the larger pressure drop provided by fin with DWP and plain plate fins, their friction factor is lower indicating a lower disturbance in the flow.

To understand the variation in the heat transfer performance of various fin patterns, local Nusselt number has been plotted along the periphery of the tubes and close to the fin surface (0.1 mm above the fin surface) in Fig. 6.6. We can observe that *Nu* decreases for plain circular, serrated, plain plate fin and fin with DWP upto θ = 120-130°. For crimped and wavy fins, the variation of *Nu* is very oscillating though it eventually decreases as move along the periphery $\theta \leq$ 120-130°. The decrease in *Nu* for plain circular, serrated, plain plate and fin with DWP is gradual upto θ = 70-80° and then it suddenly decreases to its lowest value at θ = 120-130°. This happens because of the flow separation at about θ = 70-80°, which reduces the heat transfer between the tube surface and the fluid. The flow separation for various fin patterns is

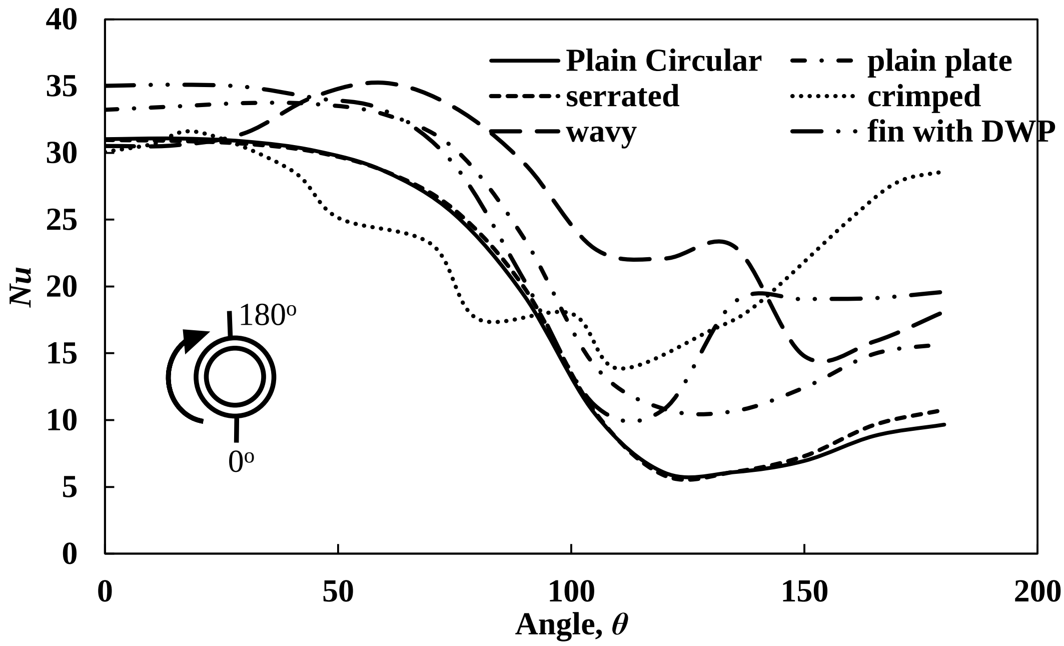

Fig. 6.6. Nusselt number variation along the periphery of the tubes in the vicinity of the fins (0.1 mm above the fin surface).

shown in Fig. 6.7. We can observe a wake region behind the tubes with recirculating vortices for all the fins except fin with DWP. Further, as move to the rear side of the tube ($\theta \geq$ 120-

130°), the Nusselt number starts increasing for all the fins. This can be understood from the flow patterns in Fig. 6.7. In Fig. 6.7A, we can see that the recirculating vortices start from the flow separation point and then move alongside the mean flow and then again comes back and touch the back side of the tube (black line). This way these recirculating vortices take heat from the tube surface and then interact with the mean flow and hence heat is transferred. We can also observe from Fig. 6.6 that recovery of the heat transfer is very high for the fin with DWP in the wake region ($\theta \geq$ 120-130°). This is due to the presence of delta winglets near the tubes, which directs the mean flow towards the rear side of the tube and reduces the wake region and hence enhances the heat transfer. From crimped and wavy fin (Figs. 6.7B and 6.7E respectively), the wake region is seen to be disturbed by the complex geometry of the fins and that is the reason that heat transfer is higher and non-uniform in the wake region also. In Fig. 6.7, the temperature contours are also shown, which are denser for fin with DWP, wavy and crimped fins, indicating higher heat transfer in the wake region.

To investigate the effect of various fin patterns on the flow field we have shown the temperature contours between the fin surfaces in *x-z* plane. We can observe that for plain fins (plain circular and plain plate) the contours are nice and uniform indicating less disturbance in the flow (Figs. 6.8A and 6.8D). However, if we observe the temperature contours for crimped, wavy and fin with DWP (Figs. 6.8B, 6.8E and 6.8F), then we can observe that the contours are disturbed and non-symmetric. This reflects the capabilities of these fins to affect the mean flow and promote mixing which leads to a higher heat transfer as have been discussed. Surprisingly, the contours for serrated fins are also uniform (Fig. 6.8C). The detailed flow patterns for serrated, crimped and fin with DWP are discussed in Section 6.3.3. Some studies have focused on the comparison of fins, for serrated fins, Kawaguchi et al. (2005) found that friction factor of serrated fins is 1.1-1.15 times the friction factor of plain circular fin. In the present work, we

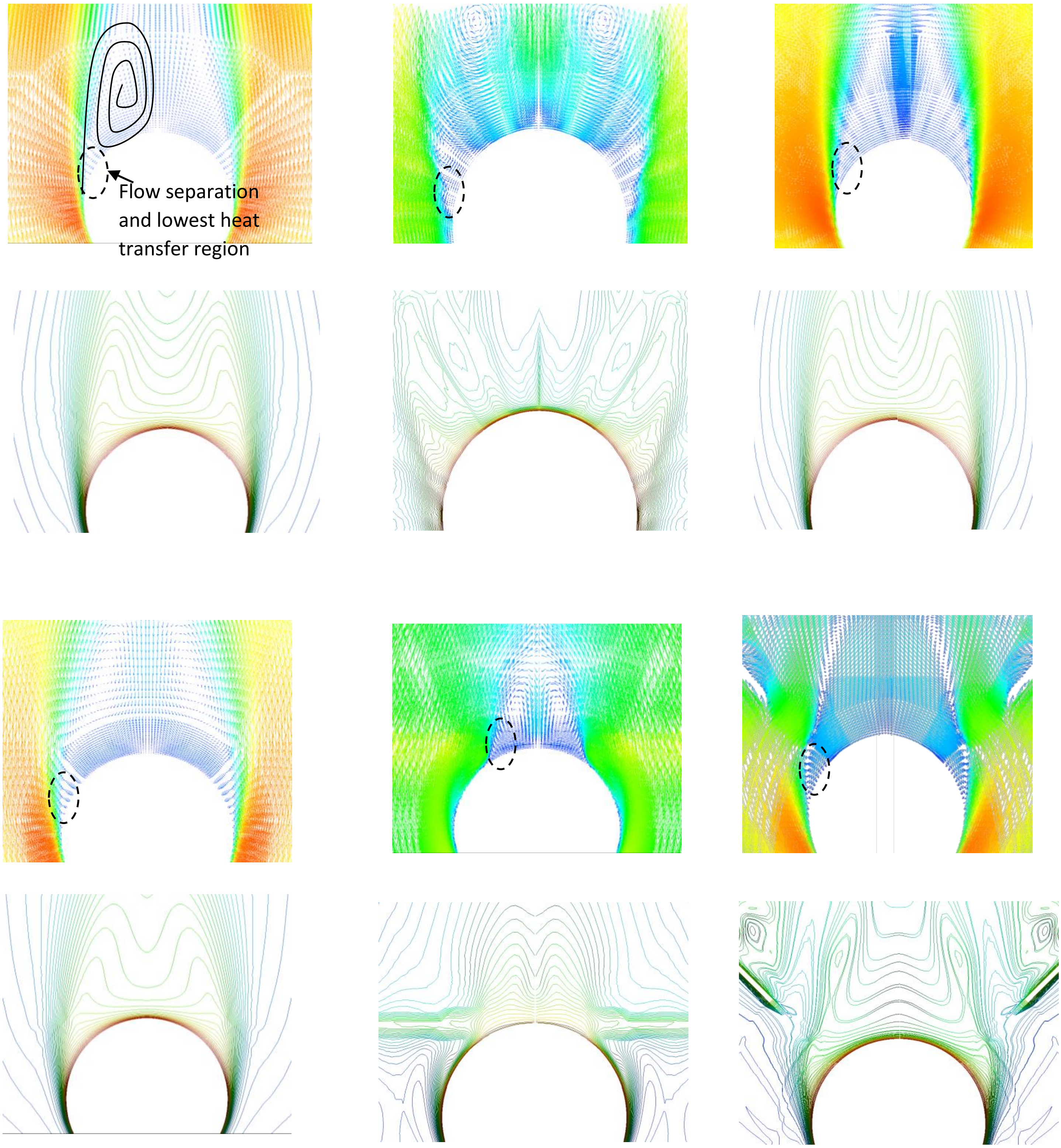

Fig. 6.7. Velocity vectors and temperature contours representing flow separation and wake region formation behind the tubes (Dotted circles show the flow separation point). (A) plain circular fin, (B) crimped fin, (C) serrated fin, (D) plain plate fin (E) wavy fn and (F) plain fin with punched delta winglet pair (DWP)

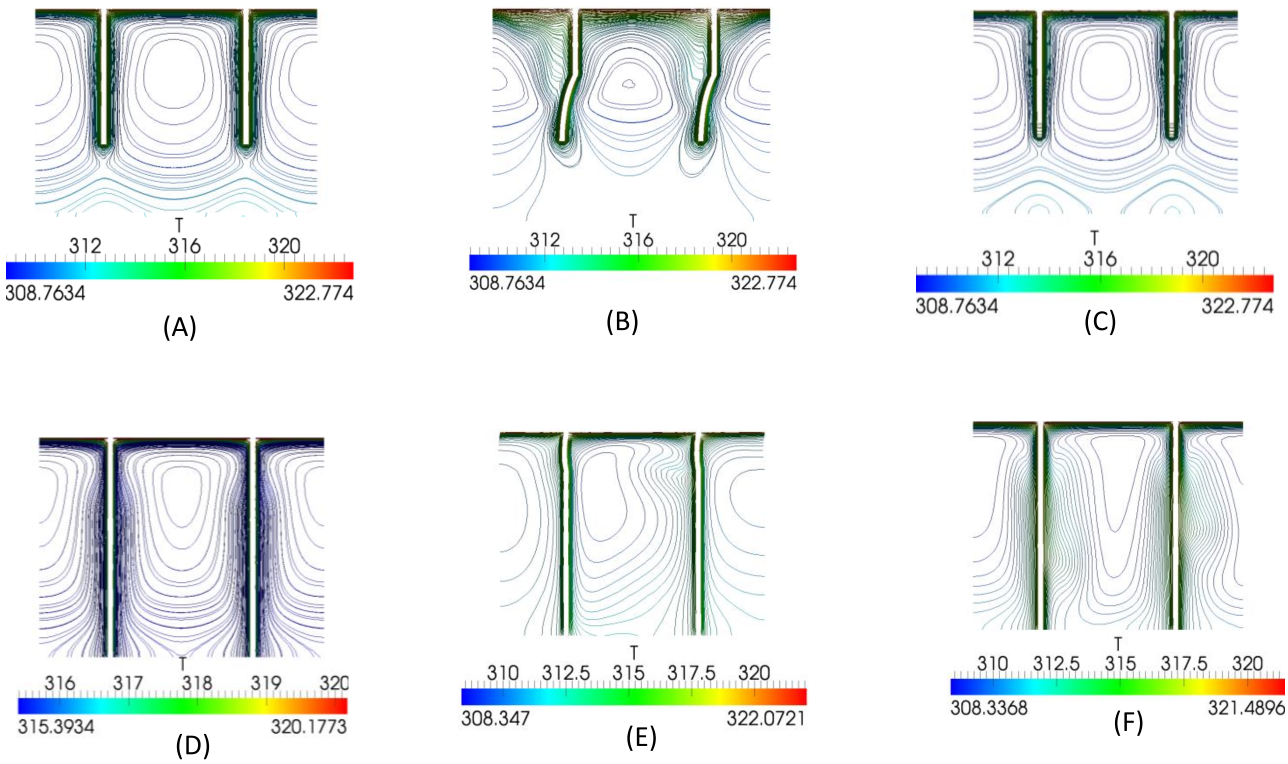

Fig. 6.8. Temperature contours between the fin gap for (A) plain circular fin, (B) crimped fin, (C) serrated fin, (D) plain plate fin (E) wavy fn and (F) plain fin with punched delta winglet pair (DWP).

find it to be 1.4-1.5 times; the reason can be larger dimensions of tube and fins used by Kawaguchi et al. (2005) which affects the performance of the finned-tubes. For the serrated fins, the only numerical study was performed by Lemoudda et al. (2011), and they observed that serrated fins provides a 9% higher heat transfer rate as compared to the plain circular fin of equivalent heat transfer area but requires larger power input also. Present results agree with Lemoudda et al. (2011).

Biswas et al. (1994) found that *Nu* for fin with DWP is 240% higher than the plain fin, Tian et al. (2009) observed an increase of 95% in the heat transfer by fin with DWP as compared to the plain fin. In the present case, we find an increase of 8-12% in heat transfer coefficient for fin with DWP as compared to the plain fin. Tang et al. (2009a, 2009b) observed that crimped fin provides a higher Colburn factor as compared to the plain fin, fin with DWP, slit fin and mixed fin. However, under identical flow rate, pumping power and pressure criterions, the fin with DWP was found to perform better than the other fins. In the present study also, we observed a higher Colburn factor for the crimped fin as compared to the fin with DWP, but found that friction factor is also higher for the crimped fin. In none of the previous studies, detailed flow patterns were given for the crimped fin.

Overall, present results agree with some of the authors and disagree with some, and to understand this we have tried to go deeper into the thermal-hydraulics of the air cooled heat exchanger and have given detailed flow patterns for all the fins in Section 6.3.3.

6.3.4. Effect of fin spacing

In the literature, there have been only few studies on the serrated and crimped fins, especially those describing detailed flow patterns. Also, of the plate fins, the performance of fin with DWP has been impressive as observed in the last section and by previous researchers. Therefore, we have extended the present work to study the effect of fin spacing for serrated fin, crimped fin and fin with DWP. The Reynolds number has been kept constant for all the fins at Re_h = 3000. Detailed flow patterns have also been investigated and presented in this section. Fig. 6.9A shows the heat transfer coefficient, and we can observe that h decreases by 10-15 % as fin spacing increases from 3 to 6 mm at a constant Re_h. This is due to the bypass flow between the fins as fin spacing increases beyond a certain value. Fig. 6.10 represents the air flow temperature between the two fin surfaces, we can observe that the air temperature is higher near the fin surface only and as we move away from the fin then the air temperature is almost 308 K, which is the inlet air temperature. This is true for all the fin spacings and proves that the heat transfer is inefficient away from the fin surfaces. Therefore, as the fin spacing increases, the amount of fluid taking part in the inefficient heat transfer process increases leading to a lower heat transfer coefficient. The crimped fin provides higher heat transfer coefficient for the range of $3 \leq S \leq 6$ mm as compared to the serrated fin and fin with DWP. Similar observations were made for constant fin spacing and varying Re_h (Fig. 6.4A). Fig. 6.9B shows the variation in the pressure drop with an increase in the fin spacing and it can be observed that the pressure drop decreases as the fin spacing increases. This is due to the less

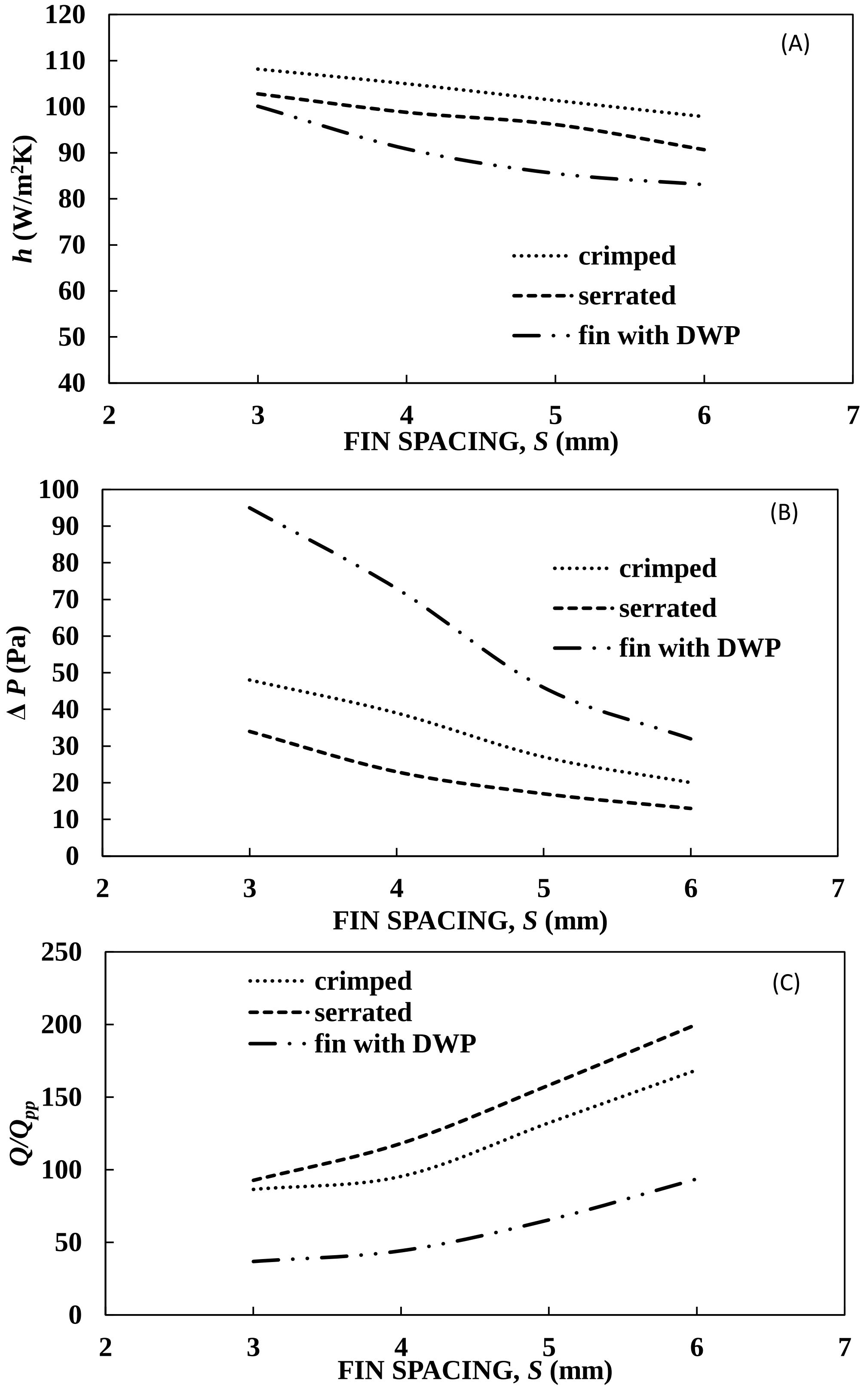

Fig. 6.9. Comparison of fins at varying fin spacing for Re_h = 3000, (A) heat transfer coefficient, (B) pressure drop, and (c) heat transfer per unit pumping power.

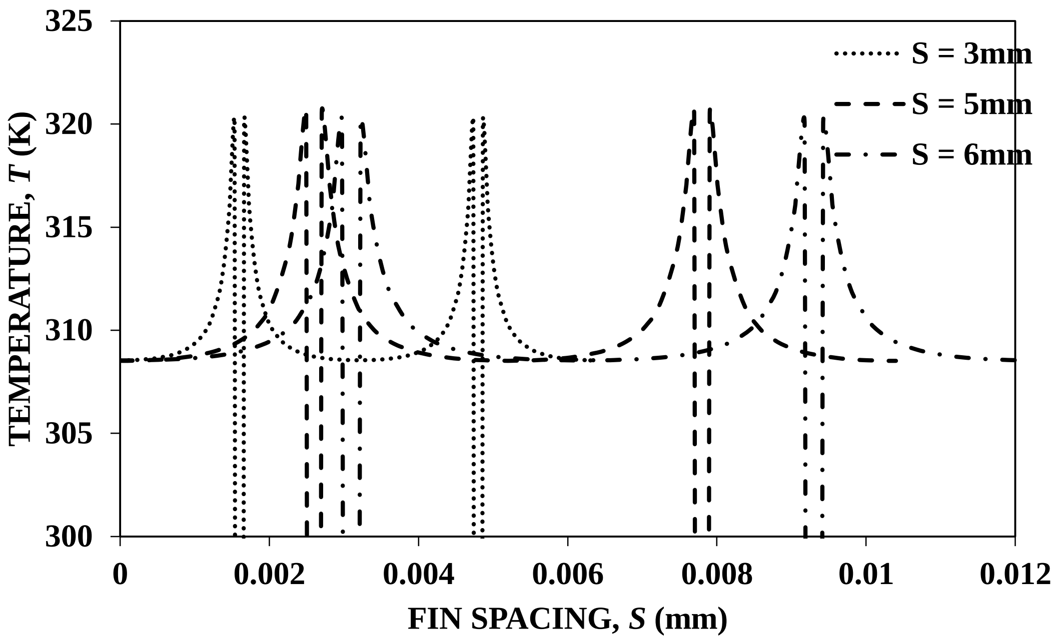

Fig. 6.10. Air flow temperature plots between the gap of the fins.

obstruction provided by the finned-tube geometry at larger fin spacing. The fin with DWP provides higher pressure drop as compared to the serrated and crimped fins, which is due to the larger area of the fin with DWP (hence larger skin friction) and the obstruction provided by the DWPs. We can also observe that as fin spacing increases the variation in the pressure drop is largest for the fin with DWP (more than 66%). This might be since DWPs produces significant disturbance in the flow and hence pressure drop and as the fin spacing increases, the free flow area increases in the domain. This results in more air flow diverting into the free flow area and bypassing the DWPs as much as possible due to the tendency of the flow of choosing less obstructing path. In Fig. 6.9C, the heat transfer per unit pumping power is presented. We can observe that, serrated fin performs best in terms of Q/Q_{pp} and fin with DWP performs worst. Also, Q/Q_{pp} increases by 90-140% as the fin spacing increases from 3 to 6 mm. This indicates that with an increase in the fin spacing, the decrease in the pressure drop is larger as compared to the decrease in the heat transfer coefficient. Therefore, larger fin spacing is beneficial to extract higher heat transfer rate for a minimum pumping power penalty for commercial heat exchangers.

The results for non-dimensional parameters, i.e., Colburn and friction factor have been presented in Figs. 6.11A and 6.11B. The behavior of Colburn factor is like the behavior of heat transfer coefficient presented in Fig. 6.9A. However, the friction factor increases as the fin spacing increases, which contrasts with the pressure drop variation presented in Fig. 6.9B. This

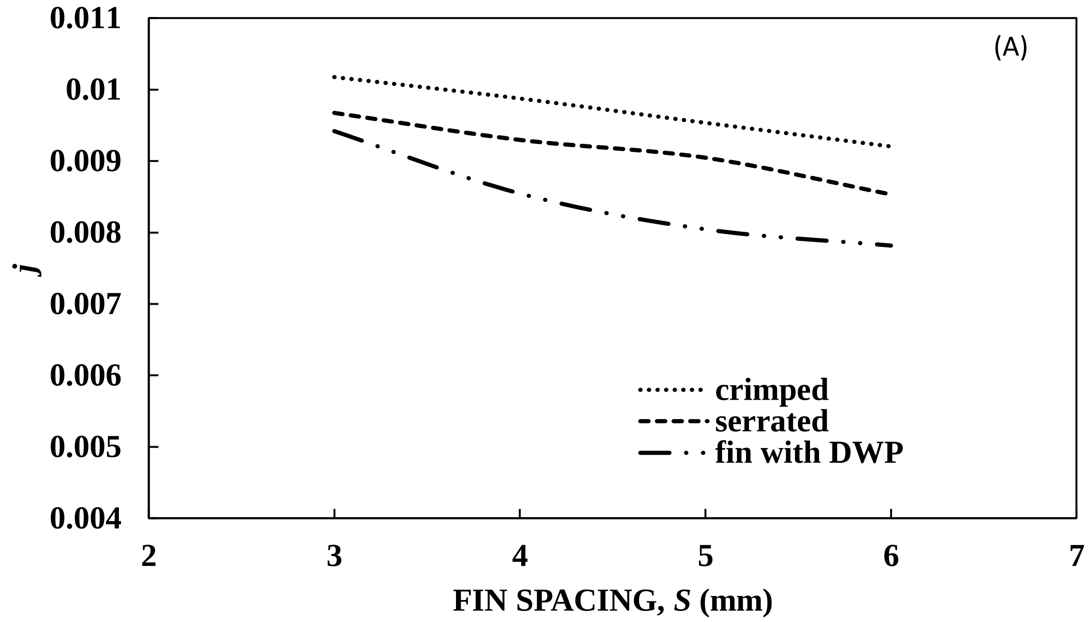

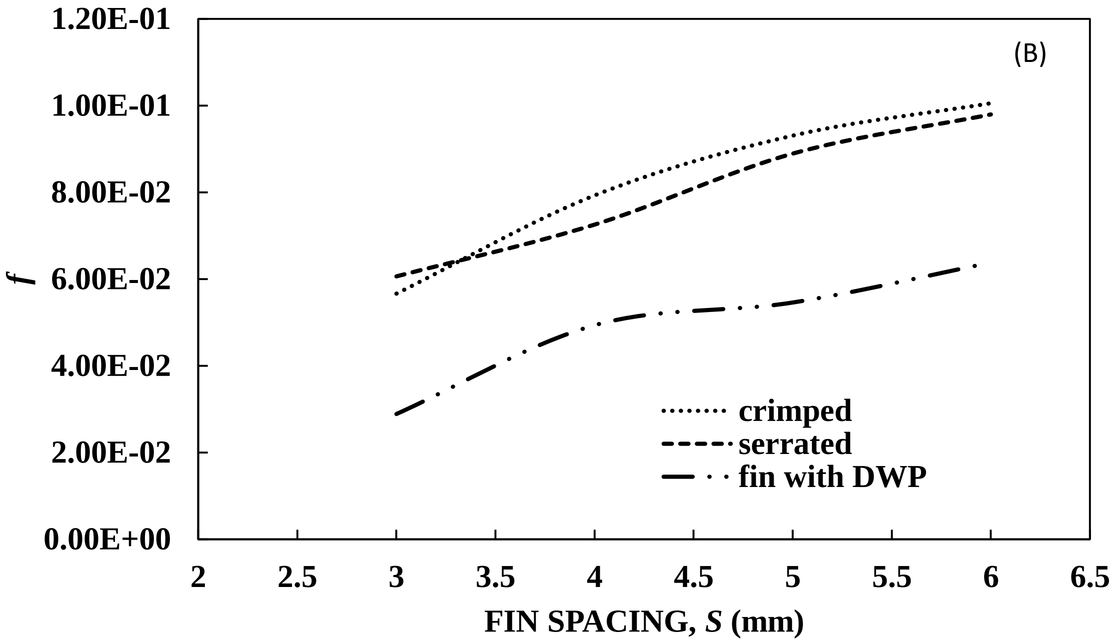

Fig. 6.11. Comparison of fins at varying fin spacing for Re_h = 3000, (A) Colburn factor (*j*), (B) friction factor (*f*).

can be understood by 6.6, as fin spacing increases, there is a decrease in pressure drop but there is a decrease in the mass flux (G_c) also. The combination of these two parameters results in an increase in the friction factor.

We have discussed about the thermal-hydraulic parameters and their variation with the geometrical parameters. To understand the flow physics associated with serrated fin, crimped fin and fin with DWP, detailed flow patterns have been studied and presented in Figs. 6.12 to 6.15. Fig. 6.12 shows the flow patterns for the serrated fin. In Fig. 6.12A, we have shown the formation of horseshoe vortices for the serrated fins and its comparison with the horseshoe vortices for the plain circular fin. At the fin surface, the flow velocity is zero due to no slip condition and as we move away from the fin surface, the flow velocity increases. This results in a pressure gradient along the tube surface [Fig. 6.12A (3)], which forces the fluid to move from the centerline of the tube towards the fin-tube junction [as discussed by Satapathy et al. (2011) and Okamoto and Sunabashiri. (1992)]. This flow then forms the horseshoe vortices and moves along the tube surface towards the rear part of the tube as can be seen in Fig. 6.12A (1) and 6.12A (2). If we compare the horseshoe vortices generated by plain circular fin [Fig. 6.12A (1)] and by serrated fin [Fig. 6.12A (2)] then we can observe that for the plain circular fin the horseshoe vortices form near the fin tube junction and moves to the rear side and mixes with the mean flow. The same phenomenon happens for the serrated fin but the difference is that the mean flow coming from the serrated fins is highly turbulent as it comes through the segments of the fin. This enhances mixing in the mean flow and as it merges with the horseshoe vortices then it further increases the heat transfer. The role of the segments of the serrated fin in enhancing the mixing in the mean flow can be understood by Fig. 6.12B. In which, we have given velocity vectors in three planes, the first plane is in the front side, plane 2 is in the middle part and third is on the rear part. We can observe that flow nicely penetrates the segments of the fin in plane 1 (front side), and this promotes turbulence and mixing in the mean flow which latter goes on and mixes with the horseshoe vortices. But as we move to the rear side, the penetration of the flow weakens as can be seen in plane 2 and 3. Therefore, we can conclude that most of the enhancement in the heat transfer is by the segments in the front part of the serrated fin. This can also be observed by the turbulent kinetic energy distribution in Fig. 6.12C, which shows a high value of turbulent kinetic energy between the segment gaps indicating highly turbulent flow.

Similarly flow patterns for crimped fin are shown in Fig. 6.13. The horseshoe vortices formation is like the case of serrated fin (Fig. 6.13A), however, the horseshoe vortices after forming at the fin tube junction travels through the wavy region of the crimped fin and latter mixes with the turbulent and wavy mean flow coming from the finned part. Also, if we observe the pressure gradient and formation of horseshoe vortices between the fin surfaces in Fig. 6.13A (2), then we can observe that pressure gradient is non-symmetric between the fin surfaces due to non-uniform shape of the fin. This results in most of the flow diverting to the upper fin tube junction as compared to the lower fin tube junction and which can affect the formation of the horseshoe vortices. Fig. 6.13B presents the detailed flow pattern around the crimped fin. We can observe the velocity vectors at three planes (Plane 1 is closest to the tube and plane 3 is farthest) on the fin surface. In plane 1, the amplitude of the crest and trough is largest, and we observe that flow penetrates in the crest and trough to some extent and local circulations are observed in the flow. As we move away from the tube to plane 2 and 3, we observe that flow becomes weaker in the crest and trough of the fins but local circulations are still present in the flow. The strong flow near the tube which penetrates deeper into the crest (plane 1) might be due to the horseshoe vortices formed at the tube surface which accelerate the mean flow in the crests of the fin. The local circulation in crests interacts with the fin surface

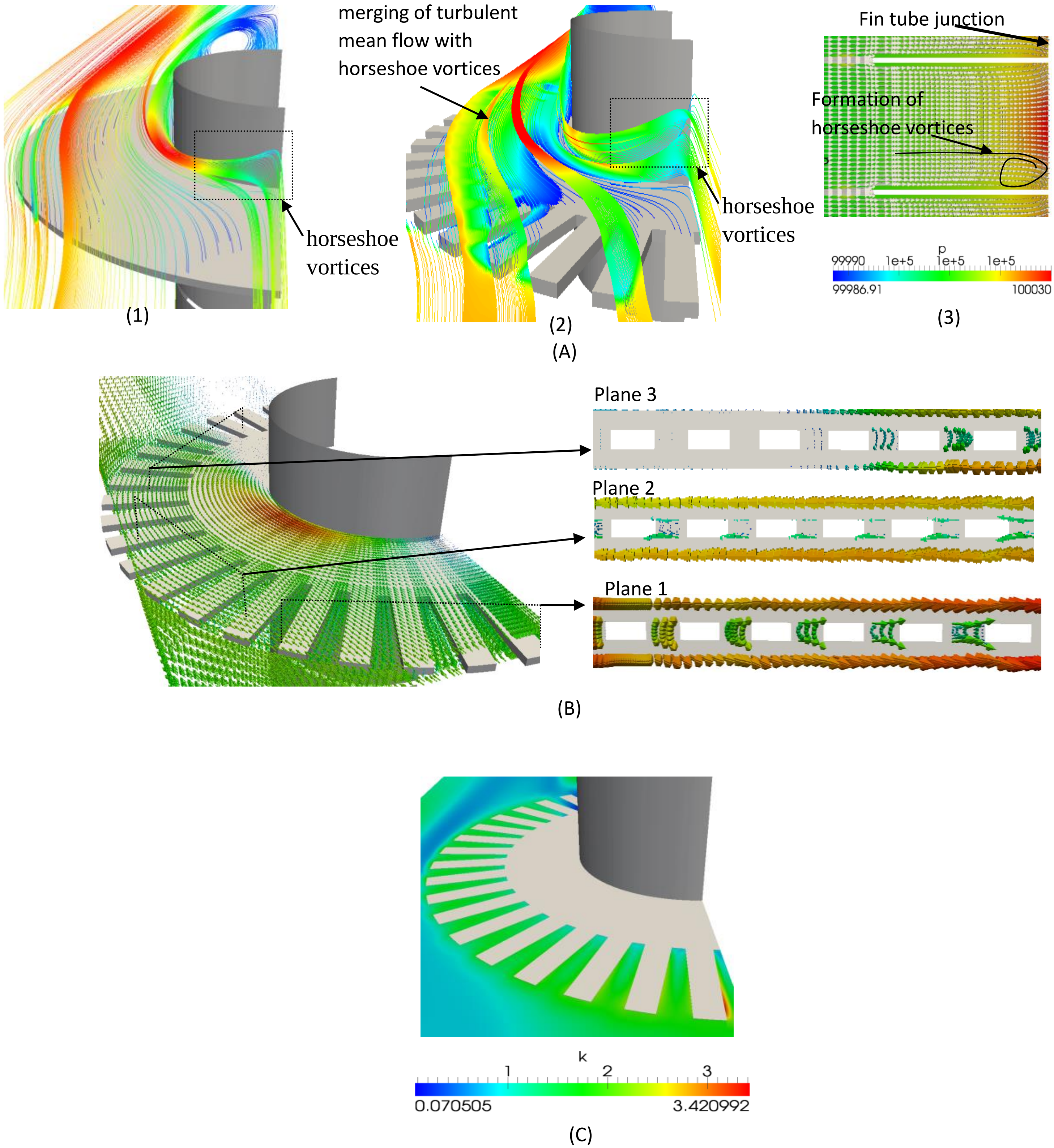

Fig. 6.12. Flow patterns for serrated fin, (A) (1) horseshoe vortices for plain circular fin, (2) horseshoe vortices for serrated fin, (3) formation of horseshoe vortices at fin tube junction, (B) velocity vectors around serrated fin (C) turbulent kinetic energy distribution around serrated fin.

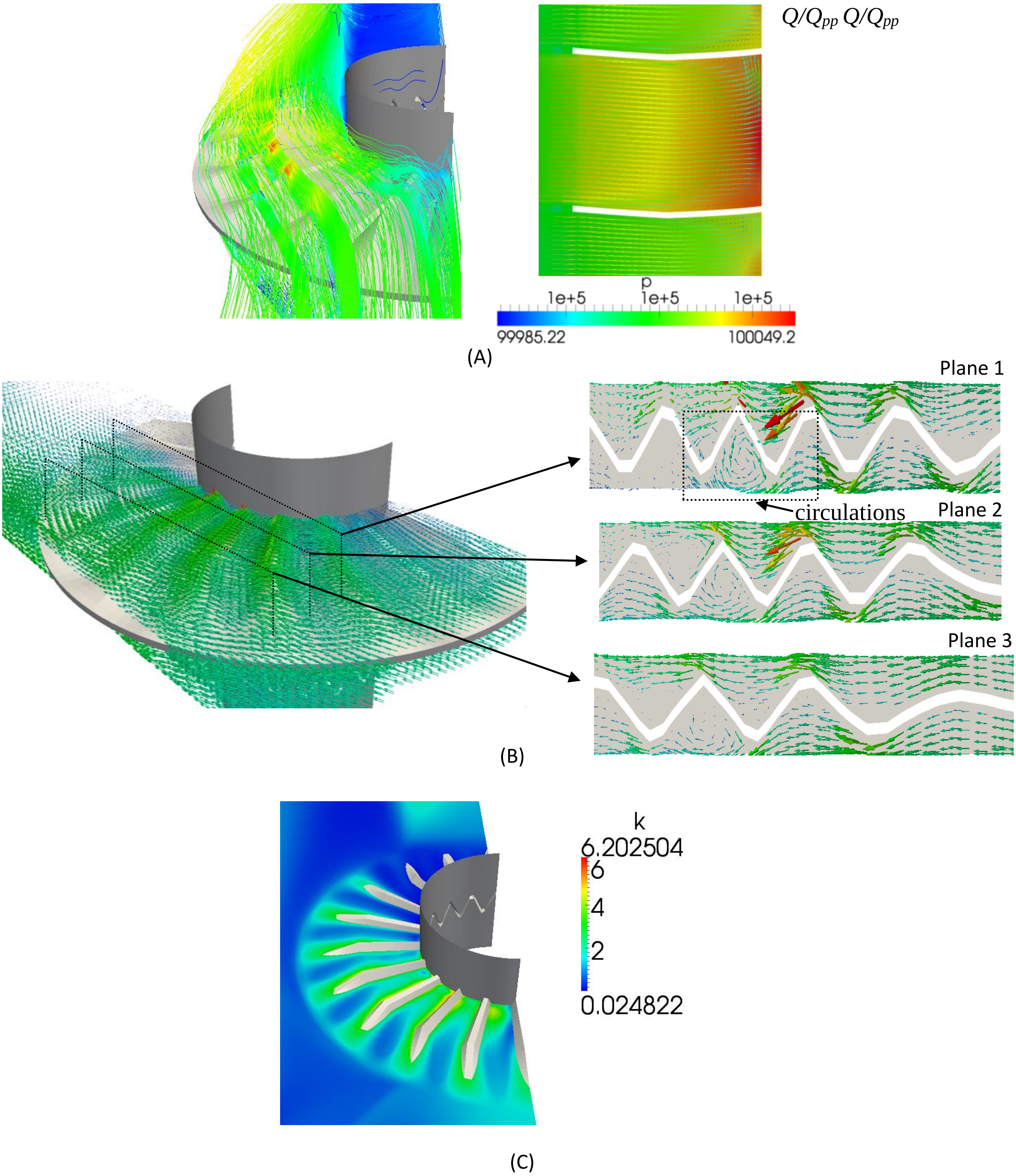

Fig. 6.13. Flow patterns for crimped fin, (A) (1) horseshoe vortices for crimped fin, (2) formation of horseshoe vortices at fin tube junction, (B) velocity vectors around crimped fin (C) turbulent kinetic energy distribution around crimped fin.

and comes back to join the mean flow resulting in higher heat transfer. Similar to the Fig. 6.12C for the serrated fin, we observe high turbulent kinetic energy distribution near the fin crests in Fig. 6.13C for the crimped fins. This indicates enhancement in the turbulent intensity in the mean flow which along with the horseshoe vortices enhances heat transfer as compared to the plain circular case.

Fig. 6.14 presents the flow patterns for the fin with DWP. Fig. 6.14A shows the classical horseshoe vortices forming at the fin tube junction and travelling to the rear side of the tube, however, as compared to the plain fin, there are delta winglets present near the wake region of the tube. It is well known that delta winglets generate longitudinal and transverse vortices in the mean flow, which have been observed by many previous researchers (discussed in Chapter 2). The primary vortices are known to form on the leading edge of the fin and secondary vortices form are on the trailing edge mixed with the flow coming from the punched part of the winglet. For the present case, the vortices generated by the DWPs are shown in Fig. 6.14A. We have analyzed these vortices for both the rows of the DWPs. We can observe in Fig. 6.14A that, for the first row of the winglet, the primary vortices are formed on the upper edge of the winglet and secondary vortices are also observed and are mainly formed by the flow coming from the punched part of the winglet mixing with the mean flow. For the second row, it can be observed that the strength of both the vortices increases but the secondary vortices seems to be stronger than the primary. The strengthening of the vortices for the second row DWP is due to the merging of the vortices from the first row DWP with the horseshoe vortices of the second row tube and primary and secondary vortices of the second row DWPs. This has also been explained by Chen et al. (1998b). Fig. 6.14B shows the distribution of turbulent kinetic energy along the flow length passing through the DWPs. We can observe a high turbulent kinetic energy distribution near the edges of the winglet, which indicates the presence of the vortices. Fig. 6.14C shows the formation of the primary vortices on the winglet (plane 1) and how it

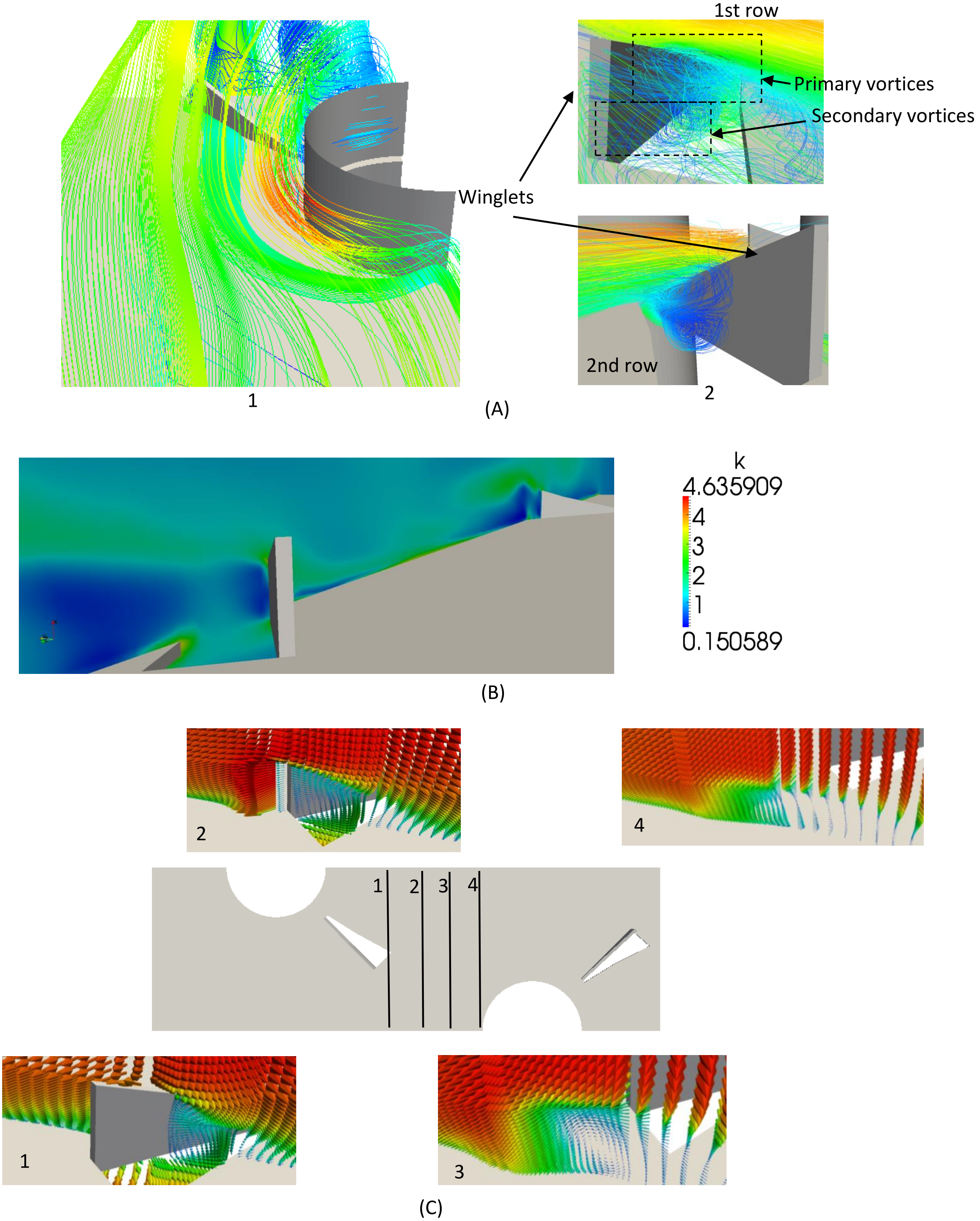

Fig. 6.14. Flow patterns for fin with DWP, (A) (1) horseshoe vortices, (2)primary and secondary vortices formation, (B) turbulent kinetic energy distribution along the air flow path, (C) formation and merging of primary vortices with the mean flow.

traverses along the flow length (though planes 2 to 3) and eventually mixes with the mean flow near plane 4. Further to observe how serrated fins and crimped fins improves heat transfer performance as compared to the plain circular fin, we have presented the temperature contours near fin surface in Fig. 6.15. We can observe that there is a continuous development of thermal boundary layer on the plain circular fin (Fig. 6.15A), whereas for the serrated fin the thermal boundary layer breaks for every segment of the fin and hence enhances heat transfer. Similarly, for the crimped fin, the thermal boundary layer formation is obstructed by the crests and troughs present on the fin surface. This leads to better heat transfer and mixing in the mean flow as can be seen by the temperature distribution around fin surface, which shows a higher heat transfer to the fluid from the fin surface.

If we compare the present results with the literature, then we can observe that, for plain circular fins, Pongsoi et al. (2012) did not observe any significant effect of fin spacing on *j* and argued that at high *Re*, the mixing is good and effect of fin spacing becomes negligible. Also, they observed that the friction factor increased slightly with fin spacing. For plain plate fin, Wang and Chang (1996) did not observe any effect of fin pitch on Colburn and friction factor.

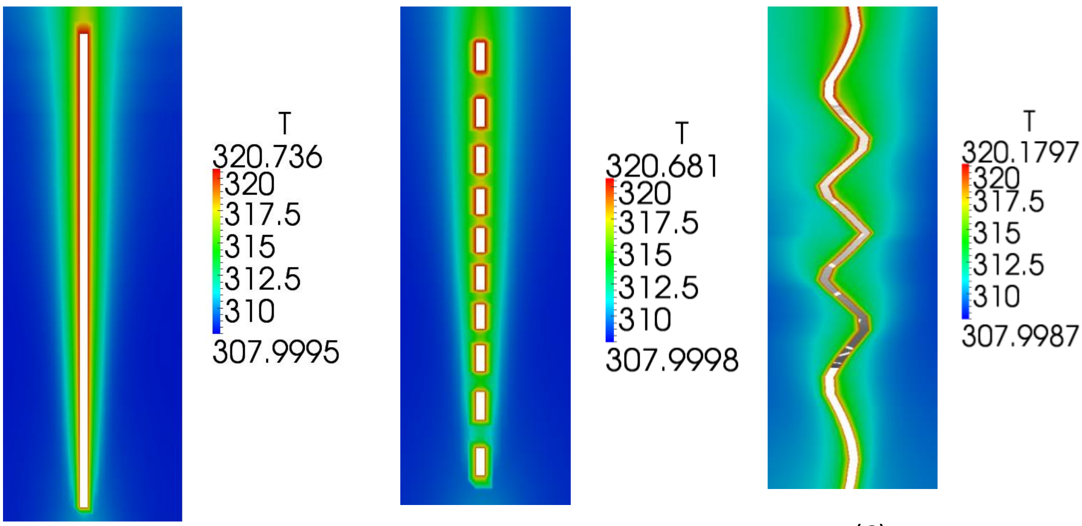

(A) (B) (C)

Fig. 6.15. Temperature contours showing thermal boundary layer development (A) plane circular fin, (2) serrated fin and (3) crimped fin.

Wang and Chi (2000) observed that Colburn factor decreases with an increase in fin spacing due to larger vortex formation behind the tubes. However, Choi et al. (2010) observed that *j* increases with the fin spacing due to delay in boundary layer interaction at higher fin spacing. Present results agree with the results of Wang and Chi. (2000) for Colburn factor and with Pongsoi et al. (2012) for the friction factor. The insignificant effect of fin spacing on Colburn factor by Pongsoi et al. (2012) can be attributed to the smaller range of fin spacing ($2.5 \leq S \leq 4.2$ mm) considered in their study. The discrepancy in the results of Wang and Chang (1996) and Wang and Chi (2000) can be attributed to accuracy of the experimental results and use of proper ε-NTU relation for the calculation as stated by Wang et al. (2000). For Choi et al. (2010), it is difficult to understand how the Colburn factor increased with an increase in the fin spacing.

6.3.5. Fin efficiency

The temperature distribution on a fin surface is non-uniform as have been presented by Chen et al. (2005, 2007) and Chen and Lai (2012). The fin efficiency is defined as the ratio of the real heat transfer to the ideal heat transfer (fin at tube surface temperature) and can be expressed as [Lin and Jang (2002)]:

$$\eta = \frac{\int (T_a - T_f) dA}{\int (T_a - T_b) dA} \quad \ldots (19)$$

Here T_a is the average air temperature calculated separately for each row fin. The temperature of the air increases as it passes through the tube rows, therefore, the average air temperature is calculated in the vicinity of a particular row number to obtain the fin efficiency for that tube row. T_b is the tube base temperature, which also varies with geometrical parameters due to consideration of finite wall thickness and dA indicates the heat transfer area under consideration. T_f is the average fin temperature.

In Fig. 6.16A, the fin efficiency is shown for varying Reynolds number for all the fins at a fin spacing of $S = 5$ mm, we can observe that as Re_h increases, the fin efficiency decreases in the range of 5-14%. Physically it means that at higher Reynolds number or inlet velocities, the ability of air flow to extract heat from the fin surface decreases. This is analogues to the results obtained by Tao et al. (2007, 2011). We can observe that the fin efficiency of all the circular fins is higher by 20-40% as compared to the plate fins. Of the circular fins, serrated fin provides highest fin efficiency and it can be due to its segmented shape which lowers the heat

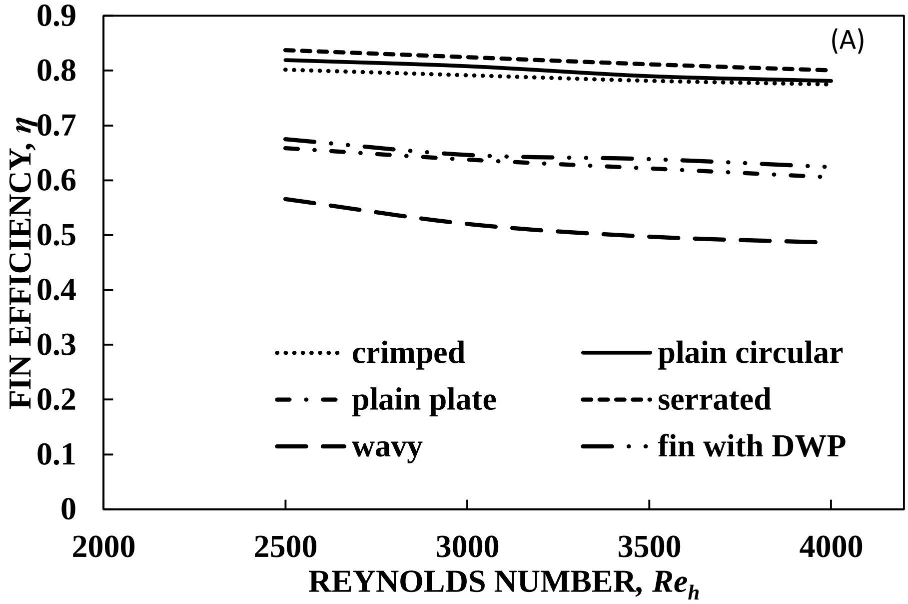

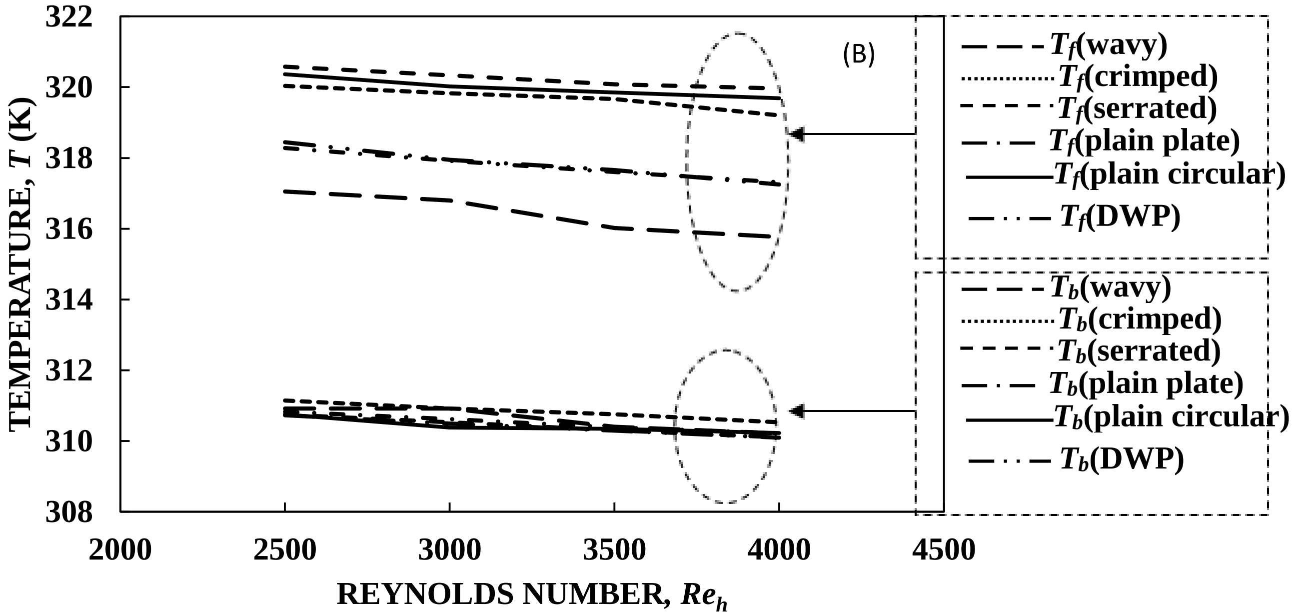

Fig. 6.16. Comparison of fins at varying Reynolds number for S = 5 mm, (A) fin efficiency, (B) temperature plots on the fin surface and in the bulk.

transfer area and improves conduction through the fin. For plate fins, the efficiency of fin with DWP and plain plate fin is equally good (only 3% difference) and is higher by 15-20% than the wavy fin. The worst performance of wavy fin in term of fin efficiency is due to its longer flow path and larger heat transfer area which increases the conduction length and hence decreases fin efficiency. The higher fin efficiency for the circular fins as compared to the plate fins is because of the smaller heat transfer area and discreet shape of the circular fins, which improves the uniformity in the temperature distribution over the fin surface. Fig. 6.16B shows the temperature values for the fin surface and the air flow. We can clearly observe that while

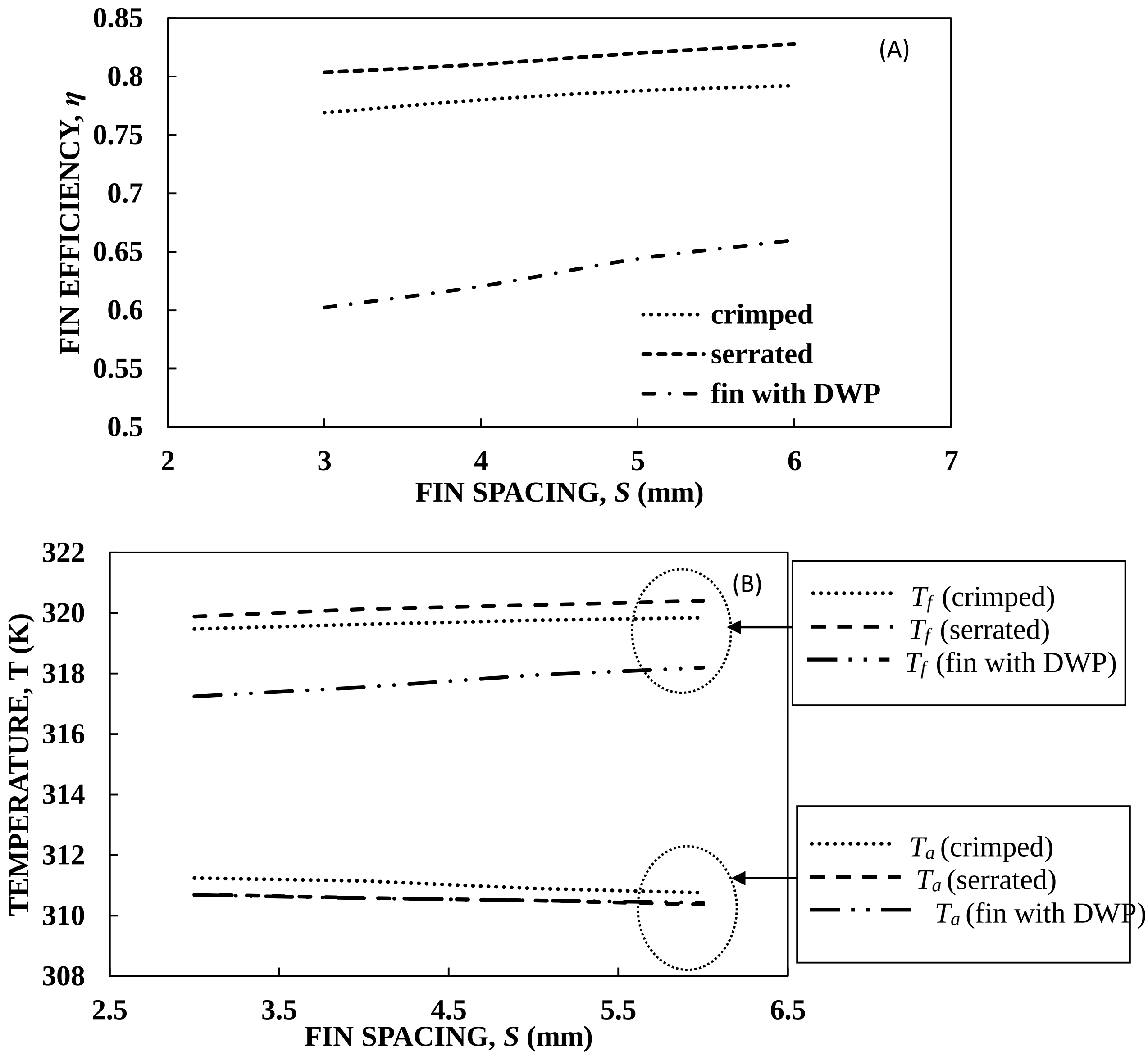

Fig. 6.17. Comparison of fins at varying fin spacing for Re_h = 3000, (A) fin efficiency, (B) temperature plots on the fin surface and bulk.

the fluid temperature is very close for all the fin patterns, the fin temperature varies in a wide range for different fin patterns. This indicates that the variation in the fin efficiency for the fin patterns is mainly due to the temperature distribution on the fin surface. Figs. 6.17A and 6.17B show the fin efficiency and temperature distribution for the serrated fin, crimped fin and fin with DWP for varying fin spacing. We can observe that as fin spacing increases, the fin efficiency decreases. The reason is the decreased mass flux in the domain for a constant Re_h at larger fin spacing, which degrades the heat transfer as we have seen for varying Re_h case.

6.3.6. Goodness factors

The performance evaluation criterion of the air cooled heat exchanger is determined by the volume goodness factor. The method to calculate the volume goodness factor was developed by Kays and London (1950), which compares the heat transfer per unit heat exchanger volume and per unit temperature difference (Z) with the power provided per unit heat exchanger volume (E).

$$Z = \frac{\eta h A}{L A_{fr}} \qquad \text{… (6.7)}$$

$$E = \Delta P \left(\frac{\dot{m}}{\rho_m}\right) \frac{1}{L A_{fr}} \qquad \text{… (6.8)}$$

A high value of Z with respect to E indicates a more compact air cooled heat exchanger and the following quantities are kept constant: (1) heat transfer rate, (2) pressure drop, (3) temperature difference between the surface and the fluid, and (4) fluid flow rate. We can observe in Fig. 6.18A that, all the plate fins offer a higher Z as compared to the circular fins (serrated and plain circular fins), whereas the crimped fin provides highest value of Z among all the fin patterns. However, the input power required (E) is also in the higher range for the plate fins. This indicates that for a fixed volume of the air-cooled heat exchanger, highest heat transfer rate can be obtained by using crimped fins and all the plate fins. However, only crimped

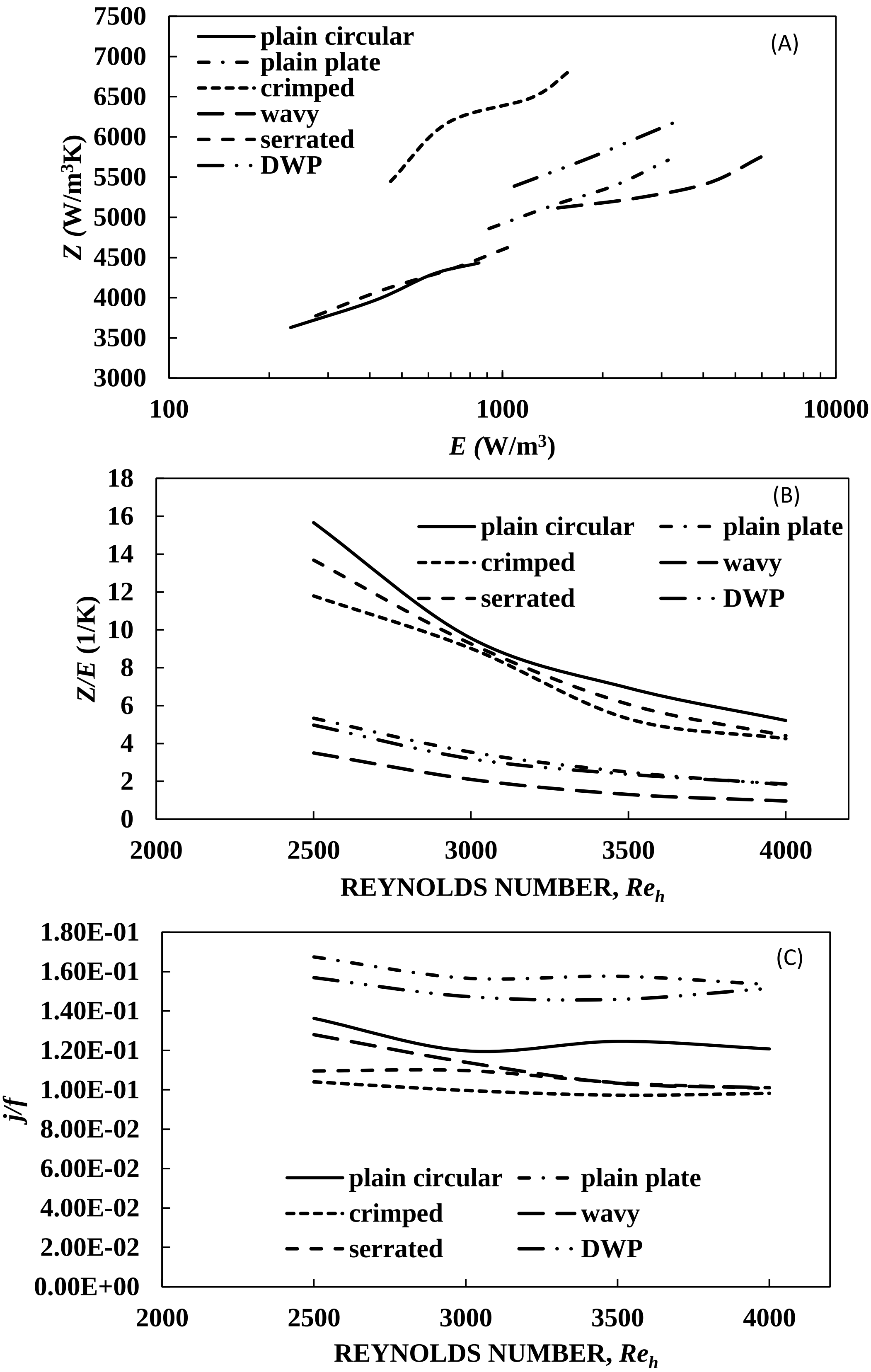

Fig. 6.18. Comparison of fins at varying Reynolds number for S = 5 mm, (A) volume goodness factor, (B) Z/E plot and (C) area goodness factor.

fin seems to perform better in terms of input power requirement. If we analyze the heat transfer per unit power input (*Z/E*) to the air-cooled condenser. We can observe in Fig. 6.18B that the plain circular fin performs best among the circular fins with highest *Z/E* (5-16% and 20-30% higher than the serrated and crimped fin resp.). For the plate fins, the plain plate fin performs better with 20-30% and 30-50% higher *Z/E* ratio as compared to the fin with DWP and wavy fin respectively. Overall, all the circular fins perform better than the plate fin with 130-170% higher *Z/E* ratio.

Table. 6.9 shows the value of *Z* and *E* for varying fin spacing for serrated fin, crimped fin and fin with DWP. It can be observed that both *Z* and *E* decreases as fin spacing is increased at a constant Re_h indicating less compact heat exchanger. However, the value of *Z/E* increases, which means we have to provide lesser power at a higher fin spacing to remove the same power.

Table 6.9. Z and E values at varying fin spacing

Fin spacing, *S* (mm)	**Serrated fin**			**Crimped fin**			**Fin with DWP**		
	Z (W/m^3K)	*E* (W/m^3)	*Z/E* (1/K)	*Z* (W/m^3K)	*E* (W/m^3)	*Z/E* (1/K)	*Z* (W/m^3K)	*E* (W/m^3)	*Z/E* (1/K)
3	7387.12	1312.53	5.62	8866.02	1801.62	4.92	9648.71	5689.68	1.70
4	5609.24	786.63	7.13	7305.38	1336.07	5.46	7054.70	3394.27	2.07
5	4703.16	486.87	9.66	5914.35	775.81	7.62	5709.08	1800.16	3.17
6	4049.48	329.26	12.30	4792.48	510.50	9.38	4888.74	1051.58	4.65

When the frontal area of the heat exchanger is the parameter of interest, then the area goodness factor is compared for the heat exchangers. The area goodness factor is used to optimize the heat exchanger frontal area. A maximum value of the area goodness factor indicates a minimum frontal area of the heat exchanger.

The *j*/*f* factor results into an expression given as: $\frac{1}{A_{fr}^2}\left(\frac{Pr^{2/3}NTU\dot{m}^2}{\rho^2 G_c \Delta P}\right)$ … (6.9)

The quantities in the bracket are dependent on the operating conditions. Therefore, for a fixed operating condition, a higher *j*/*f* indicates a lower frontal area (A_{fr}). This factor is important in determining the frontal size of the heat exchangers. Fig. 6.18C shows the area goodness factors for all the fins. We can observe that for a fixed Re_h, the plain plate fin and fin with DWP offers lower frontal area requirements for a fixed operating condition and for same heat removal capacity.

6.4. Conclusions

Various fin patterns (circular and plate fins) have been studied in this chapter and results have been presented in terms of thermal-hydraulic performance and compactness of the air cooled heat exchanger. It has been observed that among the circular fins, the crimped fin provides the highest heat transfer coefficient and among the plate fins, the wavy fin produces the highest heat transfer coefficient. The pressure drop for all the plate fins is higher as compared to the circular fins due to their longer flow path and higher skin friction. In terms of heat transfer per unit pumping power, the circular fins give 140-170% higher Q/Q_{pp} as compared to the plate fins for a fixed Reynolds number. Q/Q_{pp} decreased as the Reynolds number increased for all the fin patterns. It was observed that the friction factor for crimped fin and serrated fin was higher as compared to the plate fins, indicating high disturbance and obstruction in the flow. Local Nusselt number around the periphery of the tubes in the vicinity of the fins revealed distinct effect of each fin on the wake region of the tube. Three fin patterns (crimped, serrated, fin with DWP) were studied in much greater detail. For these three fins, it was observed that the heat transfer coefficient decreases with an increase in the fin spacing due to increase in bypass flow rate through the heat exchanger. The heat transfer per unit pumping power showed an increase with the fin spacing. Detailed flow patterns showed turbulence and mixing enhancement by these fins in flow field, which leads to higher heat transfer rate. The role of horseshoe vortices along with the vortices generated by various fin patterns in enhancing the heat transfer has been studied in details. The fin efficiency of the circular fins has been observed in the range of 77-83% and for the plate fins; it has been found to be 55-66% for a range of $2500 \leq Re_h \leq 4000$. From performance evaluation criterions, it has been observed that all the plate fins along with the crimped fin can provide a much compact heat exchanger design as compared to the plain circular and serrated fin. However, the input power requirement has also been in the higher range for the plate fins. From all the results presented, it can be concluded that, capital and operating cost of the air cooled heat exchanger can be minimized by using circular fins, however, for more compact configuration (to reduce the cost associated with space), the plate fins can be more useful.

Chapter 7
Thermal-hydraulic optimization of air cooled condenser

7.1. Introduction

Conventional power plants use river water or sea water as the ultimate heat sink. The steam coming from the turbine is condensed using the water coming from the cooling towers and then the water is recirculated back to the cooling towers (for the case of river as ultimate heat sink). However, for this type of cooling, approximately 2.11 litres of water is needed per kWh of energy produced. Due to heavy demand of water in cooling towers, substantial amount of research work has been published on the air cooled condensers (or heat exchangers) in the past 50 years. The performance of the air-cooled heat exchangers depends upon many geometrical parameters, like tube type, fin type, fin spacing, number of tube rows, tube pitch, etc. One of the major problems with the air cooling technology is the low heat transfer coefficient provided by air, which results in a large heat transfer area of the heat condenser, and therefore, a high associated capital cost as compared to the water cooled condensers. The total cost associated with the A-type air-cooled condensers includes the capital cost, operating cost, and the cost of the space used, and these three parameters must be optimized to obtain an economical air cooled condenser. Continuous efforts have been ongoing to improve the performance and the efficiency of the air-cooled heat exchangers, still, there is a scope to make the air cooling technology more economical and efficient.

The experimental and the numerical studies on the thermal-hydraulic performance of air cooled heat exchangers have been explained in chapter 2 (section 2.4). Some authors have used optimization methods to optimize the design of air cooled heat exchangers. For instance, Doodman et al. (2009) developed an optimization method for the design of air cooled heat exchangers based on stochastic approach. It was observed that the presented method for optimization converged to optimum design with better accuracy as compared to the conventional genetic algorithms. Salimpour and Bahrami (2011) performed analysis to optimize the design of air cooled heat exchanger using second law of thermodynamics. The results were analysed in terms of entropy generation in the system due to heat transfer and pressure loss. The tube side and air side Reynolds number was found to affect the entropy generation in the system. Pieve and Salvadori (2011) proposed a mathematical model based on LMTD (logarithmic mean temperature difference) method to analyse the performance of air cooled steam condenser under various environmental conditions. It was concluded that by increasing the number of cooling units, the global power consumption in the plant decreases. Kashani et al. (2013) optimized the design of air cooled heat exchanger using ε-NTU method. The objective of the study was to optimize the annual cost and temperature approach of the heat exchanger. The parameters considered were tube length, number of tube rows, number of tubes per row, number of tube passes, tube pitch ratio, fin height, fin density, fin thickness, and air blowing velocity. Manassaldi et al. (2014) presented optimization mathematical model for the air cooled heat exchangers. Three optimization criterions were considered in the study e.g., Total annual cost, heat transfer area and the operating cost. For optimization, type of flow regime, type of finned tube, number of tube rows, and number of tubes per row, number of passes, fin density and fin thickness were considered. Hatami et al. (2015) carried out numerical investigation and optimized the obtained results using artificial neural network and genetic algorithm for a finned-tube heat exchanger in diesel exhaust recovery system. 30 samples of heat exchangers were modelled with varying fin height, thickness and numbers. Two cases of heat exchangers (optimized and non-optimized) were compared and it was found that the optimized design increased the exergy recovery and provides lower pressure drop. Wu et al. (2015) performed numerical simulations to study the thermal performance of the internally finned-tubes and observed that the critical Reynolds number for the internally finned-tubes is lower than the critical *Re* for bare tubes. For the internally finned-tubes, a secondary vortex system was found to emerge, which helped in enhancing the turbulent kinetic energy in the flow field.

From the literature discussed in chapter 2 (section 2.4) and in previous paragraphs, it may be noted that, most of the studies focus on the thermal-hydraulic performance of the heat exchangers. However, only few studies have focused on the optimization of the heat exchanger design. The capital cost of the condenser can be optimized by maximizing the heat transfer coefficient, and hence minimizing the heat transfer area. However, the associated pumping power must be minimized for obtaining a minimum operating cost. Various studies have discussed the optimization of these factors, however, the practical implication of the results have not been discussed in these studies. The other costs include the cost associated with the space required, for that one needs to design a very compact heat exchanger. For this purpose, the area goodness factor and the volume goodness factor need to be optimized, however, only few studies have focused on the optimization of these factors.

Therefore, in the present chapter, 3D numerical simulations have been performed using RANS based k-ε turbulence model to analyze the thermal-hydraulic performance of the annular-finned tubes. The importance of the 3D numerical simulations to understand the heat transfer and associated physical phenomenon has been presented in Chapters 4 and 5. On the basis of these simulations, an attempt has been made to suggest an optimum design based on Taguchi method [Taguchi (1986)].

7.2 Numerical Solution

7.2.1 Geometry

The system under consideration comprises of an air cooled condenser with annular finned-tubes (Fig. 7.1). As a first step, a comparison was performed between the bare circular and elliptical tubes with varying tube dimensions and the details are given in Table 7.3. Based on the results obtained in Section 3.2, a particular dimension (elliptical tube with 30 × 10 mm dimensions) of the finned-tube geometry was chosen for further studies. The computational domain is shown in Fig. 7.2. The temperature of the inner surface of the tube is kept at 323 K (TPP steam temperature). The grid generation and meshing were executed using Gmsh 2.3 [Geuzaine and Remacle (2009)].

7.2.2 Governing equations and model assumptions

The problem under consideration is steady 3D forced convection of air around annular-finned tubes. The assumptions in the computational model are the following:

1. Flow is compressible.
2. The buoyancy is neglected in the domain and flow is assumed to be solely under forced convection conditions.

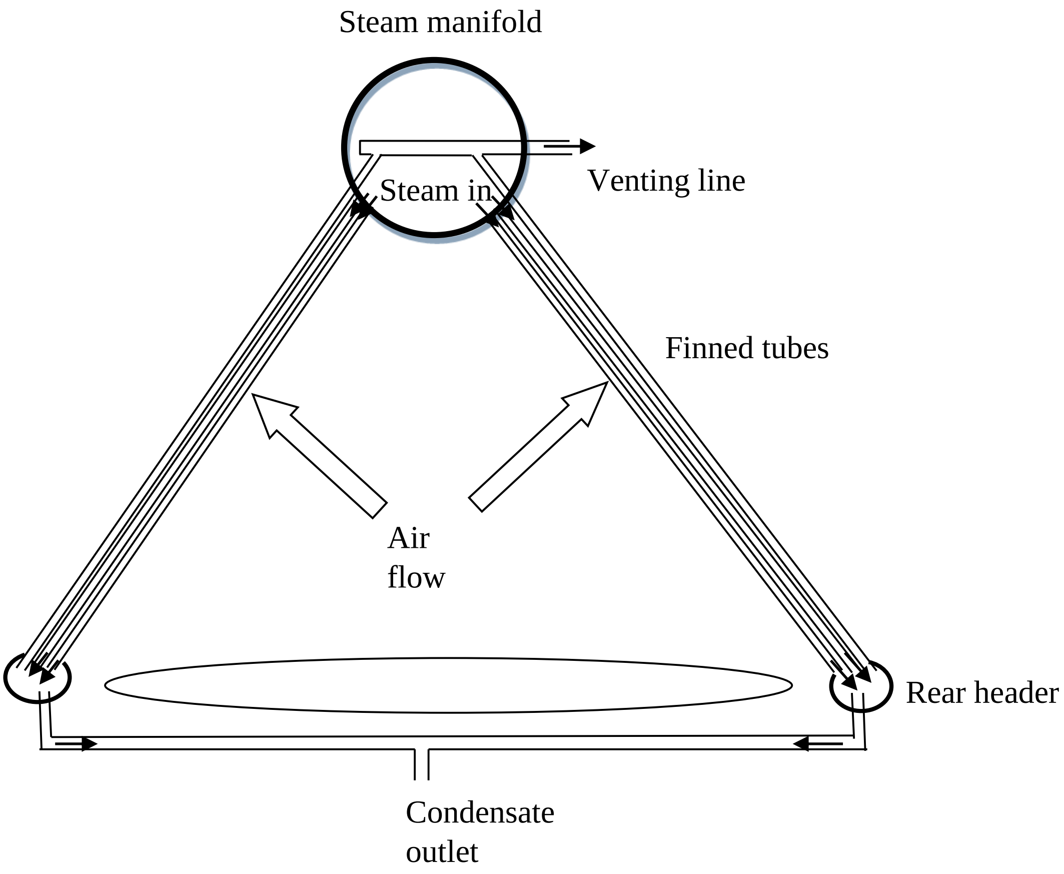

Fig. 7.1. Schematic of the Air Cooled Condenser and computational domain (dotted box)

Table 7.1. Geometrical details of the tubes

Circular tubes		Elliptical tubes	
Diameter (mm)	Thickness (mm)	Diameter (mm)	Thickness (mm)
7	1.5	30 × 10	1.5
14	1.5	30 × 15	1.5
24	1.5	30 × 20	1.5

For the finned-tube case, under natural convection conditions for a temperature difference of 15 K between ambient and the tube surface, the value of the heat transfer coefficient lies in the range of 6-8 W/m^{2}K (Chapter 4). Whereas, *h* varies in the range of 50-100 W/m^{2}K for forced convection conditions (for present work). Also, the Richardson number (*Ri*) is in the range of 10^{-04}. Therefore, simplification of the numerical problem by neglecting buoyancy is fairly justified.

The value of the *Re* is 3500-5500, therefore, the flow is considered to be in the turbulent region. At this value of *Re*, the air flow can be treated as incompressible. However, in Openfoam 2.2., the conjugate solvers are present for compressible flows only. The consideration of air flow as compressible is also justified, as the numerical results agree well with the published experimental results (see Section 7.3.2). Therefore, the flow is treated to be compressible. The governing equations for the 3D steady forced convection are continuity, momentum, turbulence kinetic energy (k), turbulence energy dissipation rate (ε) equations, and energy equation have been given in Chapter 2 (Section 3.2.2), which are given as:

The heat transfer rate is calculated using the following equations:

$$Q = \dot{m} c_p \Delta T \qquad \dots (7.1)$$

$\dot{m}$ is the mass flow rate through the finned tube heat exchanger and is calculated at the minimum flow area, A_c, of the finned heat exchanger and is given by,

$$\dot{m} = \rho A_c u_{max} \qquad \ldots (7.2)$$

Where u_{max} is the maximum velocity occurring at the minimum flow area, A_c.

After calculating Q, the heat transfer coefficient is obtained by using the following equation:

$$h = \frac{Q}{A \Delta T_{LMTD}} \qquad \ldots (7.3)$$

Where ΔT_{LMTD} is the logarithmic is mean temperature difference and is given by,

$$\Delta T_{LMTD} = \frac{(T_{in} - T_{tube}) - (T_{out} - T_{tube})}{ln\left[\frac{(T_{in} - T_{tube})}{(T_{out} - T_{tube})}\right]} \qquad \ldots (7.4)$$

7.2.3. Boundary condition

The inner tube wall is given a constant temperature boundary condition. The problem is solved as conjugated heat transfer, and the conduction through the tube wall and the fin is considered. The no slip boundary condition is used at the tube and fin surface. At the inlet a fixed velocity (4.76-6.32 m/s) and at the outlet the Neumann boundary condition is used for the velocity and the pressure is set to atmospheric. Additional details pertaining to the boundary conditions are given in Table 7.4.

Table 7.2. Boundary conditions

Physical Surface	Temperature	Velocity	Pressure
Inlet	Fixed Value (323 K)	Fixed Velocity (4.32 m/s-6.32 m/s)	$\frac{\partial p}{\partial x} = 0$
Outlet	$\frac{\partial T}{\partial x} = 0$	$\frac{\partial u}{\partial x} = 0$	Atmospheric
Tube (inner wall)	Fixed Value (323 K)	No slip	Atmospheric
Symmetry	$\frac{\partial T}{\partial x} = 0$	$\frac{\partial u}{\partial x} = 0$	$\frac{\partial p}{\partial x} = 0$

7.2.4. Method of solution

In the present work, simulations were performed under steady conditions. All the computational work was carried out using the software OpenFOAM-2.2, which is based on finite volume approach. QUICK scheme was used to discretize the divergence terms, which is a third order accurate scheme and the diffusion terms are discretized using the central difference scheme, which is a second order accurate scheme. All the discretized equations were solved in

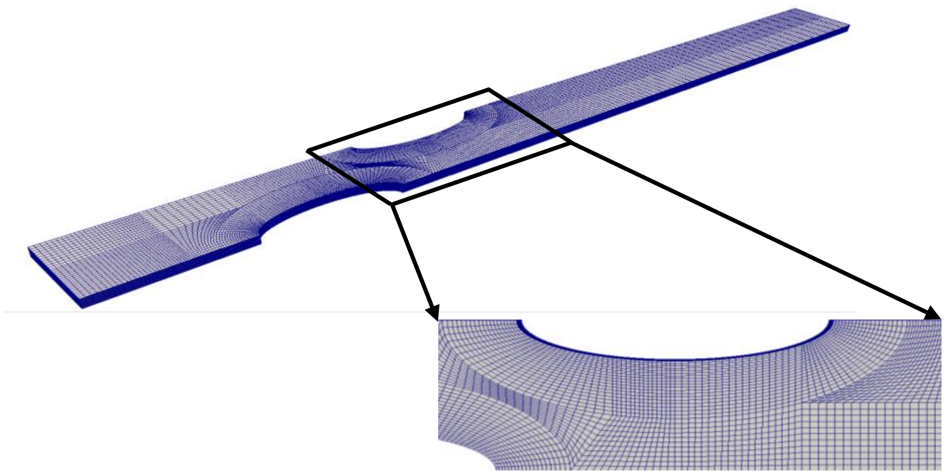

Fig. 7.2. Computational domain and grid generation

a segregated manner with the SIMPLE (Pressure Implicit with Splitting of Operators) algorithm. In SIMPLE algorithm, the equations are solved using initial guess values of flow variables, and then the values are corrected in each iteration. The iterative process continues

until the convergence criterion is satisfied. The convergence criterion was based on the scaled residuals of the velocity, when the residuals reached below 10^{-5}, the solution was considered to be fully converged.

7.2.5. Grid independence

A structured hexahedaral non-uniform mesh was generated using Gmsh 2.3. A fine mesh was generated around the tube and fins to capture the high velocity and temperature gradients (first node at Y^{+}>20). All the grid independence studies were performed for 3D simulations. A grid resolution of 150000, 300000, and 500000 was used to understand the grid senstivity for a 2 rows coil (S = 2, 5 and 10 mm). The difference in the heat transfer coefficient was within 2-3% for the three cases (Table 7.5). The grid independence study was also carried out for a 10 rows coil (S = 5 mm, h_f = 5 mm) with grid resolution of 300000, 500000, and 700000 for U_{fr} = 4.76 m/s and 6.32 m/s. The difference in the heat transfer coefficient was within 2-3% for U_{fr} = 4.76 m/s and 2-5% for U_{fr} = 6.32 m/s (higher being between cell number of 300000 and 500000). Finally a grid of 300000-500000 (higher grid number was used for the larger fin spacing and larger row number) cells was used for all the cases. The grid geometry has been schematically shown in Fig. 7.2.

7.3. **Results and discussions**

7.3.1 Effect of tube design

In the preliminary studies, bare elliptical and circular tube designs have been studied. The circular tube diameter was varied from 7 to 24 mm and the elliptical tube diameter was varied from 30 × 10 mm to 30 × 20 mm. The flow area for all the tube designs was kept equal for a fair comparison. The velocity vectors are presented in Fig. 7.4. It can be observed that the flow separation on the tube surface occurs later for the elliptical tubes. This results in a suppression of the wake region for the elliptical tubes. Further, for the round tubes, the wake

Table 7.37. Grid size independence results

N_r = 2				**N_r = 10**					
				U_{fr} = 4.76 m/s			***U_{fr} = 6.32 m/s***		
Fin spacing (mm)	Grid size= 150000 [h (W/m^{2}K)]	Grid size= 300000 [h (W/m^{2}K)]	Grid size= 500000 [h (W/m^{2}K)]	Grid size= 300000 [h (W/m^{2}K)]	Grid size= 500000 [h (W/m^{2}K)]	Grid size= 700000 [h (W/m^{2}K)]	Grid size= 300000 [h (W/m^{2}K)]	Grid size= 500000 [h (W/m^{2}K)]	Grid size= 700000 [h (W/m^{2}K)]
2	60.85	62.70	63.01						
5	77.98	80.01	79.45	65.01	66.86	65.91	90.41	95.75	96.87
10	86.32	88.45	88.01						

region is minimum for the smaller diameter tube, similarly, for the elliptical tubes, the wake region is minimum for the smaller ellipticity (*e*) of the tube. The heat transfer and pressure drop results are presented in Table 7.8. It can be observed from Table 7.8 that, for the circular tubes, the smaller diameter tube provides relatively higher heat transfer per unit pressure drop. Overall, the elliptical tubes provide 10-30% higher heat transfer coefficient and 20-80% lower pressure drop as compared to the circular tubes. The major difference is observed in the heat transfer

Table 7.4. Thermal-hydraulic performance of various tube designs

Circular tubes				**Elliptical tubes**			
D **(mm)**	***h*** **(W/m^2K)**	**ΔP (Pa)**	***Q/ (ΔP*V)***	***D*** **(mm)**	***h*** **(W/m^2K)**	**ΔP (Pa)**	***Q*/ (ΔP*V)**
7	138	16	44.66	30 × 10	155	13	178.05
14	129	34	35.61	30 × 15	152	24	85.91
24	121	58	24.61	30 × 20	149	36	54.28

per unit pumping power, which is 22-600% higher for the elliptical tubes as compared to the circular tubes. The elliptical tube with cross-section of 30 × 10 mm provides best performance among all the tube designs. Therefore, the tube design with 30 × 10 mm dimensions has been selected for carrying out further studies for the design of the air cooled condenser. The choice of finned-tubes against bare tubes for the design of an air cooled condenser is based on the fact that, the thermal-conductivity of air is very low. The convective heat transfer coefficient obtained fkl,mkl,mor air is usually in the range of 50-200 W/m^2K. Finned-tubes increases the heat transfer area of bare tubes by 60-90% (based on fin size and density), which results in a more compact condenser or heat exchanger. Also, some of the fins are known to produce 3D vortices (e.g., Fins with delta winglet, serrated fins, slit fins etc.,), which results in better surface renewal and hence an improved heat transfer coefficient. Therefore, for the design of an air cooled condenser or heat exchanger, the finned-tubes are chosen.

7.3.4 Effect of fin spacing and fin height

The effect of fin spacing has been studied for 2 rows of the tubes and at various fin heights (h_f = 5, 7 and 7 mm, *Z/E* is slightly lower than h_f =5 mm, however for h_f =10 mm, *Z/E* is very low as compared to the fin with h_f =5 mm and 7 mm.

In order to comprehend the practical implication of the results discussed, the calculations were carried out for 1 MW air cooled heat condenser. The results are shown in Figs. 7.8A, 7.8B and 7.8C. Fig. 7.8A shows the heat transfer area requirement for the air cooled heat exchanger for varying fin spacing for the three diameters of the fin. It can be observed that for a fixed heat removal capacity, the fin with h_f =5 mm requires 7-10% less heat transfer area than the fin with h_f =7 mm, and 16-30% less heat transfer area as compared to the fin with h_f =10 mm to remove 1 MW of heat. The required heat transfer area decreases with an increase in the fin spacing for all the fin diameters. This is due to the increase in the heat transfer coefficient with an increase in the fin spacing as discussed earlier in this section. Fig. 7.8B shows the pumping power requirement for varying fin spacing for h_f =5, 7 and 10 mm. For 1 MW, the fin with h_f =5 mm requires larger pumping power (0-10%) as compared to the fin with h_f =7 mm for all the range of fin spacing. The fin with h_f =10 mm requires the highest pumping power (0-20% larger as compared to h_f =7 mm) at lower fin spacing (S< 5 mm). However, at larger fin spacing, all the fins perform equally well. This can be related to the fact that, at larger fin spacing, the obstruction to the flow reduces and pressure drop becomes almost constant for all the fin diameters, hence the pumping power curve shows a similar behavior. Fig. 7.7C shows the space requirement (represents the frontal area) for the air cooled condenser for 1 MW of heat removal capacity. It can be observed that fin with h_f =10 mm requires more area as compared to the other fins. The difference is prominent at lower fin spacing with 7-30% more area requirement for h_f=10 mm as compared to the fin with h_f =5 mm. However, at larger fin spacing, all the

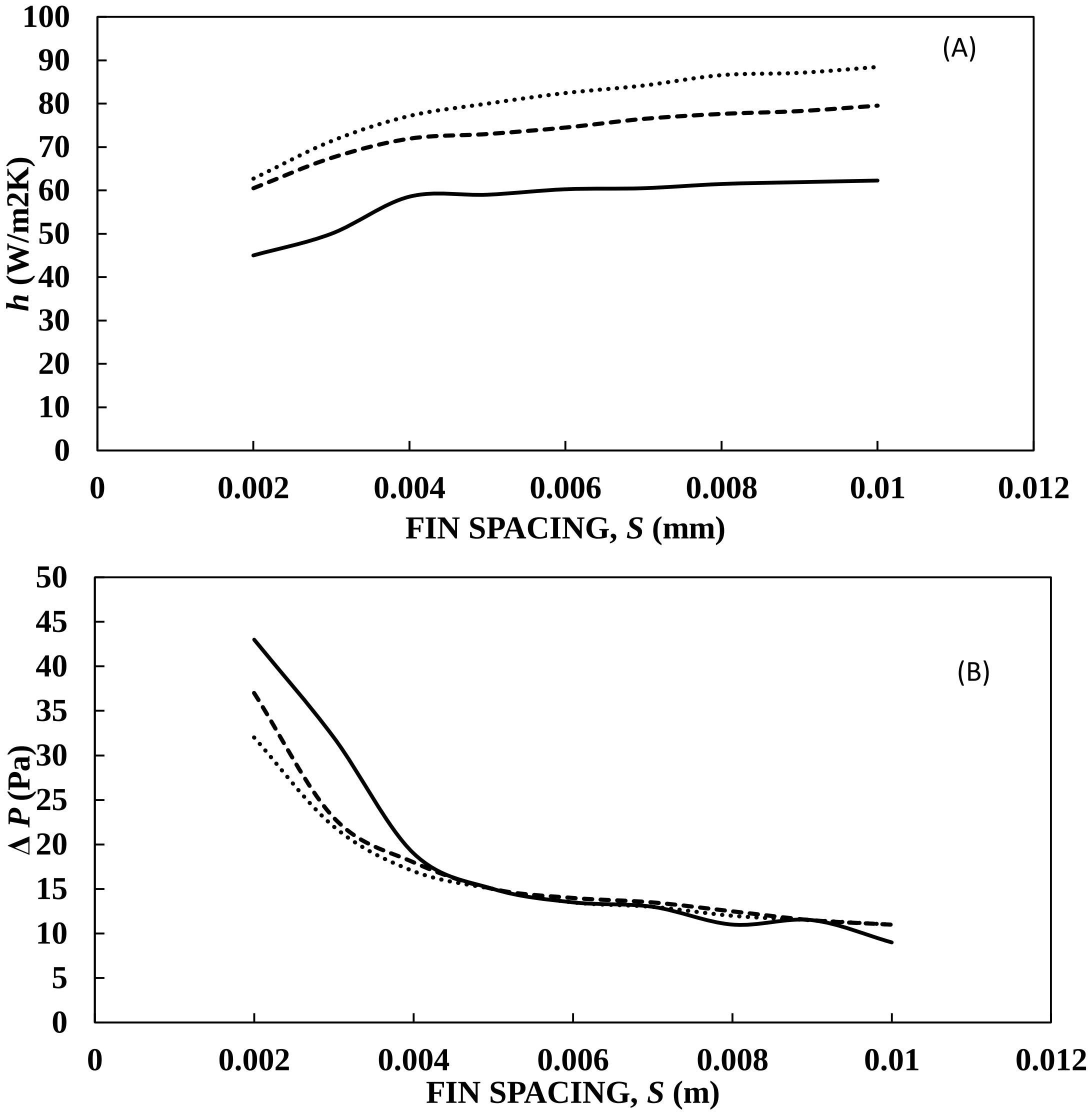

Fig. 7.4. Effect of fin spacing (A) heat transfer coefficient, (1) h_f = 5 mm, (2) h_f = 7 mm(3) h_f = 10 mm. (B) pressure drop (1) h_f = 5 mm, (2) h_f = 7 mm(3) h_f = 10 mm.

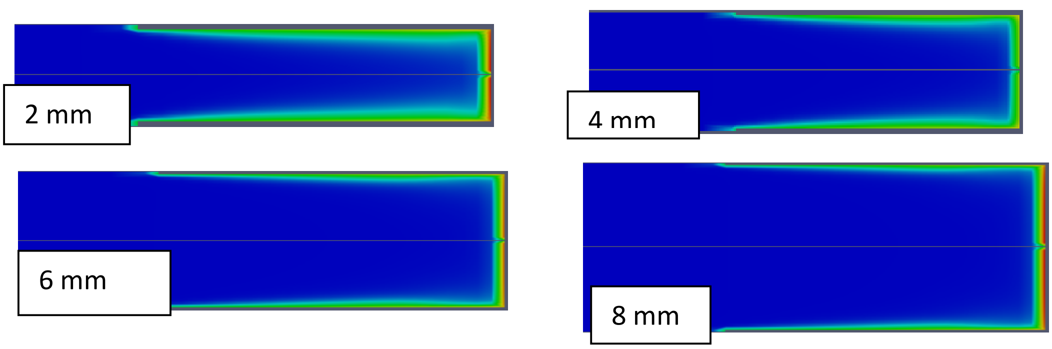

Fig. 7.5. Thermal boundary layer development

three fin diameters perform equally well. Also, with an increase in the fin spacing, the area requirement increases continuously. As fin spacing is increased from 2 mm to 10 mm, space requirement increases by 150% for all the fin diameters. Overall, from this section we can conclude that by increasing the fin spacing, the heat transfer coefficient increases and pressure drop decreases for all the fin diameters, and it may seem appropriate to use larger fin spacing in the design of the air cooled condenser. However, when we consider the space requirement associated with the design of the condenser, then we have to optimize the design in such a way that it gives highest heat transfer coefficient per unit per unit pressure drop possible for a minimum space requirement. Therefore a fin spacing of 5-6 mm is recommended from this section. Also, the fins with h_f = 5 mm performs better than the fins with h_f =7 mm and 10 mm in terms of the heat transfer, j/f factor and volume goodness factors. Therefore, the fin with a height of 5 mm is chosen for further studies with a fin spacing of 5 mm.

For plate fins, Wang and Chi (2000) and Yan and Sheen (2000) found that the heat transfer increases with a decrease in the fin spacing. Whereas, Chen et al. (2012), Huang et al. (2009) and Choi et al. (2010) found that the heat transfer coefficient increases with an increase in the fin spacing. Similar results were obtained by Watel et al. (2000a, 2000b) and Chen and Hsu (2008) for the plain annular fins. On the other hand, He et al. (2005), Liu et al. (2010) and Mon and Gross (2004) observed that, the heat transfer coefficient increases with an increase in the fin spacing due to delay in the boundary layer interaction at higher fin spacing. However, beyond a certain fin spacing, the heat transfer coefficient decreases due to bypass flow between the fins. Therefore, they recommended an optimized fin spacing in the range of 1.2 mm to 4 mm. Similarly, for crimped spiral fins, Pongsoi et al. (2011, 2012) recommended a fin spacing of 4.2 mm. The heat transfer coefficient depends on the volumetric flow rate or mass flow rate through the heat exchanger and the temperature rise of the fluid from the inlet to the outlet. From the above discussion, it can be seen that some of the authors have found the heat transfer

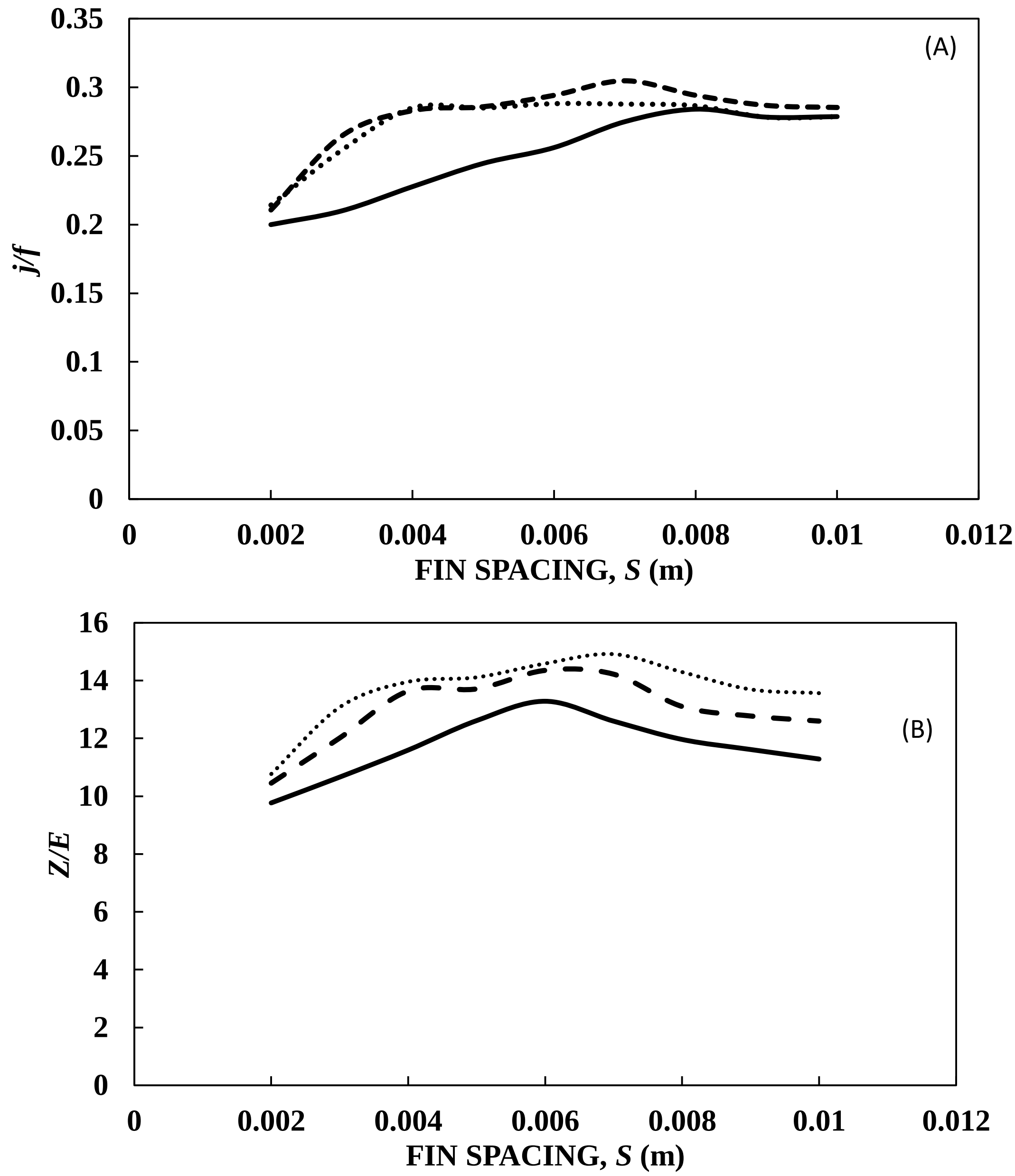

Fig. 7.6. Effect of fin spacing (A) *j/f* ratio (1) h_f = 5 mm, (2) h_f = 7 mm(3) h_f = 10 mm. (B) Volume goodness factor (*Z/E* ratio) (1) h_f = 5 mm, (2) h_f = 7 mm(3) h_f = 10 mm.

coefficient as an increasing or decreasing function of the fin spacing, and some found an optimized fin spacing and argued that the flow bypasses the finned area without efficient heat transfer. For this purpose, an attempt has been made to understand these phenomena by plotting the volumetric flow rate and the temperature profile between the fins for S = 2, 6 and 10 mm for h_f = 5 mm and N_r = 2 in Fig. 7.9. It can be observed that, the volumetric flow rate increases

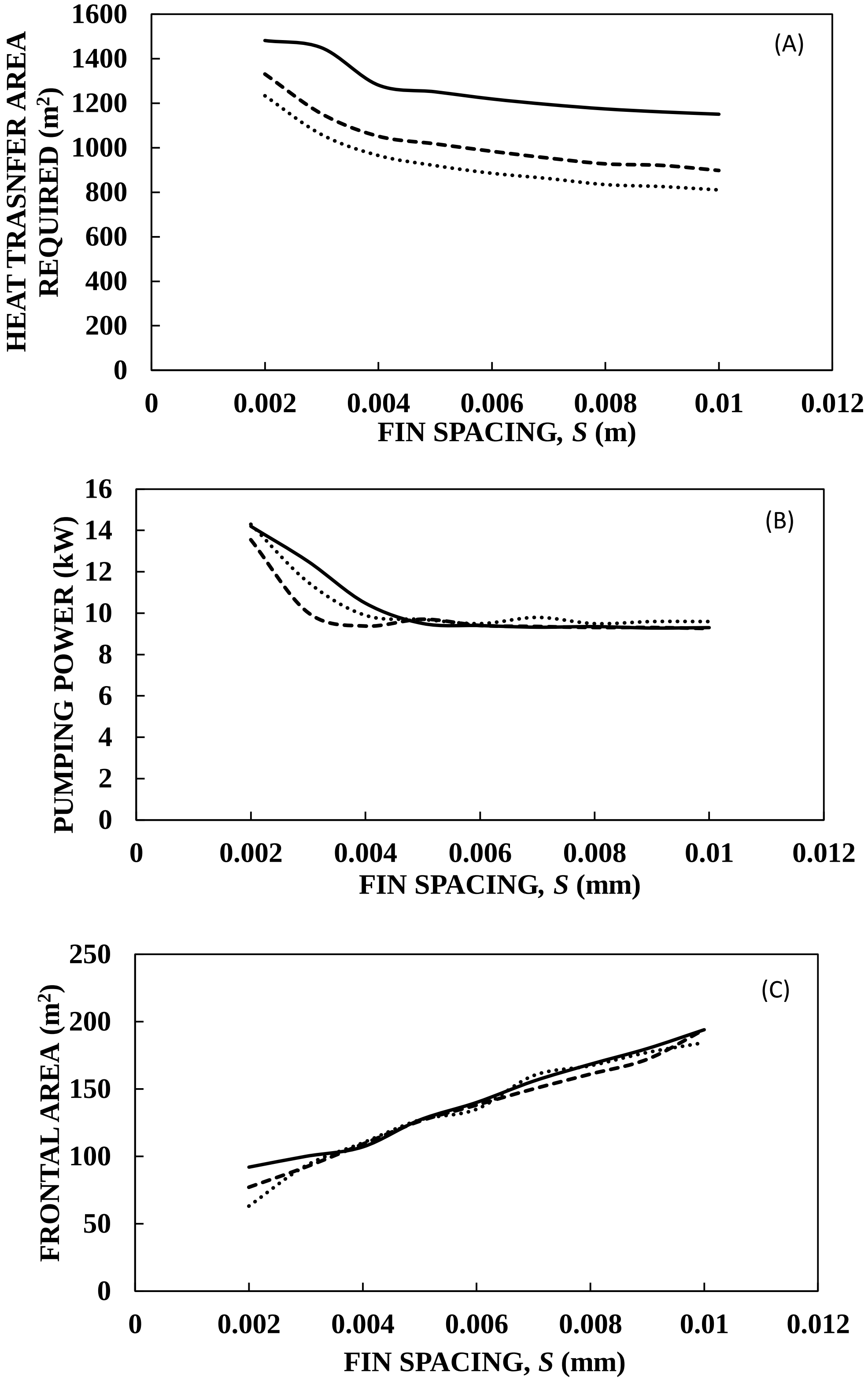

Fig. 7.7. (A) Volumetric flow rate variation between two fins (1) *S* = 2 mm, (2) *S* = 6 mm, (3) *S* = 10 mm. (B) Air temperature variation between two fins (1) *S* = 2 mm, (2) *S* = 6 mm, (3) *S* = 10 mm

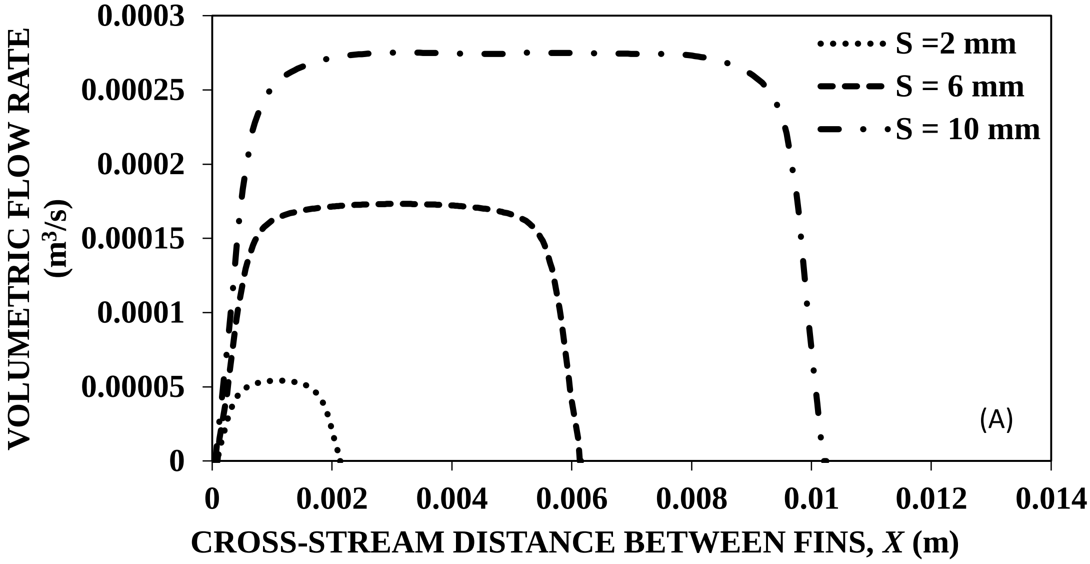

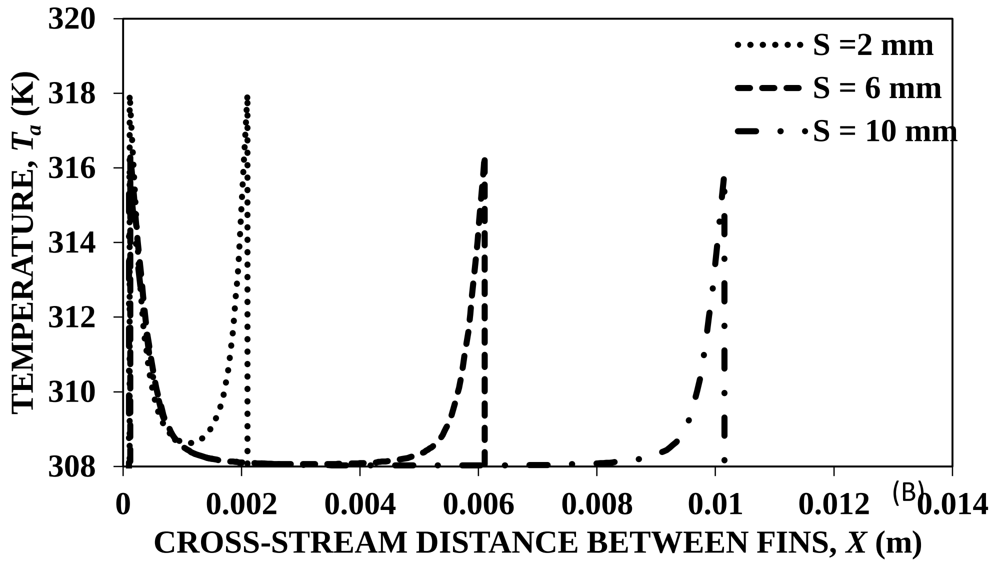

Fig. 7.8. For 1 MW heat removal capacity (A) heat transfer area requirement (1) h_f = 5 mm, (2) h_f = 7 mm(3) h_f = 10 mm. (B) pumping power requirement (1) h_f = 5 mm, (2) h_f = 7 mm(3) h_f = 10 mm. (C) space requirement (1) h_f = 5 mm, (2) h_f = 7 mm(3) h_f = 10 mm.

by a large magnitude as the fin spacing is increased from 2 to 10 mm (Fig. 7.9A). The bypass flow stream can also be observed in Fig. 7.9B. The center portion of the air flow goes at almost 308 K (inlet temperature) and the heat transfer is very low for all the fin spacing except at 2 mm, where the bypass flow is less prominent. Overall, the increase in the volumetric flow rate dominates over the flow bypass phenomenon and the heat transfer coefficient increases as the fin spacing is increased. Therefore, we can conclude that, heat transfer coefficient behavior

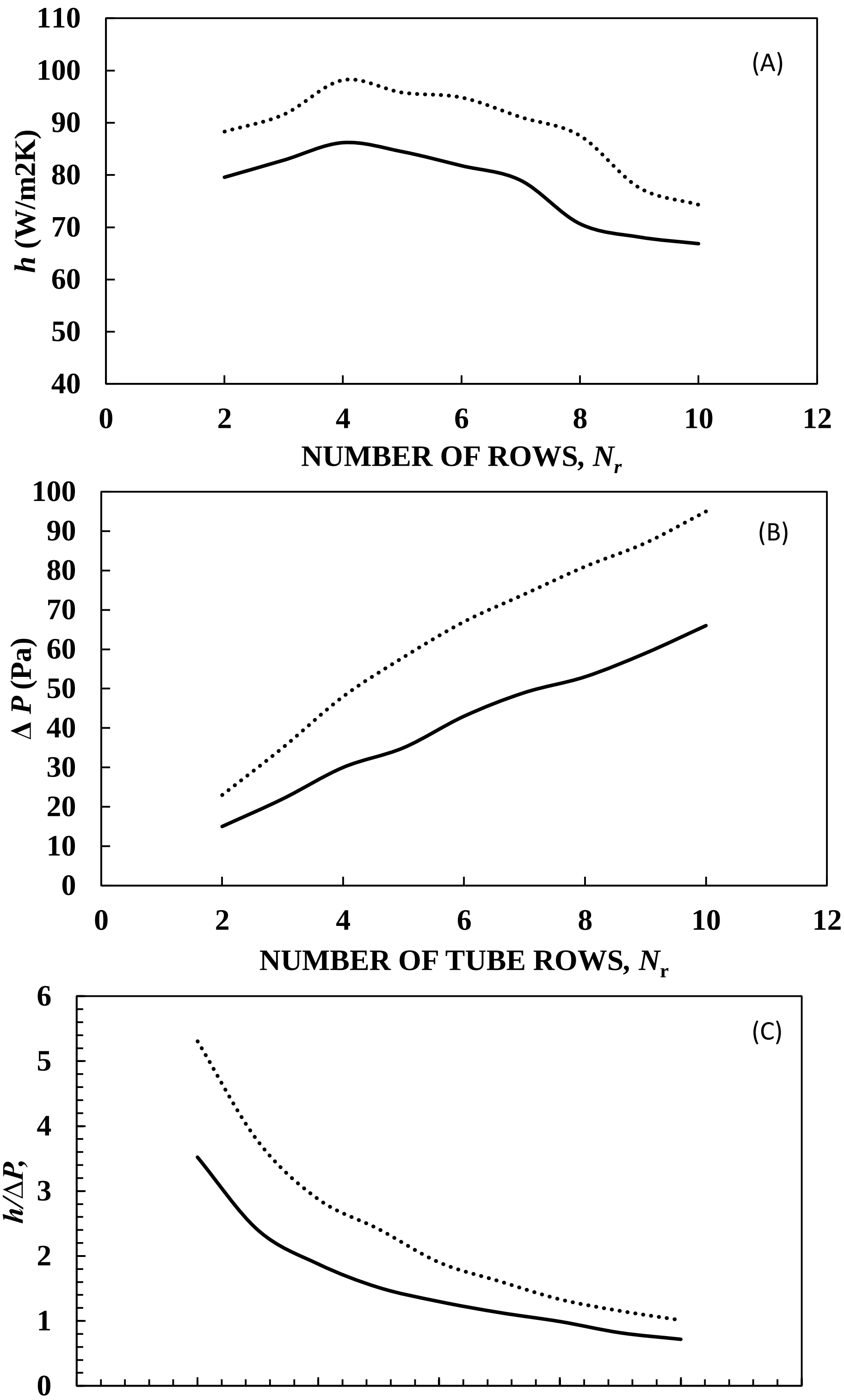

Fig. 7.9. Effect of number of tube rows (A) heat transfer coefficient (1) U_{fr} = 4.76 m/s, (2) U_{fr} = 6.32 m/s, (B) pressure drop (1) U_{fr} = 4.76 m/s, (2) U_{fr} = 6.32 m/s, (C) heat transfer coefficient per unit pressure drop (1) U_{fr} = 4.76 m/s, (2) U_{fr} = 6.32 m/s.

with respect to the fin spacing depends on the boundary layer interaction, bypass flow phenomenon and enhancement in the volumetric flow rate, especially, for a fixed inlet velocity. Also, current recommendation of a fin spacing of 5 mm is also based on the compactness of the heat exchanger along with the heat transfer and pressure drop, unlike most of the previous studies.

7 .3.5. Effect of number of tube rows

The effect of number of tube rows has been studied by varying the row number from 2 to 10 at two frontal velocities (U_{fr} = 4.76 m/s and 6.32 m/s). The results are presented in Figs. 7.10-7.14. Fig. 7.10 shows the (A) heat transfer coefficient, (B) pressure drop and (C) heat transfer coefficient per unit pressure drop from varying row number at two frontal velocities. It can be observed that, as the row number increases from 2 to 4, the heat transfer coefficient increases, and beyond N_r = 4, the heat transfer coefficient decreases gradually. On the other hand, the pressure drop increases continuously with an increase in the row number from 2 to 10 (Fig. 7.10B). This is due to the increase in the resistance with an increase in the row number. Fig. 7.10C shows the heat transfer coefficient per unit pressure drop, it can be observed that, $h/\Delta P$ is highest at lowest row number and it decreases as the row number is increased to 10. Also, it can also be observed that as the frontal velocity (or *Re*) is increased, the heat transfer coefficient per unit pressure drop decreases. However, as the number of rows is increased beyond 8, the $h/\Delta P$ becomes comparable at two frontal velocities. Wang and Chang (1996), Wang and Chi (2000), Xie et al. (2009) and Choi et al. (2010) also observed that the heat transfer coefficient decreases with an increase in the row number upto N_r = 6, and beyond this, the effect of tube rows diminishes. However, in the present case, the heat transfer coefficient shows a maxima at N_r = 4 and decreases gradually for N_r> 4. Figs. 11A and 11B show the Colburn factor (*j*) andfriction factor (*f*) with respect to the row number at two frontal velocities. It can be observed that the Colburn factor increases with an increase in the number of rows from 2 to 4, and for

N_r> 4, the Colburn factor decreases. Also in Fig. 7.11B, it can be observed that the friction factor decreases continuously with an increase in the row number. These results are analogues to the results obtained by Wongwises and chokeman (2005) for Colburn factor and friction factor. In Table 7.9, we have given Z and E with respect to the number of rows at two frontal velocities. The highest Z/E ratio is provided by row number of 5 at U_{fr} = 4.76 m/s and 6.32 m/s, which indicates a lower volume of heat exchanger for the same heat removal capacity. We can also observe that, as the frontal velocity increases from 4.76 m/s to 6.32 m/s, the value of Z increases. This implies a larger heat removal capacity with same size of the heat exchanger at larger frontal velocity. However, with an increase in U_{fr}, the value of E also increases resulting in a lower Z/E ratio. Therefore, we can conclude that at higher frontal velocity, the compactness of the heat exchanger can be maximized with an increased cost of the pumping power.

In this case also, we have carried out calculations for 1 MW heat removal capacity and the results are shown in Figs. 12A, 12B and 12C. Fig. 7.12A shows the heat transfer area requirement at U_{fr} = 4.76 m/s and 6.32 m/s. It can be observed that, at N_r= 4, minimum heat transfer area is required to remove 1 MW of heat at both the frontal velocities. This is due to the highest heat transfer coefficient obtained at N_r= 4, as we have already seen earlier in this section. As the number of rows increased beyond 4, the surface area requirement increases. The heat transfer area requirement decreases by 16-20% as the frontal velocity increases from 4.76 m/s to 6.32 m/s. Similarly in Fig. 7.12B, we can observe that the pumping power requirement increases with an increase in the number of tube rows. The pumping power requirement increases by 30-40% with an increase in the frontal velocity from 4.76 m/s to 6.32 m/s. In Fig. 7.12C, the space requirement is shown for varying row number. The space requirement at U_{fr} = 4.76 m/s is 16-27% higher than at U_{fr} = 6.32 m/s, higher being at lower number of rows. As row number is increased at both frontal velocities, the space requirement decreases till N_r= 7, and as the row number is increased further, the space requirement becomes almost constant. Therefore, we can conclude that, by increased the row number beyond 7, there is no improvement in terms of the size and space requirement of the air cooled condenser, and

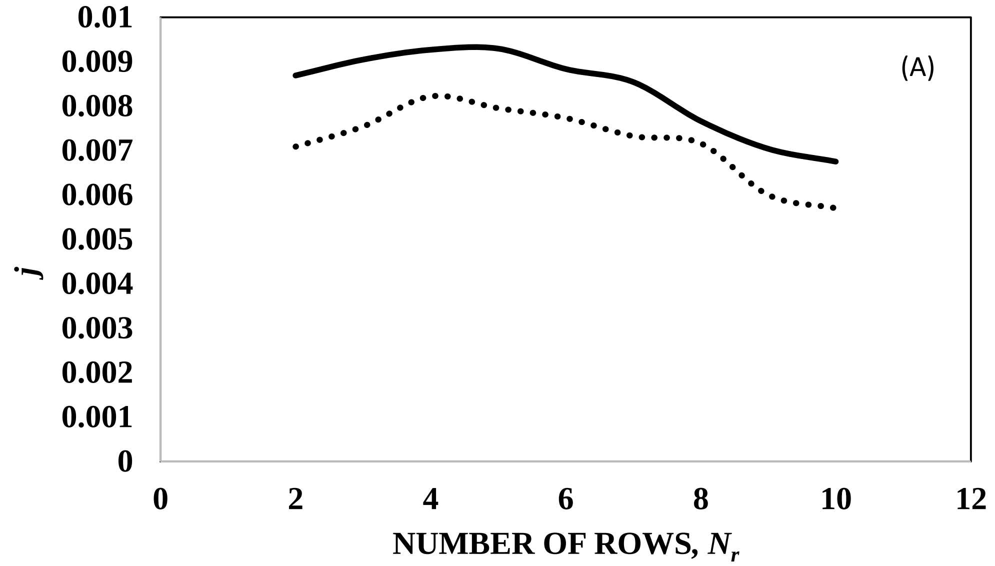

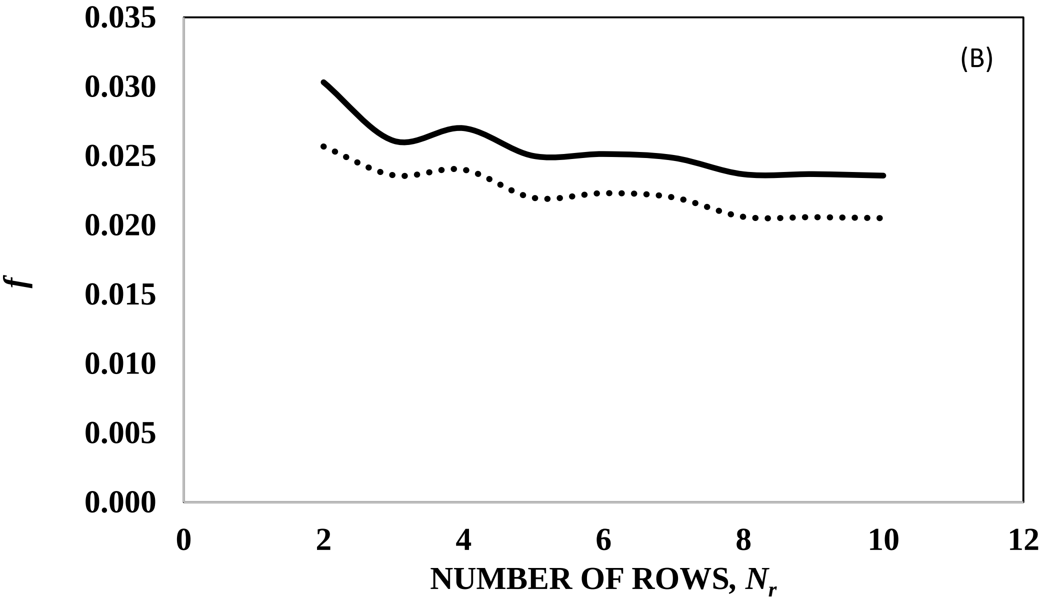

Fig. 7.10. Effect of number of tube rows (A) Colburn factor (1) U_{fr} = 4.76 m/s, (2) U_{fr} = 6.32 m/s, (B) friction factor (1) U_{fr} = 4.76 m/s, (2) U_{fr} = 6.32 m/s,

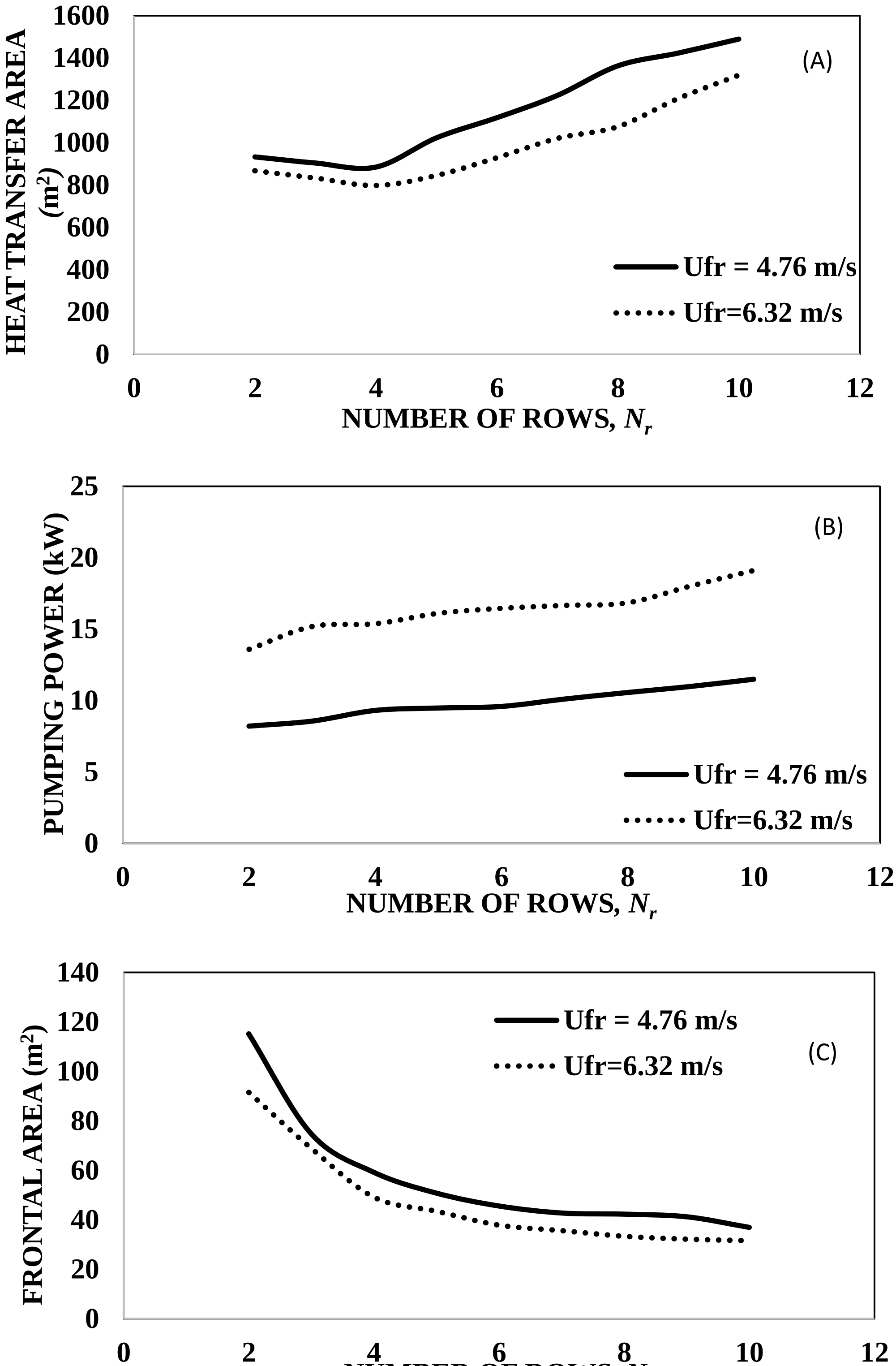

Fig. 7.11. Effect of tube rows, for 1 MW heat removal capacity (A) heat transfer area requirement (1) U_{fr} = 4.76 m/s, (2) U_{fr} = 6.32 m/s, (B) pumping power requirement (1) U_{fr} = 4.76 m/s, (2) U_{fr} = 6.32 m/s, (C) space requirement (1) U_{fr} = 4.76 m/s, (2) U_{fr} = 6.32 m/s.

therefore, this must be taken into consideration while designing. The variation in number of rows affects the downstream turbulence shedding, mixing and pressure drop. Wang and Chang (1996), Wang and Chi (2000) argued that at low Re, the effect of row number is prominent and formation of vortices takes place behind the tubes which reduces the heat transfer coefficient for larger row number. As Re is increased beyond 3000, the downstream turbulence dominates and leads to an increase in the heat transfer coefficient and the effect of row number becomes negligible. Similarly, Xie et al. (2009) observed that for larger row number coil, the recirculation zones behind the tubes were more prominent as compared to the tubes of lower row number coil. Therefore, the heat transfer coefficient was lower for the coil with larger number of rows for Xie et al. (2009). We tried to analyze the wake region and recirculation zones of the coil with row number 2, 4, 7, and 10 and the results are shown in Fig. 7.13. In Fig.

Table 7.5. Volume goodness factor for varying row number

Row Number	**U_{fr} = 4.76 m/s**			**U_{fr} = 6.32 m/s**		
	Z	***E***	***Z/E***	***Z***	***E***	***Z/E***
2	13005.20	949.45	13.69	14500.23	2002.34	7.24
3	15652.95	958.52	16.33	17761.06	2022.07	8.78
4	16537.80	968.34	17.07	19306.25	2131.17	9.058
5	17926.27	982.59	18.24	19462.07	2110.00	9.22
6	16925.81	995.53	17.00	18790.00	2055.35	9.14
7	15908.77	960.65	16.56	18470.05	2041.42	9.04
8	14770.20	935.49	15.78	17429.84	1894.73	9.19
9	14021.20	934.56	15.00	15983.20	1876.00	8.51
10	13741.68	940.72	14.60	14141.33	1889.00	7.48

7.13A, the wake region behind the tubes is shown for the 1st row, 4th row, 7th row and 9th row of the 10 row coil. It can be observed that as we move towards downstream, the wake region and recirculation cells behind the tubes becomes more prominent, which results in larger ineffective area behind the tubes. Similarly in Fig. 7.13B, the 1st row of 2 row coil, 4th row of 5 row coil, 7th row of 8 row coil is shown, and we can observe that the wake region for these tube rows is similar to those shown in Fig. 7.13A (1st row, 4th row and 7th row). This indicates that as the number of rows is added in the coil, the wake region increases continuously.

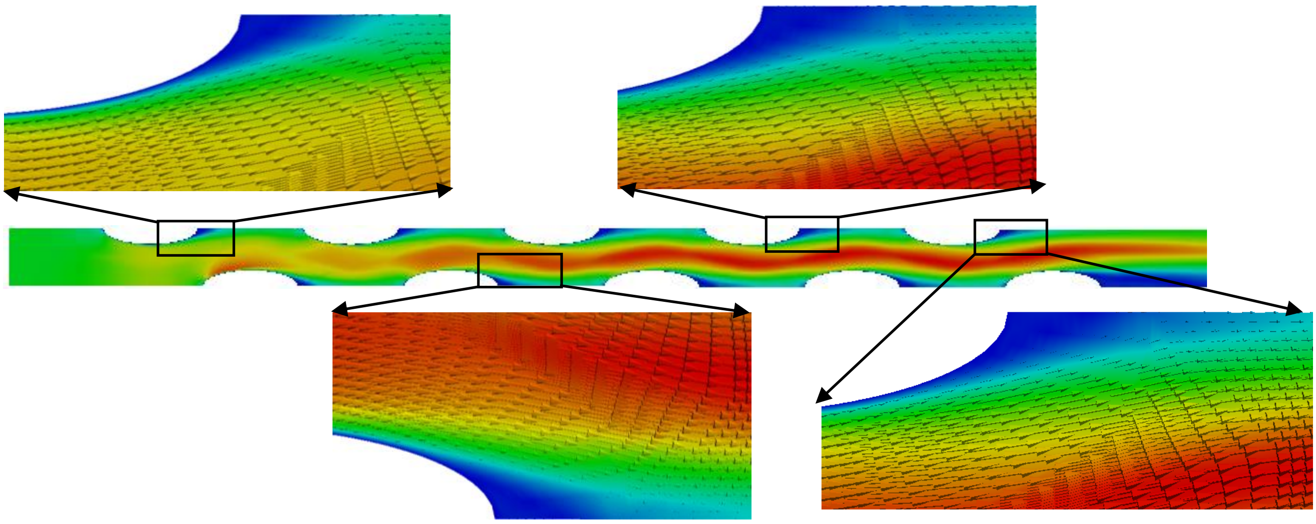

(A)

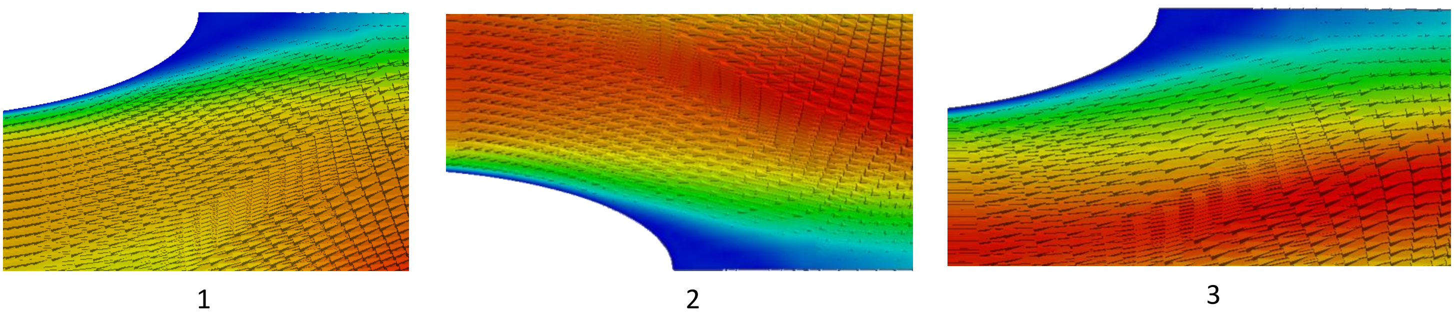

(B)

Fig. 7.12. Velocity vectors showing wake region and formation of recirculation cells (A) 10 row coil, (B) (1) 1st row of 2 row coil, (2) 4th row of 5 row coil, (3) 7th row of 8 row coil.

Therefore, for larger number of rows, recirculation cells and wake region becomes stronger leading to a lower heat transfer coefficient except for N_r<4. Also, in the present case, this behavior is observed at both the frontal velocities of 4.76 m/s and 6.32 m/s (corresponding Reynolds numbers are 3700 and 5000). Therefore, unlike the observation made by Wang and Chang (1996) and Wang and Chi (2000) that the effect of tube rows diminishes beyond Re > 3000, we observe that the effect of tube rows is still significant beyond Re> 3000. Further, in order to understand the quantitative effect of downstream turbulence, we have estimated the volume integral value of the turbulence kinetic energy for all the cases and shown in Fig. 7.14.We can observe that, when number of rows is increased from 1 to 4, the turbulence kinetic energy increases in the domain, and beyond 4 rows, it becomes constant. This indicates that the downstream turbulence increases as the number of rows is increased from 1 to 4 and this is also reflected by an increase in the heat transfer coefficient when the number of rows is increased from 1 to 4.

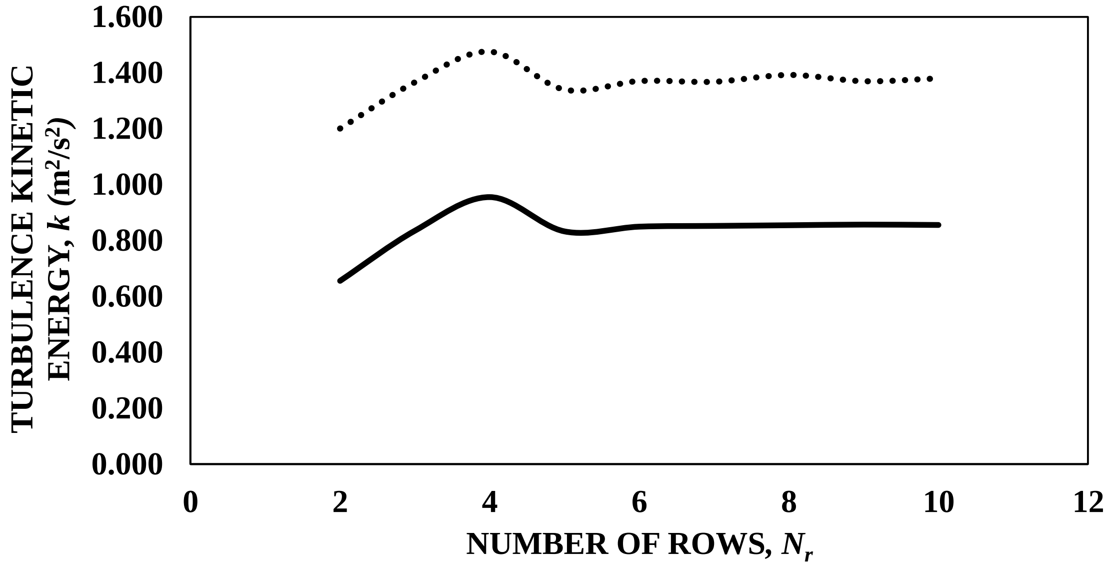

Fig. 7.13. Variation of turbulence kinetic energy with number of tube rows.

From these results, it can be concluded that, by increasing the number of rows, the turbulence generation increases in the domain, which helps in an increase in the heat transfer coefficient. However, the wake region and recirculation cells get stronger with an increase in the row number, and this tends to suppress the mixing and turbulence eddies. Also, as the row number is increased, the air temperature reaching the downstream finned-tubes increases and reduces the heat transfer coefficient for the downstream tube rows. Overall, we can conclude that beyond 4 rows, the heat transfer coefficient decreases, therefore a row number of 4 can be recommended for better heat transfer performance. However, when it comes to compactness of the heat exchanger then a row number of 5 provides maximum *Z/E* ratio and therefore can be considered where space requirement is important. Present recommendation for row number is not in agreement with He et al. (2005) who recommended a row number less than 3, however, their recommendation was based only on the *Nu* and did not consider other parameters like, compactness, pumping power, etc. The value of the frontal velocity can be chosen in the similar way, at higher value of frontal velocity, we can obtain better heat transfer coefficient, and also more compact heat exchanger. However, the pumping power requirement increases as well and hence an optimum value of frontal velocity must be chosen.

7.3.6. Effect of transverse tube pitch

The effect of transverse tube pitch depends on whether the system is operated at constant frontal velocity or constant Reynolds number (based on the maximum velocity). He et al. (2005) and Xie et al. (2009) observed an increase in the transverse tube pitch (at a constant frontal velocity) decreases the heat transfer coefficient as well as the pressure drop. We have analyzed the effect of the transverse tube pitch (for the case of $N_r = 2$ and $S = 5$ mm, $h_f = 5$ mm) on the heat transfer and pressure drop and also the effects on the parameters like material requirement, space requirement and pumping power. Fig. 7.15A, we can observe that, as the transverse tube pitch increases, the heat transfer coefficient (h) decreases. The decrease in h is steep initially for $P_t < 38$ mm, and then the rate of decrease in h reduces slightly. This is because, in all the cases, the frontal velocity is constant, and as the tube pitch is increased it leads to a

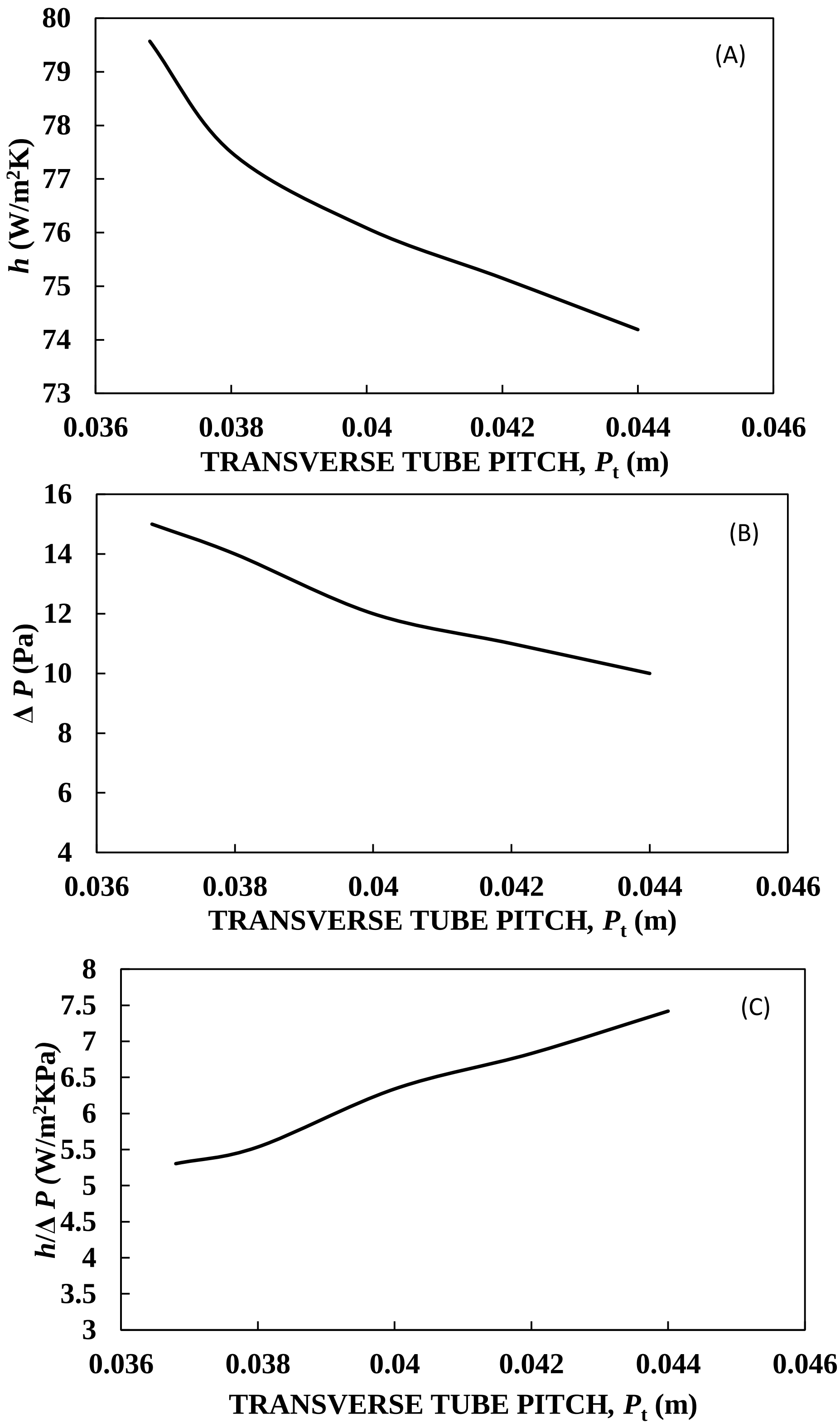

Fig. 7.14. Effect of transverse tube pitch, (A) heat transfer coefficient, (B) pressure drop (C) heat transfer coefficient per unit pressure drop.

lower maximum velocity in the minimum flow area and hence reduction in the heat transfer coefficient. The maximum variation in the heat transfer coefficient is 7% as the tube pitch is increased from 36.8 mm to 44 mm. Similarly, the pressure drop across the heat exchanger reduces by 33% as P_t is increased from 36.8 mm to 44 mm (Fig. 7.15B). The reduction in pressure drop is because as the tube pitch increases at constant frontal velocity, then the obstruction to the flow decreases. Fig. 7.15C shows that the heat transfer coefficient per unit pressure drop increases by 28.5% as P_t is increased from 36.8 mm to 44 mm. Therefore, to obtain a maximum heat transfer coefficient per unit pressure drop, a higher transverse tube pitch is suggested. However, other parameters like compactness and space requirement are also affected as the tube pitch is increased and we have given the material requirement, pumping power and space requirement in Fig. 7.16. We can observe that the surface area requirement increases as the tube pitch is increased, and the rate of increase is higher for 36.8 mm $\leq P_t \leq$ 40 mm, and the rate of increase reduces. This is due to the higher rate of reduction in h for 36.8 mm $\leq P_t \leq$ 40 mm (Fig. 7.15A). The increase in the heat transfer area requirement is 7% as P_t is increased from 36.8 mm to 40 mm. Similarly in Fig. 7.16B, the pumping power decreases by 15% as the tube pitch is increased in the same range, and this is due to the decrease in the pressure drop with an increase in the transverse tube pitch (Fig. 7.15B). In Fig. 7.16C, the space requirement is shown for varying tube pitch. The space requirement can be seen to increase with an increase in the tube pitch, and the overall increase is 21% across the tube pitch range of 36.8 mm to 44 mm. Therefore, we can conclude that by varying the tube pitch the variation in the heat transfer coefficient or heat transfer area requirement is not so large (only 7%), however, the decrease in the pumping power is significant (15%). This results in a larger heat transfer coefficient per unit pressure drop at higher tube pitch. However, the frontal area (space) requirement also increases (21%) significantly as the tube pitch is increased, and therefore we

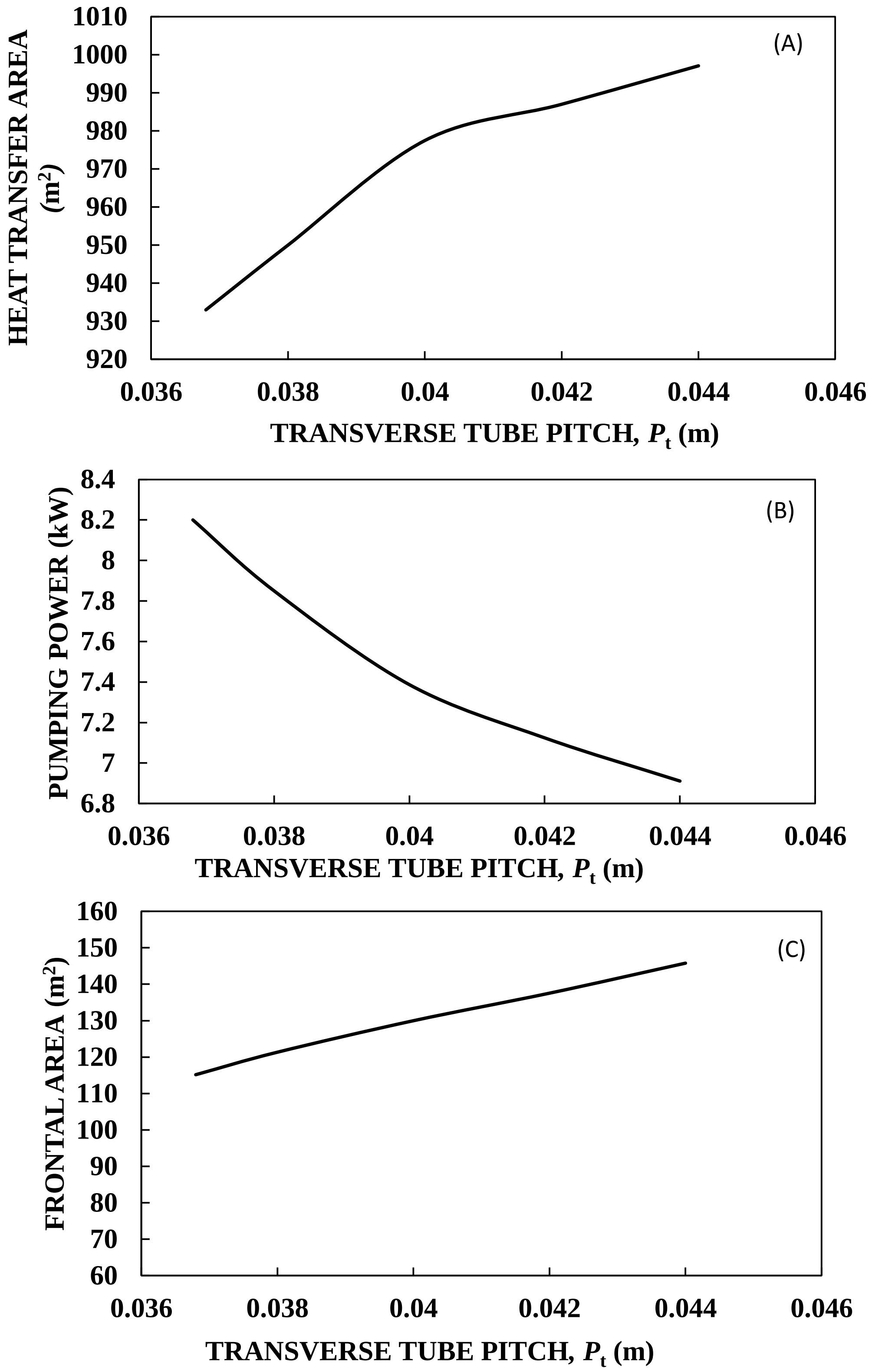

Fig. 7.15. Effect of transverse tube pitch, For 1 MW heat removal capacity (A) heat transfer area requirement, (B) pumping power requirement (C) space requirement.

need to optimize all these parameters. conclude that the effect of tube pitch is dependent on the fin type and the value of P_t/D_f ($1.26 \leq P_t/D_f \leq 1.47$ for the present case).

7.3.7. Fin efficiency

The temperature distribution on a fin surface is not uniform as have been presented by Chen et al. (2005, 2007), Chen and Lai (2012), and Chen and Hsu (2008). The fin efficiency is defined as the ratio of the real heat transfer to the ideal heat transfer (fin at tube surface temperature) and can be expressed as [Lin and Jang (2002)]:

$$\eta = \frac{\int (T_a - T_f) dA}{\int (T_a - T_b) dA} \qquad \ldots (7.11)$$

Here T_a is the average air temperature calculated separately for each row fin. The temperature of the air increases as it passes through the tube rows, therefore, the average air temperature is calculated in the vicinity of a particular row number to obtain the fin efficiency for that tube row. *dA* indicates the heat transfer area under consideration. In Fig. 7.17A, the fin efficiency is shown for varying fin spacing, we can observe that as the fin spacing increases, the fin efficiency decreases. The reason can be understood by Fig. 7.17B, in which average air temperature and average fin temperature is plotted with respect to the varying fin spacing. The average air temperature around finned-tubes decreases as the fin spacing is increased due enhanced mass flow rate with an increase in the fin spacing. Also, the fin temperature decreases, however, the decrease in the air temperature is larger, which results in a decrease in the fin efficiency. Similar results were obtained by Tao et al. (2007) for the wavy fins. We can also observe in Fig. 7.17A, that the fin efficiency decreases as the fin height is increased. This is due to the decrement in the conduction heat transfer with an increase in the fin height, which lowers the average fin temperature.

Fig. 7.18A shows the variation of fin efficiency with an increase in the number of tube rows. It can be observed that, as the number of rows is increased, the fin efficiency initially increases slightly for $N_r < 4$, and then decreases as the number of rows increases. The increase in the fin efficiency for $2 < N_r < 4$ can be attributed to the increase in the turbulence as explained in Section 3.4., the increase in the turbulence promotes mixing in the flow and enhances heat transfer and fin efficiency. Beyond $N_r > 4$, the air reaching the fin surfaces is at a higher

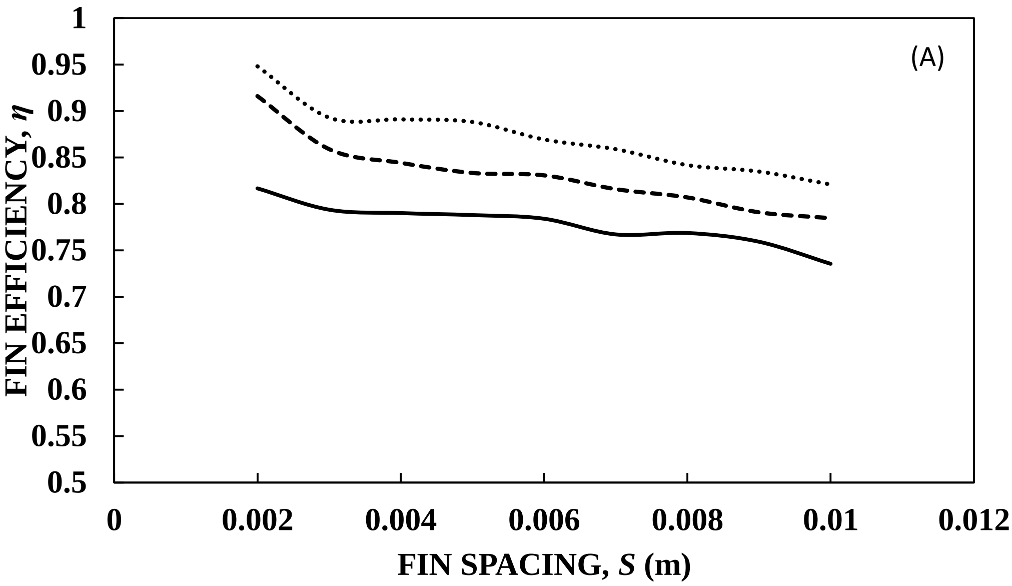

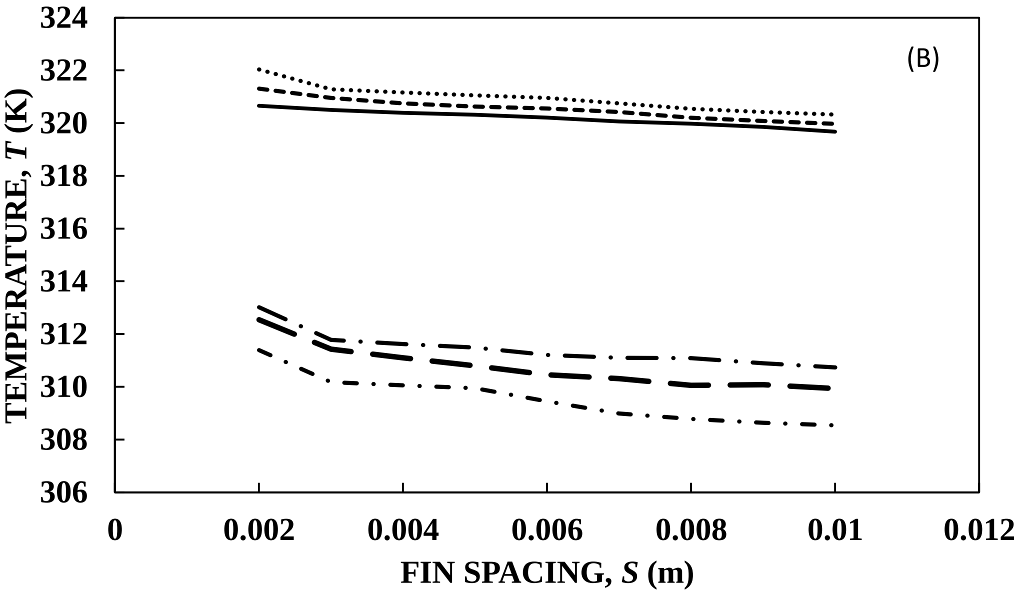

Fig. 7.16. (A) Variation of fin efficiency with fin spacing for various fin heights and $N_r = 2$. (1) $h_f = 5$ mm, (2) $h_f = 7$ mm (3) $h_f = 10$ (B) Variation of fin temperature and average air temperature with fin spacing for various fin heights and $N_r = 2$. (1) T_f at $h_f = 5$ mm, (2) T_f at $h_f = 7$ mm (3) T_f at $h_f = 10$ mm, (4) T_a at $h_f = 5$ mm, (5) T_a at $h_f = 7$ mm (6) T_a at $h_f = 10$ mm.

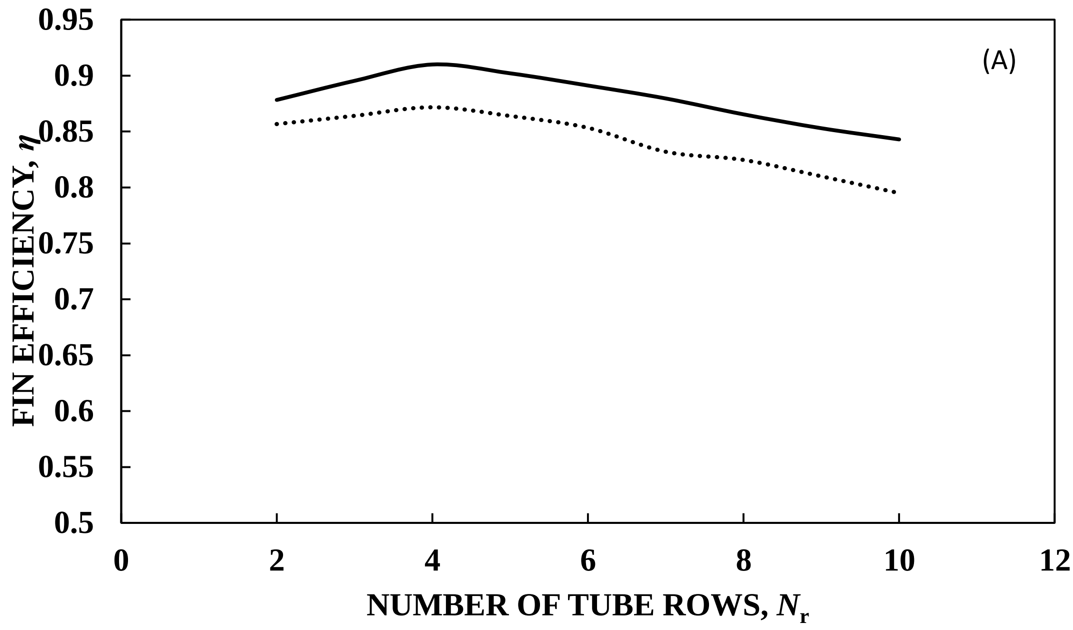

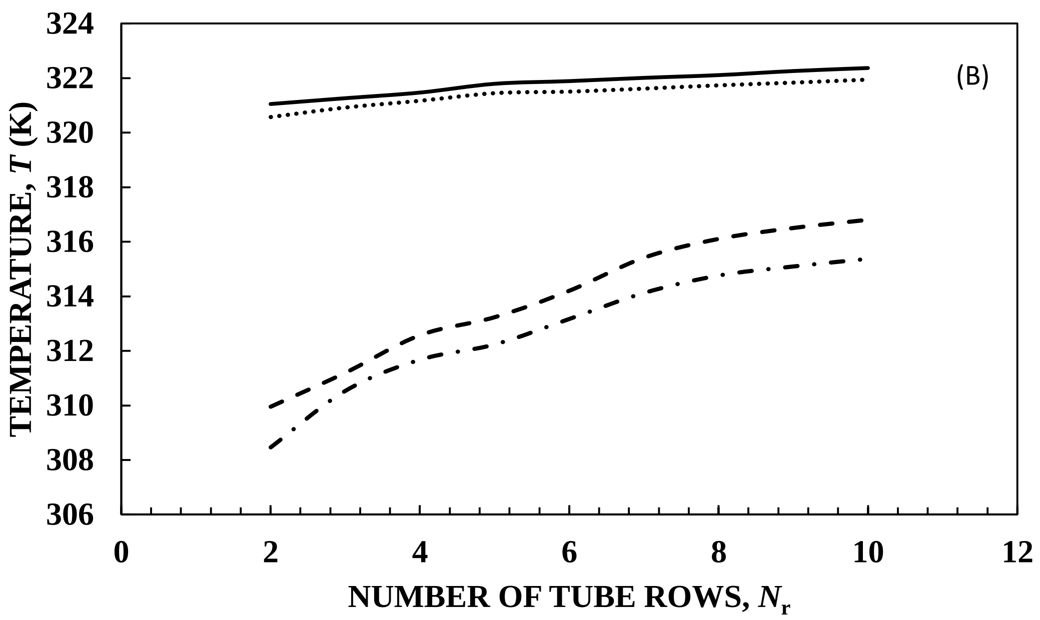

Fig. 7.17. (A) Variation of fin efficiency with number of tube rows for S = 5 mm and h_f = 5 mm. (1) U_{fr} = 4.76 m/s, (2) U_{fr} = 6.32 m/s (B) Variation of fin temperature and average air temperature with number of tube rows for S = 5 mm and h_f = 5 mm. (1) T_f at U_{fr} = 4.76 m/s, (2) T_f at U_{fr} = 6.32 m/s (3) T_a at U_{fr} = 4.76 m/s, (4) T_a at U_{fr} = 6.32 m/s.

temperature, which reduces the temperature difference between the fin and air and hence the fin efficiency decreases as can be observed from Fig. 7.18B. Tao et al. (2011) observed that the fin efficiency increases along the length of the flow for a two row coil. The reason was assumed to be the low temperature at the fin near the inlet due to high heat transfer coefficient and the high temperature of the fin in the rear part of the coil. However, a higher heat transfer should be an indication of higher fin efficiency, and it does not provide a clear picture of variation in fin efficiency along the length of the coil. Also, it can be observed that the fin efficiency decreases with an increase in the frontal velocity or *Re*. As the frontal velocity is increased, the average air temperature through the heat exchanger decreases, however, the fin temperature also comes down as shown in Fig. 7.18B. Overall, this leads to a decrease in the fin efficiency as observed in Fig. 7.18A. This is analogues to the results obtained by Tao et al. (2007, 2011). In Fig. 7.19, the temperature distribution on the fin surfaces of 1^{st} row, 4^{th} row, 7^{th} row and 10^{th} row of 10 row coil is shown. It can be observed that, the temperature distribution is non-uniform for all the tube rows, however, the average temperature of the fins increases as the tube row number is increased. This also indicates that the heat transfer deteriorates as the heat exchanger depth increases.

7.3.8. Thermal-hydraulic optimization

Based on the results obtained from the numerical simulations in Sections 3.1 to 3.7, the design of the air cooled condenser has been optimized using Taguchi method [Taguchi (1986)]. Taguchi method is a multi-parameter optimization procedure, which is very useful in identifying and optimizing dominant process parameters with a minimum number of experiments or numerical simulations. The method is based on an orthogonal array [Taguchi and Konishi (1987)] of numerical simulations. An orthogonal array is a minimal set of numerical simulations with various combinations of parameter levels. Output of the orthogonal array, which indicates the relative influences of various parameters on the formation of the desired product, is used to optimize an objective function. There are three types of objective functions: larger-the-better, smaller-the-better and nominal-the-best. The influences are commonly referred in terms of *S/N* (signal to noise) ratio.

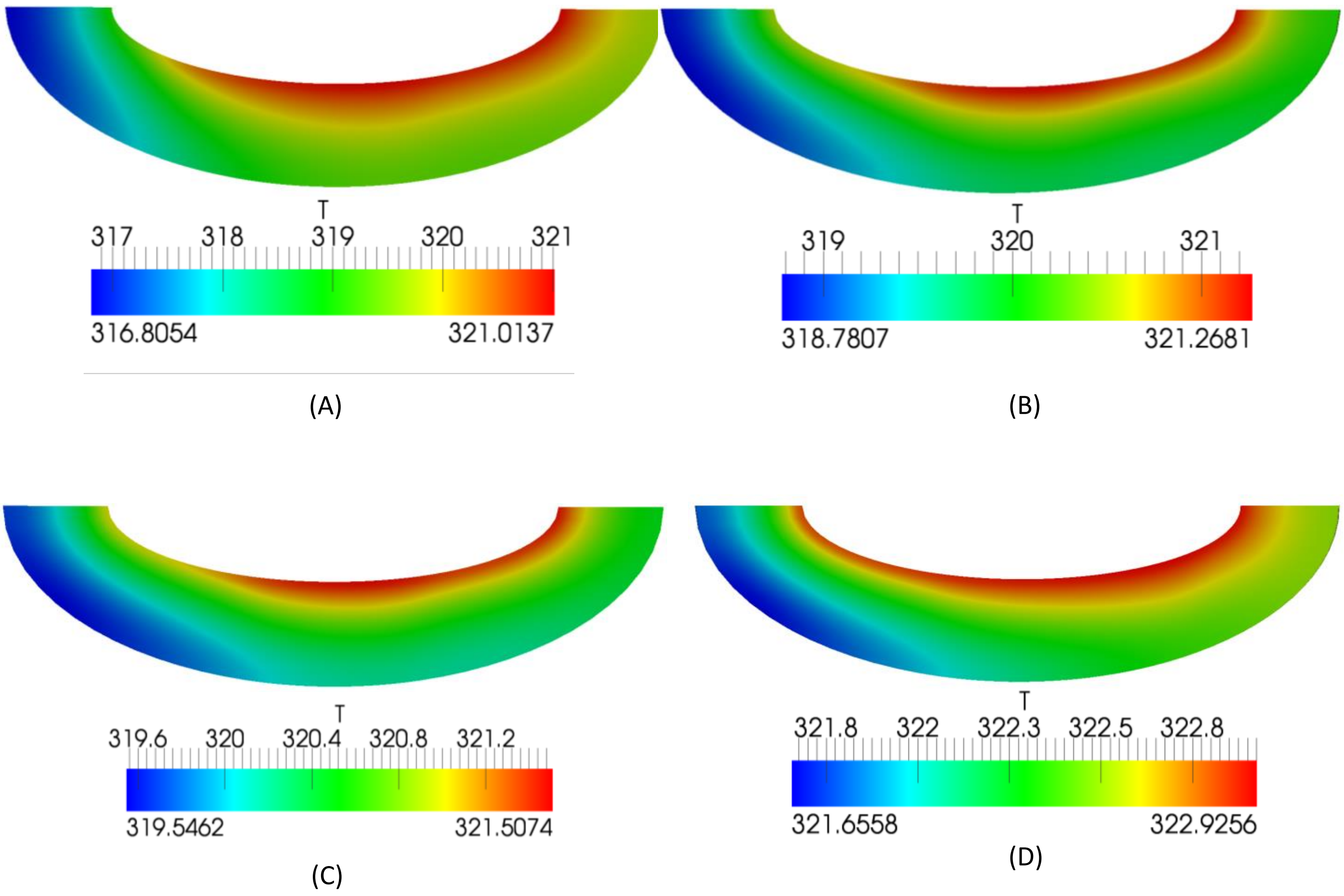

Fig. 7.18. Temperature distribution (Units in Kelvin) over fin surface for the 10 row coil, (A) 1st row, (B) 4th row, (C) 7th row, (D) 10th row.

For the optimization purpose, four input parameters (fin spacing, fin height, number of tube rows and transverse tube pitch) are considered with three levels each and for output, heat transfer coefficient per unit pressure drop, surface area required, pumping power and *Z/E* (compactness) are considered. The L-9 orthogonal array has been chosen as per design and shown in Table 7.10. It is to be noted that simulation number 6 and 8 have not been performed due to geometrical constraints, therefore, are provided with random minimal values. For optimization of pumping power and material requirement (surface area), smaller-the-better type of objective function has been used. In this case the exact relation between *S/N* ratio and

Table 7.6: L-9 orthogonal array for numerical simulations

Simulation no.	Fin spacing, S	Fin height, h_f	No of tube rows, N_r	Transverse tube pitch, P_t
1	3	5	2	36.8
2	3	7	4	40
3	3	10	10	44
4	5	5	4	44
5	5	7	10	36.8
6	5	10	2	40
7	10	5	10	40
8	10	7	2	44
9	10	10	4	36.8

the signal is given by

$$S/N = -10\log(\frac{1}{n})\sum_{i}^{n} y_i^2 \qquad \text{… (7.12)}$$

Whereas, for optimization of heat transfer coefficient per unit pressure drop and *Z/E* ratio, larger-the-better type of objective function has been used. Here, the exact relation between S/N ratio and the signal is given by

$$S/N = -10\log(\frac{1}{n})\sum_{i}^{n} 1/y_i^2 \qquad \text{… (7.13)}$$

where y_i is the signal (value of output) predicted by simulations. The effect of a parameter level on the *S/N* ratio, i.e., the deviation it causes from the overall mean of signal, is obtained by analysis of mean (ANOM). The relative effect of process parameters can be obtained from analysis of variance (ANOVA) of S/N ratios. Computation of ANOM and ANOVA are done by using following relations.

$$m_i = (\frac{1}{N_l})\sum S/N \qquad \ldots (7.14)$$

and

$$Sum\,of\;\,squares\,(SoS) = \sum_{i=i}^{i=j} N_l\,(m_i - \langle m_i \rangle)^2 \qquad \ldots (7.15)$$

where m_i represents the contribution of each parameter level to *S/N* ratio, $\langle m_i \rangle$ is the average

Table 7.7: Output values and corresponding *S/N*

h/ΔP (W/m^{2}KPa)	S/N	Surface area required (m^2)	S/N	Pumping power (kW)	S/N	*Z/E*	S/N
3.24	102.109	1059	-60.4979	11.5	-21.214	12.01	215.9086
1.9	55.75072	1180	-61.4376	7.69	-17.7185	20.78	263.5291
0.527	-55.6379	2534	-68.0761	10.36	-20.3072	14.43	231.8533
4.06	121.7052	946.5	-59.5224	6.7	-16.5215	20.19	261.0273
0.9	-9.1515	1647	-64.3339	11.34	-21.0923	15.1	235.7954
0.00001	-1000	0.00001	100	0.00001	100	0.00001	-1000
5.35	145.6708	1422	-63.058	8.94	-19.0268	17.19	247.0552
0.00002	-939.794	0.00001	100	0.00001	100	0.00001	-1000
3.53	109.5549	1104	-60.8594	10.51	-20.4321	13.36	225.1613

of m_i's for a given parameter and the coefficient and N_l represents the number of times the simulation is conducted with the same factor level in the entire simulation region. *SoS* is obtained by using ANOVA. This term is divided by corresponding degrees of freedom (DoF=number of parameter level minus 1) to derive relative importance of various numerical parameters by utilizing equation (6.16)

$$Factor\ effect = \frac{SoS}{\{DoF\ X\ \sum(SoS/DoF)\}} \qquad \dots (7.16)$$

Several researchers [Chee et al. (1996), Dasgupta et al. (2010), Nasab et al. (2011), Taghisadeh et al. (2008)] have extensively used this technique in optimization of parameters in various processes.

The *S/N* values for different outputs are shown in Table 7.11. The effect of each parameter on the four outputs is shown in Table 7.12. We can observe that the effect of fin height is maximum on the $h/\Delta P$ and is about 37%, the effect of fin spacing is second highest and is about 28.18%. The effect of number of tube rows is dominant on rest of the outputs (Surface area required, pumping power and *Z/E*) as compared to other input parameters. Also, from Table 7.12, we can find optimum value of the parameters corresponding to each of the outputs. For $h/\Delta P$, (based on larger value of S/N or m_i in Table 7.12), the effect of fin height and fin spacing is dominant as compared to the number of tube rows and tube pitch, therefore, this corresponds to the simulation number 7 in Table 7.10 with optimum value of the parameters as S = 10 mm, h_f = 5 mm, N_r =10, P_t = 40 mm. For surface area requirement, the effect of number of tube rows and fin height is dominant, which corresponds to S = 3 mm, h_f = 5 mm, N_r = 2, P_t = 36.8 mm (simulation 1 in Table 7.10), respectively. Similarly, for pumping power and *Z/E*, the optimum values come out to same and is given by S = 3 mm, h_f = 7 mm, N_r = 4, P_t = 40 mm (simulation 2 in Table 7.10).

From the results obtained by Taguchi method, it can be observed that the effect of number of tube rows is dominant in almost all the cases. Except $h/\Delta P$, a lower number of tube rows are found to be beneficial for the performance of air cooled condenser, as mentioned in previous sections also. The fin height is found to be an important parameter for a better heat transfer with an optimum value of 5 mm. The tube pitch is the second important parameter affecting the pumping power and compactness of the condenser and the optimum value is found to be 40 mm. The fourth parameter is fin spacing which affects the $h/\Delta P$ value only (considered to be one of the primary factor affecting the performance by most of the researchers). Overall, the optimum value of all the parameters can be chosen based on the application and interest. For example, if interest is to minimize the pumping power and space then tube pitch and number of tube rows are important parameters and must therefore be optimized.

7.4. Design methodology

The design process involves certain input parameters, constraints and output parameters. In the present case, we have identified input parameters as:

- Tube design and dimensions (tube diameter, tube shape)
- Fin design (fin type, fin height, fin spacing, fin thickness)
- Flow variables (velocity)
- Ambient conditions (air temperature)

The constraints are basically dependent on the economics of the air cooled condenser, and air cooled condenser should be enough economical to make it competitive with the conventional cooling towers. Therefore, constraints are:

- Capital cost
- Operating cost
- Space requirement

The output parameters of the process are:

- Heat transfer coefficient
- Pressure drop

We can show the process as

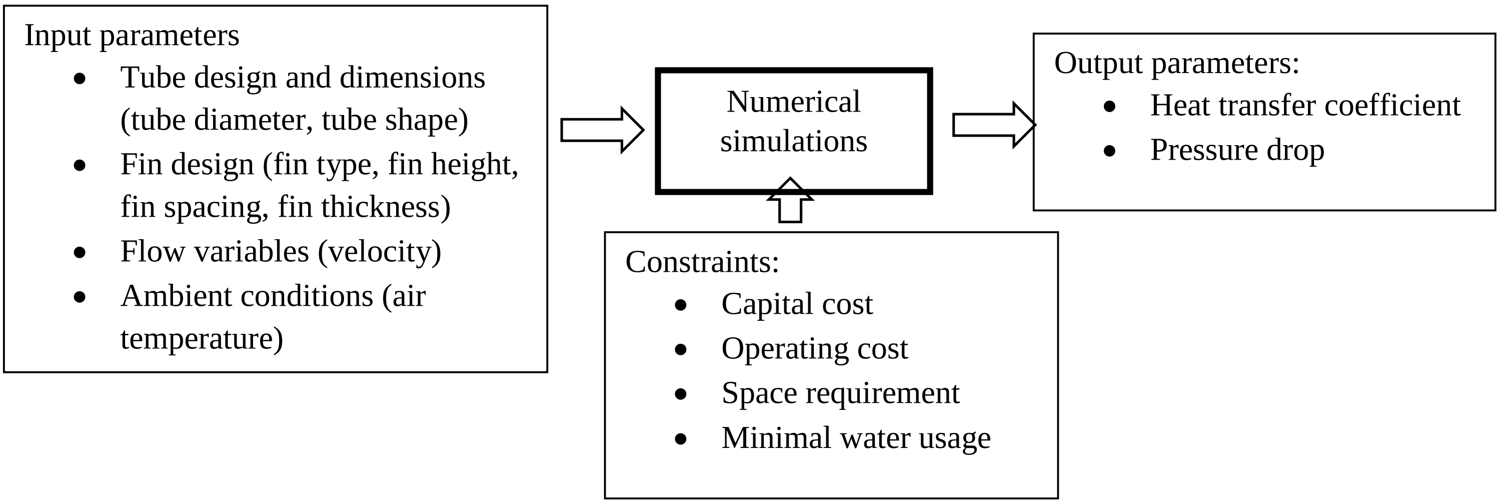

For conventional cooling towers in power plants, the capital cost is around Rs 120 Cr (Data from Paharpur Pvt. Ltd.) for a 600 MW power plant and the operating power required is about 6500 kW. The space requirement is about 12000 m^2 and the water consumption is 4 m^3/h/MW.

For same power plant, for air cooled condenser (currently employed) the capital cost is approximately Rs 150 Cr, operating power required is 14000 kW and space requirement is 18000 m^2 with no water loss.

The basis of design methodology in the present work is to achieve a more economical air cooled condenser design as compared to the conventional cooling towers per MW of the power. If we calculate the costs per MW of heat removal capacity then,

(A) For conventional cooling towers,

Capital cost/MW: 120/600 Cr/MW= Rs 20 lakhs,

Operating cost:

operating power/MW = 6500 kW/600 MW = 11 kW

cost per unit electricity (per kW) = approx. Rs 6 (assumption), therefore, operating cost/MW/day = 6 × 11 × 24 = Rs 1584

Space requirement/MW = 12000/600 = 20 m^2

Therefore, total operational cost for one day = Rs 1584/ MW

For one year (first year of commissioning of plant), the total cost (excluding space) is (capital + operating)= Rs 1584 × 365 + 2000000 = Rs 26 lakhs/MW

(B) For currently employed air cooled condensers,

Capital cost/MW: 150/600 Cr/MW = 25 lakhs/MW.

Operating cost:

operating power/MW = 14000/600 = 23 kW

operating cost/MW/day = 23 × 6 × 24 = Rs 3312

Space requirement/MW = 18000/600 = 30 m^2

Therefore, total operational cost for one day = Rs 3312/MW

For one year (first year of commissioning of plant), the total cost (excluding space) is (capital + operating)= Rs 3312 × 365 + 2500000 = Rs 37 lakhs/MW

From the above discussion, it is clear that air cooled condensers are more costly than conventional cooling towers. Therefore, current objective is to lower the capital and operating costs of the air-cooled condenser to make it competitive with the conventional cooling towers.

So the constraints can be identified as:

Capital cost < Rs 25 lakhs/MW

Operating cost/MW/day < Rs 3000/MW

Space required < 30 m^2

Based on our numerical simulations for one of the cases presented in Chapter 6 (section 6.3.3, circular fin, Re_h = 3500) the input parameters are:

Heat transfer coefficient = 90 W/m^2K

LMTD = 13.98 K,

For 1MW, the heat transfer area required= $Q/h*LMTD$ = 1000000/90*13.98 = 790 m^2.

Heat transfer area of one meter length of the tube= 0.0956 m^2

Total length of the tube = 790/0.0956 = 8300 m.

Based on quotation, the price for 1 m length of the tube= Rs. 300.

Therefore, the total capital cost of the condenser = 250 × 8300 = 20 lakhs

Pumping power/MW = pressure drop × volumetric flow rate = 16 kW /MW.

Operating cost/MW/day = 16 ×24 × 6 =Rs 2304/day/MW

Space required (for A frame) = Length of the tube (10 m) × transverse tube pitch (0.023 m) × number of tubes per row (118) = 27 m^2.

For one year (first year of commissioning of plant), the total cost (excluding space) is (capital + operating) = Rs 2304 × 365 + 2000000 = Rs 28 lakhs/MW

From the calculations presented above, we can conclude that present work proposes a more economical design of the air-cooled condenser as compared to the presently employed air cooled condensers in industry.

Bases on the research carried out in the present work, the design methodology can be generalized as:

Step 1: Identifying the type of location, where air cooled condenser must be placed.

If it is in urban area, then space is important and compact design of the fins (plate fins, chapter 6) are to be used for the numerical simulations.

It it is in rural area, then space becomes cheaper and annular fins are to be used for the numerical simulations.

Step 2: Carry out detailed numerical analysis by varying all the input parameters (fin spacing, fin diameter, tube diameter, number of tube rows, flow variables etc.) and obtain results in terms of heat transfer and pressure drop.

Detailed results have been presented in Chapter 6 and 7 for all the tube and fin designs for a wide range of input parameters.

Step 3: Perform optimization using optimization methodologies (Taguchi method for the present case).

We have found optimum fin spacing = 5 mm, fin height = 5 mm, number of tube rows = 2-4, transverse tube pitch = 3 times the tube diameter (approximately) .

Step 4: After optimization, carry out detailed cost analysis.

The cost analysis should consider the constraints. For the present case, the constraints are, capital cost < 25 lakhs, operating cost < Rs. 3000 /MW/day and space requirement < 30 m^2.

In the present work, we could achieve the optimized results under all constraints.

Incase the results do not satisfy the constraints, we need to change the input parameters.

7.5. Conclusion

The effects of various parameters such as tube type, tube dimensions, fin spacing, fin height, number of tube rows, frontal or inlet velocity, and transverse tube pitch on the thermal-hydraulic performance of the air cooled condenser have been studied in the present work. It has been shown that the elliptical tubes with minimum ellipticity (0.33) performs better in terms of heat transfer per unit pumping power as compared to the other tube designs. Therefore, further studies were performed with the tube with e = 0.33. The heat transfer coefficient increased and the pressure drop decreased with an increase in the fin spacing for various fin heights. A fin spacing of 5 mm was chose to be optimum by comparing the heat transfer performance and the compactness of the condenser. The fin with a height of 5 mm performed better than the fin with larger heights and hence was chosen for further studies. As the row number was varied from 2 to 10, the heat transfer coefficient showed a maxima at $N_r = 4$, and then decreased gradually. The pumping power was highest for largest row number coil; however, less frontal area was required for the largest row number. The transverse tube pitch has been varied from 36.8 mm to 44 mm, and the heat transfer coefficient decreased with an increase in the tube pitch. However, the pressure drop and pumping power also reduced with an increase in the tube pitch. Overall, the tube pitch has to be optimized by taking care of thermal-hydraulic performance and space requirement for the condenser. The fin efficiency was observed to decrease with an increase in the fin spacing and number of tube rows ($N_r > 4$). The fin efficiency depends majorly on the temperature distribution on the fin and also on the variation of average air temperature through the heat exchanger. Taguchi method was applied to optimize the design of the air cooled condenser and it was observed that, number of tube rows is the most important parameter affecting the performance of the condenser, whereas, tube pitch affects the pumping power and compactness, fin height affects the heat transfer per unit pressure drop and surface area required, and fin spacing affects the heat transfer per unit pressure drop only. Overall, based on the results obtained the optimized value of the number of tube rows, fin height, transverse tube pitch and fin spacing is 2-4, 5 mm, 40 mm, and 3-5 mm, respectively. The research work is a progress to understand the hydrodynamic stability of air flow through tube bundles [Lee and Korpella (1983), Joshi et al. (2001), Thorat and Joshi (2004)].

Table 7.8: Effect of different parameters on the output values

Factor		$h/\Delta P$ (W/m^{2}KPa)				Surface area required (m^2)				Pumping power (kW)				*Z/E*			
	level	mi	<mi>	SoS	%effect	mi	<mi>	SoS	%effect	mi	<mi>	SoS	%effect	mi	<mi>	SoS	%effect
	3	34.07				-63.33				-19.76				237.09	240.53		
S	5	56.27	72.65	4777.5	28.18	-61.92	-62.40	1.30	5.53	-18.80	-19.42	0.58	5.54	248.41		93.45	6.76
	10	127.34				-61.95				-19.72				236.10			
	5	123.16				-61.02				-18.92				241.33			
h_f	7	23.29	57.80	6413.61	37.83	-62.88	-62.79	5.94	25.34	-19.40	-19.56	1.08	10.37	249.66	239.83	227.12	16.44
	10	26.95				-64.46				-20.36				228.50			
	2	102.10				-60.49				-21.21				215.90			
N_r	4	95.67	74.91	3469.93	20.04	-60.60	-62.08	14.14	60.04	-18.22	-19.86	4.58	43.75	249.90	234.68	596.82	43.20
	10	26.96				-65.15				-20.14				238.23			
	36.8	67.50				-61.89				-20.91				225.62			
P_t	40	100.71	67.08	2290.35	13.5	-62.24	-62.60	2.04	8.75	-18.37	-19.23	4.23	40.35	255.29	242.45	464.03	33.59
	44	33.03				-63.79				-18.41				246.44			

Chapter 8
Conclusions and recommendations for future work

In the present work, numerical simulations have been performed to study the thermal-hydraulic characteristics of air cooled condenser and optimize its design under forced convection and natural convection conditions. Chapter 2 presented a detailed literature survey and listed many unresolved issues in the literature. In Chapters 4 and 5, studies on the natural convection of air around bare and finned tubes were presented. The main findings from these chapters are:

(1) It was found that the small aspect ratio of the cavity causes the wall-cylinder interaction, which results in a 3D, unstable, oscillatory and complex flow. The merging of the primary recirculating eddies and formation of secondary eddies was observed along the length of the cavity. By performing the 3D numerical simulations, the surface averaged Nusselt number was found to increase by 20% as compared to the 2D numerical simulations performed by Cesini et al. (1999), and by 10 % as compared to the experimental results of Cesini et al., (1999).

(2) From the simulations performed (Cesini et al., (1999), Newport et al., (2001) and present case) in the present work, it can be concluded that the interaction of enclosure walls and cylinder can lead to a 3D, oscillating, and complex fluid flow. Therefore, it can be concluded that the 3D numerical simulations need to be performed to capture the 3D flow phenomenon in natural convection especially in the presence of cylinder-cavity interaction.

(3) It has been found that, with an increase in the fin spacing for a particular fin diameter, the heat transfer coefficient increases due to the separation of the thermal boundary layers between the finned surfaces and formation of horseshoe vortices. However, as the fin spacing is increased beyond a certain value, the heat transfer coefficient decreases due to

the bypass flow stream between the fins. The optimum value of the fin spacing has been found to be 8 mm.

(4) An increase in the fin diameter increases the heat transfer coefficient, however, beyond D_f > 41 mm, the rate of increase in h decreases due to enhanced thermal boundary layer thickness. The heat transfer coefficient increases with an increase in the chimney height and tube surface temperature.

(5) A comparison of tube designs showed that elliptical tube with minimum ellipticity (0.5) performs better than the other elliptical and circular tubes in terms of heat transfer coefficient.

Chapter 6 represented a comparison of thermal hydraulic performance of various fins (Plain circular, plate, serrated, crimped and wavy). The main conclusion from this study are:

(1) Serrated fin provides highest heat transfer coefficient (12-16% higher than plain annular fin and 40-45% higher than plain plate fin) as compared to the other fins and crimped fin provides the second highest heat transfer coefficient. However, plain circular fin provides the maximum heat transfer per unit pumping power as compared to other fins.

(2) With an increase in the frontal velocity from 4.76 m/s to 6.32 m/s, the heat transfer coefficient and pressure drop increases for all the fins, however the heat transfer per unit pumping power decreases.

(3) In terms of the compactness of the heat exchanger, it was observed that a more compact heat exchanger can be designed using plain circular fin as compared to the other fins.

(4) Serrated fin showed a maximum fin efficiency of 80-82%, and the wavy fin showed the worst fin efficiency (53%) as compared to other fins. As the frontal velocity was increased, the efficiency decreased.

After a comparison of various fins, an optimization of the air cooled condenser design was performed using elliptical tubes with plain annular fins. 3D numerical simulations were performed and the effects of fin spacing, fin diameter, transverse tube pitch, Reynolds number and number of tube rows were studied. These results have been presented in Chapter 7, and the main findings are listed below:

(1) Elliptical tubes with minimum ellipticity (0.5) performs better in terms of heat transfer per unit pumping power as compared to the other tube designs.

(2) A fin spacing of 5 mm was chosen to be optimum by comparing the heat transfer performance and the compactness of the condenser. The fin with a height of 5 mm performed better than the fin with larger heights and hence was chosen for further studies.

(3) As the row number was varied from 2 to 10, the heat transfer coefficient showed a maxima at $N_r = 4$, and then decreased gradually. The pumping power was highest for largest row number coil; however, less frontal area was required for the largest row number.

(4) The fin efficiency was observed to decrease with an increase in the fin spacing and number of tube rows ($N_r > 4$). The fin efficiency was found to depend mainly on the temperature distribution on the fin and on the variation of average air temperature through the heat exchanger.

(5) Based on the results obtained the optimized value of the number of tube rows, fin height, transverse tube pitch and fin spacing is 2-4, 5 mm, 40 mm, and 3-5 mm, respectively.

Recommendations for future work

In the second chapter of literature survey, the gap areas and the recommendation for the future work were mentioned. In the present work, some of the gap areas and recommendations have been addressed. For example, an optimization of the air cooled condenser has been performed by considering all the design parameters and output parameters. The thermal-hydraulic performance of the condenser has been optimized along with the compactness of the condenser and hence all the costs associated (capital, operating and space requirement) have been taken care of in the present work.

The natural convection around finned-tube heat exchangers under a chimney has been studied in the present work, which has not been studied in the past by other researchers. Also, we showed a significant difference between the results of 2D numerical simulations and 3D numerical simulations for the natural convection of air. Which shows that natural convection is multidimensional in nature and hence requires a 3D treatment of the problem.

However, there is some scope remains for the future work and can be stated as:

(1) From the discussion in Section 2.4.2 and 2.4.3, it is clear that the estimation of heat loss in the published literature has been addressed using two types of approaches: (1) development of empirical correlations and (2) use of CFD. The latter approach permits the understanding of physics of the system through the insights in (a) fluid mechanics and (b) the relationship between the fluid mechanics and design objectives such as heat losses. Secondly, during the past 25 years, CFD is being increasingly used because of the development in computational power as well as numerical techniques. Joshi and Ranade (2003) have given an overview of opportunities and scope of CFD. Ranade et al. (1989, 1990, 1992), Murthy et al. (2008), Ekambra et al. (2005), and Joshi et al. (2011a, 2011b) have given the details pertaining to governing equation, method of solution and appropriate precautions for the implementation of CFD. Further, some examples of relationship between the fluid mechanics and design objectives have been described in the published literature. For instance, heat transfer [Thakre et al. (1999)], mixing [Patwardhan and Joshi (1999), Nere

et al. (2003), Kumaresan and Joshi (2006), Joshi and Sharma (1978), Joshi and Shah (1981)], solid suspension [Rao et al. (1988), Rewatkar and Joshi (1991), Murthy et al. (2007)] and the rate of gas induction [Murthy et al. (2007), Joshi and Sharma (1977)]. Similar methodology needs to be employed in the future work for the estimation of heat losses and pressure drop. In particular, LES (and if possible DNS) simulations need to be undertaken for developing better insight.

(2) For better understanding of transport phenomenon, the future work should include the identification and dynamics of flow structures. [Joshi and Sharma (1976), Shnip et al. (1992), Thorat et al. (1998, 2004), Kulkarni et al. (2001, 2007), Bhole et al. (2008), Joshi et al. (2009), and Mathpati et al. (2009). Additional work is also needed to understand the relationship between the structure dynamics and heat transfer as well as pressure drop.

(3) For crimped and serrated fins, only few numerical studies have been performed. These fins generate 3D vortices and enhances turbulence in the flow. Thus the understanding of 3D flow patterns is very important in order to design an optimum fin. Therefore, more 3D numerical simulations are required for these types of fins.

(4) In the heat exchangers, a combination of fins can be used and the combinations of the fins can be optimized by analyzing the flow structure and dynamics in the heat exchangers. For that purpose 3D numerical simulations are still needed, so far, only one has been reported by Tang et al. (2009b), which considered a combination of VGs and the slit fins. More combinations of this sort can be studied for the practical purpose.

(5) The natural convection studies can be extended to big chimney and larger size of the condenser. However, it takes large computational time and a lot of efforts in the modeling part. Therefore, it is recommended to find a efficient way of performing numerical

simulations for larger heat removal capacity. The use of periodic boundary condition is one of the possible ways.

(6) In the present work, the overall enhancement in the thermal-hydraulic performance has ben observed in the range of 30-40% over currently used design of air cooled condenser. More innovative methods should be discovered for a drastic improvement in the design (brining the overall cost of air cooled condenser down by 70-80%).

Nomenclature

A	Total outside heat transfer surface area (m^2)
AR	Aspect ratio (2b/c) for delta winglet and W/D for cavity
A_c	minimum flow area (m^2)
A_{fr}	frontal area (m^2)
a	Elliptical tube major axes (mm)
b	Elliptical tube minor axes (mm)
B	Winglet span (mm)
C	Winglet chord length (mm)
C_p	Specific heat (KJ Kg^{-1} K^{-1})
D	tube outer diameter (mm)
D_f	fin tip diameter (mm)
D_h	heat exchanger hydraulic diameter ($4*A_c/P_w$) (mm)
e	tube ellipticity (b/a)

g_s Segment gap (mm)

f friction factor $\left(\frac{2\Delta P D_h}{L\rho U_{fr}^2}\right)$ or $\left(\frac{2\Delta P A_c\,\sigma^2}{A\rho U_{fr}^2}\right)$

h heat transfer coefficient (W m^{-2} K^{-1})

h_l length averaged heat transfer coefficient (W m^{-2} K^{-1})

h_θ circumferential averaged heat transfer coefficient (W m^{-2} K^{-1})

h_l^* normalized length averaged heat transfer coefficient

h_{avg} Surface averaged heat transfer coefficient(W m^{-2} K^{-1}).

h^* Dimensionless heat transfer coefficient (h/h_{max})

h_{max} Maximum value of the heat transfer coefficient at a particular surface temperature for fixed fin spacing and diameter (W m^{-2} K^{-1})

H^* distance between the top wall and cylinder upper surface (mm)

H height of the box (mm) or chimney height (mm)

g acceleration due to gravity (m/s^2)

h_s height of the segment (mm)

j Colburn factor $\left(\frac{Nu}{RePr^{\frac{1}{3}}}\right)$

j_m Mass transfer coefficient

k Thermal conductivity (W m^{-1}K^{-1})

L Length of the coil (or array length) (mm) or length of the box incase of cavity

l length of the cylinder (mm)

L_{pf} Length of the plate fin (mm)

NTU Number of transfer units

n	infinitesimal distance in the vicinity of the wall (mm)
N_r	Number of tube rows
Nu	local Nusselt number
Nu_l	length averaged Nusselt number
Nu_θ	circumferential averaged Nusselt number
Nu_l^*	normalized length averaged Nusselt number (Nu_l / Nu_{lo})
Nu_{lo}	length averaged Nusselt number at the lower stagnation point of cylinder when $H^*/D = 1$.
Nu_{avg}	Surface averaged Nusselt number.
ΔP	Pressure drop (Pa)
P_w	Wetted perimeter
Pr	Prandtl number$\left(\frac{C_p\mu}{k}\right)$
Q	Heat flux (W)
Ra	Rayleigh number, $Ra = \left(\frac{g\beta\Delta T D^3}{\nu\alpha}\right)$
Re	Reynolds number based on tube outer diameter and air maximum velocity$\left(\frac{\rho U_{max}D}{\mu}\right)$
Re_a	Reynolds number based on array length $\left(\frac{\rho U_{max}L}{\mu}\right)$
Re_c	Reynolds number based on tube collar diameter and air maximum velocity$\left(\frac{\rho U_{max}D_c}{\mu}\right)$

Re_{fr}	Reynolds number based on tube outer diameter and air frontal velocity $\left(\frac{\rho U_{fr} D_h}{\mu}\right)$
Re_h	Reynolds number based on hydraulic diameter $\left(\frac{\rho U_{max} D_h}{\mu}\right)$
Re_{lw}	Reynolds number based on the length of the winglet
Re_p	Reynolds number based on tube perimeter $\left(\frac{\rho U_{max} D_h}{\mu}\right)$ (Jang and Yang, 1998)
S	fin spacing (mm)
S_f	fin pitch (mm)
S_l	Longitudinal tube pitch (mm)
S_t	Transverse tube pitch (mm)
t_f	fin thickness (mm)
T	Temperature (K)
T_a	Average air temperature (K)
T_b	Average tube base temperature (at the outer surface) (K)
T^*	Dimensionless fluid temperature (T/T_{max})
T_{max}	Maximum fluid temperature at a particular surface temperature for fixed fin spacing and diameter (K)
T_{in}	air temperature at the inlet (K)
T_{out}	air temperature at the outlet (K)
T_{tube}	temperature of the tube (K)
$T_{ceiling}$	temperature of the ceiling (K)
$T_{cylinder}$	temperature of the cylinder (K)
u	Mean velocity (m s^{-1})

U_{fr}	Air frontal velocity (m s^{-1})
u_{max}	Maximum air velocity in the narrows finned space (m s^{-1})
W	width of the box (mm)
W_{pf}	Width of the plate fin (mm)
W_s	Segment width (mm)
x	spatial coordinate (m)

Greek symbols

α	thermal diffusivity (m^2 s^{-1})
$\boldsymbol{\beta}$	thermal expansion coefficient (K^{-1})
$\boldsymbol{\delta}$	Dimensionless temperature $\left(\frac{T-T_{ceiling}}{T_{cylinder}-T_{ceiling}}\right)$
$\boldsymbol{\upsilon}$	kinematic viscosity (m^2 s^{-1})
$\boldsymbol{\rho}$	density of fluid (kg m^{-3})
$\boldsymbol{\theta}$	angle along the surface of the cylinder in degrees (zero at the top)

Bibliography

Ay H, Jang J Y and Yeh J N 2002 Local heat transfer measurements of plate finned-tube heat exchangers by infrared thermography Int J Heat Mass Transf 45: 4069–4078

Atmane M A, Chan V S S and Murray D B 2003 Natural convection around a horizontal heated cylinder: The effects of vertical confinement. Int. J. Heat Mass Transf. 46: 3661–3672.

Arora A, subbarao P M V and Agarwal R S 2015 Numerical optimization of location of ‘common flow up’ delta winglets for inline aligned finned tube heat exchanger. Appl. Therm. Eng. 82: 329-340.

Ashjaee M, Yazdani S, Bigham S and Yousefi T 2012 Experimental and numerical investigation on free convection from a horizontal cylinder located above an adiabatic surface. Heat Transf. Eng. 33: 213–224.

Aziz A and Kraus A D 1996 Optimum Design of Radiating and Convecting-Radiating Fins, Heat Transfer Eng. 17: 44–78.

Badr H M 1994 Mixed convection from a straight isothermal tube of elliptic cross section. . Int. J. Heat Mass Transf. 37 (15): 2343-2365

Banerjee R K, Karve M, Ha J H and Hwan D 2012 Evaluation of enhanced heat transfer within a four row finned tube array of an air cooled steam condenser. Numer. Heat Transf. Part A: Appl. 61: 735–753

Beecher D T and Fagan T J 1987 Effects of fin pattern on the air-side heat trasnfer coefficient in plate finned-tube heat exchangers. ASHRAE Trans. 93 (2): 1961-1984

Bettanini E 1970 Simulataneuos heat and mass transfer on a vertical surface. Int. Inst. Refrig. Bull. 70 (1): 309-317

Bhole M R, Joshi J B and Ramkrishna D 2008 CFD simulation of bubble columns incorporating population balance modelling. Chem. Eng. Sci. 63: 2267-2282

Biswas G, Mitra N K and Fiebig M 1994 Heat transfer enhancement in fin-tube heat exchangers by winglet type vortex generators. Int. J. Heat Mass Transf. 37: 283–291

Brauer H 1964 Compact heat exchangers. Chem. Process Eng. 45 (8): 451-460

Briggs D E and Young E H 1963 Convection heat transfer and pressure drop of air flowing across triangular pitch banks of finned tubes. Chem. Eng. Prog. Symp. Ser. 59 (41): 1-10

Brockmeier U, Guentermann T and Fiebig M 1993 Performance evaluation of a vortex generator heat transfer surface and comparison with different high performance surfaces Int. J. Heat Mass Transf. 36: 2575–2587

Butler C, Newport S and Geron M 2013 Natural convection experiments on a heated horizontal cylinder in a differentially heated square cavity. Exp. Therm. Fluid Sci. 44: 199–208.

Cesini G, Paroncini M and Cortella M 1999 Natural convection from a horizontal cylinder in a rectangular cavity. Int. J. Heat Mass Transf. 42: 1801–1811.

Chao B and Fagbenle R 1974 On merk's method of calculating boundary layer transfer. Int. J. Heat Mass Transf. 17: 223-240

Chee K K, Wong M K and Lee H K 1996 Optimization of microwave-assisted solvent extraction of polycyclic aromatic hydrocarbons in marine sediments using a microwave extraction system with high-performance liquid chromatography-fluorescence detection and gas chromatography-mass spectrometry. J. Chromatogr. A. 723: 259-271.

Chen H T and Hsu W L 2008 Estimation of heat-transfer characteristics on a vertical annular circular fin of finned-tube heat exchangers in forced convection. Int. J. Heat Mass Transf. 51: 1920–1932

Chen H T and Chou J C 2006 Investigation of natural-convection heat transfer coefficient on a vertical square fin of finned-tube heat exchangers. Int. J. Heat Mass Transf. 49: 3034–3044

Chen H T and Hsu W L 2007 Estimation of heat transfer coefficient on the fin of annular-finned tube heat exchangers in natural convection for various fin spacings. Int. J. Heat Mass Transf. 50: 1750–1761.

Chen H T and Lai J R 2012 Study of heat-transfer characteristics on the fin of two-row plate finned-tube heat exchangers. Int. J. Heat Mass Transf. 55: 4088–4095

Chen H T, Chou J C and Wang H C 2007 Estimation of heat transfer coefficient on the vertical plate fin of finned-tube heat exchangers for various air speeds and fin spacings. Int. J. Heat Mass Transf. 50: 45–57

Chen H T, Song J P and Wang Y T 2005 Prediction of heat transfer coefficient on the fin inside one-tube plate finned-tube heat exchangers. Int. J. Heat Mass Transf. 48: 2697–2707

Chen Y Fiebig M Mitra N 1998a Conjugate heat transfer of a finned oval tube with a punched longitudinal vortex generator in form of a delta winglet: parametric investigations of the winglet. Int. J. Heat Mass Transf. 41: 3961-3978

Chen Y, Fiebig M and Mitra N 1998b Heat transfer enhancement of a finned oval tube with punched longitudinal vortex generators inline. Int. J. Heat Mass Transf. 41: 3040-3055

Chen Y, Fiebig M and Mitra N 2000 Heat transfer enhancement of finned oval tubes with staggered punched longitudinal vortex generators. Int. J. Heat Mass Transf. 43: 417-435

Cheng Y P, Lee T S and Low H T 2007 Numerical Analysis of Periodically Developed Fluid Flow and Heat Transfer Characteristics in the Triangular Wavy Fin-and-Tube Heat Exchanger Based on Field Synergy Principle. Numer. Heat Transf. Part A: Appl. 53 821–842

Cheng Y P, Lee T S and Low H T 2009 Numerical prediction of periodically developed fluid flow and heat transfer characteristics in the sinusoid wavy fin-and-tube heat exchanger. Int. J. Numer. Methods Heat Fluid Flow 19: 728–74

Cheng Y P, Qu Z G, Tao W Q and He Y L 2004 Numerical design of efficient slotted fin surface based on the field synergy principle. Numer. Heat Transf. Part A: Appl. 45: 517–538

Choi J M, Kim Y, Lee M and Kim Y 2010 Air side heat transfer coefficients of discrete plate finned-tube heat exchangers with large fin pitch. Appl. Therm. Eng. 30: 174–180

Chokeman Y and Wongwises S 2005 Effect of fin pattern on the air side performance of herringbone wavy fin-and-tube heat exchangers. Heat Mass Transf. 41: 642–650

Churchill S W and Chu S S 1975 Correlating Equations for Laminar and Turbulent Free Convection from Horizontal Cylinder c 18: 1049-1053.

Colburn A P 1942 Heat transfer by natural and forced convection. Eng. Bull. Purdue Univ. Res. Ser. 26 (84): 47–50.

Crow S C 1970 Stability theory for a pair of trailing vortices. AIAA J. 8: 2172-2179

Dasgupta K, Sen D, Mazumder S, Basak C B, Joshi J B and Banerjee S, Optimization of parameters by Taguchi method for controlling purity of carbon nanotubes in chemical vapour deposition technique. J. Nanosci. Nanotechnol. 10: 4030-4037.

Dejong N C and Jacobi A M 1997 An experimental study of flow and heat transfer in parallel-plate arrays: local, row-by-row and surface average behavior. Int. J. Heat mass Transf. 40: 1365-1378

Dogan A, Akkus S and Baskaya S 2012 Numerical analysis of natural convection heat transfer from annular fins on a horizontal cylinder. J. Therm. Sci. Tech. 32 (2): 31-41.

Dhotre M T and Joshi J B 2004 CFD Simulation of heat transfer in turbulent pipe flows. Indus. Eng. Chem. Res. 43: 2816-2829.

Ding H, Shu C, Yeo K S and Lu Z L 2005 Simulations of natural convection in eccentric annuli between a square outer cylinder and a circular inner cylinder using local Mq-Dq method. Num. Heat Transf., Part A: Appl. 47: 291–313.

Doodman A R, Fesanghary M and R. Hosseini, A robust stochastic approach for design optimization of air cooled heat exchangers, Appl. Energy 86 (2009) 1240-1245.

Du Y J and Wang C C 2000 An experimental study of the airside performance of the superslit fin-and-tube heat exchangers. Int. J. Heat Mass Transf. 43: 4475–4482

Eckels P W and Rabas T J 1987 Dehumidification: on the correlation of wet and dry transport processes in plate finned-tube heat exchangers. J. Heat Trasnf. 109: 575-582

Ekambara K, Dhotre M T and Joshi J B 2005 CFD simulations of bubble column reactors: 1D, 2D and 3D appraoch. Chem. Eng. Sci. 60: 6733-6746

Elmahdy A H 1975 Analytical and experimental multi-row, finned-tube heat exchanger performance during cooling and dehumidification process. Ph.D thesis, Mech. Eng. Dept., Carleton Univ., Ottawa, Canada

Elmahdy A H and Biggs R C 1979 Finned Tube Heat Exchanger: Correlation of Dry Surface Heat Transfer Data. ASHRAE Trans. 85(2): 262-273

ElSherbini A I and Jacobi A M 2002 The thermal-hydraulic impact of delta-wing vortex generators on the performance of a plain-fin-and-tube heat exchanger. HVAC&R Research 8 (4): 357-370

Erek A, Özerdem B, Bilir L and İlken Z 2005 Effect of geometrical parameters on heat transfer and pressure drop characteristics of plate fin and tube heat exchangers. Appl. Therm. Eng. 25: 2421–2431

Farhadi F, Davani N and Ardalan P 2005 New correlation for natural convection of finned tube A-type air cooler. Appl. Therm. Eng. 25: 3053–3066.

Fiebig M 1998 Vortices, generators and heat transfer. Inst. Chem. Engrs. Trans. IChemE 76: 108-122

Fiebig M, Chen Y, Grosse-Gorgemann A and Mitra N K, 1995 Numerical analysis of heat transfer and flow loss in a parallel plate heat exchanger element with longitudinal vortex generators as fins. J. Heat Transf. Trans. ASME 117: 1064-1067

Fiebig M, Valencia A and Mitra N K 1993 Wing-type vortex generators for fin-and-tube heat exchangers. Exp. Therm. Fluid Sci. 7: 287–295

Fiebig M, Valencia A and Mitra N K 1994 Local heat transfer and flow losses in fin-and-tube heat exchangers with vortex generators: a comparison of round and flat tubes. Exp. Therm. Fluid Sci. 8: 35-45

Ganapathy V 2003 Industrial boilers and heat recovery steam generators: design, applications and calculations. Marcel Dekker

Gandhi M S, Sathe M J, Joshi J B and Vijayan P K 2011 Two phase natural convection: CFD simulations and PIV measurements. Chem. Eng. Sci. 66: 3152-3171.

Gandhi M S, Sathe M J, Joshi J B and Vijayan P K 2013 Study of two phase thermal stratification in cylindrical vessels CFD simulations and PIV measurements. Chem. Eng. Sci. 98: 125-151.

Gandhi M S, Sathe M J, Joshi J B and Vijayan P K 2013 Reduction in thermal stratification in two phase natural convection in rectangular tanks CFD simulations and PIV measurements. Chem. Eng. Sci. 100: 300-325.

Ganguli A A, Gudekar A S, Pandit A B and Joshi J B 2009 CFD Simulation of Heat Transfer in a Two-Dimensional Vertical Enclosure. Trans. Inst. Chem. Engs. (U.K.).-A: Chem. Eng. Res. Des. 87: 711-727.

Ganguli A A, Gudekar A S, Pandit A B and Joshi J B 2012 A novel method to improve the efficiency of a cooking device via thermal insulation. Can. J. Chem. Eng. 90: 1212-1223.

Geuzaine C and Remacle J F 2009 Gmsh: a three-dimensional finite element mesh generator with built-in pre- and post-processing facilities. Int. J. Num. Method. Eng. 79 (11): 1309-1331.

Ghasemi E, Soleimani S and Bararnia H 2012 Natural convection between a circular enclosure and an elliptic cylinder using control volume based finite element method. Int. Comm. Heat Mass Transf. 39: 1035–1044.

Gray D L and Webb R L 1986 Heat transfer and friction correlations for plate fin-and-tube heat exchangers having plain fins, in: Proc. Eighth Int. Heat Transf. Conf., San Francisco, California 6: 2745–2750

Guillory J and McQuiston F 1973 An experimental investigation of air dehumidification in a parallel plate. ASHRAE Trans. 79 (2): 146-151

Hahne E and Zhu D 1994 Natural convection heat trasnfer on finned tubes in air, Int. J. Heat Mass Transfer 37: 59-63.

Hatami M, Ganji D D and Gorji-Bandpy M 2015 Experimental and numerical analysis of the optimized finned-tube heat exchanger for OM314 diesel exhaust exergy recovery. Energy Convers. Manage. 97: 26-41.

Harraez J V and Belda R 2002 A study of free convection in air around horizontal cylinder of different diameters based on holographic interferometry. Temperature field equations and heat transfer coefficients. Int. J. Therm. Sci. 41: 261-267.

Hashizume K, Morikawa R, Koyama T and Matsue T 2002 Fin efficiency of serrated fins. Heat Transf. Eng. 23: 6–14

He Y L, Tao W Q, Song F Q and Zhang W 2005 Three-dimensional numerical study of heat transfer characteristics of plain plate fin-and-tube heat exchangers from view point of field synergy principle. Int. J. Heat Fluid Flow 26: 459–473

Hu X and Jacobi A M 1993 Local heat transfer behavior and its impact on a single-row annularly finned tube heat exchanger. Trans. ASME 115: 66-74

Huang C H, Yuan I C and Ay H 2003 A three-dimensional inverse problem in imaging the local heat transfer coefficients for plate finned-tube heat exchangers. Int. J. Heat Mass Transf. 46 3629–3638

Huang C H, Yuan I C and Ay H 2009 An experimental study in determining the local heat transfer coefficients for the plate finned-tube heat exchangers. Int. J. Heat Mass Transf. 52: 4883–4893

Hussain S H and Hussein A K 2010 Numerical investigation of natural convection phenomena in a uniformly heated circular cylinder immersed in square enclosure filled with air at different vertical locations. Int. Comm. Heat Mass Transf. 37: 1115–1126.

Ibrahim T A and Gomaa A 2009 Thermal performance criteria of elliptic tube bundle in crossflow. Int. J. Therm. Sci. 48: 2148–2158

Idem S A, Jacobi A M and Goldchmidt V M 1990 Heat transfer characterization of a finned-tube heat exchanger (with and without condensation). Trans. ASME 112: 64-70

Idem S A, Jacobi A M and Goldchmidt V M 1993 Sensible and latent heat transfer to a baffled finned-tube heat exchanger. Heat Transfer Eng. 14 (3): 26-35

Ishiguro H, Nagata S, Yabe A and Nariai H 1991 Augmentation of forced-convection heat transfer by applying electric fields to disturb flow near a wall. ASME J. 3: 25–31

Jacobi A M and Goldschmidt V W 1990 Low Reynolds number heat and mass transfer measurements of an overall counterflow, baffled, finned-tube, condensing heat exchanger. Int. J. Heat Mass Trasnf. 33 (4): 755-765

Jacobi A M and Shah R K 1995 Heat transfer surface enhancement through the use of longitudinal vortices: A review of recent progress. Exp. Therm. Fluid Sci. 11: 295–30

Jakob M 1938 Heat transfer and flow resistance in cross flow of gases over tube banks. Trans. ASME 60: 384–386

Jang J Y and Yang J Y 1998 Experimental and 3d numerical analysis of the thermal-hydraulic characteristics of elliptic finned-tube heat exchangers. Heat Trasnf. Eng. 19 (4): 55-67

Jin W W, He Y L, Qu Z G, Zhang C C and Tao W Q 2006 Optimum design of two-row slotted fin surface with x-shape strip arrangement positioned by “front coarse and rear dense” principle part ii: results and discussion. Numer. Heat Transf. Part A Appl. 50: 751–771

Joshi J B and Sharma M M 1976 Mass transfer characteristics of horizontal sparged contactors, Trans. Instn. Chem. Engrs. 54: 42-43.

Joshi J B and Sharma M M 1978 Liquid phase backmixing in sparged contactors. Can. J. Chem. Eng. 56: 116-119.

Joshi J B 1980 Axial mixing in multiphase in multiphase contactors- a unified correlation, Trans. Instn. Chem. Engrs. 58: 155-165.

Joshi J B, Dinkar M, Deshpande N S and Phanikumar D V 2001 Hydrodynamic Stability of Multiphase Reactors, Advanc. Chem. Eng. 26: 1-130.

Joshi J B and Shah Y T 1981 Hydrodynamic and mixing models for bubble column reactors, Chem. Eng. Commun. 11: 165-199.

Joardar A and Jacobi A M 2008 Heat transfer enhancement by winglet-type vortex generator arrays in compact plain-fin-and-tube heat exchangers. Int. J. Refrig. 31: 87–9

Joshi J B and Ranade V V 2003 Computational fluid dynamics for desiging process eqiupment expectations, current status and path forward. Ind. Eng. Chem. Res. 42: 1115-1128

Joshi J B, Sharma M M, Shah Y T, Singh C P P, Ally M and Klinzing G F 1980 Heat transfer in multiphase contactors. Chem. Eng. Comm. 6: 257-271.

Joshi J B and Shah Y T 1981 Gas-liquid solid reactor design. Proc. Eng. Found. Conf. Mah. RSH and Sieder, W.D. Eds., A. I. Ch. E. J. 277-333

Joshi J B and Ranade V V 2003 Computational fluid dynamics for designing process equipment: expectations, current Status and path forward. Indus. Eng. Chem. Res. 42: 1115-1128.

Joshi J B and Sharma M M 1977 Mass transfer and hydrodynamic characteristics of gas inducing type of agitated contactors. Can. J. Chem. Eng. 55: 683-695

Joshi J B and Sharma M M 1978 Liquid phase backmixing in sparged contactors. Can. J. Chem. Eng. 56: 116-119

Joshi J B, Nere N K, Rane C V, Murthy B N, Mathpati C S, Patwardhan A W and Ranade V V 2011 CFD simulations of stirred tanks: comparison of turbulence models, Part I: radial flow impellers. Can. J. Chem. Eng. 89: 23-82

Joshi J B, Nere N K, Rane C V, Murthy B N, Mathpati C S, Patwardhan A W and Ranade V V 2011 CFD simulations of stirred tanks: comparison of turbulence models, Part II: axial flow impellers, multiple impellers and multiphase dispersions. Can. J. Chem. Eng. 89: 754-816

Joshi J B, Tabib M V, Deshpande S S and Mathpati C S 2009 Dynamics of flow structures and transport phenomena-1: Experimental and numerical techniques for identification and energy content of flow structures. Ind. Eng. Chem. Res. 48: 8244-8284

Joshi J.B and Sharma M.M 1976 Mass transfer characteristics of horizontal sparged contactors. Trans. Instn. Chem. Engrs. UK 54: 42-53

Kang H C and Kim M H 1999 Effect of strip location on the air-side pressure drop and heat transfer in strip fin-and-tube heat exchanger. Int. J. Refrig. 22: 302–312

Kang H J, Li W, Li H J, Xin R C and Tao W Q 1994 Experimental study on heat transfer and pressure drop characteristics of four types of plate fin-and-tube heat exchanger surfaces. J. Therm. Sci. 3: 34–42

Kannan K, Vinod V, Padmakumar G, Rudramoorthy R and Rajan K K, Effect of geometric factors on performance of a sodium to air heat exchanger in a fast reactor. Ann. Nucl. Energ. 75: 428-437.

Kashani A H A, Maddhai A and Hajabdollahi H 2013 Thermal-economic optimization of an air-cooled heat exchanger unit. Appl. Therm. Eng. 54: 43-55.

Katsuki R, Shioyama T, Iwaki C and Yanazawa T 2015 Study on free convection heat transfer in a finned-tube array. Int. J. Air Cond. Refrig. doi: 10.1142/S2010132515500078.

Kawaguchi K, Okui K and Kashi T 2004 The heat transfer and pressure drop characteristics of finned tube banks in forced convection (comparison of the pressure drop characteristics of spiral fins and serrated fins). Heat Transf. Res. 33: 431–444

Kayansayan, N 1993 Heat transfer characterization of flat plain fins and round tube heat exchangers. Exp. Therm. Fluid Sci. 6: 263-272

Kayansayan N 1993 Thermal characteristics of fin-and-tube heat exchanger cooled by natural convection. Exp. Therm. Fluid Sci. 7: 177–188.

Kays W M and London A L 1950 Heat-transfer and flow-friction characteristics of some compact heat-exchanger surfaces. Trans. ASME 72: 1087–1097.

Kays W M and London A L 1955 Compact heat exchangers, second edition, McGraw Hill 7- 224

Kim N H, Youn B and Webb R L 1999 Air-side heat transfer and friction correlation for plain fin and tube heat exchangers with staggered tube ar- rangements. J. Heat Transfer. 121: 662-667.

Koizumi H and Hosokawa I 1996 Chaotic behavior and heat transfer performance of tlhe natural convection around a hot horizontal cylinder affected by a flat ceiling. Int. J. Heat Mass Transf. 39 (5): 1081–1091.

Kreith F and Bohn M S 1993 Principles of Heat Transfer, fifth ed., New York, West Publishing Co.

Korzen A and Taler D 2015 Modeling of transient response of a plate fin and tube heat exchanger. Int. J. Therm. Sci. 92: 188-198.

Kulacki FA 1983 In: Augmentation of low reynolds number forced convection channel flow by electro- static discharge, in low Reynolds number flow heat exchangers, S Kakac [(ed.)], Washington, Hemisphere, 753–782

Kulkarni A A, Joshi J B, Ravikumar V and Kulkarni B D 2001 Application of multi-resolution analysis for simultaneous measurement of gas and liquid velocities and fractional gas hold-up in bubble column using LDA. Chem. Eng. Sci. 56: 5037-5048

Kulkarni A A, Ekambara K and Joshi J B 2007 On the development of flow pattern in a bubble column reactor: experiments and CFD. Chem. Eng. Sci. 62: 1049-1079.

Kumaresan T and Joshi J B 2006 Effect of impeller design on the flow pattern and mixing in stirred tanks. Chem. Eng. J. 115: 173-193

Kuvannarat T, Wang C C and Wongwises S 2006 Effect of fin thickness on the air-side performance of wavy fin-and-tube heat exchangers under dehumidifying conditions. Int. J. Heat Mass Transf. 49: 2587–2596

Kwak K M, Torii K and Nishino K 2005 Simultaneous heat transfer enhancement and pressure loss reduction for finned-tube bundles with the first or two transverse rows of built-in winglets. Exp. Therm. Fluid Sci. 29: 625–632

Kwak K, Torii K and Nishino K 2002 Heat transfer and flow characteristics of fin-tube bundles with and without winglet-type vortex generators. Exp. Fluids 33: 696–702

Kwak K, Torii K and Nishino K 2003 Heat transfer and pressure loss penalty for the number of tube rows of staggered finned-tube bundles with a single transverse row of winglets. Int. J. Heat Mass Transf. 43: 417-435

Kumar A, Joshi J B, Nayak A K and Vijayan P K 2014 3D CFD simulation of air cooled condenser-I: Natural convection over a circular cylinder. Int. J. Heat Mass Transf. 78: 1265-1283.

Kumar A, Joshi J B, Nayak A K and Vijayan P K 2015a A review on the thermal-hydraulic characteristics of air cooled heat exchangers in forced covnection. Sadhana 40 (3): 673-655.

Kumar A, Joshi J B, Nayak A K and Vijayan P K 2015b 3D CFD simulation of air cooled condenser-II: Natural draft around a single finned tube kept in a small chimney. Int. J. Heat Mass Transf. 78: 1265-1283.

Lee J M, Ha M Y and Yoon H S 2010 Natural convection in a square enclosure with a circular cylinder at different horizontal and diagonal locations. Int. J. Heat Mass Transf. 53: 5905–5919.

Lee Y and Korpela S A 1983 Multicellular natural convection in a vertical slot.J. Fluid Mech. 126: 91-121.

Lemouedda A, Schmid A, Franz E, Breuer M and Delgad A 2011 Numerical investigations for the optimization of serrated finned-tube heat exchangers. Appl. Therm. Eng. 31: 1393–1401

Lin C W and Jang J Y 2005 3D Numerical heat transfer and fluid flow analysis in plate-fin and tube heat exchangers with electrohydrodynamic enhancement. Heat Mass Transf. 41: 583–593

Liu Y C, Wongwises S, Chang W J and Wang C C 2010 Airside performance of fin-and-tube heat exchangers in dehumidifying conditions – Data with larger diameter. Int. J. Heat Mass Transf. 53: 1603–1608

London A L and Ferguson C K 1949 Test results of high-performance heat-exchanger surfaces used in aircraft intercoolers and their significance for gas-turbine regenerator design. Trans. ASME 71: 17–26

Lopata S and Oclon P 2015 Numerical study of the effect of fouling on local heat transfer conditions in a high-temperature fin-and-tube heat exchanger. Energy ISSN 0360-5442, http://dx.doi.org/10.1016/j.energy.2015.03.048.

Ma Y, Yuan Y, Liu Y, Hu X and Huang Y 2012 Experimental investigation of heat transfer and pressure drop in serrated finned tube banks with staggered layouts. Appl. Therm. Eng. 37: 314–323

Manassaldi J I, Scenna N J and Mussati S F 2014 ptimization mathematical model for the detailed design of air cooled heat exchangers. Energy 64: 734–746.

Madi MA, Johns RA and Heikal MR 1998 Performance characteristics correlation for round tube and plate finned heat exchangers. Int. J. Refrig. 21 (7): 507–517

Martinez E, Vicente W, Soto G, and Salinas M 2010 Comparative analysis of heat transfer and pressure drop in helically segmented finned tube heat exchangers. Appl. Therm. Eng. 30: 1470–1476

Martinez E, Vicente W, Vazquez M S, Carvajal I and Alvarez M 2015 Numerical simulation of turbulent air flow on a single isolated finned tube module with periodic boundary conditions. Int. J. Therm. Sci. 92: 58-71.

Mathpati C S, Tabib M V, Deshpande S S and Joshi J B 2009 Dynamics of flow structures and transport phenomena-2: Relationship with design objectives and design optimization. Ind. Eng. Chem. Res. 48: 8285-8311

Matos R S, Laursen T A, Vargas J V C and Bejan A 2004a Three-dimensional optimization of staggered finned circular and elliptic tubes in forced convection. Int. J. Therm. Sci. 43: 477–487

Matos R S, Vargas J V C, Laursen T A and Bejan A 2004b Optimally staggered finned circular and elliptic tubes in forced convection Int J Heat Mass Transf 47: 1347–1359

McQuiston F C 1978a Correlation of heat, mass and momentum transport coefficient for plate-fin-tube heat trasnfer surfaces with staggered tubes. ASHRAE Trans. 84 (1) 294-308

McQuiston F C 1978b Heat, mass and momentum transfer data for five plate-fin-tube heat trasnfer surfaces. ASHRAE Trans. 84 (1) 266-293

McQuiston F C 1981 Finned tube heat exchangers: state of the art for the air side. ASHRAE Trans. 87: 1077-1085

Merkin J 1977 Free Convection boundary layers on cylinders of elliptic cross section, ASME J. Heat Transf. 99: 453-457

Mirth D R and Ramadhyani S 1993 Prediction of cooling-coil performance under condensing conditions. Int. J. Heat Fluid Flow 14 (4): 391-400

Mirth D R and Ramadhyani S 1994 Correlations for Predicting the Air-Side Nusselt Numbers and Friction Factors in Chilled-Water Cooling Coils. Exp. Heat Transf. 7: 143–162

Misumi T, Suzuki K and Kitamura K 2003 Fluid flow and heat transfer of natural convection around large horizontal cylinders: Experiments with air, Heat Transf. Res. 32: 293–305.

Mochizuki S, Yagi Y and Yang W J 1987 Transport phenomena in stacks of interrupted parallel-plate surfaces. Exp. Heat Transf. 1: 127-140

Mon M S and Gross U 2004 Numerical study of fin-spacing effects in annular-finned tube heat exchangers. Int. J. Heat Mass Transf. 47: 1953–1964

Morgan V T 1975 The overall convective heat from smooth circular cylinder, in: T.F. Irvin, J.P. Harnett (Eds.), Advances in heat transfer, eleventh ed., Academic Press, New York. pp. 199-264.

Moukalled F and Acharya S 1996 Natural convection in the annulus between concentric horizontal circular and square cylinders, J. Thermophys. Heat Transf. 10 (3): 524–531.

Mullisen R S and Loehrke R I 1986 A study of the flow mechanism responsible for the heat transfer enhancement in interrupted-plate heat exchangers. ASME J. Heat Tranf. 108: 377-385

Murthy B N and Joshi J B 2008 Assesment of standard k-ϵ, rsm and les turbulence models in a baffled stirred vessel agitated by various impeller designs. Chem. Eng. Sci. 63: 5468-5495

Murthy B N, Deshmukh N, Patwardhan A W and Joshi J B 2007 Hollow self-inducing impeller: flow visualisation and CFD simulation. Chem. Eng. Sci. 62: 3839-3848.

Murthy B N, Ghadge R S and Joshi J B 2007 CFD simulations of gas-liquid-solid stirred reactor: prediction of critical impeller speed for solid suspension. Chem. Eng. Sci. 62: 7184-7195

Myers R J 1967 The effect of dehumidification on the air-side heat transfer coefficient for finned-tube coil. M.S. Thesis, Mech. Eng. Dept., Univ. Minnesota, Minneapolis, MN

Næss E 2010 Experimental investigation of heat transfer and pressure drop in serrated-fin tube bundles with staggered tube layouts. Appl. Therm. Eng. 30: 1531–1537

Nasab M E, Sam A and Milani S A 2011 Determination of optimum process conditions for the separation of thorium and rare earth elements by solvent extraction, Hydrometallurgy 106: 141-147.

Nakayama W and Xu L P 1983 Enhanced fins for air-cooled heat exchangers - heat transfer and friction correlations, in: Proc. 1st ASME/JSME Therm. Eng. Joint Conf. 1: 495-502

Naphon P and Wongwises S 2005 Heat transfer coefficients under dry- and wet-surface conditions for a spirally coiled finned tube heat exchanger. Int. Commun. Heat Mass Transf. 32: 371–385

Nelson D A, Ohadi M M, Zia S and Whipple R L 1991 Electrostatic effects on heat transfer and pressure drop in cylindrical geometries. ASME J. 3: 33–39

Nere N K, Patwardhan A W and Joshi J B 2003 Liquid phase mixing in stirred vessels: turbulent flow regime. Ind. Eng. Chem. Res. 42: 2661-2698

Newport D T, Dalton T M, Davies M R D, Whelan M and Forno C 2001 On the thermal interaction between an isothermal cylinder and its isothermal enclosure for cylinder Rayleigh numbers of Order 10^4. J. Heat Transf. 123: 1052-1061.

Nir A 1991 Heat transfer and friction factor correlations for crossflow over staggered finned tube banks. Heat Transf. Eng. 12: 43–58

Nuntaphan A, Kiatsiriroat T, and Wang C C 2005a Air side performance at low Reynolds number of cross-flow heat exchanger using crimped spiral fins. Int. Commun. Heat Mass Transf. 32, 151–165

Nuntaphan, A, Kiatsiriroat, T., Wang, C.C., 2005b Heat transfer and friction characteristics of crimped spiral finned heat exchangers with dehumidification. Appl. Therm. Eng. 25, 327–340

Ogata J, Iwafuji Y, Shimada Y and Yamazaki T 1992 Boiling heat transfer enhancement in tube-bundle evaporators utilizing electric field effects. ASHRAE Trans. 98(2): 435–444

Ohadi M M, Nelson D A and Zia S 1991 Heat transfer enhance- ment of laminar and turbulent pipe flow via corona discharge. Heat Mass Transf. J. 4: 1175–1187

Ota T, Nishiyama H, and Taoka Y 1984 Heat transfer and flow around and elliptic cylinder. Int. J. Heat Mass Transf. 27: 1771-1779

Paeng J G, Kim K H and Yoon Y H 2010 Experimental measurement and numerical computation of the air side convective heat transfer coefficients in a plate fin-tube heat exchanger. J. Mech. Sci. Technol. 23: 536–543

Patil R G, Kale D M, Panse S V and Joshi J B 2014 Numerical study of heat loss from a non-evacuated receiver of a solar collector, Energ. Conv. Manage. 78 (2014) 617-626.

Patwardhan A W and Joshi J B 1999 Relation between flow pattern and blending in stirred tanks. Ind. Eng. Chem. Res. 38: 3131-3143

Pathak S P, Velusamy K, Rajan K K and Balaji C 2015 Numerical and experimental investigation of heat removal performance of sodium-to-air heat exchanger used in fast reactors. Heat Transf. Eng. 36: 439-451.

Patwardhan A W and Joshi J B 1999 Relation between flow pattern and blending in stirred tanks, Industrial Engineering and Chemical Research 38: 3131-3143.

Pieve M and Salvadori G 2011 Performance of an air-cooled steam condenser for a waste-to-energy plant over its whole operating range. Energy Convers. Manage. 52: 1908-1913.

Pesteei S M, Subbarao P M V and Agarwal R S 2005 Experimental study of the effect of winglet location on heat transfer enhancement and pressure drop in fin-tube heat exchangers. Appl. Therm. Eng. 25: 1684–1696

Pirompugd W, Wang C C and Wongwises S 2007a Finite circular fin method for heat and mass transfer characteristics for plain fin-and-tube heat exchangers under fully and partially wet surface conditions. Int. J. Heat Mass Transf. 50: 552–56

Pirompugd W, Wang C C and Wongwises S 2007b A fully wet and fully dry tiny circular fin method for heat and mass transfer characteristics for plain fin-and- tube heat exchangers under dehumidifying conditions. J. Heat Transf. 129 (9): 1256–1267

Pirompugd W, Wang C C and Wongwises S 2008 Finite circular fin method for wavy fin-and-tube heat exchangers under fully and partially wet surface conditions. Int. J. Heat Mass Transf. 51 4002–4017

Pirompugd W, Wang C C and Wongwises S 2009 A review on reduction method for heat and mass transfer characteristics of fin-and-tube heat exchangers under dehumidifying conditions. Int. J. Heat Mass Transf. 52: 2370–2378

Pirompugd W, Wongwises S and Wang C C 2005 A tube-by-tube reduction method for simultaneous heat and mass transfer characteristics for plain fin-and-tube heat exchangers in dehumidifying conditions. Heat Mass Transf. 41: 756–765

Pirompugd W, Wongwises S and Wang C C 2006 Simultaneous heat and mass transfer characteristics for wavy fin-and-tube heat exchangers under dehumidifying conditions. Int. J. Heat Mass Transf. 49: 132–143

Pongsoi P, Pikulkajorn S and Wang C C, and Wongwises S 2011 Effect of fin pitches on the air-side performance of crimped spiral fin-and-tube heat exchangers with a multipass parallel and counter cross-flow configuration. Int. J. Heat Mass Transf. 54: 2234–2240

Pongsoi P, Pikulkajorn S and Wongwises S 2012a Experimental Study on the Air-Side Performance of a Multipass Parallel and Counter Cross-Flow L-Footed Spiral Fin-and-Tube Heat Exchanger. Heat Transf. Eng. 33: 1251–1263

Pongsoi P, Pikulkajorn S and Wongwises S 2012c Effect of fin pitches on the optimum heat transfer performance of crimped spiral fin-and-tube heat exchangers. Int. J. Heat Mass Transf. 55: 6555–6566

Pongsoi P, Pikulkajorn S, and Wang C C, and Wongwises S 2012b Effect of number of tube rows on the air-side performance of crimped spiral fin-and-tube heat exchanger with a multipass parallel and counter cross-flow configuration. Int. J. Heat Mass Transf. 55: 1403–1411

Pongsoi P, Promoppatum P, Pikulkajorn S and Wongwises S 2013 Effect of fin pitches on the air-side performance of L-footed spiral fin-and-tube heat exchangers. Int. J. Heat Mass Transf. 59: 75–82

Poulter R, Allen PHG 1986 Electrohydrodynamically augmented heat and mass transfer in the shell/tube heat exchanger. In: Proceedings of the 8th international heat transfer conference, San Francisco, 2963–2968

Qu Z G, Tao W Q and He Y L 2004 Three-dimensional numerical simulation on laminar heat transfer and fluid flow characteristics of strip fin surface with x-arrangement of strips. J. Heat Transf. 126: 697-707

Raghav Rao K S M S, Rewatkar V B and Joshi J B 1988 Critical impeller speed for solid suspension in mechanically agitated solid liquid contactors, A. I. Ch. E. J. 34: 1332-1340

Raithby G D and Hollands K G T 1985 Natural convection, in: Handbook of Heat Transfer Fundamentals, second ed., W M Rohsenow, J P Hartnett and E N Ganic [(ed (s)], New York, McGraw-Hill

Ranade V V and Joshi J B 1990 Flow generated by a disc turbine I: experimental. Trans. Instn Chem. Eng. (UK)-A: Chem. Eng. Res. Des. 68: 19-33

Ranade V V, Mishra V P, Saraph V S, Deshpande G B and Joshi J B 1992 Comparison of axial flow impellers using LDA. Indus. Eng. Chem. Res. 31: 2370-2379.

Ranade V V, Joshi J B and Marathe A G 1989 Flow generated by pitched bladed turbine part II: mathematical modelling and comparison with experimental data. Chem. Eng. Comm. 81: 225-248.

Ranade V V, Joshi J B and Marathe A G 1989 Flow generated by pitched blade turbine part II: mathematical modelling and comparison with the experimental data. Chem. Eng. Comm. 81: 225-248

Ranade V V, Mishra V P, Saraph V S, Deshpande G B and Joshi J B 1992 Comparison of axial flow impellers using LDA. Ind. Eng. Chem. Res. 31: 2370-2379

Rewatkar V B and Joshi J B 1991 Critical impeller speed for solid suspension in mechanically agitated three phase reactors I: experimental part. Ind. Eng. Chem. Res. 30: 1770-1784.

Rich D G 1973 The Effect of fin spacing on the heat transfer and friction performance of multi-row, smooth plate fin-and-tube heat exchangers. ASHRAE Trans. 79(2): 137 -145

Rich D G 1975 The Effect of the number of tube rows on heat transfer performance of smooth plate fin-and-tube heat exchangers. ASHRAE Trans. 81(1): 307-317

Robinson K K and Briggs D E 1966 Pressure drop of air flowing across triangular pitch banks of finned tubes. Chem. Eng. Prog. Symp. Ser. 62 (64): 177-184

Rocha L A O, Saboya F E M and Vargas J V C 1997 A comparative study of elliptical and circular sections in one- and two-row tubes and plate fin heat exchangers. Int. J. Heat Fluid Flow 18: 247-252

Rosman E C, Carajilescov P and Saboya F E M 1984 Performance of one and two-row tube and plate fin heat exchangers. J. Heat Transf. 106: 627-632

Rosman E C, Carajilescov P and Saboya F E M 1984 Performance of one- and two-row tube and plate fin heat exchangers. ASME J. Heat Transf. 106: 627–632

Saboya F E M, Sparrow E M 1976 Transfer characteristics of two-row plate fin and tube heat exchangers configurations. Int. J. Heat Mass Transf. 19: 41-49

Saboya S M and Saboya F E M 2001 Experiments on elliptic sections in one- and two- row arrangements of plate fin and tube heat exchangers. Exp. Therm. Fluid Sci. 24: 67–75

Sahiti N, Durst F and Dewan A 2006 Strategy for selection of elements for heat transfer enhancement. Int. J. Heat Mass Transf. 49: 3392-3400

Salimpour M R and Bahrami Z 2011 Thermodynamic analysis and optimization of air-cooled heat exchangers. Heat Mass Transf. 47: 35-44.

Sheu T W H and Tsai S 1999 A comparison study on fin surfaces in finned-tube heat exchangers. Int. J. Numer. Methods Heat Fluid Flow 9: 92–106

Shnip A I, Kolhatkar R V, Dinkar S and Joshi J B 1992 Criterion for transition from homogeneous to heterogeneous regime in two dimensional bubble columns. Int. J. Multiphase Flow 18: 705-726.

Shu C and Zhu Y D 2002 Efficient computation of natural convection in a concentric annulus between an outer square cylinder and an inner circular cylinder. Int. J. Heat Mass Transf. 38: 429–445.

Sun L, Yang L, Shao L L and Zhang C L 2015 Overall thermal performance oriented numerical comparison between elliptical and circular finned-tube condensers. Int. J. Therm. Sci. 89: 234-244.

Taghizadeh M, Ghasemzadeh R, Ashrafizadeh S N, Saberyan K and Ghanadi M 2008 Determination of optimum process conditions for the extraction and separation of zirconium and hafnium by solvent extraction, Hydrometallurgy 90: 115-120.

Taler D and Oclon P 2014a Determination of heat transfer formulas for gas flow in fin-and-tube heat exchanger with oval tubes using CFD simulations. Chem. Eng. Process.: Process Intensif. 83: 1-11.

Taler D and Oclon P 2014b Thermal contact resistance in plate fin-and-tube heat exchangers, determined by experimental data and CFD simulations. Int. J. Therm. Sci. 84: 309-32.

Taguchi G 1991 Taguchi on robust technology development, Bring Quality Engineering (QE) Upstream. ASME.

Taguchi G 1986 Introduction to Quality Engineering: Designing Quality into Products and Processes, Asian Product. Org.

Taguchi G and Konishi S 1987 Orthogonal Arrays and Linear Graphs, ASI Press, Dearborn, MI.

Tahseen T A, Ishak M and Rahman M M 2015 An overview on thermal and fluid flow characteristics in a plain plate finned and un-finned tube banks heat exchanger. Renew. Sust. Energ. Review 43: 363-380.

Taguchi G, Elsayed A E and Thomas C H 1989 Quality Engineering in Production Systems. New York, McGraw-Hill

Tang L H, Min Z, Xie G N and Wang Q W 2009a Fin pattern effects on air-side heat transfer and friction characteristics of fin-and-tube heat exchangers with large number of large-diameter tube rows. Heat Transf. Eng. 30: 171–180

Tang L H, Xie G N, Zeng M, Wang H G, Yan X H and Wang QW 2007a Experimental investigation on heat transfer and flow friction characteristics in three types of plate fin-and-tube heat exchangers. J. Xi'an Jiaotong Univ. 41: 521–525

Tang L H, Xie G N, Zeng M, Wang Q W 2007b Numerical simulation of fin patterns on air-side heat transfer and flow friction characteristics of fin-and-tube heat exchangers, in: Proceedings of ASCHT07, First Asian Symp. Comp. Heat Transf. Fluid Flow, Xi'an, China

Tang L H, Zeng M and Wang Q W 2009b Experimental and numerical investigation on air-side performance of fin-and-tube heat exchangers with various fin patterns. Exp. Therm. Fluid Sci. 33: 818–827

Tao Y B, He Y L, Huang J, Wu Z G and Tao W Q 2007a Numerical study of local heat transfer coefficient and fin efficiency of wavy fin-and-tube heat exchangers. Int. J. Therm. Sci. 46: 768–778

Tao W Q, Cheng Y P and Lee T S 2007b The Influence of Strip Location on the Pressure Drop and Heat Transfer Performance of a Slotted Fin. Numer. Heat Transf. Part A Appl. 52: 463–480

Tao W Q, Jin W W, He Y L, Qu Z G and Zhang C C 2006 Optimum design of two-row slotted fin surface with x-shape strip arrangement positioned by ‘‘front coarse and rear dense’’principle, part I: physical/mathematical models and numerical methods. Numer. Heat Transf. Part A 50: 731–749

Tao Y, He Y, Qu Z and Tao W 2011 Numerical study on performance and fin efficiency of wavy fin-and-tube heat exchangers. Prog. Comput. Fluid Dyn. 11: 246-254

Thakre S S and Joshi J B 2000 CFD modeling of heat transfer in turbulent pipe flow. A. I. Ch. E. J. 54: 5055-5060.

Thakre S S and Joshi J B 1999 CFD simulation of flow in bubble column reactors: importance of drag force formulations. Chem. Eng. Sci. 54: 5055-5060

Thorat B N, Shevade A V, Bhilegaonkar K R, Agalave R H, Parasu Veera U, Thakre S S, Pandit A B, Sawant S B and Joshi J B 1998 Effect of sparger design and height to diameter ratio on gas hold-up in bubble column reactors. Trans. Instn. Chem. Engrs. – A: Chem. Eng. Res. Des. 76: 823-834

Thorat B N and Joshi J B 2004 CFD Regime trasnsition in bubble columns: experimental and predictions. Exp. Therm. Fluid Sci. 28: 423-430.

Threlkeld J L 1970 Thermal environmental engineering, New York, Prentice-Hall

Tian L, He Y, Tao Y and Tao W 2009 A comparative study on the air-side performance of wavy fin-and-tube heat exchanger with punched delta winglets in staggered and in-line arrangements. Int. J. Therm. Sci. 48: 1765–1776

Tiggelbeck St., Mitra N K and Fiebig M 1994 Comparison of wing-type vortex generators for heat trasnfer enhancement for heat trasnfer enhancement in channel flows. Trans. ASME 116: 880-885

Torii K, Kwak K M and Nishino K 2002 Heat transfer enhancement accompanying pressure-loss reduction with winglet-type vortex generators for fin-tube heat exchangers. Int. J. Heat Mass Transf. 45: 3795–3801

Tree D and Helmer W 1976 Experimental heat and mass transfer data for condensing flow in a parallel plate heat exchanger. ASHRAE Trans. 82: 289-299

Tsai S F and Sheu W H 1998 Some physical insights into a two-row finned-tube heat transfer.

Tsai SF, Sheu TWH and Lee S M 1999 Heat transfer in a conjugate heat exchanger with a wavy fin surface. Int. J. Heat Mass Transf. 42: 1735-1745

Wang W, Bao Y and Wang Y 2015 Numerical investigation of finned-tube heat exchanger with novel longitudinal vortex generators. Appl. Therm. Eng. 86: 27-34.

Wang C and Chang Y 1996 Sensible heat and friction characteristics of plate fin-and-tube heat exchangers having plane fins. Int. J. Refrig. 19 (4): 223–230

Wang C C and Chi K Y 2000 Heat transfer and friction characteristics of plain fin-and-tube heat exchangers part I: new experimental data. Int. J. Heat Mass Transf. 43: 2681-2691

Wang C C, Chi K Y and Chang C J 2000a Heat transfer and friction characteristics of plain fin-and-tube heat exchangers part II: Correlation. Int. J. Heat Mass Transf. 43: 2693–2700

Wang C C, Fu W L and Chang C T 1997 Heat transfer and friction characteristics of typical wavy fin-and-tube heat exchangers. Exp. Therm. Fluid Sci. 14: 174-186

Wang C C, Hwang Y M and Lin Y T 2002 Empirical correlations for heat transfer and flow friction characteristics of herringbone wavy fin-and-tube heat exchangers. Int. J. Refrig. 25 (5): 673–680

Wang C C, Tao W H and Chang C J 1999 An investigation of the airside performance of the slit fin-and-tube heat exchangers. Int. J. Refrig. 22: 595-603

Wang C C, Tao W H and Du Y J 2000c Effect of waffle height on the air-side performance of wavy fin-and-tube heat exchangers under dehumidifying conditions. Heat Trasnf. Eng. 21: 17-26

Wang C C, Webb R L and Chi K Y 2000b Data reduction for air-side performance of fin-and-tube heat exchangers. Int. J. Heat Mass Transf. 43: 2693–2700

Wang J and Hihara E 2003 Prediction of air coil performance under partially wet and totally wet cooling conditions using equivalent dry-bulb temperature method. Int. J. Refrig. 26: 293–301

Wangnippanto S, Tiansuwan J, Jiracheewanun S, Wang C C and Kiatsiriroat T 2001 Air side performance of thermosyphon heat exchanger in low Reynolds number region with and without electric field. Energy Conserv. Manage. 43: 1791–1800

Watel B, Harmand S and Desmet B 1999 Influence of flow velocity and fin sapcing on the forced convective heat trasnfer from an annular-finned tube. JSME Int. J. 42 (1): 56-64

Watel B, Harmand S and Desmet B 2000a Influence of fin spacing and rotational speed on the convective heat exchanges from a rotating finned tube. Int. J. Heat Fluid Flow 21 (2): 221-227

Watel B, Harmand S and Desmet B 2000b Experimental study of convective heat transfer from a rotating finned tube in transverse air flow. Exp. Fluids 29: 79-90

Webb P L 1994 Principles of Enhanced Heal Transfer. New York, Wiley

Webb R L 1990 Air-side heat transfer correlations for flat and wavy plate fin-and-tube geometries. ASHRAE Trans. 96 (2): 445-449.

Weierman C 1976 Correlations ease the selection of finned tubes. Oil Gas J. 74 (36): 94-100

Weierman C, Taborek J and Marner W J 1978 Comparison of the performance of in-line and staggered banks of tubes with segmented fins. The American Inst. Chem. Engs. Symp. 74 (174): 39-46

Wongwises S and Chokeman Y 2003 Effect of fin thickness on air-side performance of herringbone wavy fin-and-tube heat exchangers. Heat Mass Transf. 41: 147-154

Wongwises S and Chokeman Y 2005 Effect of fin pitch and number of tube rows on the air side performance of herringbone wavy fin and tube heat exchangers. Energy Convers. Manag. 46: 2216–2231

Wongwises S and Chokeman Y 2005 Effect of fin pitch and number of tube rows on the air side performance of herringbone wavy fin and tube heat exchangers. Ener. Convers. Manag. 46: 2216–2231

Wongwises S and Naphon P 2006a Thermal performance of a spirally coiled finned tube heat exchanger under wet-surface conditions. Heat Transf. Eng. 20 (2): 212-226

Wongwises S and Naphon P 2006b Heat transfer characteristics of a spirally coiled, finned-tube heat exchanger under dry-surface conditions. Heat Transf. Eng. 27: 25–34

Wu F and Zhou W J 2015 Numerical simulation of convective heat transfer and pressure drop in two types of longitudinally and internally finned tubes. Heat Transf. Res. 46 (1): 31-48.

Xie G, Wang Q and Sunden B 2009 Parametric study and multiple correlations on air-side heat transfer and friction characteristics of fin-and-tube heat exchangers with large number of large-diameter tube rows. Appl. Therm. Eng. 29: 1–16

Xin R C, Li H Z, Kang H J, Li W and Tao WQ 1994 An experimental investigation on heat transfer and pressure drop characteristics of triangular wavy fin-and-tube heat exchanger surfaces. J. Xi’an Jiaotong Univ. 28 (2): 77–83

Yabe A 1991 Active heat transfer enhancement by applying electric fields. ASME J. 3: 15-23

Yabe A, Mori Y and Hijikata K 1978 EHD study of the corona wind between wire and plate electrode. AIAA J. 16(4): 340–345

Yabe A, Mori Y and Hijikata K 1987 Heat transfer enhancement techniques utilizing electric fields. Heat Transfer High Technol. Power Engineer: 394–405

Yan W M and Sheen P J 2000 Heat transfer and friction characteristics of fin-and-tube heat exchangers. Int. J. Heat Mass Transf. 43: 1651–1659

Yaghoubi M and Mahdavi M 2013 An investigation of natural convection heat transfer from a horizontal cooled finned tube. Exp. Heat Transf. 26 (2013) 343-359.

Yildiz S and Yuncu H 2004 An experimental investigation on performance of annular fins on a horizontal cylinder in free convection heat transfer. Heat Mass Transf. 40: 239–251.

Yoshii T, Yamamoto M and Otaki T 1973 Effects of dropwise condensate on wet surface heat transfer of air cooling coils. Proc. 13th Int. Congress Refrig. 285-292

Yu Z T, Xu X, Hu Y C, Fan L W and Cen K F 2011 Unsteady natural convection heat transfer from a heated horizontal circular cylinder to its air-filled coaxial triangular enclosure. Int. J. Heat Mass Transf. 54: 1563–1571.

Yun J Y and Lee K S 2000 Influence of design parameters on the heat transfer and flow friction characteristics of the heat exchanger with slit fins. Int. J. Heat Mass Transf. 43: 2529–2539

Yun J Y and Lee K S 1999 Investigation of heat transfer characteristics on various kinds of fin-and-tube heat exchangers with interrupted surfaces. Int. J. Heat Mass Transf. 42 (13): 2375-2385

Zeng M, Tang L H, Lin M and Wang QW 2010 Optimization of heat exchangers with vortex-generator fin by Taguchi method. Appl. Therm. Eng. 30: 1775–1783

Zhang L W, Balachandar S, Tafti D K and Najjar F M 1997 Heat transfer enhancement mechanisms in inline and staggered parallel-plate fin heat exchangers. Int. J. Heat Mass Transf. 40: 2307-2325

Zhang W, Chen F and Lan F 2013 A numerical simulations of combined radiation and natural convection heat transfer in a square enclosure heated by a centric circular cylinder, Heat Mass Transf. 49: 233-246.

Zhao H, Yan C, Sun L, Zhao K and Fa D 2015 Design of a natural draft air-cooled condenser and its heat transfer characteristics in the passive residual heat removal system for 10 MW molten salt reactor experiment. Appl. Therm. Eng. 76: 423-434.

ZukausKas A A 1972 Heat transfer from tubes in cross flow. Adv. Heat Transf. 8: 93–160